DYNAMIC BEHAVIOUR OF HEAD LOSS IN A DEEP BED GRANULAR FILTER BASED ON DEPOSITION MORPHOLOGY

BY

AL Beldawi M. Fadhil

M.Sc.(Eng.)

A Thesis

Submitted To The School Of Graduate Studies

In Partial Fulfilment Of The Requirements

For The Degree

Doctor Of Philosophy

McMaster University

DOCTOR OF PHILOSOPHY (1993)
(Civil Engineering and
Engineering Mechanics)

McMASTER UNIVERSITY
Hamilton, Ontario
Canada

TITLE: Dynamic Behaviour of Head Loss in A Deep Bed Granular Filter Based on Deposition Morphology.

AUTHOR: AL Beldawi Mohammad Fadhil
B.Sc. (Eng.) – Mosul University, IRAQ
M.Sc.(Eng.) – Baghdad University, IRAQ

SUPERVISORS: Dr. John C. Doering
Dr. D.F.E. Stolle
Dr. James M. Dickson

NUMBER OF PAGES: xxiv, 253

ABSTRACT

A review of the literature related to assessing treatment efficiency and head loss build-up using particle count and size distribution indicates some deficiencies and limitations. These deficiencies and limitations indicate several shortcomings in the available head loss models. It was noted that previous research work, which used particle size analyzers, have experienced difficulty and uncertainty in obtaining the true particle count. A procedure to correct the particle count, supported by quantitative and qualitative validation, is provided. Result obtained from past investigations on floc geometry, and its mode of deposition, have also displayed a pronounced disparity. Furthermore, no photographic evidence has been published that shows the particle dendrites in liquid. Most observations of deposition patterns relate to conditions that exhibit a substantially different behaviour from conventional filter media characteristics.

The objective of this work was to develop a mathematical model which describes the head loss in deep bed granular filter based on different modes of deposition. The deposition models include parameters that account for the dynamic fraction of particles that contribute to additional surface area and the change in geometry. The dynamic fraction of particles that contribute to smooth coating and dendrite deposition in filter containing deposit are also included in the model. The deposition morphology was validated visually using an optical fibre endoscope and quantitatively using the filtration test.

Three mathematical models have been developed for describing the effect of different deposit morphologies on the head loss build-up in sand filters. The models predict the head loss for a specific deposition mode and a combination of (different) modes. The first model is based on the assumption that retained particles form a relatively smooth coating around the filter grains (smooth coating model). The second model is based on the assumption that retained particles can act as additional collectors, forming chain-like depositions (dendrites mode model) as proposed

by O'Melia and Ali (1978). A refinement to the O'Melia model is also proposed. In particular, the variation in porosity and the factor which represents the fraction of retained particles that contribute to the additional surface area were considered in the model refinement. The effect of change on the geometry of the filter grains were considered as well. In the third model, adsorption and bridging were proposed as combined mechanisms of polyelectrolyte action during filtration of small silica (5 um) suspension. Therefore, this model is based on the assumption that the deposition takes place in two stages: smooth coating and dendrite deposition (combined mode model). It is also hypothesized that more than one mode of deposition may govern the deposition process during the filter time.

A comprehensive experimental program was conducted in which the size and concentration of silica suspension, as well as the filtration velocity and type of coagulant, were varied while the filter column and media characteristics were held constant.

Results from the experimental program and analytical modelling were used to validate the proposed deposition morphologies and to map-out the important factors responsible for different geometries and their contribution to head loss build-up. Reasonable agreement was observed between the measured and predicted head loss. The proposed models are general in nature and may be extended to conditions other than those used for validation, provided that the deposit morphology is the same. The accuracy of the proposed combination of different deposit morphologies was confirmed using experimental data.

An analysis and possible explanation for the similarity and dissimilarity of the optimum coagulant dosage between the results from a jar test and filtration test are presented.

ACKNOWLEDGEMENT

I would like to express my sincere gratitude to Dr. A. Ghobarah (Chairman) for his guidance, advice and effort in reviewing the first working draft of this thesis. I am especially indebted for him for his financial contribution.

This gratitude is also extended to Drs. John C. Doering, D.F.E. Stolle and James M. Dickson, members of my supervisory committee for their valuable comments and suggestions in editing this thesis.

I would like to express thanks to the members of my examination committee, and in particular to Professor K.J. Ives (London University, London, England) for his many constructive and helpful suggestions, for the many worthwhile correction and comments, he provided in every aspect of this work. It seems hardly adequate to briefly acknowledge Professor K.J. Ives for his honesty, fairness and judgement in evaluating this work. Professor Ives are also providing a firm background for every comment and letting me benefit from his vast knowledge and enthusiasm in the field of water filtration.

I wish to thank my great wife, Eman, for her help, patience, understanding and encouragement towards the completion of this thesis. Special thanks are to my mother for her inspiration. I wish to thank my brothers and sisters for their continuous encouragement too.

I would specially like to thank Mr. Jim Wood (Wastewater Technology Centre) for his effort in the experimental program.

This thesis is dedicated to the memory of my father Fadhil Albeldawi and to the memory of my brother Qassem Albeldawi.

TABLE OF CONTENTS

TABLE OF CONTENTS (continued)

TABLE OF CONTENTS (continued)

TABLE OF CONTENTS (continued)

LIST OF TABLES

LIST OF TABLES (continued)

LIST OF FIGURES

LIST OF FIGURES (continued)

LIST OF FIGURES (continued)

LIST OF FIGURES (continued)

LIST OF FIGURES (continued)

LIST OF FIGURES (continued)

LIST OF FIGURES (continued)

LIST OF FIGURES (continued)

LIST OF SYMBOLS

Symbol	Definition	Units
A_c	Surface area of filter grains containing deposit	cm^2
A_p	Surface area of total retained particles	cm^2
A_{co}	Surface area of clean filter grains	cm^2
A_{ps}	Surface area of retained particles which contribute to smooth coating deposit	cm^2
A_{pd}	Surface area of retained particles which contribute to dendrites formation	cm^2
A_s	Specific surface of the filter grains	cm^{-1}
A	Geometry parameter coefficient (smooth coating model)	[−]
a_1, a_2	Empirical constant describing the increase and eventual decrease infiltration efficiency with time (Ives)	cm^{-1}
B	Geometry parameter coefficient (smooth coating model)	[−]
b	Bulking factor of deposit	[−]
C_o, C	Influent and effluent suspended solids concentration	mg/L
C_e	Filtrate suspended solids concentration	mg/L
c_2	Empirical constant related to filter coefficient equation (Stein)	mg/L
c	Empirical constant related to filter coefficient equation (Iwasaki)	[−]
c'	Empirical constant related to filter coefficient equation which has the value of 0.45 (Mohanka)	cm-g-min
c_γ	Coefficient related to the empirical expression for γ	[−]
d	Coefficient related to the empirical expression for γ	[−]
D	Single collector efficiency due to Brownian motion	[−]
d_c	Diameter of filter grain	cm
d_p	Diameter of average particle size	cm

LIST OF SYMBOLS (continued)

Symbol	Definition	Units
d_{pi}	Diameter of i sized particles	cm
d_f	Diameter of floc	cm
F	Theoretical filter capacity	[−]
FP	Flow path of the suspended particles	[−]
G	Single collector efficiency due to settling	[−]
g	Acceleration due to gravity	cm/s^2
h_o	Initial head loss through the filter bed	cm
h	Head loss at time t, through the filter bed	cm
H_s	Head loss due to straining	cm
I	Single collector removal efficiency due to interception	[−]
i_o, i	Hydraulic gradient of clean and filter containing deposit	[−]
K_1	Filter coefficient parameter due to interception of diffusion	cm
K_o, K	Kozeny's coefficients of clean and filter containing deposit	[−]
K_B	Boltzmann's constant (1.38×10^{-23})	$J\ K^{-1}$
KS	Geometry parameter of filter grain	[-]
k	Head loss empirical constant	[-]
k_1	Constant in head loss equation for surface mat deposit	cm
k_2	Rate constant in head loss equation for surface mat deposit	sec^{-1}
K_g	Geometry parameter coefficient (dendrite mode model)	[−]
L	Depth of filter bed	cm
m	Positive head loss parameter	
n	Geometry parameter exponential coefficients (dendrite mode model)	[−]

LIST OF SYMBOLS (continued)

Symbol	Definition	Units
N_c	Number of filter grains per unit filter layer	[−]
N_{pi}	Number of particles retained of ith size	
N_{ij}	Number of influent particles at j time interval	[−]
N_{ej}	Number of effluent particles at j time interval	[−]
N_o	Initial number of flow path in filter bed	[−]
$n_{L,t}$	Fractional volume of blocked flow path per total initial pore volume	[−]
N_p	Total number of particles retained	cm^{-3}
P	Constant which depend on the grain diameter	
P_{50}	Equivalent uniform size of sand grain	cm
Q	Feed volumetric flow rate	
r	Positive head loss parameter	[-]
r m	Compaction coefficient with measured values in the range of 0.05-0.4	g/L
Re	Reynold's number	[−]
S_1	Shape factor of the suspended particles	[−]
S_o, S	Shape factor of clean and containing deposit filter grain	[−]
t	Filtration time	sec
T	Absolute temperature	Kelvin
V_o	Filtration velocity	cm/s
V_c	Volume of clean filter grains	cm^3
V	Volume of coated grains	cm^3
V_g	Volume of one single grain	cm^3
V_{co}	Filter grain volume per unit volume	[−]

LIST Of SYMBOLS (continued)

Symbol	Definition	Units
V_p	Volume of total retained particles	cm^3
V_{ps}	Volume of retained particles which contribute to smooth coating deposit	cm^3
V_{pd}	Volume of retained particles which contribute to dendrites formation	cm^3
x,y,z	Empirical exponents in filter coefficient equation	[−]
α	Fraction of contact between a filter grain and suspended particles that result in attachment and removal	
α_{ao},α_a	Surface area shape factor of clean and filter grain containing deposit	[−]
α_d	Fraction of retained particles which contribute to dendrites formation	[−]
α_p	Fraction of contact between retained particles and particles in suspension that results in attachment and removal	[−]
α_s	Fraction of retained particles which contribute to smooth coating	[−]
α_{Vo},α_V	Volume shape factor of clean and filter grain containing deposit	[−]
β	Fraction of retained particles that is exposed to the flowing fluid and contribute to additional surface area	[−]
β_1,β_2,β_3	Empirical exponents in filter coefficient equation (general form)	[-]
Δd	Increase in diameter due to accumulation of deposit	cm
$\varepsilon_o,\varepsilon$	Porosity of clean and filter containing deposit	[−]
$_t$	Porosity at time, t	[−]
$\Delta\varepsilon$	Change in filter layer porosity	[−]
ε_d	Porosity of deposit	[−]
$\varepsilon_{L,o}$	Initial porosity at depth L	[−]
ρ_p	Zeta potential of the particles	mV
ξ	Constant in head loss equation, account for the combination of all variables	

LIST OF SYMBOLS (continued)

Symbol	Definition	
λ_o, λ	Filter coefficient of clean and filter containing deposit	cm^{-1}
λ_{20}, λ_T	Filter coefficient at 20°C and at particular temperature, T	cm^{-1}
λ_m	Filter coefficient when start to decrease	cm^{-1}
μ	Dynamic viscosity of liquid	g/cm.sec
ν_{20}, ν_T	Kinematic viscosity of water at 20 and T °C	cm^2/sec
ρ_p	Density of particles	g/cm^3
ρ_w	Density of water	g/cm^3
ρ_i	Density of particles of i size	g/cm^3
σ	Specific deposit (volume of deposit per bed volume)	cm^3/cm^3
σ_u	Ultimate quantity of specific deposit in a pore when the filter efficiency is zero	cm^3/cm^3
σ_m	Specific deposit, when the filter coefficient start to decrease	cm^3/cm^3
$\sigma_{L,t}$	Amount of specific deposit at depth L and time, t	cm^3/cm^3
ϕ	Empirical filter constant, describing the eventual decrease in filtration efficiency with time	cm^{-1}

CHAPTER ONE

INTRODUCTION

1.1 Statement Of The Problem

Knowledge of the mode of deposition of suspended particles within the filter bed element is necessary in order to develop a reliable mathematical description of the removal of suspended solids and head loss build-up, and to develop a reasonable understanding of the mechanism(s) involved. As particles are removed by filter grains, they tend to accumulate in a variety of different configurations. These configurations are related not only to the surface area and/or surface characteristics of the filter grains, but also to the size of the particles in suspension. They are also related to coagulant type and dose, particle concentration, as well as to the particles that are removed, which act as an additional collector. These effects result in a change in the structure of the filter bed.

Many investigators recognize that a change in the structure of the filter bed plays a primary role in the particle deposition process, as well as determining the local head loss. Many of the proposed head loss equations are based on Kozeny's equation for head loss in clean, granular, porous medium. The proposed equations differ from one another because of different assumptions made regarding the mode of deposition around the filter grains and the difficulty in determining the change in the filter medium characteristics (i.e., porosity, surface area to volume ratio, and geometry parameter). As a result, investigators have obtained conflicting results concerning the mode of deposition and the factors that control deposition. The most critical factors that vary in the Kozeny's equation are considered in the model formulation. These factors

are: a) the change in porosity of the filter bed due to deposition; b) the change in surface area/volume ratio of the filter grains, which depend on the specific deposit and/or the number of particles retained (varied with mode of deposition); and c) change in the geometry parameter (the ratio of the shape factor times Kozeny's coefficient for filter containing deposit to the clean filter) that results from the change in the cross-sectional area of the flow path.

The possible existence of long particle dendrites in water filtration is a subject of controversy among researchers involved in modelling deep bed filtration. Ives (1985) indicated that no visible photographic evidence showing these particles in a liquid was obtained. To validate the proposed morphology qualitatively and quantitatively, direct observation of a floc's geometry and its mode of deposition within the filter column is an asset.

Although most of the filter models developed for close observation of deposition morphology use different techniques, they do offer some insight and information, their value is however rather limited due to the filter model used. An example of such limitations is the assumption that the pores of the prototype can be represented by straight, perpendicular channels (Maroudas and Eisenklam, 1965). The dimensions of these channels (one order of magnitude larger than those in a typical sand filter) are not considered to be representative of sand filter pores. Other visualization experiments are of somewhat limited value because of the very large grain diameter of the model filter, e.g., 5 mm used by Ison and Ives (1969). Payatakes et al. (1977) and Pendse et al. (1978) do not account for the behavioral variation in morphology while the filter run is active. Some observations for deposition patterns are related to the ferric, or alum flocs, which might show substantially different behaviour from naturally occurring particles in drinking water sources; these mixtures are often metal oxides, carbonates, silicates, organic debris, and microorganisms. Other research directed towards deposition morphology studies uses

monosized particles in suspension. This approach does not govern the expected filtration mechanisms, (O'Melia and Ali, 1978; Tien et al., 1979; Payatakes et al. 1981).

Thus, there is a pronounced disparity between results obtained by different investigators under different circumstances. At this stage, it should be recognized that an adequate model for describing head loss under different operating conditions has yet to be developed. This necessitates the need for a thorough investigation of each and/or a combination of different deposition morphology within the filter media.

The available literature concerning the use of particle count and size distribution in assessing treatment efficiency and head loss build-up is limited. In particular, in water treatment, comprehensive research on continuously monitored particle counts and size distribution using on-line measuring techniques is lacking. Deficiencies in available studies and modelling procedure include issues which relate to:

1. single mode of deposition,
2. use of mono-sized particles for most of the suspensions,
3. short filter runs,
4. bench-scale models,
5. mode of deposition using small and large particles with metal and polymer, respectively, as a filter aid are yet to be identified,
6. fine filter grains in most filter models give no information about particle size distribution (PSD) and depth removal,
7. most head loss equations predict the build-up of head loss under constant physical and chemical conditions, and
8. direct qualitative or quantitative observations are lacking to validate the proposed

morphologies.

These deficiencies contribute to several shortcomings in the available head loss models, and demonstrate the need for a more comprehensive head loss model.

1.2 Objective And Hypotheses

The objective of the research is to develop a mathematical model which describes the complete cycle of head loss based on different modes of deposition.

The developed model will be used to investigate the following aspects:

1. the most important factors responsible for the pattern of deposition;
2. the effect of ferric chloride using 5 μm (Min-U-Sil) silica and the effect of cationic polymer (percol 728) using 30 μm Silica on the deposition process and head loss development;
3. the verification of the combined (smooth coating and dendrites) modes of deposition when small particles are used with a cationic polymer as a filter aid;
4. the effect of using settled silica 5 μm ($<$ 5 μm) with ferric chloride on the mode of deposition and head loss development;
5. the validation of the proposed deposition morphology visually and quantitatively, using different techniques;
6. the mapping out of the effect of various physical variables (filtration rate, particle size, and influent concentration) and chemical filtration variables (coagulant type and dose) on the evolution of any kind of deposition, and its associated rate of head loss developmen; and
7. the best means of inducing any of the deposition morphology and under what conditions.

The following hypotheses are adopted in the proposed mathematical model.

Hypothesis 1: Smooth coating and bridging mechanisms act as a combined deposition mode, when using small particles, 5 μm silica and polymer (cationic) as a filter aid.

Hypothesis 2: Significant change in the geometry parameter $KS^2/K_oS_o^2$ occurs due to deposition during the filter run.

Hypothesis 3: A single mode of deposition does not govern the deposition process for the entire filter run.

Analysis of the data presented by Yao et al. (1971), and O'Melia and Ali (1978), indicate that the observed head loss in the early stage of the filter run can be predicted using the smooth coating head loss equation, however it is not applicable in the later stage of the filter run. This indicates that a single mode of deposition does not govern the deposition process over the entire cycle of a filter run. On this basis, it is hypothesized that the deposit is initially in the form of a relatively smooth coating on the surface of the filter grain related to the direct adhesion of the individual particles to the filter grain. As the filter run progresses, the attachment takes place by a bridging mechanism that connects one particle to another, and particle to the coating. Subsequently, the bridged deposits act as additional sites for collecting particles and this tends to inhibit further deposition at the adjacent sites of the retained particles. This effect is a direct consequence of the finiteness of the particle sizes (Rajagopalan and Tien, 1979). Inhibition of further deposition within the shadow area leads to a nonuniform deposition. The deposited particles protrude above the filter grains and, hence, provide new surfaces that are greater than

the surface area occupied. The zeta potential of the particle and the filter grain is another plausible explanation for bridging within the filter bed. The zeta potential of the filter grain has a larger negative magnitude than that of the deposited material. Therefore, there will be less repulsive force associated with a particle-to-particle interaction than a particle-to-grain interaction. The particles have a greater chance for capture on deposited particles resulting in the formation of a deposit consisting of chains, or dendrites, protruding into the pore space and causing an increase in both removal efficiency and head loss.

Hypothesis 4: Particle size and filter aid control the mode of deposition.

Hypothesis 5: The retained particles, which contribute to additional surface area, are changing with time.

1.3 Scope of The Work

The scope of this research program can be summarized as follows:

1. Analysis of the data by Yao et al. (1971), and O'Melia and Ali (1978) for the purpose of relating the head loss model to the mode of deposition.
2. Development of mathematical models to predict different deposition morphologies; in particular, smooth coating, dendrites, and a combined (smooth coating and dendrites) deposition modes are considered. The mathematical models are developed in four steps

    2.1 research hypothesis,

    2.2 model assumption and formulation,

2.3 experimental program, and

2.4 model calibration, validation, and modifications.

3. Development of a computer program to a) correct the particle concentration data, b) derive the values of parameters and terms included in the models, and c) simulate the dynamic behaviour of head loss under different conditions.

4. Validation of floc geometry and floc deposition morphology qualitatively and quantitatively. Jar test and zeta potential measurements in conjunction with a camera mounted on a microscope photographing the flocs are analyzed. An analysis of optical fibre endoscope observations using image analysis technique is also presented. The head loss data obtained from a pilot-scale filter are analyzed by comparing PSD and/or particle volume of samples obtained from a batch flocculation test for different conditions.

1.4 Outline of Thesis

A review of previous work in water filtration with respect to clarification performance and head loss is presented and discussed in Chapter 2. In particular, filtration mechanisms, deposition morphology and the factors controlling the mode of deposition are outlined. Chapter 3 describes the modelling of the dynamic behaviour of head loss in a deep bed granular filter. Parameter calibration and model verifications are also presented. Experimental material and method are described in Chapter 4. A pilot-scale plant, equipment, experimental conditions, filter media and suspension are briefly discussed.

The credibility of the zeta potential measurements in conjunction with jar test is demonstrated in Chapter 5. Visual and quantitative validation of the floc geometry and modes of floc deposition using different techniques are presented and discussed. The difficulty in

accurately measuring particle size and count is considered in chapter 6. Deficiencies and/or possible sources of errors are presented and some of the accessible deficiencies are examined. The magnitude of sizing and particle count error introduced by uncertainty of the system and measurement errors are also presented. Setting the procedure to correct the size and number concentration supported with quantitative and qualitative validation is provided. Experimental results and analysis, for no aid, ferric chloride and polymer (percol 728) using 5 and 30 μm silica at different filtration velocity is presented in Chapter 7. Comparison of model prediction and observed head loss are also presented and discussed. The research conclusions, contribution and recommendations for further research are summarized in Chapter 8.

CHAPTER TWO

LITERATURE REVIEW

2.1 Introduction

The rapid filtration of water through sand beds is a major unit in water purification plants. Its main function is the final clarification of settled water. Many attempts have been made to enhance this process in order to cope with demands for larger amount of higher quality water. Early developments focused on refining the structural features of filters, followed by a period of refinement in filter operation. Subsequently, emphasis was placed on proper conditioning of the water prior to the filtration. In recent decades, attention has been directed toward understanding the mechanism of the filtration process and the chemical parameters related to the capture efficiency to obtain more insight into and information about the deposition process. Direct observation within the filter media using different techniques and approaches are the latest of these efforts to examine the deposition morphology and/or filtration mechanisms.

The mechanisms involved in removal of suspended solids by a granular filter, and its effect on the mode of deposition and head loss build-up are complex. The large number of variables associated with the filtration process and the complexity of the physical and chemical mechanisms, means sophisticated models are necessary to represent the process. Numerous studies and many mathematical formulations mainly directed toward describing the clean bed filter removal efficiency and head loss development were made in the past two decades. As the filtration proceeds, the retained particles modify the filter performance, and the equations become inapplicable. The other approaches, which are directed toward representing the filter containing

deposit, lack generality and have limitations by predicting constant physical and chemical conditions.

Despite progress towards a better understanding of the dynamic behaviour of filter performance, there has been little progress directed towards predicting the dynamic behaviour of head loss in a granular filter, even for suspensions of monosized particles. In most of the previous work, head losses are evaluated as a function of time, where no meaningful information can be obtained in term of deposition morphology. To achieve a better understanding of the effect of changes in the basic parameters such as solids loading, particle size, filtration velocity and filter aid on the head loss build-up, and mode of deposition, an investigation was undertaken on how head loss and the deposition mode vary with these basic parameters. Emphasis is placed on the new approach to evaluate head loss in terms of mass retained or specific deposit. From the experimental data, some principles are described. The principles involved are the influence of changes in basic parameters on head loss build-up and the controlling factor in predominating one kind of deposition on another.

2.2 Background

2.2.1 Mechanisms and Modelling

The primary objective of filtration techniques in water and wastewater treatment is the the removal of particles from the water. A large part of the early work in filtration was associated with an effort to describe the performance of sand filters used in water purification process. An early attempt at mathematical formulation of the mechanism of filtration through a sand filter was made by Iwasaki (1937). The removal per unit filter depth is proportional to the concentration of suspension giving an exponential decrease in suspended particles through the

depth of the filter medium, Iwasaki (1937). Other studies and the development of a number of predictive models were directed essentially at increasing the understanding of removal efficiency following the filtration equation proposed by Iwasaki (1937), viz.,

$$\frac{\partial C}{\partial L} = -\lambda C, \tag{2.1}$$

where C is the concentration of suspension, λ is the filter coefficient or measure of filter efficiency and L is the depth of filter media. At the commencement of filtration, t=0 , λ is constant with L (clean, unisize media). Integration of Equation (2.1) yields

$$C = C_o \exp(-\lambda_o L). \tag{2.2}$$

However, there are changes in the suspension concentration and amount of deposit with respect to time and distance. Therefore, Equation (2.1) is valid only at the commencement of filtration, or as the suspension takes a finite time to traverse a layer of the filter. The filter coefficient in Equation (2.1) has been found to increase initially, causing improvement in the filtrate quality due to local initial deposit helping to remove more of the suspended particles. This dependency has been expressed by many researchers (e.g. Iwasaki 1937; Ives, 1960) as

$$\lambda = \lambda_o + c\,\sigma, \tag{2.3}$$

in which λ_o, is the initial impediment modulus (initial filter coefficient) when the filter grains are clean (t=0), c is a constant, and σ is the specific deposit (volume of deposited material per unit volume of bed) of the filter bed. From experiments conducted in a model transparent filter, and as a result of data analysis of Eliassen's (1935) experiments, Stein (1940) described the filter behaviour in terms of filter coefficients as follows:

1. The increase in the amount of material deposited tends to increase as long as the

increasing shear forces in the filter medium do not inhibit removal; this dependency was expressed as in Equation (2.3).

2. When the shear force reaches intensities that inhibit the removal, λ is decreased accordingly. For this phase Stein suggested

$$\lambda = \lambda_m \left[\frac{1 - c_2 \sigma}{1 - c_2 \sigma_m} \right]^4, \tag{2.4}$$

where λ_m is the filter coefficient when starts to decrease, σ_m is the specific deposit when $\lambda=\lambda_m$, and c_2 is a constant.

In 1951, Mints developed a concept of filtration in which two processes act simultaneously in the filter. These two processes are deposition on the filter grains and detachment of existing deposit by flowing water. Mints (1951) assumed that λ is constant throughout the run. Further research revealed that λ is no longer constant after the commencement of the filter run Ives (1960). Ives (1960) was concerned with the ideal case of homogeneous suspension applied at a constant rate under laminar flow conditions to isotropic homogeneous porous filter medium. Ives (1960) found that the filter coefficient increased initially, causing improvement in the filtrate quality, as local initial deposit helped to remove more of the suspended particles. As the filtration proceeds, the filter coefficient diminishes due to straightening of streamlines and increasing interstitial velocity carrying suspended material through the partly blocked pores. The above statement was expressed by Ives (1960) as

$$\lambda = \lambda_o + c\sigma - \frac{\phi \sigma^2}{\varepsilon - \sigma}. \tag{2.5}$$

Sholji (1963) derived the effluent concentration and filter coefficient as a function of the flow path (FP), i.e, the flow path of the settling suspension onto the grain, is designated by an unspecified

function f(FP),

$$\frac{C}{C_o} = e^{-\left(\frac{6 \cdot K \cdot f(FP)}{V_o \cdot d_c} (1-\varepsilon) \cdot L\right)}. \tag{2.6}$$

From Equation (2.2), then

$$\lambda_o = \frac{6 \cdot K \cdot f(FP)}{V_o \cdot d_c} (1 - \varepsilon). \tag{2.7}$$

After deposition takes place and if the hydrodynamic forces are not dominating, the value of porosity would decrease and become $(\varepsilon - \sigma)$, therefore

$$\lambda = \frac{6 \cdot K \cdot f(FP)}{V_o \cdot d_c} [1 - (\varepsilon - \sigma)]. \tag{2.8}$$

Simplifying Equation (2.8) gives

$$\lambda = \frac{6 \cdot K \cdot f(FP)}{V_o \cdot d_c} (1 - \varepsilon) + \frac{6 \cdot K \cdot f(FP)}{V_o \cdot d_c} \cdot \sigma. \tag{2.9}$$

where K is a factor depending on the size, the shape of packing, the orientation of the grains, and is less than one (surface area constant); V_o is the filtration velocity; and d_c is the filter grain diameter. Since $\lambda = \lambda_o + c \cdot \sigma$, then $c = \frac{6 \cdot K \cdot f(FP)}{V_o \cdot d_c}$ where c is a function of V_o, dc and FP (not constant). Cleasby (1966) used the hydrous ferric oxide flocs to evaluate the validity of Ives filtration Equation and indicated that the result obtained in the laboratory shows that Ives mathematical expression does not adequately describe the removal of ferric flocs by sand filtration. Mackrle and Mackrle (1961) stated that there would be a volume around each grain that may be designated "adhesive space" and suspended particles entering this space would be removed from the flow as they would be attracted to adhere to the grain surface. Camp (1964) stated that nearly all conventional filters operate well within the laminar flow region at a

Reynolds number much lower than 12. Camp expressed the Reynold number in term of porosity and found that the Reynold number always increase during a filter run, but that the total increase is less than 2.5 fold.

O'Melia and Stumm (1967) proposed a model for filtration in which the process is in two stages, a transport stage and an attachment stage. First, a transport mechanism must bring the particles from the bulk of the fluid close to the surface of the media. The mechanisms which are believed to affect solid/liquid separation within a granular media filter are summarized in Table (2.1). From the Work of Yao et al. (1971), Craft and Eichhortz (1970), Rajogopalan and Tien (1979), Ives (1980) and others, it may be concluded that there is a general agreement among researchers as to the nature of mechanisms, and that the main transport mechanisms for depth filtration are interception, gravitational settling, diffusion, and hydrodynamic forces. The action of particles caused by these forces (transport mechanisms) are discussed more fully by Ives (1975). Convection or fluid motion affect the suspended particle transport. In water filtration, suspended particles following the flowing fluid in the pores of the filter bed can collide with stationary filter grains in a process called interception. The gravitational settling process produces vertical transport of particles and depends upon the buoyant weight of these particles. Gravity has been found to be a significant mechanism as, in downflow filtration, particles collect preferentially on the top of the grain, forming caps. Ives (1960) visually noted that particles collect on the top of grains forming a "cap", even in upflow filtration. Brownian diffusion caused by the random motion of small particles is brought about by thermal effects. Hydrodynamic effects cause particles to leave stream lines and may lead to particle-to-grain and/or particle-to-particle contact. Yao et al. (1971) stated that if the density of the suspended particles is greater than that of water, the particles will follow a different trajectory due to the

influence of the gravitational force field. In Figure (2.1) a suspended particle following a streamline of the flow may come in contact with the collector by virtue of its own size (case A). This transport process is interception. Sedimentation (case B) is the transport process caused by gravity force. Finally, Brownian movement causes bombardment of the particles (case C). It is important to recognize that straining (particles large enough to form a mat and clog the filter surface rapidly) is not caused by any forces acting on the particles, but is due to the geometry of the particle-grain-pore system. Hall (1957) showed that if straining is the predominant mechanism the filter coefficient is indirectly proportional to the particle diameter.

$$\lambda \alpha \left[\frac{\textit{Filter Media Diameter}}{\textit{Particle Diameter}}\right]^{3/2}. \qquad (2.10)$$

An attachment of the suspended particles at the solid-liquid interface presented by the filter bed can be controlled by the surface properties of these solids. An attachment mechanism is required to retain particles at the surface of the filter medium, or to existing deposits of particles. These attachment forces act on a particle when it is in close proximity (separated by less than 1 μm) to the grain surface (Ives, 1980). The attachment mechanisms may involve London-Van der Waals' attraction forces (these universal attractive forces between atoms and molecules are due to their electronic nature, leading to an interaction of attraction between grain surfaces and particles in water, Ives and Cleasby (1971)). Other forces involved are electrostatic forces, chemical bridging, or specific adsorption, all of which are affected by the coagulant employed and the chemical characteristic of the water, the particles, and the filter medium. In a physical filtration mechanism, suspended particles may be transported to the surface of a filter grain. In order for the particles to be removed from the flow these particles must then adhere to the grain. Particle attachment has been described as a chemical process, that is influenced by both physical and

chemical parameters (Hsiung et al., 1968). The attachment was described by two empirical coefficients, α and α_p (O'Melia and Ali, 1978). The fraction of the contact between a filter grain and suspended particles that result in attachment and removal is termed α. Similarly, α_p is the fraction of contact between retained particles and suspended particles that results in attachment and removal. The attachment coefficient ranges from 0 to 1. The diameter of particles with minimum contact efficiency is approximately 3 μm. The contact efficiency increases with decreasing particle size below 3 μm. The surface interaction arises due to the so-called London interaction between molecules of particles and collector, together with the interaction between the electrical double layers which surround the particles and collector. The interaction of electrical double layers can lead to an attraction or repulsion depending on whether the surfaces have electrokinetic (zeta) potential of an unlike, or like sign, respectively. Between similar colloid particles with sufficiently high zeta potentials, the repulsion prevents contact and the colloidal dispersion is stable. Theories of colloid stability enable such attraction or repulsion to be calculated, provided that the electrokinetic potentials of the grain surface and of the particles are known, together with ionic strength of the solution (Ives and Cleasby, 1971). Since sand surfaces and the great majority of the colloidal impurities in water have negative zeta potentials, the double layer interaction usually inhibit attachment. The range of action however, is dependent on the concentration of dissolved salts in water, for instance, the range only be of the order of 1×10^{-8}m. At such small distances, attractive forces become significant and may overcome the repulsion. Van der Waals' force is the most important of the many intermolecular forces and manifests itself in a variety of phenomena, such as surface tension, adsorption, and adhesion between solid surfaces in contact.

Ives and Gregory (1967) indicated that between nearly all materials in water, the Van der

Waals' interaction is attractive, though the range rarely exceeds 5×10^{-8}m. Rajagopalan and Tien (1976) state that surface forces operate over a very short distance, say 10×10^{-8}m. Although most investigators agree that the Van der Waals-London force becomes negligible beyond a distance of 1×10^{-8}m, Boyd and Ghosh (1973) have demonstrated that within this zone of influence the London force may be significant.

The transport mechanism is primarily physical mass transport. The attachment mechanism is influenced by both physical and chemical parameters. The physical phenomena tends to control the process for larger particles > 30 μm, while chemical factors dominates for particles of < 1 μm. Gravitational settling occurs when particles with a density greater than water follow a trajectory which departs from the streamlines and contact a collector. The single collector efficiency due to settling is (Yao et al., 1971),

$$G = \frac{(\rho_p - \rho_w) g d_p^2}{18 V_o \mu}, \tag{2.11}$$

where ρ_p and ρ_w are the density of the particles and the water respectively, d_p is the average diameter of the particles, μ is the dynamic viscosity of the water, and V_o is the filtration velocity.

Diffusion occurs as a result of Brownian motion and the theoretical value of different, D, for a single collector efficiency due to Brownian motion is (Yao et al., 1971),

$$D = 0.9 \left[\frac{K_B T}{\mu \, d_p \, d_c \, V_o} \right]^{2/3}, \tag{2.12}$$

where K_B is Boltzmann's constant, T is the absolute temperature (Kelvin) and d_c is the equivalent uniform size ($\simeq P_{50}$) of the collector.

The third mechanism is interception and the single collector removal efficiency due to interception is given by (Yao et al., 1971),

$$I = \frac{3}{2}\left[\frac{d_p}{d_c}\right]^2 . \qquad (2.13)$$

These three mechanisms are assumed to yield the total single collector efficiency approximated by the sum of the analytical expressions. As presented by Ives (1971), Ison (1969) in his experimental studies, characterized the hydrodynamic mechanism by a simple Reynolds number of the filter, $Re = V_o\, d_c/\nu$, where ν is the kinematic viscosity of the fluid. The filter efficiency was found to vary as $Re^{-2.7}$ for the kaolinite suspension, thus indicating the importance of this mechanism. Theoretical relationships between filter performance and other variables such as grain diameter, filtration rate, water viscosity, and the density of the suspended particles were predicted by many researchers. The first of these, was credited to Stein (1940) who proposed the following equation based on the geometry of the constriction in filter pores and the deposit around the grain,

$$\lambda \propto \left[\frac{1}{d_c^3}\right] . \qquad (2.14)$$

Hall (1957) developed two equations for the filter coefficient that may be expressed as $\lambda \propto 1/d_c^{2.5}$ (straining), and $\lambda \propto 1/(\mu\ Vo\ d_c)$ (settling). Mints and Krishtul derived an equation of the form $\lambda \propto 1/(V_o^{0.7}\, d_c^{1.7})$. Maroudas (1965) proposed that the filter coefficient is inversely proportional to the velocity $\lambda \propto 1/V_o$. Mackrle and Mackrle (1961) proposed $\lambda \propto \mu^{0.5}/V_o\, d_c^2$. This indicates that the filter performance deteriorates as the water temperature rises. Stanley (1955) indicated that filter coefficient is directly proportional to filter depth and inversely proportional to filtration velocity and grain size $\lambda \propto L/(V_o^{1.56}\, d_c^{2.46})$. A general expression for most of these theoretical and empirical equations is of the form

$$\lambda \propto \left[\frac{1}{V_o^{\beta_1} d_c^{\beta_2} \mu^{\beta_3}} \right]. \tag{2.15}$$

The dependency of the filter coefficient on filtration variables for different mechanisms is indicated in Table (2.2). In his paper, Mohanka (1969) dealt with the extension of filter theory to cover the case of multilayer filtration. Almost independently of the mechanisms which control filtration, Mohanka (1969) assumed that for a given suspension at a given temperature the filter efficiency is dependent on the surface area available for the particle deposition and on the rate of flow past such surfaces. An approximate correction for temperature was made by Mohanka (1969) as the filter coefficient, λ, is inversely proportional to μ as given by Ives and Sholtji (1965).

$$\lambda_{20} = \lambda_T \frac{\nu_T}{\nu_{20}}. \tag{2.16}$$

In which λ_{20} is the filter coefficient at 20 C°, λ_T is the filter coefficient at particular temperature, T, and ν_{20} and ν_T represents the kinematic viscosity of water at 20 and T C°, respectively. The physical transport mechanism and filter coefficient models are given in Table (2.3). Ives (1971) stated that most proponents of mathematical models of filtration recognize that the filter coefficient λ is not constant during the filtration process. Since the deposited particles alter the characteristic of the filtration action, it follows that λ must be written as some function of the specific deposit σ. The most general of all proposed functions is one formulated by Ives (1969):

$$\lambda = \lambda_o \left[1 + \frac{b\sigma}{\varepsilon_o} \right]^y \left[1 - \frac{\sigma}{\varepsilon_o} \right]^z \left[1 - \frac{\sigma}{\sigma_u} \right]^x, \tag{2.17}$$

where b is a geometric constant relating to the packing of the filter grains, σ_u is the ultimate or

saturation value of the specific deposit, and x, y, z are empirical exponents. By suitable choice of the exponents x, y, and z, previous mathematical models, notably Iwasaki (1937), Ives (1960), Mackrle (1965), Heertjes and Lerk (1967), Maroudas (1965) and Mohanka (1969) can be expressed as the following equations, respectively (Iwasaki: x=z=0, y=1),

$$\lambda=\lambda_o\left[1+\frac{b\sigma}{\varepsilon_o}\right]. \tag{2.18}$$

(Ives: x=y=z=1),

$$\lambda=\lambda_o+a_1\sigma-\frac{a_2\sigma^2}{(\varepsilon_o-\sigma)}. \tag{2.19}$$

(Mackrle et al.: x=0),

$$\lambda=\lambda_o\left[1+\frac{b\sigma}{\varepsilon_o}\right]^y\left[1-\frac{\sigma}{\varepsilon_o}\right]^z. \tag{2.20}$$

(Heertjes and Lerk: x=y=0, z=1),

$$\lambda=\lambda_o\left[1-\frac{\sigma}{\varepsilon_o}\right]. \tag{2.21}$$

(Maroudas: y=z=0, x=1),

$$\lambda=\lambda_o\left[1-\frac{\sigma}{\sigma_u}\right]. \tag{2.22}$$

(Mohanka: x=1.5, y=0.75, $z=c' A_s^{0.61}/V_o^{0.24}$)

All the parameters are evaluated from experimental observations. z was found to be a function of filtering velocity and grain size. c′ is a constant which has the value of 0.45 cm-gm-min, and

A_s is the specific surface).

2.2.2 Deposition Morphology

Review of the previous research work suggested that the deposition morphologies likely to occur in deep bed filtration are 1) smooth coating around the grains, 2) cap formation deposit, 3) blocking of the pores in the filter bed, 4) chain-like (dendrites) formation extending from the grain surface into the pore space and 5) constriction mode of deposition. Each of these deposition morphologies may be associated with a set of physical and/or chemical conditions which lead to a certain morphology evolution. Identifying and quantifying the conditions leading to each of the modes has been emphasized. In particular, more detailed investigation is directed toward the smooth coating, dendrites and the combined (smooth coating and dendrites) mode of deposition. Some of the above deposition modes do not evolved initially, but rather their evolution may be associated with certain conditions related to the transient behaviour in a deep bed filter. The result of the resuspension of flocs, for example, is the formation or the transition to some other kind of deposition. It is interesting to note that it has been observed experimentally (Ives, (1961), Camp (1964), and Deb (1969)) that the filter coefficient, λ, first increases with σ and then decreases, suggesting that perhaps the deposit morphology may undergo a change from one type to another during a filtration cycle depending upon the extent of particle deposition.

The effectiveness of the deposited solids on head loss build-up appears to be related to two factors, namely, the mode of deposition and the extent of deposition at any given depth and time. Head loss distribution emphasizes the former, whereas the overall solids removal efficiency and the head loss distribution over depth at different time intervals determines the degree of penetration. Most of the models developed are formulated on the basis that the deposits are in

a relatively smooth coating form. Camp (1964), and Stein (1940), in a study which employed the use of an experimental filter composed of cylindrical rods, observed the formation of a relatively smooth coating over the collecting bodies during the filtration of ferric flocs. A pattern of sheath-like deposit was noted to accumulate on the upper half of the grains in the case of ferric flocs (1-20 μm), and calcium carbonate particles (1-10 μm) by Cleasby and Baumann (1962). Accumulation on the upper half of the filter grains was also observed by Ison and Ives (1969) for kaolinite particles. Maroudas and Eisenklam (1965) performed a series of experiments using a specially designed filter containing a two-dimensional network of interconnecting channels of a regular staggered square pattern. They observed that even with the same filter and the same kind of particles, differences in flow rate and particle size may lead to three different results: gradual constriction of all junctions leading to nonretention, blocking of some junctions leading to nonretention, and blocking of some junctions leading to complete blocking of the bed. They showed experimentally that spherical 390 μm particles (constriction mode of deposition) gave lower pressure drops compared to angular particles (blocking mode), where in both cases the final state of the bed was nonretaining. Some previous works on particle deposition inside filter media have assumed for the sake of calculation that particles deposit uniformly along the pore walls of the filter medium, and that the increase in head loss during clarification is due to a uniform decrease in pore diameter (Grace, 1956).

An indirect method of evaluating the deposition morphology was developed by Pendse et al., (1978). They used a tracer dispersion measurement in conjunction with head loss data as an indirect diagnostic technique. Pendse et al. (1978) considered two limiting cases of morphology; they were:

1) Deposition forms a relatively uniform and smooth coating on the surface of the filter

grain, i.e. smooth coating mode; and

2) Particle deposits are lodged at the pore constrictions of the filter bed and thus block the flow of the suspension through these pore space, i.e., blocking mode.

Habibian and O'Melia (1975) suggested that particles removed during the early stage of a filter run can serve as a collector or deposition sites for particles reaching the bed at a later time, thereby improving filtration efficiency during the ripening period of filtration. As a consequence, the utility of theories for head loss and removal efficiency of clean filter bed is restricted. O'Melia and Ali (1978) argued that the major role of deposited particles is to act as additional collectors forming chain (dendrites). Ives (1985) wrote:

> "This seems unlikely in liquid filtration in which the liquid force would cause such dendrites if they ever commence to form, to lie down on the grain surface. The evidence for such dendrites is slight and circumstantial; no visible of photographic evidence ever shows them in liquid filtration".

Formation of smooth coating and/or dendrites modes depend on the particle size to be removed, concentration of suspension, coagulant type and dose. Payatakes (1977) showed that the main mechanism causing alteration of the geometry of the flow channels within the filter media is throat-clogging. The study by O'Melia and Ali (1978), using a polymer coagulant system, mathematically related the improving phase of filtration to the accumulation of particles and the formation of dendrites within the media pores, which have been shown to increase the capture of influent particles. Many researchers, e.g., O'Melia and Ali (1978), Yapijakis (1982), Payatakes et al. (1981), Francois and Van Haute (1985), have proposed that the accumulation of particles within the filter media pore results in the improving phase of the filter ripening sequence, whether by dendrites formation, pore clogging or discrete particle accumulation. This is not the case as maximum particle removal efficienty was observed in a run belonging to experiments with filter aid over the entire cycle of the filter run where head loss, but not the

breakthrough were the termination criteria. In an earlier study, Payatakes and Tien (1976) and Payatakes et al. (1977) proposed a theory for the formation and growth of particle dendrites on a single cylindrical collector. This earlier theory considers the kinetics of particle dendrites growth as a function of the angular position of deposition on the collector. Yao et al. (1971) stated that when polymers are used a short filter run with conventional beds due to rapid clogging of the filter pores will result; retention of small (0.1 μm) particles produces considerable head loss. Chi Tien et al. (1977) proposed a theory for the formation and growth of particle dendrite on a collector placed in an aerosols stream using the following values of the physical parameters: d_p (particle diameter)=1.305 μm; d_f (fibre diameter)=9.6 μm; ρ_p (particle density)=1.01 gm/cc. They point out that the manner in which the particle deposit forms on the collector surface is strongly influenced by two intrinsic properties of suspended particles: (1) their finite size and (2) the randomness of the location of individual paticles in the fluid stream. The effect of dendrites from adjacent collectors were not taken into consideration; dendrites will eventually touch each other, thereby clogging the filter media. The possibile existence of long particle dendrites in water filtration was a subject of controversy among the researchers involved in modelling deep bed filtration. Nevertheless, the fact that filtration efficiency changes as filtration progress and that exponential increase in head loss clearly indicates that the deposited particles play a significant role.

Predicting of the response of a filter bed to the structural changes in its pore geometry, which is caused by particle deposition, makes understanding deep bed filtration difficult. In recent years, advances have been made in modelling the retention efficiency, but to a lesser extent the head loss.

2.2.3 Head Loss Models

For clean porous media of grain diameter d_c, the hydraulic gradient is accurately predicted by the Kozeny's equation,

$$i = \left[\frac{K \cdot S^2 V_o}{g}\right] \frac{(1-\varepsilon_o)^2}{\varepsilon_o^3} \left[\frac{\nu}{d_c^2}\right], \tag{2.23}$$

where i represents the clean bed gradient, K S^2 characterizes the shape and geometry of the media, ν is the kinematic viscosity, ε_o is the porosity, g is the gravity constant, V_o is the approach filtration rate and d_c is the filter media grain diameter.

Based on Kozeny's equation, Camp (1964) developed a head loss equation to determine the hydraulic gradient i at various depths of the filter bed for different stages of the run. As clogging progresses, it is assumed to be characterized by sheath formation over the media grains. This assumption implies that the clogging of the filter would result in a porosity reduction, noted by σ, which is defined as specific deposit, and an increase in grain diameter, noted by Δd.

$$i = \left[\frac{KS^2 V_o}{g}\right] \frac{(1-\varepsilon_o+\sigma)^2}{(\varepsilon_o-\sigma)^3} \frac{\nu}{(d_c+\Delta d)^2}. \tag{2.24}$$

Solving the equation and dropping the (negligible or small) term Δd^2, the hydraulic gradient equation is obtained in the form:

$$i = \frac{KS^2 \nu}{g} \frac{(1-\varepsilon_o+\sigma)^2}{(\varepsilon_o-\sigma)^3} \frac{V_o}{\sqrt{\frac{\sigma}{3(1-\varepsilon_o)}+\frac{1}{4}} + \frac{\sigma}{3(1-\varepsilon_o)}+\frac{1}{2}}. \tag{2.25}$$

Mohanka (1969) derived an equation similar to equations derived empirically by other authors.

$$\left[\frac{\partial h}{\partial L}\right] = \left[\frac{\partial h}{\partial L}\right]_o + F(\sigma). \tag{2.26}$$

Experimentally, the function has been found to be linear with the specific deposit for a number of different suspension (Ives and Sholji, 1965); consequently, the equation can be written as

$$\left[\frac{\partial h}{\partial L}\right] = \left[\frac{\partial h}{\partial L}\right]_o + k\sigma. \tag{2.27}$$

The head loss through the entire depth of the filter at any given time was found by integrating the above equation, i.e.,

$$\int_0^L \frac{\partial h}{\partial L} dL = \int_0^L \left[\frac{\partial h}{\partial L}\right]_o dL + \int_0^L k\sigma dL. \tag{2.28}$$

Mohanka found that $\int_0^L k\,\sigma\,dL$ is approximately equal to $k\,V_o\,C_o\,t$, in which t is the time from commencement of filtration and

$$h = h_o + kV_oC_ot. \tag{2.29}$$

The equation is valid only when the filtrate concentration is less than 10 percent of the inlet concentration. For other cases, Equation (2.29) takes the form:

$$h = h_o + kV_o(C_o - C_e)t, \tag{2.30}$$

in which C_e is the filtrate concentration for a particular depth, L, and time, t.

Ives (1969), observed that when flow starts, the head loss experienced through the media increases linearly with depth conforming to the Kozeny equation. This linearity is not maintained, however, as the clogging proceeds since the amount of clogging is not uniform in all layers. Consequently, the pressure lines are distorted as the filter run proceeds. Simultaneous measurement of particle concentration, specific deposit, and hydraulic gradient is attempted within

a filter. The spacing of the manometer ports for determining hydraulic gradient and of sampling ports for measuring suspended particles concentration were often much further apart. A number of studies using radioactive tracer or x-ray absorbing material have directly measured particle deposit within a filter at 1 cm intervals. Sampling and manometer ports were again spaced at various intervals in other work (Camp 1964; Cleasby, 1969; Adin and Rebhun 1974, 1977; and Rebhun et al. 1984). In recent research, particle size distributions were measured on samples taken at different depth and times, accompanied with continuous monitoring of head loss at the same locations (Darby et al. 1990, 1991, 1992; Mackie and Bai, 1992).

Sakthivadivel et al. (1972) believed that four components of the Kozeny-Carman equation play an important role in head loss development: 1) change in porosity with time, 2) change in surface area with time, 3) change in geometry parameter ($K \cdot S^2$), which is partly represented by the Carman shape factor, and 4) change in the flow path (tortuosity factor). Sakthivadival adds that:

> "The inability to determine these variables exactly during filtration often lead to approximation and simplified assumptions, which in turn give rise to different head loss equations depending on the validity of the assumptions."

As stated by Sakthivadivel et al. (1972), Ives (1960) advocated the use of a modified form of the Kozeny equation for the head loss in which he introduces a constant to account for the change in surface area and the Kozeny-Carman constant during filtration. He suggests that the constant be determined experimentally.

Mackrle (1961) proposed a mathematical model for the change in surface area per unit volume of matrix with respect to three factors x, y and p.

$$S=S_o\left[1+\frac{p\sigma}{\varepsilon_o}\right]^x\left[1-\frac{\sigma}{\varepsilon_o}\right]^y, \tag{2.31}$$

where p is a constant depending on the grain size. Mackrle assumes for simplicity that x=y=1. The head loss equation is:

$$h=h_o\left[1+\frac{p\sigma}{\varepsilon}\right]^3\left[1-\frac{\sigma}{\varepsilon}\right]^{-3/2}. \tag{2.32}$$

Mohanka (1969) determined the value of x, y and b experimentally. However, in his proposed equation for head loss during filtration, he considered x=y=1 and $p=29/(S')^{0.65}$ and assumes that the Kozeny-Carman constant remains unchanged during filtration. Hence his equation, in effect, takes into account only the change in surface area and porosity of the matrix.

$$h=h_o\left[1+\frac{p\sigma}{\varepsilon_o}\right]^2+\left[1-\frac{\sigma}{\varepsilon_o}\right]^{-1}. \tag{2.33}$$

Sakthivadivel (1966) and Shektman (1961) as reported by Sakthivadivel et al. (1972) only accounted in their equations for the change in porosity of the matrix. In addition, they introduce a constant to account for the other variables,

$$h=h_o\frac{(1-\varepsilon_o+\sigma)^2}{(\varepsilon_o-\sigma)^3}\frac{\varepsilon_o^3}{(1-\varepsilon_o)^2}\cdot\frac{1}{\xi^2}, \tag{2.34}$$

where ξ^2 is denoted for the combination of all the other variables such as the interstitial velocity, filter grain diameter.

Shektman proposed Equation (2.35) to predict the headloss.

$$h = h_o \frac{1}{\left[1 - \sqrt{1 - \frac{\varepsilon_o - \sigma}{\varepsilon_o}}\right]^3}, \tag{2.35}$$

Based on Stein's experimental results, Camp (1964) assumed that clogging forms as a sheath on each grain. His model fails to consider the point of contact between the matrix grains. Camp also assumed that the value of k does not significantly change during filtration.

$$h = h_o \left[1 + \frac{\sigma}{\varepsilon_o}\right]^{4/3} \left[1 - \frac{\sigma}{\varepsilon_o}\right]^{-3}. \tag{2.36}$$

Hsiung (1972) assumed a mathematical equation for the increase in head loss due to clogging in the pores of the media during the filtration process:

$$h_t - h_o = k \sum Q(C_o - C_e)\Delta t, \tag{2.37}$$

in which h_o = initial head loss; h_t = head loss at time t; Q = filtration rate; Δt = Filtration Time after starting the run; C_o = influent concentration; C_e = effluent concentration; and k = head loss constant.

Maroudas (1965) worked with particles of relatively large dimension (> 25 μm). She describes the head loss by the formula:

$$i = i_o \left[\frac{1-\varepsilon}{1-\varepsilon_o}\right]^{4/3} \left[\frac{\varepsilon_o}{\varepsilon}\right]^3, \tag{2.38}$$

in which $\varepsilon = \varepsilon_o - b\sigma$, where b is the bulking factor.

As reported in the literature, Sakthivadivel studied the retention of large particles, and proposed two models in which the tortuosity remains constant. The first was a model of uniform

coating of parallel pores. However, the defined expression does not correspond to his hypothesis, as it does not allow for the variation of bed specific surface. This model, given by Equation (2.39), was verified experimentally for very fine particles.

$$i = i_o \left[\frac{\varepsilon_o}{\varepsilon} \right]^3 . \tag{2.39}$$

In the second model, he assumed that the grain diameter, d_c, remains constant. As a consequence, the grain specific surface is constant,

$$i = i_o \left[\frac{1-\varepsilon}{1-\varepsilon_o} \right]^2 \left[\frac{\varepsilon_o}{\varepsilon} \right]^3 . \tag{2.40}$$

Ling (1955) also used the same concept of Sakthivadivel since he assumed that grain specific surface varies very slowly, whereas $(1-\varepsilon)^2/\varepsilon^3$ varies rapidly. Maroudas and Eisenklam (1965) proposed a simple equation for head loss in case of pore blockage, with non-blocked passages free of deposit.

$$h = h_o \frac{V}{V_o} = h_o \left[\frac{1}{1-n_{l,t}} \right], \tag{2.41}$$

where $n_{l,t}$ is the fraction volume of blocked flow paths per total initial pore volume.

The principal difference between the various head loss models notably, Ives (1960), Camp (1964), Mohanka (1969), Mackrle (1965), and Sakthivadivel (1966), is the value of the constant assumed in the equation, and the substitution of the expression representing the components which change in the Kozeny equation. Comparing the various head loss equations by plotting h/h_o versus σ Figure (2.2), Sakthivadivel et al. (1972) concluded that the available models could each be fitted to experimental data, but the models were not predictive under new situations.

Sakthivadivel et al. (1972) and Chi Tien and Gimbel (1982) presented summaries of proposed models for increased head loss by deposited particles. Proposed equations as presented by McDowel et al. (1986), are of the form:

$$i = i_o \frac{1}{(1-r\sigma)^m}, \tag{2.42}$$

where r and m are positive parameters. This equation is frequently expanded into a power series in r σ:

$$i = i_o \left[1 + mr\sigma + \frac{m(m+1)}{2} r^2\sigma^2 + ... \right]. \tag{2.43}$$

When the term in σ^2 and above are dropped, the hydraulic gradient increases linearly with particle deposition. However, this is not always observed in the filter column. McDowell et al. (1986) wrote that Kavanaugh (1974) termed the parameter combination r m, a compaction coefficient with measured values in the range of 0.05-0.4 g/L. Larger media have smaller values at constant flow rates. Frequently, those equations are incorrectly applied to deep bed granular filter where substantial depth variation in deposit occurs.

Ives (1963) and Heertjes and Lerk (1967) show that the total pressure drop i across the entire filter was in certain conditions a linear function of time. The expression can be written as:

$$i = i_o(1 + rm\sigma). \tag{2.44}$$

Adin and Rebhun (1977) and Rebhun et al. (1984) observed that the hydraulic gradient during filtration could fit the Shektman formula:

$$ri = i_o \left[1 - \sqrt{\frac{\sigma}{F}} \right]^{-3}, \tag{2.45}$$

where F is the theoretical filter capacity and is evaluated from filtration data.

Chi Tien et al. (1979) proposed the following smooth coating model for blocking mode particle deposition:

$$i = i_o \left[\frac{1}{1 - \frac{\sigma}{\varepsilon_o (1-\varepsilon_d)}} \right]^3 \left[1 + \frac{\sigma}{(1-n_o)(1-\varepsilon_d)} \right]^{4/3}. \tag{2.46}$$

The model in equation (2.46) results in the change in the interstitial velocity, the dimension of the collector, and the overall porosity, but has no effect on the geometrical configuration of the collector. None of the flow passages are completely blocked unless the pores are completely filled.

Some theories have been developed for ripening the filter in water and wastewater treatment. Habibian and O'Melia (1975) suggested that particles removed during the early stage of a filter run serve as collectors or deposition sites for particles reaching the bed at a later time, thereby improving filtration efficiency during the ripening period of filtration. As a consequence, the utility of theories for the head loss of a clean filter bed is restricted. Yao et al. (1971) also mentioned such particle attachment in water filtration. O'Melia and Ali (1978) developed a model for filter clogging based on particles captured on clean filter media and on previously captured particles that form dendrites. The head loss model represented by Equation (2.48) was based on Kozeny equation for clean filter bed. The change in surface area as dendrites form was considered in the model formulation, while the change in porosity was assumed negligible. This assumption is justified only in case of dilute suspension. The model could fit experimental data

on particle removal and increase in hydraulic gradient, but the model could not be verified with data not used for parameter calibration.

$$\frac{h}{L}=\frac{36}{d_c^2}\frac{K\mu V_o}{\rho_w g}\frac{(1-\varepsilon_o)^2}{\varepsilon_o^3}\left[\frac{1+\beta'\frac{N_p}{N_c}\left[\frac{d_p}{d_c}\right]^2}{1+\frac{N_p}{N_c}\left[\frac{d_p}{d_c}\right]^3}\right]^2, \qquad (2.47)$$

where N_c and N_p are the number of filter grains and retained particles in the filter bed with length L, and β' is an empirical coefficient that represents the fraction of retained particles which are exposed to the flowing fluid and contribute to the additional surface area.

In an earlier study, Payatakes and Tien (1976) and Payatakes et al. (1977) proposed a theory for the formation and growth of particle dendrites on a single cylindrical collector. This earlier theory considers the kinetics of particle dendrites growth as function of the angular position of deposition on the collector. Payatakes et al. (1977) calculated the increase in hydraulic gradient with filter depth as a function of the specific deposit using the constricted tube model. Based on different hypotheses of the morphology of deposits, different hydraulic gradient increases were predicted. A Comparison of these predictions with experimental data suggests that throat-clogging was dominant in the filtration of a clay suspension. However, in the filtration of ferric and alum flocs, the deduced deposit morphology was that of smooth and nearly uniform coating on the grains. Constriction clogging results from polyelectrolyte flocs. However, this study was unable to represent the transient behaviour in deposit morphology. Modelling transient behaviour from one deposition mode to another was attempted in modelling the removal efficiency, but not in head loss development (Tien et al., 1979, Mackie and Horner, 1987). Another diagnostic approach developed by Pendse et al. (1978) was based on the axial dispersion

of tracers in clogged filters. Using head loss measurements and by assuming a given deposit morphology, axial dispersion in the filter can be predicted theoretically. Comparison of the predicted and measured axial dispersion can be used to validate or reject the assumed deposit morphology. Formation and growth of chain-like particles or dendrites was originally observed in air filtration experiments, Billing (1966). Dendritic modelling was originally developed for air filtration by Payatakes and Tien (1976). Many of the mechanisms employed in air filtrations (inertial impaction, Brownian diffusion, and direct interception) are identical to those in solid-liquid separation. In air filtration, inertia and diffusion is the major capture mechanism. The inertia force has been shown to be negligibly small in the case of liquid media (Herzig et al., 1970); this is in contrast to the case of aerocolloidal suspension where the inertial force is almost always significant. In water filtration, the effect of other capture mechanisms, such as gravitational settling, pore space flocculation, and straining are involved.

The major differences between the controlling mechanisms of particle collection in the clarification of air and liquid is the higher liquid viscosity compared to the lower viscosity in case of air filtration, different surface characteristic of the filter media and the lack of similarity between filter grains in water filtration and fibre in air filtration. The forces on the particles increase with fluid viscosity, velocity, and particle size. It is expected that the drag force on particles in liquid filtration system should be much higher than in air filtration system because liquids have higher viscosities than air.

Ives (1970) has suggested that particles do not become detached from filter grains under most operating conditions, particularly if the filtration rate is kept constant. The resuspension of single particles and clusters of particles may occur when the force exerted on the deposited particles by the fluid flowing through the pore spaces exceeds the cohesive strength of the

deposit.

It was postulated that the filtration process consist of two consecutive stages: smooth coating followed by a transition to a constriction clogging Tien et al. (1979). They also grouped the models employed by various investigators into three categories: Capillaric collector (Payatakes, Rajagopalan and Tien, 1974; Hsiung and Tien, 1976); spherical collector (Yao, Habibian and O'Melia, 1971; Spielman and Fitzpatrick, 1973; Payatakes, Rajagopalan and Tien, 1974; Rajagopalan and Tien, 1976); and the constricted tube collector (Payatakes, Tien and Turan, 1974).

Letterman (1976) proposed a head loss equation without specifying what morphology should be fit.

$$h = h_o \, e^{\frac{\sigma}{k}}. \tag{2.48}$$

Under straining and cake formation conditions the head loss would be expected to increase dramatically as the fluid would have to pass through a layer of porous media containing particles considerably smaller than the original media. Ives (1982) showed that this head loss exhibits an exponential increase pattern, given by

$$H_s = k_1 \exp(k_2 t), \tag{2.49}$$

in which H_s is the head loss due to straining and k_1 and k_2 are constants. Considering the change in surface area and porosity, Sembi and Ives (1982) developed the following equation for the hydraulic gradient through a layer containing deposit:

$$\left[\frac{\partial H}{\partial L}\right]_{L,t} = \left[\frac{\partial H}{\partial L}\right]_{L,0} \left[\frac{1-\varepsilon_{L,0}+b\sigma_{L,t}}{1-\varepsilon_{L,o}}\right]^{1.33} \left[\frac{\varepsilon_{L,o}}{\varepsilon_{L,o}-b\sigma_{L,t}}\right]^{3} \qquad (2.50)$$

The term $(\varepsilon_{L,o}-b\sigma_{L,t})$ represents the porosity remaining open to flow.

It is well-established that deposited particles act as additional collectors (Payatakes et al., 1981). Other models have been developed to calculate the effect of deposited particles on the collection efficiency (Wang et al., 1977). However, the head loss model was not considered to the same extent as that of the removal efficiency.

Vigneswaran and Tulachan (1988) modified the O'Melia and Ali (1978) model by considering the change in surface area and porosity due to deposition of particles on the filter grain. They introduced the coefficients S_1 and S_0, which take into account the shape factor of the suspended particles and filter grains, respectively:

$$\frac{h}{L} = \frac{K\mu V_o}{\rho_w g} \frac{(1-\varepsilon_o)^2}{\varepsilon_o^3} \frac{36}{d_c^2} \left[\frac{S_0}{6}\right]^2 \left[\frac{1 + \gamma' \frac{Np}{Nc}\left[\frac{dp}{dc}\right]^2 \left[\frac{S_0}{S_1}\right]^2}{1 + \frac{Np}{Nc}\left[\frac{dp}{dc}\right]^3 \left[\frac{S_0}{S_1}\right]^3}\right]^2 . \qquad (2.51)$$

The value of γ' was determined by fitting the theoretical head loss profile with the experimental head loss profile. However, the expression included in the model S_1 and S_0 does not account for the variation in shape factor of the flocs and/or the filter grains as they assume that the shape factors are constant and equal to 6.1. This assumption is the major inadequacy of the model.

In summary this present work is an improvement over and extension of the earlier work to study the morphology of particle deposit, specifically, the present study, 1) Using pilot scale plant with filter depth and media characteristic, the same as in the field; 2) Using a heterodisperse silica particles suspended in tap water; 3) Direct observation within the filter media using the

optical fibre endoscope techniques, and video recording of the process without disturbing neither the porous matrix nor the particle deposit. This allows for further image analysis; 4) Employ an experimental design covering a broad range of particle size, filtration velocity with different solids concentration.

Table (2.1) Mechanisms operative within a granular-medium filter (After Metcalf and Eddy, 1979)

Mechanism	Description
1. Straining	
a. Mechanical	Particles larger than the pore space of the filtering medium are strained out mechanically
b. Chance contact	Particles smaller than the pore space are trapped within the filter by filter by chance contact
2. Sedimentation	Particles settle on the filtering medium within the filter
3. Impaction	Heavy particles will not follow the flow streamlines
4. Interception	Many particles that move along in the stream line are removed when they come in contact with the surface of the filtering medium
5. Adhesion	Flocculant particles become attached to the surface of the filtering medium as they pass by. Because of the force of the flowing water, some material is shearing away before it become firmly attached and is pushed deeper into the filter bed. As the become clogged, the surface force increases to a point at which no additional material can be removed. Some material may break through the bottom of the filter, causing the sudden appearance of turbidity in the effluent
6. Chemical adsorption a. Bonding b. Chemical interaction	Once a particle has been brought in contact with the surface of the filtering medium or with other particles, either one of these mechanisms, or both, may be resposible for holding it there
7. Physical adsorption a. Electrostatic forces b. Electrokinetic forces c. Van der Waals forces	
8. Flocculation	Large particles overtake smaller particles. These particles are then removed by one or more of the above removal mechanisms
9. Biological growth	Biological growth within the filter bed will reduce the pore volume and may enhance the removal of particles with any of the above mechanisms

Table (2.2) **Dependence Of λ_o on d_p, V_o and Zeta Potential (ζ) For Various Transport and Attachment Mechanism**

Transport or Attachment Mechanism	d_p	V_o	ζ
Straining	$d_p^{3/2}$		
Gravity Settling	d_p^2	V_o^{-1}	
Interception	d_p^2		
Brownian Diffusion	$d_p^{-2/3}$	$V_o^{-2/3}$	
Electrostatic Forces	d_p^{-1}	V_o^{-1}	ζ^{-1}
London Van der Waals' Forces	d_p^2	Weak	

Table (2.3) **Transport Mechanism And Filter Model Coefficient (extracted from Russell and Ghosh, 1973)**

Mechanism	Model
Gravity Settling	$\lambda_o = k1\ (g.(\rho_p - \rho_s).d^2_p/18.\mu.V_o)$
Interception	$\lambda_o = 1.5 \times K_1 \times (d_p/d_c)^2$
Diffusion	$\lambda_o = K_1 \times 0.9 \times \left[\frac{K_B T}{\mu d_p d_c V_o}\right]^{2/3}$
	Where $K_1 = 1.5\ (1-\varepsilon_o)\ d_c$

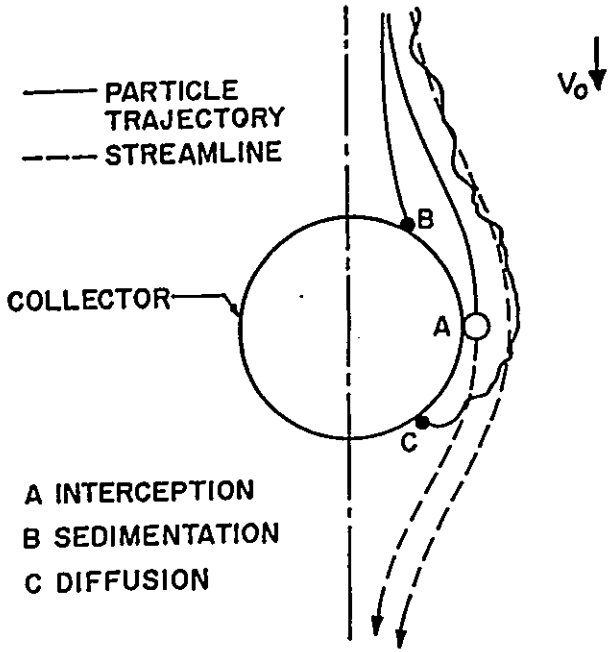

Figure (2.1) Filtration Mechanism extracted from Yao et al. (1971)

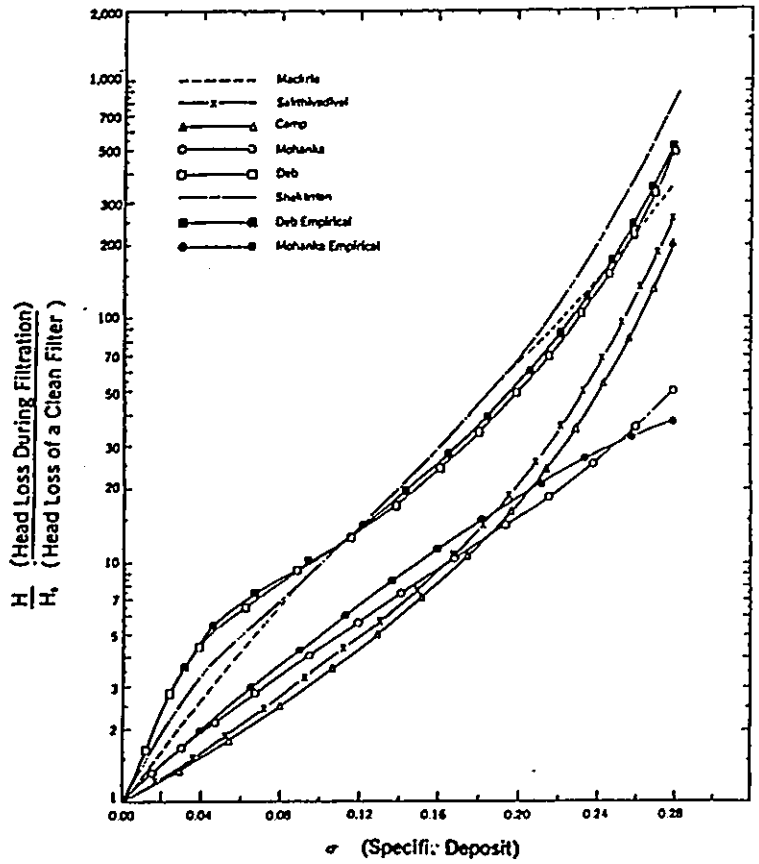

Figure (2.2) Comparison of head-loss equations during filtration (after Sakthivadivel et al., 1972)

CHAPTER THREE

DEPOSITION MODEL

3.1 Introduction

The knowledge of the mode of deposition of suspended particles within a filter is necessary to obtain a reliable mathematical description for the removal of suspended particles and head loss, and to develop an understanding of the mechanism(s) involved. As particles are removed by filter grains they tend to accumulate in a variety of different configurations. These configurations are related not only to the surface area and/or surface characteristic of the filter grain. but also to the size of the particles in suspension, coagulant type and dose, filtration velocity and particle concentration, which results in a change of the structure of the filter bed.

This change in structure is believed to play a primary role in the particle deposition process, and in determining the local head loss. Despite progress in better understanding the dynamic behaviour of the filter bed, there has been little advancement in predicting the dynamic behaviour of head loss in a granular filter. Most of the previous theories that have dealt with mono-sized particles for slurries used a single mode of deposition in all models (typically bench-scale filters) that assume a constant filter grain geometry, constant porosity over the filter run, short filter run, and small filter grains that provide no information about PSD, and depth removal. Recently, publications on the filtration of heterodisperse suspension were contributed by Darby and Lawler (1990), Darby et al. (1991). The primary focus of their studies was to investigate ripening under conditions typical of tertiary wastewater filtration without specifying what morphology should fit their experimental conditions. The effect of coarse and fine particles

was studied in a simple case of bidimensional particles in the suspension (i.e., two different sizes of particles at known concentration were mixed in the suspension), Vingeswaran and Aim (1985). The size distribution of particles used as very narrow and can be considered as monodisperse. Darby et al. (1992) revised an existing depth filter ripening model designed for monodisperse suspension to account for heterodisperse suspension with the primary emphasis on particle removal; head loss was of secondary importance. Mackie and Bai (1992) examined the importance of suspended particle size distribution in deep bed filtration. Changes in the structure of the filter bed as a result of particle deposition can be described adequately in terms of the morphology of deposition. In the present research work, the influence of the morphology of deposition on head loss is described by considering three limiting cases of deposit structure. The three cases are: smooth coating mode, dendrites formation mode, and combined deposition mode (smooth coating and dendrites formation).

For the first case, particle collection on the filter grains results in the formation of a reasonably smooth deposit layer outside the filter grains. This approach represents a generalization of earlier work, which assumes particle deposition in the form of uniform coating over filter grains by using multi-sized particles in suspension. This allows for a change in porosity during the filtration process in a conventional filter run. In addition, the present model provides a new approach for evaluating the geometry parameter which overcomes the effect of collector geometry.

For the second case, it was assumed that retained particles can act as an additional collector, thereby enhancing removal efficiency and increasing head loss O'Melia and Ali (1978). The model is also based on the assumption that porosity remains constant throughout the filtration process, where the experiments were short and only operated in ripening period. This concept

seems appropriate as the model agrees within the limit of experimental data observed. The model is refined by considering a change in collector geometry over time (function of mode and amount of deposition). However, the O'Melia and Ali (1978) dendrite collector model describes only the improving (ripening) stage where porosity changes are questionable if a certain amount of deposition occurs. It was found by analysing the data of Yao et al. (1971) that about a three percent decrease in porosity results in about a ten percent increase in predicted head loss. Therefore, the change in porosity and the change in the fraction of particles which contribute to additional surface area is also considered in the dendrite model formulation. Finally, the model is generalized to predict the head loss for multi-sized particles in suspension.

In the third instance, the model is based on the assumption that deposition takes place in two stages, smooth coating in the first stage, and dendrites formation in the second stage (combined model). The model is formulated in mathematical terms, calibrated with experimental data from current and previous research work, and tested using another set of experimental data. These models allow a description for the change of head loss with retention. In addition, these results provide some insights into deposition morphology and suggest a new direction in coagulant use. Coad and Ives (1981b) used the tracer technique (conductimetric measurement) to carefully measure porosity change during clogging. The use of a conductimetric experimental techniques indicates that their model of pore structure does not support a smooth coating - dendrite model. Flow of two principal types were observed: clear channels and clogged channels. It is likely that different experimental conditions will give different internal structures of deposit and flow. The filter material used by Coad and Ives (1981) was sand, sieved between 0.60 and 0.71 mm mesh sieves, $\varepsilon_o = 0.35$, influent solid concentration were much higher (150 mg/L was typical) than the settled 5 μm (5 mg/L) and 5 μm (15 mg/L) silica used with cationic polymer (percol 728).

At higher solids concentration, it would be expected that mean floc size would be larger; these arise from the high rate of interparticle contact. The large flocs and small media size in particular may result in clogging as the predominating mode of deposition. However, at lower influent suspended solids concentration and large media size (1.71 mm), it was observed that the filter run lasted much longer (about 48 hours) in some experiments. In these experiments a terminal head loss is being attained without a turbidity breakthrough. Clogging was not visually observed to occur under the experimental condition during most of the filter run, indicating that clogging was not the predominant mode of deposition.

3.2 Model Formulation

Accumulation of suspension inside the filter bed affects the filtration process, as it increases the resistance to fluid flow. This aspect has been studied at length by many investigators, viz., Ives (1967), Mohanka (1969), Deb (1969), Camp (1964), and others. The equations proposed by these researchers differ primarily with respect to their assumptions regarding the mode of deposition of suspended particles around the filter grains, and with respect to insufficient knowledge regarding changes occurring in the shape of the filter grains and/or the pore space during filtration.

In recent years, a different approach has been adopted to evaluate the qualitative effect of these changes on filter performance. Although this had led to some success in predicting removal efficiency (Rajagopalan and Tien, 1976), there has been little improvement in predicting the dynamic behaviour of head loss in a granular filter, even for suspension of mono-sized particles. Therefore, a reliable mathematical description of head loss development across a filter

bed is necessary for a reasonable understanding of the mechanism involved. This requires knowledge of the mode of deposition of suspended particles within the filter bed.

The head loss formulation for different modes of deposition of suspended particles within a filter bed are examined in three limited cases. These cases represent a generalized head loss equation because they consider the change in surface area of the filter grains and its attached particles (which depend on the amount and mode of deposition), and the change in Kozeny's coefficient and the filter grain shape factor.

3.2.1 Smooth Coating Model

This model attempts to develop a relationship between head loss and the specific deposit by incorporating the change in the collector geometry in terms of a specific deposit over time. This model was developed based on Kozeny's equation for head loss in clean, granular, porous medium.

$$(h/L)_o = K_o \frac{\mu V_o (1-\varepsilon_o)^2}{\rho g \varepsilon_o^3} \left[\frac{A_c}{V_c}\right]_o^2. \qquad (3.1)$$

by substituting the specific surface (A_c/V_c) value of spherical filter grains and simplifying equation (3.1) becomes:

$$(h/L)_o = K_o S_o^2 \frac{\mu V_o (1-\varepsilon_o)^2}{\rho g \varepsilon_o^3} \frac{1}{d_c^2}. \qquad (3.2)$$

Where $(h/L)_o$ is the initial hydraulic gradient, K_o is the Kozeny coefficient of clean filter, μ is the dynamic viscosity of the liquid, ρ is the density of filtering liquid, g is the acceleration gravity, V_o is the approach velocity, ε_o is the clean filter bed porosity, A_c is the surface area of

the filter grains, V_c is the volume of the filter grains, S_o is the shape factor of clean filter grain, and d_c is the filter grain diameter.

As the filter run proceeds, the equation is modified for a change in the surface area to volume ratio of the media arising from the deposition of suspended particles. It is assumed that deposition occurs by coating the filter grains uniformly. The change in porosity, the change in the surface area of the filter grain due to deposition, and the change in collector geometry, which is represented by the change in Kozeny's coefficient and shape factor (a result of the change in the cross-sectional area of the flow path), are considered necessary for uniform coating mode.

Following the same assumptions used by Ives (1969), let V_g be the volume of a single grain, ε_o the initial porosity, and σ the volume of deposit per unit filter volume. The specific surface area of filter grains coated with deposit are formulated as follows:

filter grain volume per unit volume = $1 - \varepsilon_o = V_{co}$,

volume of one spherical grain = $V_g = (\pi/6)\, d_c^3$,

volume of non-spherical grain = $\alpha_v\, d_c^3$,

number of grain per unit volume = $(1 - \varepsilon_o)/V_g$,

volume of deposit per grain = $\sigma\, V_g/(1 - \varepsilon_o)$, and

volume of coated grain = $V = V_g + V_g\, \sigma/(1 - \varepsilon_o) = V_g\, (1 + \sigma/(1 - \varepsilon_o))$.

The surface area per unit filter volume of clean and deposit containing filter are $(A_c/V_c)_o$ and (A_c/V_c), respectively. The porous medium is assumed to be composed of N_c non-spherical grains of diameter d_c per unit volume of filter, i.e.,

$$(A_c/V_c)_o = (N_c\ \alpha_{ao}\ d_c^2)/(N_c\ \alpha_{vo}\ d_c^3) = (\alpha_{ao}/\alpha_{vo})\ (1/d_c) = S_o/d_c. \qquad (3.3)$$

where α_{ao} and α_{vo} represent the surface area and volume factor. By regular deposition on the filter grain, the diameter increases to $(d_c + \Delta d_c)$. Hence, the specific surface of the filter grain after the smooth coating, can be represented by

$$(A_c/V_c) = \frac{N_c\ \alpha_a\ (d_c + \Delta d_c)^2}{N_c\ \alpha_v\ (d_c + \Delta d_c)^3}\ . \qquad (3.4)$$

Expanding and simplifying the square and cubic terms in the equation above yields,

$$(A_c/V_c) = \frac{N_c\ \alpha_a(d_c^2 + 2\ d_c\ \Delta d_c + \Delta d_c^2)}{N_c\alpha_v(d_c^3 + 3\ d_c^2\ \Delta d_c + 3\ \Delta d_c^2\ d_c + \Delta d_c^3)}\ . \qquad (3.5)$$

Retaining first-order terms gives

$$(A_c/V_c) = \frac{\alpha_a\ a_c^2\ (1 + 2\Delta d_c/d_c)}{\alpha_v\ d_c^3\ (1 + 3\Delta d_c/d_c)}$$

$$= \frac{S\ (1 + 2\Delta d_c/d_c)}{d_c\ (1 + 3\Delta d_c/d_c)}\ , \qquad (3.6)$$

The solid fraction of the clean porous medium of N_c spherical grain of diameter d_c per unit volume of filter is

$$1 - \varepsilon_o = N_c(\pi/6)\ d_c^3. \qquad (3.7)$$

For a deposit containing filter $= 1 - \varepsilon = N_c\ (\pi/6)\ (d_c + \Delta d_c)^3$. Expanding the cubic term in the equation, and simplifying it gives

$$1-\varepsilon = V_{co}\ (1 + 3\Delta d_c/d_c)$$
$$= (1-\varepsilon_o)\ (1 + 3\Delta d_c/d_c). \qquad (3.8)$$

$$\frac{3\Delta d_c}{d_c} + 1 = \frac{(1-\varepsilon)}{(1-\varepsilon_o)}$$
$$\frac{3\Delta d_c}{d_c} = \frac{1-\varepsilon-1+\varepsilon_o}{1-\varepsilon_o}$$
$$= \frac{\varepsilon_o-\varepsilon}{1-\varepsilon_o}$$
$$= \frac{\sigma}{1-\varepsilon_o}\ . \qquad (3.9)$$

and

$$\frac{2\Delta d_c}{d_c} = \frac{2\sigma}{3(1-\varepsilon_o)}\ .$$

Substituting the values of these two terms into the specific surface equation (3.6) yields

$$\frac{A_c}{V_c} = \frac{S}{d_c}\left[1 + \frac{2\sigma}{3(1-\varepsilon_o)}\right] / \left[1 + \frac{\sigma}{(1-\varepsilon_o)}\right]\ . \qquad (3.10)$$

By substituting for A_c/V_c in the filter containing deposit head loss equation, equation (3.1) gives

$$(h/L)_t = \frac{K S^2}{d_c^2}\ \frac{\mu V_o}{\rho g}\ \frac{(1-\varepsilon)^2}{\varepsilon^3}\left\{\frac{1 + 2\sigma/3(1-\varepsilon_o)}{1 + \sigma/(1-\varepsilon_o)}\right\}^2\ . \qquad (3.11)$$

The final form of the head loss equation is obtained by dividing the head loss equation for filter containing deposit by the head loss equation for a clean filter bed; it can be expressed as follows:

$$h = h_o \left[\frac{K S^2}{K_o S_o^2}\right] \left[\frac{1-\varepsilon}{1-\varepsilon_o}\right]^2 \left[\frac{\varepsilon_o}{\varepsilon}\right]^3 \left[\frac{1 + 2\sigma/3(1-\varepsilon_o)}{1 + \sigma/(1-\varepsilon_o)}\right]^2, \qquad (3.12)$$

where ($K S^2/K_o S_o^2$) is the overall geometry parameter which is evaluated experimentally. Additional details about the parameter determination are included in the next section.

3.2.2 Dendrites Mode Model

Dendritic modelling was originally developed for air filtration, where chains of particles have been observed to form (Payatakes and Tien, 1976). Habibian and O'Melia (1975) suggested that particles removed during the early stage of a filter run can serve as collectors, or deposition sites for particles reaching the bed later, and thereby improving filtration efficiency. Other detailed models have been developed to calculate the effect of deposited particles on collection efficiency (Wang et al., 1977). However, head loss models are not discussed to the same degree as removal efficiency models.

Tien et al. (1977) presented a theory for the formation and growth of particle dendrites on a collector placed in an aerosol, or hydrosol system. O'Melia and Ali (1978) developed a mathematical model which simulates head loss through granular media filter during the filter run. Their model is based on the theory that some retained particles can act as additional collectors, and thereby improve removal efficiency and increase head loss. The model also assumes that porosity remains constant throughout the filtration process, and is justified in the case of dilute suspension. This concept is appropriate, and the model agrees within certain limits of experimental data. The model is refined by considering the change in collector geometry as variable over time (function of specific deposit). In addition, the change in porosity is also

studied. Finally, the model is generalized to predict the head loss for multi-sized particles in suspension.

The development of a head loss model is based on the Kozeny's equation for head loss in a clean filter bed. As filtration proceeds, the retained particles will modify the performance of the filter. Hence, the equation that governs the clean bed filter becomes inapplicable. Therefore, in this study an attempt is made to modify the model of O'Melia and Ali's (1978) for a better representation of the filtration cycle.

The suspended particles are deposited on the filter grains and protrude into the pore space; this contributes additional surface area A_p and volume V_p within the filter. Hence, the head loss equation can be written as

$$(h/L) = K \frac{\mu V_o}{\rho g} \frac{(1-\varepsilon)^2}{\varepsilon^3} \left[\frac{A_c + A_p}{V_c + V_p}\right]^2 . \tag{3.13}$$

Substituting the area of the collector and particles retained in a unit volume of filter (A_c and A_p), and the volume of collectors and particles retained in a unit volume of filter (V_c and V_p), gives:

$$\left[\frac{A_c + A_p}{V_c + V_p}\right] = \frac{N_c \pi d_c^2 + N_p \pi d_p^2}{N_c (\pi/6) d_c^3 + N_p (\pi/6) d_p^3}$$

$$= \frac{N_c \pi d_c^2 \left[1 + \dfrac{N_p d_p^2}{N_c d_c^2}\right]}{N_c (\pi/6) d_c^3 \left[1 + \dfrac{N_p d_p^3}{N_c d_c^3}\right]} . \tag{3.14}$$

For non-spherical grains, the specific surface is given by:

$$\left[\frac{A_c + A_p}{V_c + V_p}\right] = \frac{S}{d_c} \frac{\left[1 + \frac{N_p\, d_p^2}{N_c\, d_c^2}\right]}{\left[1 + \frac{N_p\, d_p^3}{N_c\, d_c^3}\right]}, \qquad (3.15)$$

where $S = \frac{\alpha_a}{\alpha_v}$.

Hence, by substituting for the specific surface and dividing the head loss equation for deposit containing filter by the head loss equation for clean filter bed, the dendrite mode head loss equation can be expressed as follows,

$$(h/L) = \frac{K\, S^2}{d_c^2} \frac{\mu\, V_o}{\rho\, g} \frac{(1-\varepsilon)^2}{\varepsilon^3} \left[\left[1 + \frac{N_p\, d_p^2}{N_c\, d_c^2}\right] / \left[1 + \frac{N_p\, d_p^3}{N_c\, d_c^3}\right]\right]^2 . \qquad (3.16)$$

By dividing equation (3.16) by equation (3.2), gives

$$h = h_o \left[\frac{K\, S^2}{K_o\, S_o^2}\right] \left[\frac{\varepsilon_o}{\varepsilon}\right]^3 \left[\frac{1-\varepsilon}{1-\varepsilon_o}\right]^2 \left[\left[1 + \frac{N_p\, d_p^2}{N_c\, d_c^2}\right] / \left[1 + \frac{N_p\, d_p^3}{N_c\, d_c^3}\right]\right]^2 . \qquad (3.17)$$

The geometry parameter ($K\, S^2/K_o\, S_o^2$) is evaluated using the data from O'Melia and Ali (1978). The change in porosity (specific deposit) is computed by the volume of deposited particles per volume of filter bed, i.e.,

$$\Delta\varepsilon = \frac{\sum (N_{ij} - N_{ej})\, (\pi/6)\, d_p^3}{\text{Volume of filter}}, \qquad (3.18)$$

where N_{ij} = Number of influent particles at j^{th} time interval, and

N_{ej} = Number of effluent particles at j^{th} time interval.

Assuming the porosity at time t = $\varepsilon_t = \varepsilon_o - \Delta\varepsilon$, the assumption of constant porosity can be eliminated in predicting head loss development by taking the appropriate value of porosity at any time. In order to apply the model for multi-sized particles in suspension some modification is required. This modification along with the inclusion of a factor, gamma (γ), which represents the fraction of retained particles contributing to additional surface area, the head loss equation becomes,

$$h = h_o \left[\frac{K S^2}{K_o S_o^2}\right] \left[\frac{\varepsilon_o}{\varepsilon}\right]^3 \left[\frac{1-\varepsilon}{1-\varepsilon_o}\right]^2 \left[\frac{1 + \gamma \Sigma (N_i d_i^2/N_c d_c^2)}{1 + \Sigma (N_i d_i^3/N_c d_c^3)}\right]^2 . \qquad (3.19)$$

Due to the non-uniform deposition of particles in different layers of the bed, the head loss in each layer will be different. Therefore, the head loss can be calculated in each layer. The sum of the head loss for all layers will result in the total head loss across the filter bed. For this model, the values of the geometry parameter are determined experimentally using Kozeny's equation for head loss in a clean filter, and the refined dendrites mode model using data from O'Melia and Ali (1978).

3.2.3 Combined Mode Model

In this model, an attempt is made to derive a relationship between head loss and the specific deposit based on the following assumptions:

1. The deposition take place in two stages, smooth coating for the first stage and dendrite formation for the second stage. This assumption is justified as follows:

During the first stage of deposition, particles form a relatively smooth coating by the direct adhesion of individual particles to the filter grains. As the filter run proceeds the attachment occurs by a bridging mechanism that connects one particle to another in the aggregate that is formed. Subsequently, the bridged deposit provides additional sites for particles to collect. This tends to inhibit further deposition at the adjacent sites (shadow area) of the retained particles. Inhibition of further deposition within the shadow area leads to non-uniform deposition around the filter grain, where the deposited particles protrude into the pore space, with free surface available for further deposition resulting in a new surface area greater than the area it previously occupied. Hence there is a greater possibility for the particles to be captured on approaching particles. The zeta potential of the filter grain has a larger negative magnitude than the deposited material, thus, there is less repulsive force associated with particle-to-particle interaction than a particle-to-collector interaction. Both result in the formation of a deposit consisting of dendrites (chain-like) formation. Under effective coagulation (rapid mixing) the polymers adsorb on the silica surface decreasing its effective negative zeta potential (ζ = -10 mV). This will lower the potential energy barrier between particles causing deposited particles (flocs) to intercept many oncoming particles and flocs that pass by that region. Ives and Gregory (1967) reported values of zeta potential for sand, anthracite and ballotini (glass spheres), of less than -25 mV. Therefore less repulsive force is concluded to be associated with particle-to-particle, particle-to-floc and floc-to-floc than a particle or floc-to-collector interaction. Payatakes et al. (1981) reported that during the filtration of 2.0 μm polystyrene latex particles, maximum removal efficiency occurred when the zeta potential was less negative than its actual value, less removal observed as zeta potential

become highly negative or positive. Various floc shapes were observed, including chain flocs and clusters. Particle clusters frequently deposit on other causing already attached clusters to form bulky dendrites.

2. The retained particles act as additional collectors contributing to both increasing and/or decreasing the surface area enhancing filter performance and increasing the head loss.
3. The porous media is composed of N_c non-spherical filter grains.
4. Eventually, the presence of deposited particles modifies the geometry of the collectors, which contributes to the mode function and amount of deposition.
5. The change in the surface area of the collector depends on the amount and mode of deposition.

The head loss equation for a clean and deposit containing filter can be represented by Kozeny's equation; as before the initial surface area and volume of the filter grains are

$$A_{co} = N_c\, \alpha_{ao}\, d_c^2, \quad \text{and} \qquad V_{co} = N_c\, \alpha_{vo}\, d_c^3. \tag{3.20}$$

Substituting respectively for the area of the collector, the particles adsorbed on the collector, and the particles protruding into the pore space ($A_{co} + A_{ps} + A_{pd}$) in a unit volume of filter, and the volume of the collector and particles ($V_{co} + V_{ps} + V_{pd}$) in a unit volume of filter gives

$$A_c = A_{co} + A_{ps} + A_{pd}$$

$$A_c = N_c\, \pi\, (d_c + \Delta d_c)^2 + N_{pi}\, \pi\, d_{pi}^2. \tag{3.21}$$

$$A_c = N_c\, \alpha_a\, d_c^2 \left[\left[1 + \frac{2\Delta d_c}{d_c} + \frac{\Delta d_c^2}{d_c^2} \right] + \frac{N_{pi}\, d_{pi}^2}{N_c\, d_c^2} \right]. \tag{3.22}$$

where the symbol i refers to the ith particle size. Noting that $\frac{\Delta d_c^2}{d_c^2}$ is small; i.e. Δd_c^2 is small compared to d_c^2, then

$$A_c = N_c\ \alpha_a\ d_c^2 \left[\left[1 + \frac{2\Delta d_c}{d_c} \right] + \left[\frac{N_{pi}\ d_{pi}^2}{N_c\ d_c^2} \right] \right]. \tag{3.23}$$

The volume of filter grains after smooth coating and dendrites formation is:

$$V_c = V_{co} + V_{ps} + V_{pd}$$

$$V_c = N_c\ \alpha_v \left((d_c^3 + 3d_c^2\Delta d_c + 3\Delta d_c^2 d_c + \Delta d_c^3) + N_{pi}\ d_{pi}^3 \right). \tag{3.24}$$

The second and third-order thickness of coating around the filter grain is small in comparison to grain diameter and are neglected. Equation (3.24) is rewritten as

$$V_c = N_c\ \alpha_v\ d_c^3 \left[\left[1 + \frac{3\Delta d_c}{d_c} \right] + \left[\frac{N_{pi}\ d_{pi}^3}{N_c\ d_c^3} \right] \right]. \tag{3.25}$$

Substituting the initial clogging surface area and volume expression into Kozeny-Carman's equation for a clean and filter containing deposit, and dividing the head loss equation for a filter containing deposit by the head loss equation for a clean bed, the head loss equation becomes

$$h = h_o \left[\frac{K S^2}{K_o S_o^2} \right] \left[\frac{\varepsilon_o}{\varepsilon} \right]^3 \left[\frac{1 - \varepsilon}{1 - \varepsilon_o} \right]^2 \left[\left[1 + \frac{2\Delta d_c}{d_c} + \frac{N_{pi}\ d_{pi}^2}{N_c\ d_c^2} \right] / \left[1 + \frac{3\Delta d_c}{d_c} + \frac{N_{pi}\ d_{pi}^3}{N_c\ d_c^3} \right] \right]^2, \tag{3.26}$$

where $S = \frac{\alpha_a}{\alpha_v}$ and from smooth coating derivation

$$(3\Delta d_c/d_c) = \sigma/(1-\varepsilon_o); \text{ and } (2\Delta d_c/d_c) = 2\sigma/3(1-\varepsilon).$$

Substituting the above expression into Equation (3.26), introduction of coefficients α_s, α_d, and (γ), that account for the fraction of particles, which contribute to smooth coating, the fraction of particles which contribute to dendrites formation, and the fraction of particles contributing to additional surface area, respectively, and by considering multi-sized particles in suspension, the final form of the head loss equation is,

$$h = h_o \left[\frac{K S^2}{K_o S_o^2}\right] \left[\frac{\varepsilon_o}{\varepsilon}\right]^3 \left[\frac{1-\varepsilon}{1-\varepsilon_o}\right]^2 \left[\left[1 + \frac{2\,\alpha_s\,\sigma}{3(1-\varepsilon_o)} + \alpha_d\,\gamma\,\frac{\sum N_{pi}\,d_{pi}^2}{N_c\,d_c^2}\right] \Big/ \left(1 + \frac{\alpha_s\,\sigma}{(1-\varepsilon_o)} + \alpha_d\,\frac{\Sigma\,N_{pi}\,d_{pi}^3}{N_c\,d_c^3}\right)\right]^2 \quad (3.27)$$

The geometry parameter ($K\,S^2/K_o\,S_o^2$) is varied between smooth coating and dendrites mode deposition by considering the relative value of α_s and α_d, respectively.

3.3 Model Validation

Validation of the model is achieved in two steps. Firstly, the model is calibrated, i.e. values of the coefficients in the model are evaluated experimentally and/or adjusted so that the output from the model is in agreement with observations. Secondly, the model is re-run using other input data and the output is compared with observation.

3.3.1 Model Calibration

Using the three models developed to predict the head loss behaviour requires evaluation of the parameters α_s, α_d, γ and $K\,S^2/K_o\,S_o^2$. Numerous studies with extensive data and many

mathematical formulations are available with different sets of operation and system variables. However, the lack of information on particle size distribution stands as a major obstacle in utilizing such data for verifying the developed models. Experimental results obtained from this study are used to determine the model coefficients.

The geometry parameter ($K\ S^2/K_o\ S_o^2$) in the smooth coating model is evaluated using experimental data obtained in the current research work. An experimental run used to evaluate this parameter is conducted on a pilot plant filter 20 cm in diameter and 86 cm depth (d_c = 1.738 mm, ε_o = 0.4274) operated at 0.6 cm/s filtering a suspension of Min-U-Sil (silica), with surface average particle diameter of 30 μm (size range, 0.48-137 μm), and concentration of 15 mg/L. Ferric chloride is added continuously throughout the run at a dosage selected to maximize particle-to-particle attachment and removal (0.25 mg/L Fe^{+3}). The optimum dose value is obtained based on jar test and zeta potential determination.

The value of each term in the parameter can be estimated separately, where the value of $K_o\ S_o^2$ is evaluated from the initial filter conditions and for different layers using Kozeny's equation for head loss in clean, granular, and porous medium. While the value of $K\ S^2$ is evaluated using the smooth coating head loss model developed in this study. An overall parameter value ($K\ S^2/K_o\ S_o^2$) is evaluated for each layer of the filter bed based on the specific deposit σ. The geometry parameter versus specific deposit for different filter bed layers is presented in figure (3.1). An empirical equation is suggested to predict the observed geometry parameter value.

$$\frac{KS^2}{K_o\ S_o^2} = A + B * \sigma. \qquad (3.28)$$

The intercept A was found to be 1 for all layers. The value of the slope B was calculated for each layer and found to be $K_oS_o^2$ dependent. The slope versus $K_oS_o^2$ are plotted and an empirical equation were used to fit the data. Observed and predicted values of the slope is presented in figure (3.2). The empirical equation used to predict the observed value of B is

$$B = 85 + 2.0 * 10^5 * \exp(-0.019 * K_oS_o^2).$$

Therefore, the overall equation suggested to predict the observed geometry parameter value can be written as follows:

$$\frac{KS^2}{K_o\ S_o^2} = 1 + (85 + 2.0 * 10^5 * \exp(-0.019 * K_o\ S_o^2)) * \sigma. \qquad (3.29)$$

Figure (3.3) shows the geometry parameter values experimentally derived.

The same procedure is used for the dendrites mode model. Habibian (1971) conducted an extensive study on filtration using different particle sizes in the suspension. Data is obtained by this study is used to calibrate the dendrites mode model. The experimental conditions are d_c = 0.38 mm, ε_o = 0.36, 1 = 14 cm, operated at 0.136 cm/s filtering a suspension of latex sphere particles of different particle sizes (0.1, 1, and 7.6 μm) with different concentrations. Filter media are coated with polymer, prior to use, and polymer added continuously throughout the run at a dosage selected to maximize particle-to-particle attachment. The sum of squares of the weighted difference between the calculated and observed head loss was minimized. The minimization was performed using the non-linear parameter estimation package UWHAUS.

UWHAUS is used to solve the geometry parameter and γ in multivariate, non-linear regression equation and for different runs with different particle size and concentration.

$$\gamma = 1 - \exp(-c_\gamma * \sigma^{-d})$$
$$\frac{K S^2}{K_o S_o^2} = 1 + K_g \sigma^n . \tag{3.30}$$

The value of the coefficients c_γ, d, K_g, and n are determined using particle size of 0.1 μm and concentration of 11.0 mg/L and is found to be $5.5*10^{-3}$, 0.8, 625.0, and 0.8, respectively. The value of γ and n are considered as a base when different particle size and concentration are used, and the value of K_g is then evaluated as a function of d_p (μm):

$$\frac{K S^2}{K_o S_o^2} = 1 + 366.0 * \sigma^{0.8} * d_p^{-0.38}, \tag{3.31}$$

where the value 0.38 is obtained by trial and error until the predicted value and observation correspond.

Combined mode model coefficients are the geometry parameter, γ, α_s, and σ_d. Data obtained from the current research work is used to determine α_d and γ. The filter operated at 0.6 cm/s filtering a suspension of silica (concentrations 15 mg/L, d_p = 5 μm), particle size range from 0.48 to 13.7 μm. Cationic polymer (Percol 728) is added continuously throughout the run at a dosage selected to maximize particle-to-particle attachment and removal (0.05 mg/L). Particle size effects were demonstrated as the values of the coefficients as changed in the geometry parameter equation for smooth coating model. Therefore the equation used to predict the observed value of B is achieved by considering the data from the initial stage of the filter run, using polymer with 5 μm silica.

$$B = 266.0 + 1.0*10^4 * \exp(-0.014 * K_o S_o^2).$$

The value of the geometry parameter is a combination of both smooth coating and dendrites deposition by considering the relative values of α_s and α_d, respectively. Hence, the only coefficients that is remain to be evaluated are γ and α_d, where α_s can be derived from $\alpha_d(\alpha_s = 1 - \alpha_d)$. It is assumed that the value of γ determined from the dendrites mode model is applicable for the filter bed in the combined mode model. Therefore, α_d value are varied until an optimum value is obtained (0.55) based on the least square estimate of the residuals and the geometry parameter expression for the combined mode model

$$\frac{K S^2}{K_o S_o^2} = 1 + \left(266.0 + 1.0*10^4 * Exp(-0.014 * K_o S_o^2)\right) * \alpha_s * \sigma + (366.0 * \alpha_d * \sigma^{0.8} * d_p^{-0.38}). \quad (3.32)$$

3.3.2 Model Verification

The model is tested by using data from other experiments conducted in the current research work, in which one or more filtration variables are significantly different from conditions in the runs used for calibration. Data from different filtration experiments in this work use two suspended particle sizes and two types of coagulants with five filter bed elements over the filter depth, 14 cm for the first layer, and 18 cm for the other elements (Total depth = 86 cm) are presented in Chapter Seven. Model prediction is also depicted. Comparison between observed and predicted values using the models developed are appropriate.

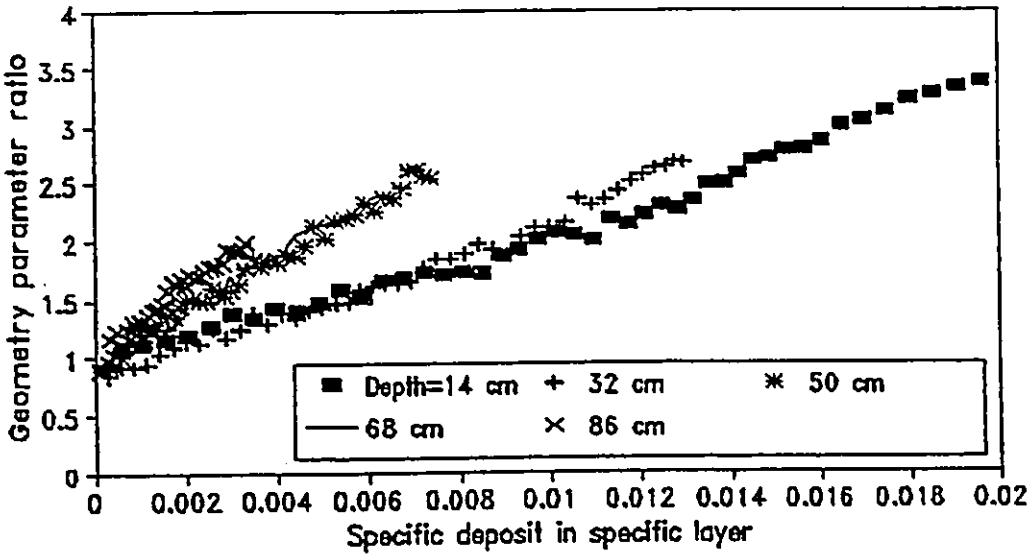

Figure (3.1) Observed geometry parameter versus specific deposit (Fe^{3+}, 30 μm, 15 mg Si/L, V_0 = 0.6 cm/s)

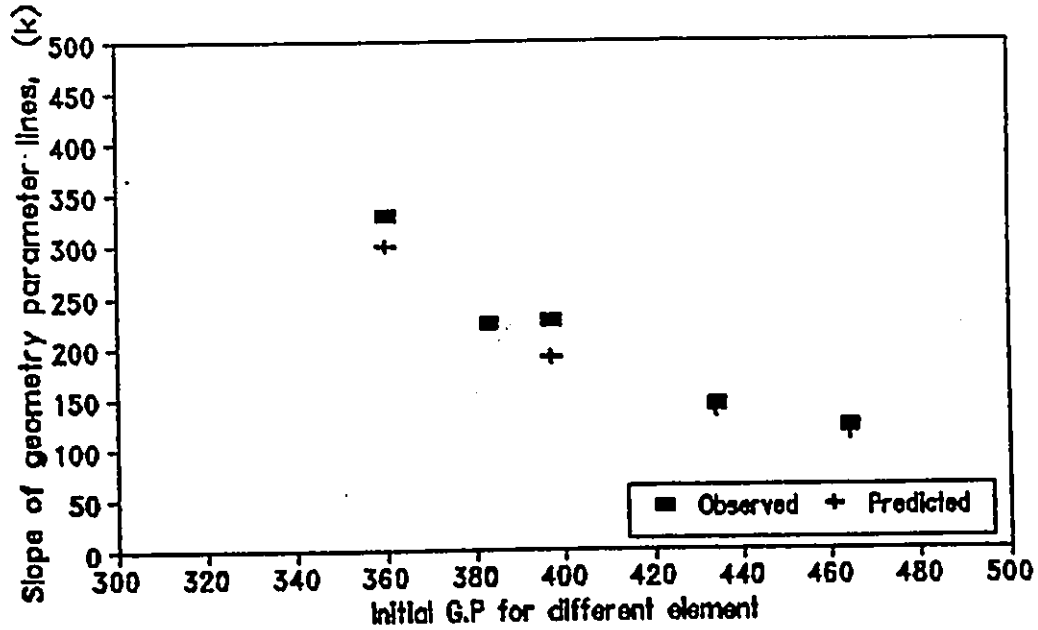

Figure (3.2) Observed and predicted values of the smooth coating geometry parameter coefficient (slope)

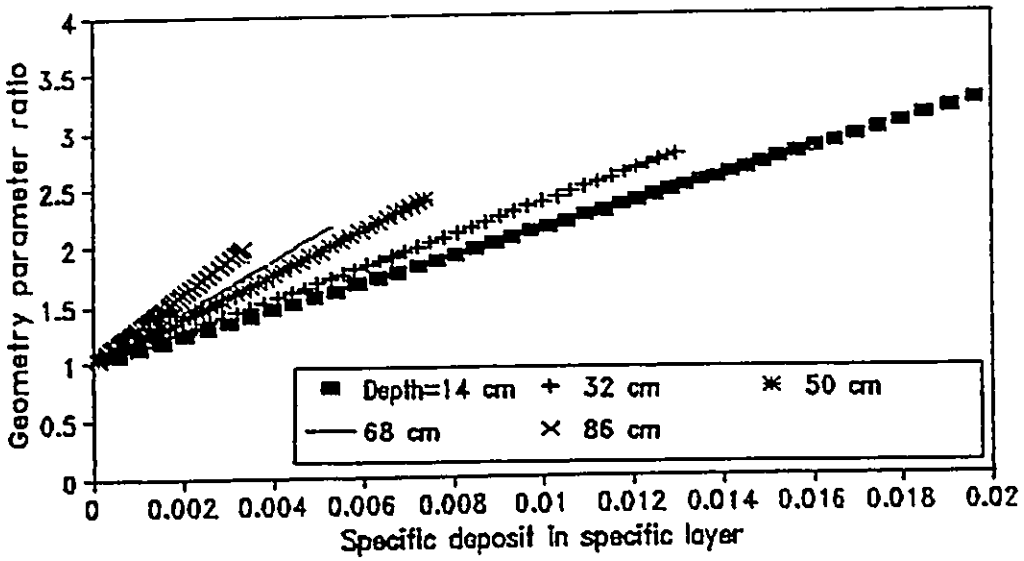

Figure (3.3) **Predicted geometry parameter values versus specific deposit (Fe^{3+}, 30 μm, 15 mg Si/L, V_0 = 0.6 cm/s)**

CHAPTER FOUR

EXPERIMENTAL PROGRAM

4.1 Introduction

The pilot-scale filtration plant used by Averil (1987) was used to conduct the experimental program in this study. The influence of different design variables on head loss build-up and developing different deposition modes are investigated by using stable (polydisperse) suspension (as a control) and a suspension destabilized using a metallic cation such as ferric chloride and cationic polymer (percol 728) as coagulants. Provision was made for PSD analysis and for measuring head loss across the filter bed. Particle size distribution were measured on samples taken at different depths and times; head loss and suspended solids measurements were made continuously at the same locations. Continuous monitoring of flow and temperature was made. Well controlled laboratory experiments were performed under varying conditions of suspended particle size and concentration, flow rate, coagulant dosages and filter depth with filter grain pore structure identical to the conventional water filtration system. The system automatically performs sampling, sample dilution, particle counting and data handling. Two limiting criteria are used during all runs, an accumulated head loss of 3.0 meter and/or effluent breakthrough. The pilot-scale test plant is controlled and monitored by a Hewlett Packard HP-1000 minicomputer.

4.2 Apparatus

A schematic diagram of the experimental apparatus is shown in Figure (4.1). The main components of the apparatus include: a stock suspension tank; slurry tank; raw water pump;

slurry pump; filter trough (overflow constant head trough); experimental filter column; two Hiac/Royco particle size analyzers with custom-built interface to the pilot plant and the process computer; and the coagulant tank (flash mixer). Dilution water for the system (reverse osmosis permeate water) and optical fibre endoscope, together with a video tape recorder and monitor for visual observation are also included with the system. The function of the selected instruments is:

1) To provide count data for 7 sample stations: 5 samples within the filter media depth, 1 influent sample, 1 dilution water sample to gather in-depth information about PSD with a wide range.
2) To monitor head loss in each of the 15 media element including the total filter driving head and total filter head loss, Figure (4.2)
3) Visual observation of the deposition mode and the change in filter grain geometry.

The experimental filter column is made of a plexiglass cylinder 20 cm in diameter with 1 meter filter media depth. The filter media is coarse sand grains with 1.71 mm diameter. Coarse gravel bed is placed at the bottom of the filter bed (20 cm depth) to support the filter media. Fifteen head loss measurement stations are located as shown in Figure (4.2). Six of these stations are used to monitor suspended solids concentration, and particle count, in addition to head loss measurement. The first station is represented by the influent, the second is located 14 cm below the surface of the filter bed. The other four stations are 18 cm apart. Suspended solids determinations is made by filtering a liquid sample on a pre-weighted glass fibre filter. The filter, was dried in an oven at 105 °C and accurately weighed using an analytical balance.

4.3 Experimental Material

Filter Grain. Coarse sand was used as a filter grain to overcome shortcomings in the system operation and to have a longer duration of the filter run with more information about the filter behaviour. Hsiung and Cleasby (1968) explained that for long filter runs, which is the case in this experimental program, a larger portion of the filter bed contributed to a significant removal. The representative equivalent grain size may be calculated from the expression

$$d_{eq} = \frac{\Sigma\, p_i\, d_i}{100},$$

in which p_i weight percent of sample separated between adjacent sieves; d_i is the geometric mean (square root of product) size of adjacent sieve openings and d_{eq} is about the size of p_{50}. Results of the sieve analysis are listed in Table (4.1) and represented by Figure (4.3). These sand grains, with an average diameter of 1.71 mm (p_{50}), were used. Sieve analysis of the sand grains shows that size was approximately uniform.

Fine sand used as a filter media had a mean grain size of 0.45 mm and a uniformity coefficient of 1.61. Specific gravity of 2.65 and porosity of 35.5% were measured. Sand was sieved using United States Standard sieves (ASTM). As sample of 1000 grams was sieved for a period of 15 minutes. Results are listed in Table (4.2) and represented by Figure (4.4). Mean grain size in Table (4.2) refers to the square of the product of the opening size of adjacent sieves. The same procedure was followed by several other filtration investigators, (Diaper and Ives, (1965), Hsiung and Cleasby (1969)).

Hsuing and Cleasby (1969) explained that when a graded sand of a given effective size (p_{10}) and uniformity coefficient are used, the equivalent uniform size can be calculated as follows:

$$d_{eq} = \frac{1}{2} \text{ (effective size) } (1 + \text{uniformity coefficient}).$$

d_{eq} is about the size of p_{50}. They found that a graded sand of certain equivalent uniform size can be used in place of a certain effective sand size and a certain uniformity coefficient to obtain the same results. Hence for the fine sand media grain with 0.32 mm effective size and 1.6 uniformity coefficient, the d_{eq} is 0.416 mm. Based on data rather than above equation the size of about p_{50} which is equal to 0.45 mm were used.

Because an equivalent uniform size of 0.45 mm is used, the locations of the sampling ports are not necessarily specific. Three sample ports for particle concentration determination were located as follows: at the bottom of the filter bed (3rd port), 18 cm from the bottom for (2nd port) and 36 cm from the bottom (1st port).

Suspended Particles. The suspended particles used in this study are silica particles (Min-U-Sil) that were supplied by L.V. Lomas Chemical Co. Ltd. The measured size distribution of the particles by the manufacturer, are shown in Figure (4.5). Characteristics for the two grades 5 and 30 μm silica as specified by the silica suppliers are reported in Table (4.3). Min-U-Sil 5 μm with an average of 1.9 μm is reported to have a surface area of 2.06 m^2/g. Min-U-Sil 30 μm with average particle size of 8.8 μm is rated at 0.54 m^2/g.

Microscopic observations of 5 μm, 30 μm, and settled 5 μm silica particles suspended in distilled water are shown in Figure (4.6). For the purpose of viewing a sample a small drop of the slurry applied on the surface of a glass cell. The drop immediately spreads on the glass to a diameter of 1 to 3 cm. This procedure thins the liquid depth so that particles and/or flocs may be readily viewed at different location of the drop. The colloids can best be viewed with

the 8X objective which with 15X eyepiece provides a magnification of 120X. The "spread drop" method produces good results, and even better after the drop has been permitted to stand for some time as shown in Figure (4.6). The shape of settled silica particles can be described as being generally spherical. The shape of 5 μm and 30 μm silica demonstrate particle size dependency, with larger particles being more irregular in shape. The zeta potential of silica particles in aqueous suspensions (suspended in distilled water) was measured by means of zeta-meter (Riddick Inc.). The average value of fourteen measurements gave the silica particles zeta potential an -26 mV.

Coagulants. A cationic polyelectrolyte (percol 728) was used as a filter aid in the pilot-scale filtration test operated under different sets of conditions. An optimal dosage of polymer (optimum removal efficiency) is determined by jar test and zeta potential measurements. Stock solution was prepared and used within 4 hours to avoid any ageing possibility and loss of flocculation activity of aqueous solutions of polymer. Ferric chloride was also used as a coagulant, with optimum dosages determined by jar test and zeta potential measurements. A stock solution of Fe^{+3} ($Fe\ Cl_3$) was prepared to last for the entire run.

4.4 Experimental Procedure

Preparation of Suspension. To prepare the predetermined concentration of test suspensions, a suitable amount of silica material is added to a 300 litre tank equipped with a mechanical mixer. The tank was filled with tap water (pH = 7.75, conductivity = 359 μs/cm, alkalinity = 92 mg/L, total hardness = 130 mg/L, calcium = 40 mg/L, chloride = 29.4 mg/L) and the mixer

operated 24 hours in advance of the filter run to ensure homogeneity of the suspension and the absence of flocculation. A high power mixer was used to keep particles in suspension.

Preparation Of Filter Bed. The filter is packed with sand grains (1.71 mm) to the specified height and the bed backwashed by fluidizing for 10 minute using air and then water, to approximately 50 percent volumetric expansion. This same procedure is repeated 2 or 3 times to ensure that all deposited material is removed and that no gas bubbles are present in the filter. The bed is then carefully reformed to the original height. Media porosities (0.43) were kept constant by tapping the sides of the filter after backwash to obtain a specific depth of media.

Determination Of Particle Concentration. Particle concentration and size distribution of samples taken are determined using a multi-channel particle-size analyzer for measuring both small particles (346B Laser) up to 3.1 μm and large particles, (CMH-150) up to 150 μm in diameter. This system was designed by Wood (1988) to manipulate the on-line sampling from several locations and dilution control. A laser based sensor and CMH-150 sensor with size classification in 36 channels over the range of 0.5 to 150 μm are used. A Hiac/Royco model 346B laser sensor measures the amount of low-angle forward scattered light refracted by an individual particle passing through the beam of a Helium Neon laser. This sensor, capable of sizing particles in the 0.45 to 25 μm range, is required to provide data on submicron particles. A second sensor, model CMH-150 uses the light obscuration technique to detect particles from 4 to 150 μm. As a result of sensor overlap, the integrated system produces results in 41 size channels over a range from 0.45 to 150 μm. The laser-based sensor is utilized over a size range from 0.45 to 3.1 μm for 18 channels; while the CMH-150 sensor monitors the size from 3.96

to 150 μm with 23 channels. Although the system is designed to give data in 41 channels, the number of particles counted in the last channels was essentially zero for most of the runs. Occasional counts in the large-size channels are also observed. These channels were recovered and are included in analysis of results, using the correction procedure as outlined in Chapter Six.

Filtration Run. The suspension prepared in the mixing tank is pumped to the constant head and constant effluent rate filter column which is packed with the sand grains to a specific height. Influent sample, four intermediate station sample, and effluent samples are selected using manifolds consisting of solenoid-activated valves, to connect five intermediate sample ports in the filter wall to differential pressure cells for head loss monitoring. Particle analysis system for PSD monitoring is also connected. For each of the 15 elements, the head loss is measured from one of two differential pressure cells (DP). The DP cells are calibrated over 2 different ranges (0-1 and 0-2.5 m) to provide sufficient accuracy for both clean bed and run termination conditions. Samples for suspended solids (S.S.) are collected by dripping techniques (6 sample stations) and measured gravimetrically on an hourly basis. Filter runs are made at different conditions with no aid, and with the continuous addition of either ferric chloride or polymer (percol 728). This subject is covered in more detail in Chapter Five. As presented by Graham (1988), for a cationic polymer and silica particles the relationship is linear between the optimal polymer concentration and the solid content (Black et al., 1965), and linearity in the polymer-particle stoichiometry is also demonstrated in direct filtration experiments which employed latex particles (Habibian and O'Melia, 1975). Therefore, maintaining a constant polymer/kaolin concentration ratio would produce an equivalent degree of destabilization and rate of flocculation, Graham (1988). The results of this study are in agreement with the observations of Black et al., and Habibian and

O'Melia. For 30 mg silica per litre, the optimum dosage used was to approximately double that amount for 15 mg per litre. The operating conditions of experiments conducted in this work are summarized in Table (4.4). Two limiting criteria are used during all runs, an accumulated head loss of 3.0 meter, and/or effluent breakthrough.

Table (4.1) Coarse Filter Sand Size

Sieve No.	Opening Size	Geometric Grain Size mm	Amount Retained, g	Cumulative Retained, g	% Pass
8-10	2.36-2.00	2.17	10	10	99
10-12	2.00-1.70	1.84	140	150	85
12-14	1.70-1.40	1.54	740	890	11
14-16	1.40-1.19	1.29	90	980	0.02
16-18	1.19-1.00	1.09	20	1000	0.00

Table (4.2) Fine Filter Sand Size

Sieve No.	Size of opening, mm	Geometric grain size	% Pass
20 - 30	0.85 - 0.60	0.714	98.0
30 - 35	0.60 - 0.50	0.547	90.8
35 - 40	0.50 - 0.42	0.458	55.3
40 - 45	0.42 - 0.35	0.383	28.2
45 - 100	0.35 - 0.149	0.228	1.3

Table (4.3) Min-U-Sil characteristic (extracted from manufacturer brochure)

Composition	Silicon Dioxide (SiO_2)	99.7%
	Iron Oxide (Fe_2O_3)	0.023%
	Aluminium Oxide (Al_2O_3)	0.101%
	Titanium Dioxide (TiO_2)	0.019%
	Calcium Oxide (CaO)	Trace
	Magnesium Oxide	Trace
Physical Properties	Specific Gravity	2.65 g/cc
	Refractive Index	1.547
	pH	7.0

Table (4.4) Summary of experiments conducted and conditions

Exp:Run Number	Coagulant Type and Dose	Filter Loading, cm/s	Particle Size, μm	Influent S.S., mg/L	Average Removal Efficiency	Filter Time, h	Terminal Head Loss, m
200:15	No Aid	0.6	30	15	56	48	0.30
200:16	No Aid	0.6	5	15	47	48	0.41
200:331	No Aid	0.3	30	30	83	48	NA
200:332	No Aid	0.6	30	30	37	48	NIL
200:371	No Aid	0.3	5	15	67	48	0.2
200:372	No Aid	0.9	5	15	33	48	0.6
200:374	No Aid	0.9	30	15	70	48	0.7
200L375	No Aid	0.9	30	30	23	48	0.8
200:356*	No Aid	0.3	< 5	5	88	20	1.2
200:01	0.25 mg Fe^{+3}/L	0.6	5	13	62	47	1.8
200:02	0.25 mg Fe^{+3}/L	0.6	30	14	82	47	1.3
200:85	0.40 mg Fe^{+3}/L	0.6	5	16	60	31	2.9
200:261	0.25 mg Fe^{+3}/L	0.3	30	17	96	48	0.63
200:262	0.25 mg Fe^{+3}/L	0.9	30	15	57	48	1.8
200:263	0.25 mg Fe^{+3}/L	0.3	5	16	68	48	0.7

Table (4.4) Continued

Exp:Run Number	Coagulant Type and Dose	Filter Loading, cm/s	Particle Size, μm	Influent S.S., mg/L	Average Removal Efficiency	Filter Time, h	Terminal Head Loss, m
200:274	0.40 mg Fe^{+3}/L	0.6	30	33	70	40	2.6
200:315	0.25 mg Fe^{+3}/L	0.9	5	15	60	44	2.6
200:316	0.25 mg Fe^{+3}/L	0.6	5	30	40	48	2.1
200:325	0.25 mg Fe^{+3}/L	0.3	30	30	100	48	1.5
200:326	1.0 mg Fe^{+3}/L	0.3	30	30	85	30	2.9
200:343	0.5 mg Fe^{+3}/L	0.6	30	30	70	32	2.3
200:344	0.5 mg Fe^{+3}/L	0.9	30	30	53	22	2.4
200:345	0.25 mg Fe^{+3}/L	0.6	30	30	63	48	1.8
200:346	0.25 mg Fe^{+3}/L	0.9	30	15	50	42	2.5
200:363#	0.25 mg Fe^{+3}/L	0.1	< 5	6	100	48	0.7
200:370#	0.25 mg Fe^{+3}/L	0.3	< 5	7	98.5	22	2.9
200:376	0.5 mg Fe^{+3}/L	0.6	30	30	67	29	2.5
200:377	0.5 mg Fe^{+3}/L	0.6	5	30	58	28	2.4
200:03	0.05 mg 351/L	0.6	5	16	94	47	2.5
200:04+	0.05 mg 351/L	0.6	30	17	99.4	47	1.1
200:13@	0.05 mg 351/L	0.6	5	15	99.3	48	3.2

Table (4.4) Continued

Exp:Run Number	Coagulant Type and Dose	Filter Loading, cm/s	Particle Size, μm	Influent S.S., mg/L	Average Removal Efficiency	Filter Time, h	Terminal Head Loss, m
200:14@	0.05 mg 351/L	0.6	30	16	99.9	35	3.0
200:86	0.05 mg 728/L	0.6	5	16	94	47	1.4
200:160	0.05 mg 728/L	0.6	5	16	93.5	45	2.87
200:161	0.05 mg 728/L	0.6	5	14	94	45	2.48
200:259	0.05 mg 728/L	0.9	5	18	74	38	2.5
200:260	0.05 mg 728/L	0.3	5	16	96	48	0.73
200:264	0.05 mg 728/L	0.3	30	14	99	48	0.46
200:273	0.05 mg 728/L	0.6	5	32	91.5	28	2.7
200:304	0.05 mg 728/L	0.3	30	15	95	48	0.4
200:312	0.09 mg 728/L	0.9	5	15	87	27	2.8
200:313	0.05 mg 728/L	0.6	30	30	99	40	3.0
200:314	0.05 mg 728/L	0.9	30	15	95	32	2.3
200:347	0.05 mg 728/L	0.9	5	15	85	38	2.4
200:305x	0.05 mg 728/L	0.3	< 5	15	49	48	0.6
200:357	0.10 mg 728/L	0.3	< 5	5	54	38	2.4
200:358	0.05 mg 728/L	0.3	< 5	5	54	5	2.4

Table (4.4) Continued

Exp:Run Number	Coagulant Type and Dose	Filter Loading, cm/s	Particle Size, μm	Influent S.S., mg/L	Average Removal Efficiency	Filter Time, h	Terminal Head Loss, m
200:359$	0.05 mg 728/L	0.3	< 5	5	54	5	2.4
200:360$	0.05 mg 728/L	0.3	< 5	5.5	100	5	2.5
200:361#	0.05 mg 728/L	0.1	< 5	5	86	48	2.3
200:362#	0.05 mg 728/L	0.1	< 5	5.8	66	23	2.8
200:364#	0.05 mg 728/L	0.1	< 5	9	73	4	NA
200:365#	0.05 mg 728/L	0.1	< 5	12	83	7	0.4
200:366#	0.05 mg 728/L	0.1	< 5	5	80	6	2.4
200:369&	0.05 mg 728/L	0.1	< 5	7	84	48	1.5

* One meter of 0.45 mm fine sand (pilot-scale filter). The run is terminated arbitrarily (No particle size and count data).
\# 0.5 meter media depth of 0.45 mm fine sand.
\+ Nonionic polymer (percol 351), with 24 hour make up period for polymer sol'n.
@ Nonionic polymer (percol 351), with 4 hour make up period for polymer sol'n.
x Mass concentration too high for particle size analysis.
& Bed conditioning (0.25 mg polymer/gm of sand grains).
$ The media is 3.5 cm lower than one meter mark (Exp. 359), and 2.5 cm lower than one meter mark (Exp360) after repacking the filter bed.

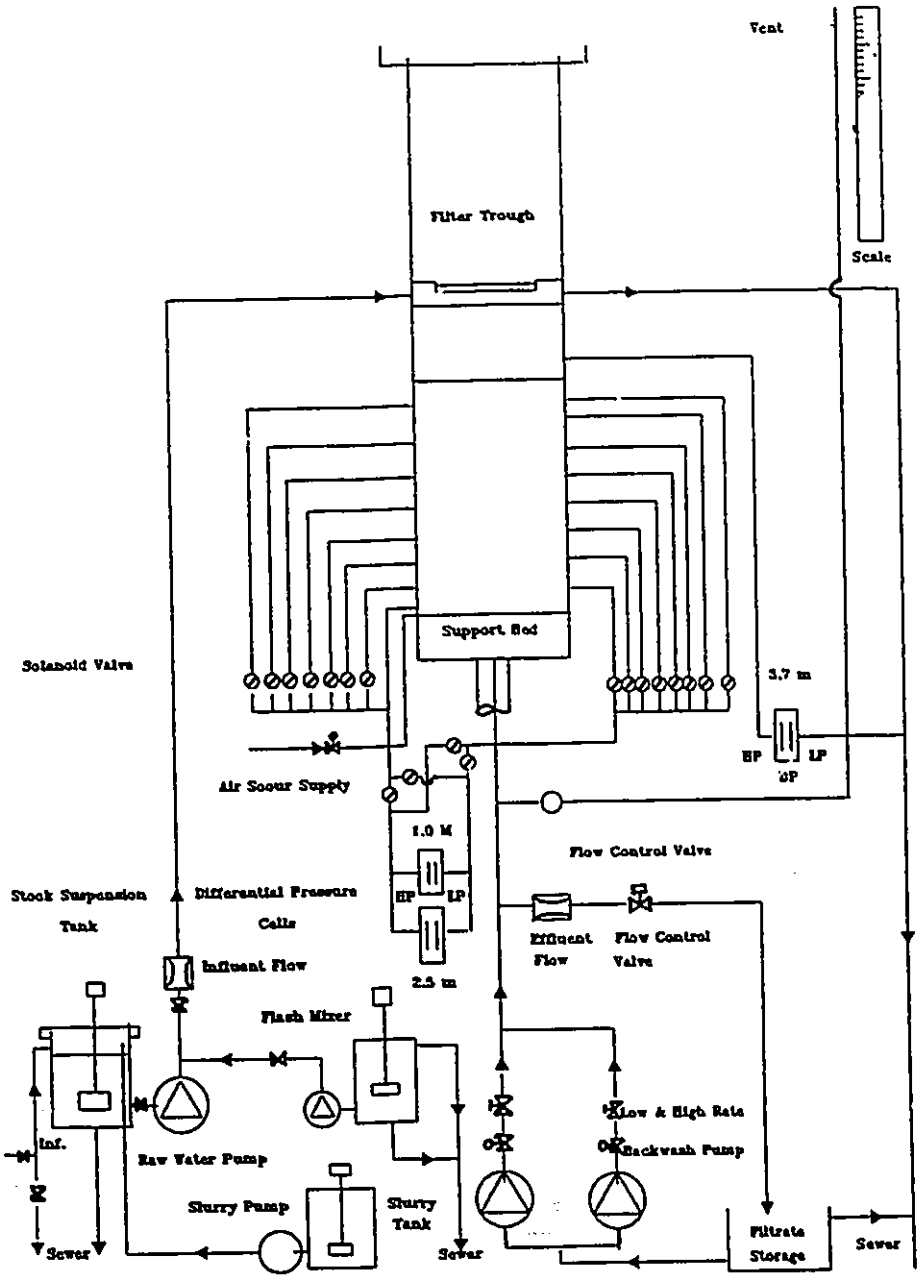

Figure 4.1 Pilot plant schematic (Adapted and Modified after Wood, 1988); HP=high pressure; LP=low pressure; DP=differential pressure cell; Inf.=influent tap water.

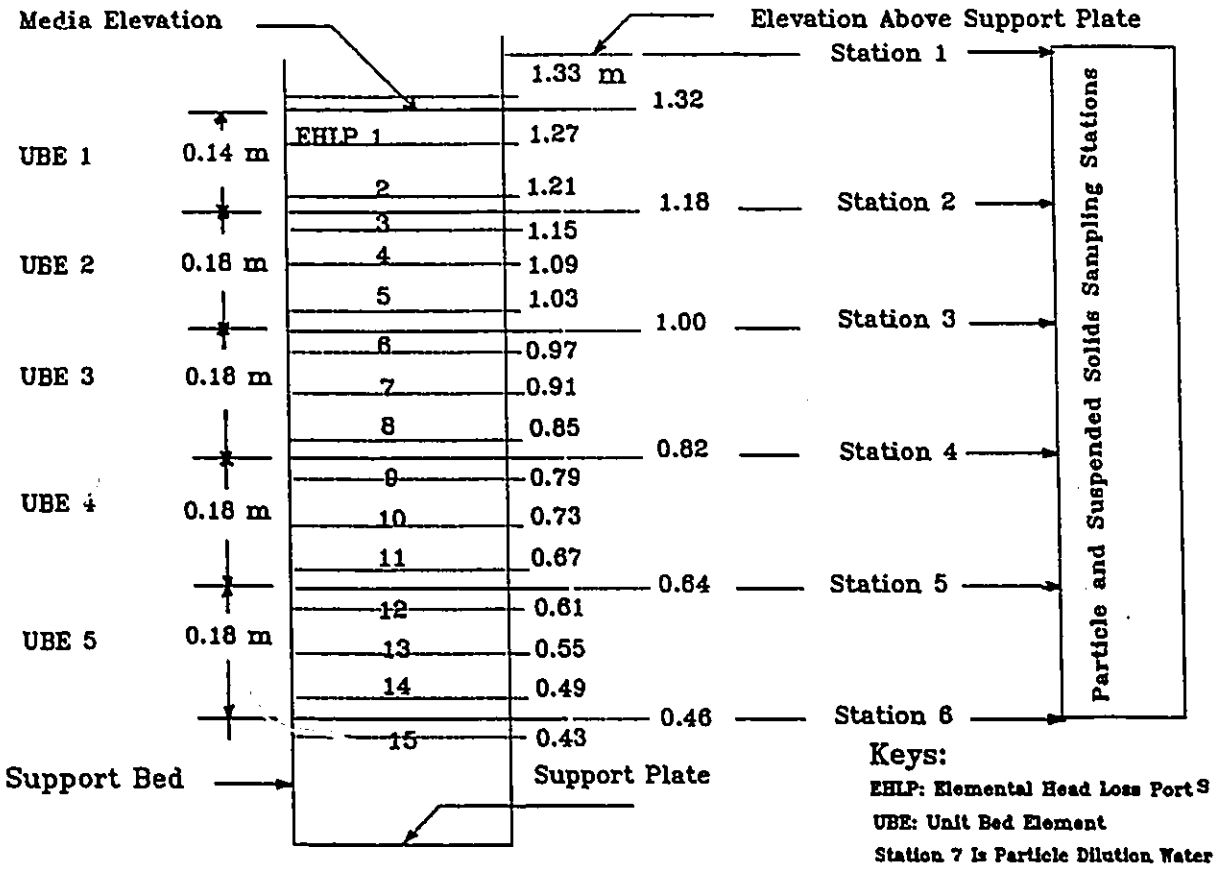

Figure 4.2 Particle/suspended solids sampling and head loss monitoring ports.

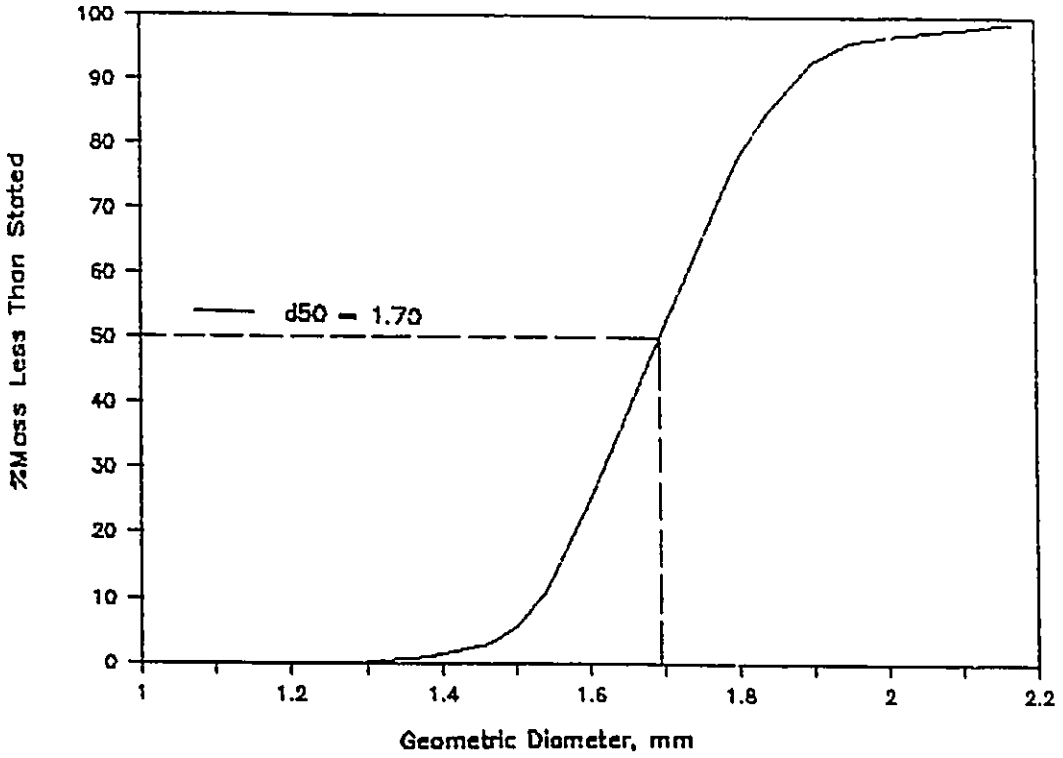

Figure 4.3 Coarse media sand size distribution.

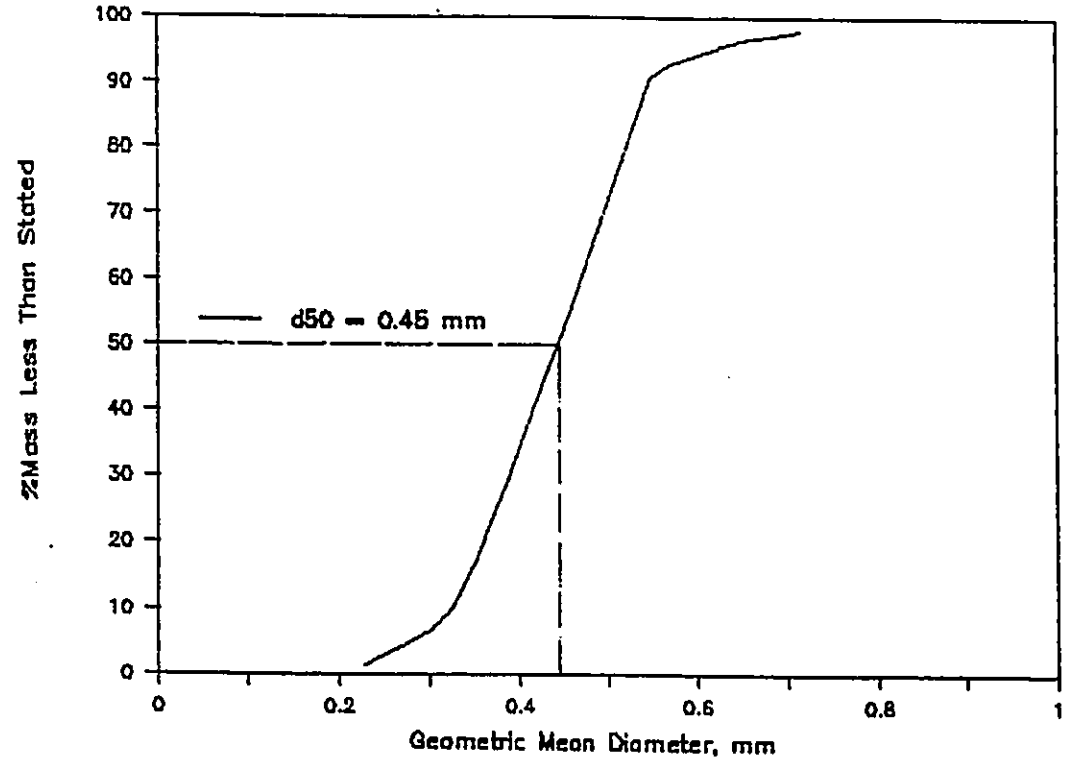

Figure 4.4 Fine media sand size distribution

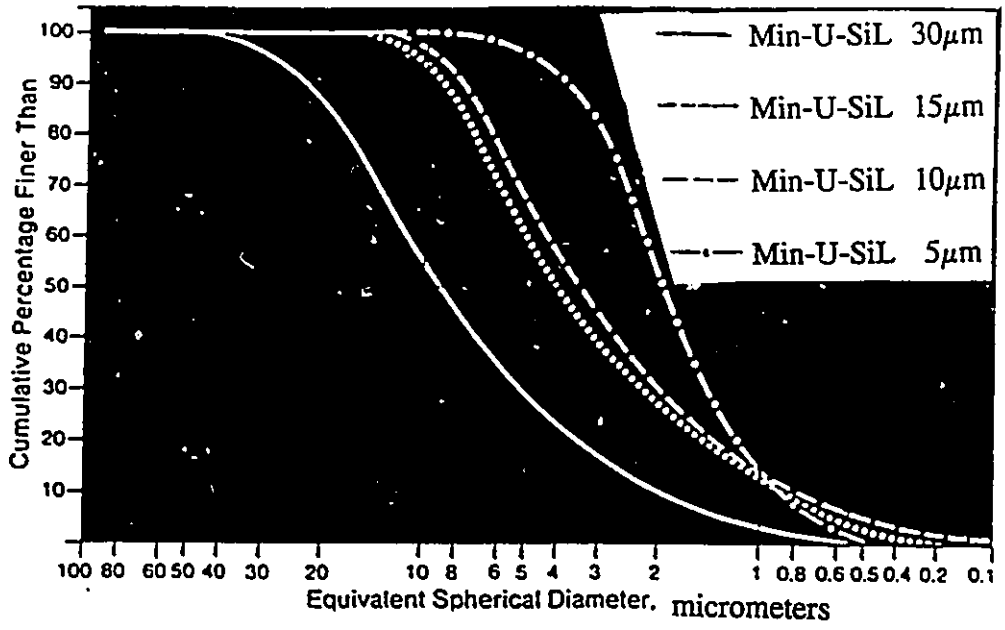

(a)

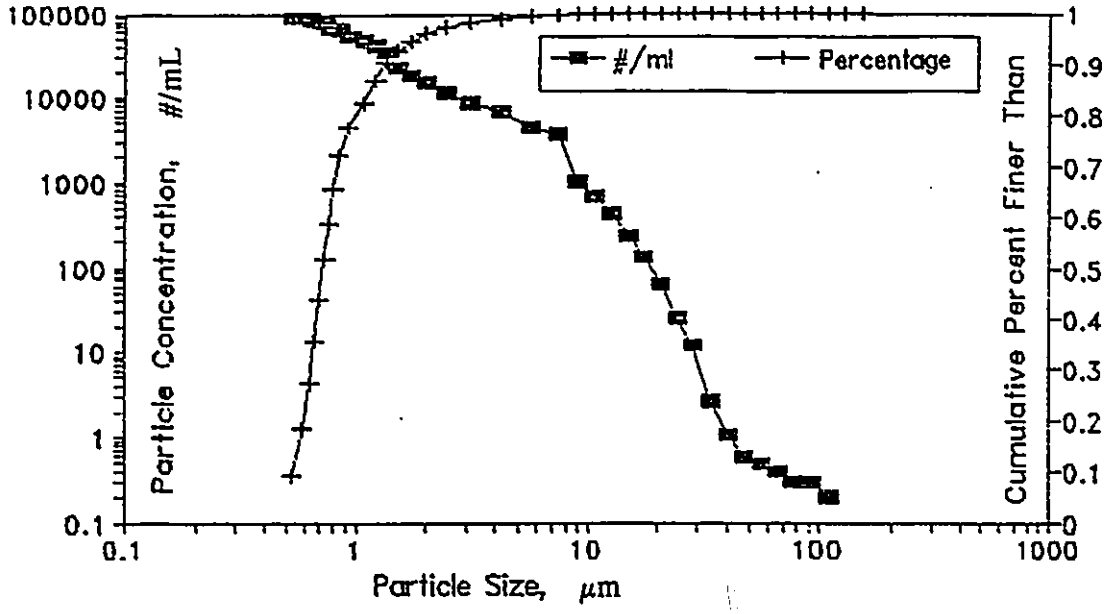

(b)

Figure 4.5 Min-U-Sil particle size distribution, a) extracted from Min-U-Sil brochure, b) stable suspension (5 μm) using Hiac/Royco particle size-analyzer model.

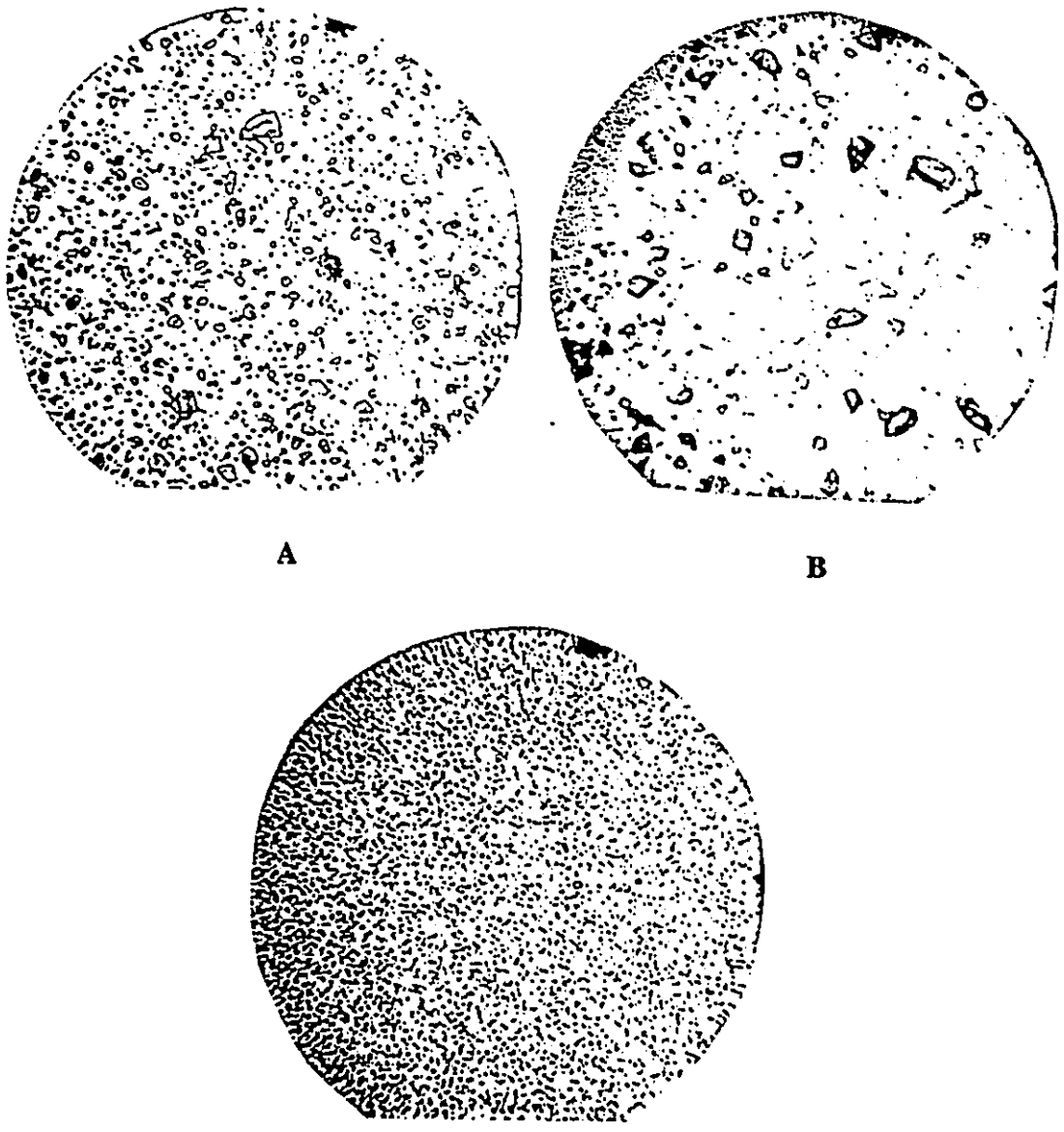

Figure 4.6 Microscopic observation of Min-U-Sil (stable) suspended in distilled water. a) 5 μm, b) 30 μm, c) settled 5 μm Silica.

CHAPTER FIVE

INVESTIGATION OF COAGULATION/FLOCCULATION MECHANISM, FLOC GEOMETRY AND THE MODES OF DEPOSITION

5.1 Introduction

In this chapter the mechanism(s) of coagulation, flocculation, floc geometry and modes of deposition are investigated experimentally. Methods used include; jar test and zeta potential measurements; a camera mounted on microscope to photograph the flocs; an optical fibre endoscope to continuously monitor the flocs geometry and the modes of deposition inside the filter bed; and finally filtration and batch flocculation test were also used.

The addition of a cationic polyelectrolyte to solid-water suspension, prior to rapid (depth) filtration can lead to increased particle capture efficiency (Adin and Rebhun, 1974). However a certain discrepancy in some results obtained in some experiments in this work indicates that no single mechanism is responsible for the removal of all types of suspension particles, but, the processes are rather complex, and yet to be adequately proven experimentally. Therefore, there is a demonstrated need for visual and quantitative information on flocs geometry and modes of deposition in this thesis.

Laboratory experiments based on jar test and zeta potential measurements are used to determine the optimum amount of coagulants and the predominant flocculation mechanism(s). Coagulant aid dosages are varied to obtain the optimum operating conditions and the subsequent results are applied to the pilot scale plant. The results of the jar test and zeta potential

measurement will show that particle surface charges are not completely neutralized by cationic polymer adsorption at the optimum polymer dosage. These results are quite consistent with the bridging hypothesis as a significant capture mechanism, in agreement with O'Melia and Ali (1978).

Visual observation is made by using a camera mounted on a microscope to photograph the flocs of silica particles when ferric chloride or polymer (percol 728) are used as a coagulant aid. Filtration experiments provided additional support for the flocs geometry using an industrial optical fibre endoscope (Lenox Rigid Probes with Fibreoptic Illumination-Lenox Instrument Co., Inc.). The endoscope visually investigates geometry of flocs, deposit build-up and the backwash phenomena. Optical fibre endoscope have been used and observation recorded on a video tape for further image analysis. In Chapter seven analyzing head loss data quantitatively, will show that the experimental data trend follows neither the "surface removal" nor "depth removal" trend, but rather tends to produce a longer filter run with exponential increase in head loss. Finally, experimental validation using batch flocculation tests are also used.

5.2 Jar Test

Jar tests are used to evaluate the ability of polymer and/or ferric chloride to destabilize particles and to estimate dosages required for filtration. Destabilization cause net reduction in surface charge of suspended solids, reducing zeta potential to a certain value, where good agglomeration can be achieved. When metallic cation (ferric chloride) is used, metallic hydroxide is initially formed as microfloc particles that adsorb colloids; while cationic polymer adsorb on negative floc particles, Lash (1975).

The amount of coagulant that is required to render a stable suspension filtrable will

depend upon the suspended solids concentration. Two different types of various sizes of flocs were recognized and categorized under the optimum amount of required coagulant. Some flocs form a settleable (large) size flocs while others shape into a filtrable (pin-point) size. It is necessary to produce a pinpoint floc that is filterable and will penetrate into the filter bed.

A six-place jar test machine (Phipps and Bird, Inc.) was used. The procedure is summarized as follows:

1. Samples are 1000 ml of solid-water suspension (silica suspended in tap water).
2. Samples are dosed with varying amounts of coagulants. Initial rapid mix for two minutes at 100 rpm is applied to disperse the coagulant.
3. To build flocs the jars are mixed at slower speed (40 rpm for 30 minutes).
4. Supernatant samples are analyzed for turbidity and zeta potential value. The jar with the lowest remaining colloidal concentration (measured by the turbidity meter [HACH 2100A]), and the corresponding zeta potential value, may represent the optimum coagulant dosage for use in the pilot scale operation.
5. Repeat steps one to four using samples with dosages of coagulant, more and less, than the optimum amount obtained in four above.
6. The optimum amount obtained in five above, is applied in the pilot scale plant.
7. For the purpose of photographing the flocs using a camera mounted on an optical microscope, a more concentrated sample is required than above. After flocculation, paddles are removed from the jars and the flocs are allowed to settle for 60 minutes, and microscope samples are withdrawn from near the bottom.

5.3 Zeta Potential

5.3.1 Introduction

In the literature the optimum coagulant dosage determined from jar test experiment is thought to understate, overstate or represent actual full scale performance as illustrated in Table (5.1), Habibian (1971). This pronounced disparity between results obtained by different investigators may question the jar test integrity and detract from the applicability of the jar test results. To avoid the uncertainty concerning the applicability of the jar test result and to emphasize the predominating mechanism involved, the optimum dosage determination is based on a jar test experiment conducted in conjunction with zeta potential measurement.

According to electrical double layer theory, the fields of ions surrounding a colloid particle occurs in two layers of opposite charges as presented in Figure (5.1). The inner layers, called the Stern layer, is concentrated and stationary. The outer layer is diffuse and mobile, with a certain amount of ion migration continually in progress. The charge in the diffuse layer weakens with distance from the particles until a zone of electroneutrality defining the outer limit is reached.

The drop in potential between the outer edge of the Stern layer and the isoelectric zone is known as the zeta potential. With the addition of inorganic and organic (cationic) coagulants, the net ionic charge or zeta potential, on the colloids can be reduced to a certain value where maximum agglomeration usually occurs. Mixing the solution brings the colloids into contact with each other and agglomeration occurs. By measuring the zeta potential of the flocs using the zeta meter, the proper dosage of coagulants that achieves maximum agglomeration can be determined and information about particle aggregation obtained.

5.3.2 Zeta Meter operation principle

The zeta meter shown in Figure (5.2), consists of a variable DC power supply with an integrally-mounted electric timer and a clear plastic electrophoresis cell with a molybdenum anode and platinium-iridium cathode. The zeta meter also includes a cell holder for reflecting a beam of light through the electrophoresis cell and a variable voltage illuminator and a stereoscopic microscope with a special mechanical stage, and ocular micrometer for measuring the rate of travel of particles in the electrophoresis cell. The zeta meter operates on the following principle: initially a constant DC-voltage equivalent to the electrophoresis cell (67 Volts) is applied, then the sample specific conductance is read. An optimum voltage used for cell electrophoresis is established by using the sample specific conductance and Table (5.2) (Zeta-meter manual, 2nd edition, 1968). Flocs with a negative charge will migrate toward the anode; while flocs with a net positive charge will migrate toward the cathode. By viewing the colloids through a microscope, their relative speed of migration can be determined and the zeta potential can be calculated. Faster rate of migration is associated with stronger charge on the flocs.

Tests were conducted on samples of 5 and 30 μm Minusil particles, 15 mg silica per litre and settled 5 μm Minusil, 5 mg silica per litre. The silica particles destabilized, used cationic polymer (percol 728) or ferric chloride as a coagulant. Destabilization of particles that used a different coagulant caused formation of flocs. Tracking a representative amount of total population of particles (flocs) in the sample was attempted with some difficulty due to sample overheating and settling of the large flocs. To avoid such difficulties and to permit tracking of small or large flocs, the test was repeated with an adjustable optical objective following different paths until a representative amount of the total population was achieved.

Three tracking paths, which was equivalent to 4X, 6X and 8X objective, were followed;

full and multi scale divisions representing different objectives (4X, 6X and 8X) as depicted in Figure (5.3). The absolute distance along the tracking path between each vertical ruling on the full scale is 960 μm. Therefore, the apparent tracking distance between the vertical ruling when employing the 4X objective is 960/4=240 μm for example. For multi-scale, the tracking distance is 60 μm (quarter scale), and 30 μm (eight scale). The 8X objective is employed for tracking larger number of colloids. If colloids are large (one micron or more) then the 6X can be more readily employed. The 4X objective was generally used for tracking large colloids which settle rapidly.

Tests using samples of 5 μm silica in tap water where the pH of the sample was altered by adding HCl or NaOH, gave zeta potential curve as shown in Figure (5.4). For the pH range (7.5-7.9), and the other characteristic found in tap water which was mentioned in Section 4.4, the sample of 5 μm silica gave a zeta potential between -20 and -28 mv.

5.4 Comparison of optimum dosages from coagulation and filtration: Review And Interpretation

Higher removal efficiency is obtained experimentally by applying the optimum dosage of coagulant obtained from the jar test to the influent suspension flowing to the filter column. Zeta potential curves for 5 μm silica particles in solutions of varying cationic polymer (percol 728) and ferric iron concentration are shown in Figure (5.5) through (5.7). Experiments using 5 or 30 μm, 15 mg silica per litre, indicate the equality between the amount of optimum coagulant using both jar test and short filter run techniques. This results is consistent with others, (Adin and Rebhun, 1974; Ghosh, et al., 1975; Tate and Trussell, 1978; and Glasser and Edzwald, 1978). The optimum polymer dosages for maximum removal efficiency, in conclusion,

can be approximated by the optimal dosage for coagulation as determined by a conventional jar test. Habibian (1971) came to the same conclusions as others provided that the polymer adsorption on surfaces of the jar is neglected. Equality was not observed in some other experiments using settled 5 μm, 5 mg Silica/L. Other investigators failed to observe such equality, as well. Dentel et al. (1988) stated:

> "Optimum polymer dose for filtration may be much less than that indicated by jar test".

Mints (1966) wrote:

> "It should be pointed out that the minimum dose which ensures the required degree of clarification in filtration and the minimum dose for the formation of large quick falling flocs are not identical in most cases. The former is usually smaller than the latter and for treatment of slightly turbid water may indeed be several time smaller."

Shull (1967) and Smith (1967) show in experiments done at the Philadelphia Suburban Water Co., that the optimum coagulant dose determined by the jar test does not necessarily produce optimum conditions for filtration.

Some of the results obtained in this experimental program are in agreement with those of Mints. For settled 5 μm, 5 mg silica/L, shown in Figure (5.6), the optimum dosage obtained from jar test and zeta potential measurements (0.6 mg polymer per litre) represents almost 10 times that required in filtration. This occurred because the influent particles concentration was changed to about 5.8 mg silica/L, instead of 5 mg/L.

Since there is a major discrepancy between results obtained by different investigators concerning equality of coagulant dosages between filtration and coagulation, the final conclusion for such equality must be based on results obtained from each individual work as related to the characteristic of water to be treated. The major discrepancy may be attributed to one, or more

of the following:

1. Amount of polymer adsorption on the surface of the jar. The amount depends on the ratio of the surface area of the jar in contact with the suspension to the surface area of the suspended particles in each jar, Habibian (1971).

2. Different experimental conditions used by investigators such as type of particles used, volume of jars, coagulant aid and mixing conditions.

3. Colloid and polymer concentration used. LaMer and Healy (1963) explain that the action of polyelectrolytes,

> "...To be effective in destabilization, polymer molecules must contain chemical groups which can interact with sites on the surface of the colloidal particles. When polymer molecules come into contact with colloidal particles, some of its active groups become attached to the particles, while the others extend away from the particle into the liquid. If a second particle with some vacant adsorption sites comes into contact with this extended segment, the two particles form a particle-polymer-particle (or grain) complex, with the polymer acting as a bridge. If a long time passes without the first particles coming into contact with other body, the group of the extended part of the adsorbed polymer may also adsorb on sites of the same particle, so that polymer is no longer available to serve as a bridge".

   This explanation illustrates why high concentration of suspended solids produces more head loss than the low concentrations, when results are compared on the basis of equal amount of mass deposit retained within the filter. This concentration effect may also be attributed to the rapid increase in the number of particle-to-particle contact per unit volume of water treated.

4. Inconsistency of variables between coagulation and filtration. The extreme variability of optimum coagulant obtained from a jar test and a filter bed may be due to variation in the quantity of colloid adsorbed. The difference is larger when the suspension pass through the filter column as a result of pore space flocculation.

5. Variability in amount of coagulant feed in filtration.

6. Surface of filter grains for added polymer competing with suspended particles, particularly if the interval between polymer addition and the arrival of suspension at the top of the filter bed are very short, Habibian (1971).

7. Ionic concentration effect (ionic strength).

O'Melia and Crapp's (1964) produced evidence that type and concentration of anions and the pH could have a significant effect on filter performance. Rong and Ghosh, (1988) assumed a flat polymer configuration on particle surface due to the strong electrostatic repulsion between charged segments.

Gregory (1986) explained:

> "It is well-known that the viscosity of polyelectrolyte solution can increase markedly as the ionic strength is reduced, indicating an expansion of the coil".

The two cases related to the equality of the optimum coagulant dosage obtained from the jar test and zeta potential measurement and that used for filtration are observed in the present work (no temperature difference was observed between the experiments conducted in this regard). The jar test experiment is highly sensitive and requires well-controlled conditions. Uncontrolled variations in operating conditions will account for some deviation from the normal trend. Therefore, without controlling such variations, the optimum coagulant dosage is inappropriate for filtration purposes and the filterability test could prove more suitable (Cleasby, 1969; Ives, 1978, Janssens, 1982).

5.5 Validity of the proposed flocculation mechanism(s)

Different approaches are used to establish the validity of the proposed flocculation mechanism(s). First, under different conditions the amount of zeta potential that corresponds to

the optimum amount of coagulant is determined. The zeta potential response was expected to be negative and zero when polymer and ferric chloride was used, respectively. Second, photographing flocs from jar test experiment, with optimum coagulant dosage, shows distinct features of the flocs. Thirdly, when using a pilot scale filter, geometry, flocs deposit build-up and backwash phenomena are observed within the filter bed element. An optical fibre endoscope was used and observations recorded on a video tape for further image analysis. Finally, experimental validation of flocculation mechanism(s) using batch flocculation test is used.

5.5.1 Visual Validation

5.5.1.1 Microscopic Observation Of Aggregated Flocs

Results of zeta potential measurement of flocs using different polymer concentration to determine the optimum coagulant dosage are shown in Figures (5.5) through (5.7). The figures illustrate that optimum coagulant dosage corresponding to the lowest remaining colloidal concentration, occurs at both negative and positive zeta potential. The positive values of zeta potential may be explained by the adsorption of positively charged amorphous $Fe(OH)_3$ colloids. It has been postulated that adsorption of polymer to a particle surface takes the forms shown in Figure (5.8). A free end of the molecule extends into solution and may adsorb onto an active site on a second colloid. The two particles join through a molecular bridge, and not by overcoming electrostatic repulsion (Stumm and O'Melia, 1968; O'Melia, 1969; Weber, 1972).

In this work, mechanisms are confirmed experimentally by visual observation through a camera mounted on a microscope for a sample withdrawn from the jar with the optimum amount of coagulant. A microscope slide was washed with detergent, flushed with tap water, followed by distilled water to lower surface tension. The microscope slide was placed on the

microscope stage and a small drop of the slurry is applied to the slide surface, and immediately expands to a diameter of 1 to 3 cm. The liquid depth thins and particles and/or flocs are viewed at different locations of the drop. Particles are aggregated by an interparticle bridging mechanism forming long chain (dendrites), mostly extended in different directions. Groups of clusters and individual particles 3, 4, and 5 particle flocs are also observed (see Figure 5.9). This provide a plausible explanation for continuous improvement in removal efficiency, and for the dramatic increase in head loss of a filter operated at a dosage of coagulant equal to the optimum dosage obtained from the jar test. Particles, which mutually adhere by direct particle-particle contact, are randomly aggregated into small floccule and are joined by polymer linkage. This morphology is associated with the rapid increase in head loss build-up. Comparison of particles (flocs) and joints in the Figures above, demonstrate that joints do not represent an individual polymer molecule linkage, but rather, may be a gel-like region formed by flocculant molecules.

5.5.1.2 Optical Fibre Endoscope Observation

Originally, the optical fibre system used was designed to investigate the change in geometry of the filter grains and flocs, and to observe the mode of deposition of particles inside the filter bed element. However, many investigators, for example Habibian (1971) and Edzwald (1984), observed equality in the optimum dosage between coagulation and filtration. Therefore, the assumption that the geometry of the flocs (flocculation mechanisms) inside the filter is similar to that obtained using the jar test may be reasonable, providing that the jar test results are obtained under well controlled conditions.

This work describes the experimental conditions and results using different coagulant and particle sizes where evidence for the proposed mechanism(s) can be drawn from the results. For

more details about the system see Clough and Ives (1986) and Ives (1989).

The experimental programme involves the filtration of silica (Min-U-Sil) particles with 5 and 30 μm, in addition to settled 5 μm silica (flocculated by ferric chloride, or polymer as coagulant aid) suspended in tap water and flowing at a filtration rate of 0.1 - 0.9 cm/s through sands of 0.45 mm and 1.71 mm in diameter.

The endoscope observation was made on the laboratory pilot-scale filter column. In the wall of this filter column is watertight fitting at different level which enables insertion of brass tubes with an end lens to permit insertion or removal of endoscope during an experiment. The directly-inserted endoscope and brass tube may be set at any distance of penetration but cannot be altered during an experiment, as the granular filter material would be disturbed. However, the endoscope can be withdrawn and relocated at a different level in the filter column without disturbing an experiment. The brass tube and endoscope are positioned at the outer surface of the filter column as alternative mean of monitoring the flocs geometry and modes of deposition to avoid problems with relocation of the endoscope.

Successful experiments were made with the above lab scale filter using ferric chloride or polymer with 5 and 30 μm grade silica. Experiments with settled 5 μm silica were unsuccessful in tracking flocs during filtration, but successful in demonstrating the deposit build-up and backwash phenomena. Figure (5.10) represents the floc size analysis for flocs resuspended by gently backwashing the filter bed; and recording observations on a video tape using an optical fibre endoscope, then analyzed using image analysis "IMIX" system. The movement of flocs is unclear because the resolution limit is about 10 μm, Ives (1989), and the flocs are small. Hsiung, (1974) investigated a backwash technique measuring the specific deposit and concluded that the sludge from backwash waste seems to retain the identity of the deposited flocs within the filter

bed. Hsiung (1974) give no firm evidence for his conclusion. Breaking up the flocs using a conventional backwashing rate is very likely. Visual observation using optical fibre endoscope techniques showed breakup of some of the flocs while others retained the flocs identity even when a low backwashing rate was used (1.0 cm/sec). In the studies reported by Coad and Ives (1981a), it is stated that the volume of deposit within the sand matrix was shown to be less than the volume the same material occupied after it was washed out of the bed and allowed to settle freely.

Many previous observations are confirmed in this work by using the optical fibre system. Firstly, when the velocity of the suspending fluid is great, the suspended solids are prevented from depositing on the grains of the filter medium, unless the suspended solids are attached strongly to the surface of the grains, or to previously deposited particles, secondly when the velocity of the suspending fluid is low, the suspended particles are deposited on the filter grain and/or the previously-deposited particles by sedimentation, interception, and diffusion. Thirdly, resuspension and recapturing of the flocs can be observed. Fourthly, as the filter run proceeds it was observed in some experiments that most of the pore space was completely blocked, particularly, in the first filter bed element (depth=14 cm), while others were completely clean, which confirm Coad and Ives (1981b) observations in experiments conducted using the tracer technique (conductimetric measurement) to measure porosity change during clogging.

5.5.2 Quantitative Validation

5.5.2.1 Filtration Test

The observed and predicted head loss values are obtained using exp361 and the smooth coating model prediction. For example settled 5 μm, 5 mg Si/L, cationic polymer (0.05 mg

percol 728/L), 0.45 mm sand grains, 50 cm bed depth, 5 cm filter column diameter and V_o = 0.1 cm/s are analyzed as a function of specific deposit, see Figures (5.11) and (5.12). The specific deposit (volume of deposited material per unit volume of bed) are determined by calculating the volume of particles and flocs retained, using the procedure outlined in Section 6.4 (particle count correction). Oulman et al. (1979) compared "surface removal" tendency with the "depth removal" tendency. He demonstrated that surface removal tends to produce short filter runs with an exponential increase in head loss while depth removal tends to produce longer filter runs with a relatively linear increase in head loss. Figures (5.11) and (5.12) demonstrated that neither the smooth coating, nor the surface removal are predominant mechanisms, as the head loss for different stations within the same bed element are approximately equally distributed. Initially in the filter run, there was no large increase in head loss observed which indicates an absence of filter performance improvement due to straining, or surface removal effect during the first 400 min.

In this work, results are inclined to produce a longer filter run with exponential increase in head loss which indicates that flocs are penetrated reasonably deep and the deposited flocs are protruded into the pore space. As mentioned earlier, by analyzing the head loss data quantitatively, the experimental data trend follows neither the "surface removal" nor "depth removal" trend, but rather tends to produce a longer filter run with exponential increase in head loss. A small amount of deposit material was expected to cause gradual increase in head loss. A deposited amount of approximately, four percent of the void space was found to contributes to a drastic increase in head loss and to a longer filter run (48 hours). Clearly, these drastic changes in head loss and filter run time cannot be cause by deposit that form smooth coating on the grains nor by clogging of the filter bed.

5.5.2.2 Batch Flocculation Test

In the particle flocculation process, destabilization of particles is attributed to charge neutralization and bridging mechanisms that produce flocs with distinct features. Generally flocs formed by bridging are stronger than those produced by charge neutralization, Gregory (1987). However, bridged flocs broken by shear may not be easily reformed, Pelton (1981) because of scission, or rearrangement, of absorbed polymer chains, Gregory (1987). Other investigators also observed such phenomena. Abdel-Alim and Hamielec (1973) explained that different mixing intensity for different periods of time to achieve complete solution tends to be too severe and scission of polymer chains into small unit may occur.

When charge neutralization becomes the dominant mechanism, floc broken by shear can be reformed when shear was reduced. This property has been used by Ditter et al., (1982) to distinguish the mechanism of flocculation. A simple experimental procedure similar to that used by Ditter et al. (1982) is proposed. It was intended to compare the particle size characteristic of the aggregated flocs before and after strong agitation of the batch sample. Such a comparison was expected to provide some evidence for judging the mechanisms of a coagulated action. To accomplish this, the optimum coagulant dosage required for the destabilization of a given suspension are determined using the jar test experiment. The batch was 18 litre in volume, 10 cm pitched turbine, and baffled tank. Particle size characteristic results are analyzed and compared for the following samples.

1. Samples after complete mixing (1 minute rapid mix at 425 rpm) of particles in suspension ("Initial").
2. Destabilized particles flocculated under gentle agitation (20 minute flocculation period at 60 rpm) until an almost steady particle size distribution is achieved as a result of the

equilibrium between aggregation and break up is achieved (Reddick (1964) observed that the floc size remained constant after 20 minutes flocculation) ("Flocculated").

3. Flocs from 2 are then subjected to strong agitation for a certain time (10 minutes is suggested as it is equal time required to back wash the filter after termination) ("Resuspended").

4. Particles from 3 are allowed to reaggregate under the original gentle agitation ("Reflocculated").

Similarity of PSD and/or vol/vol (volume of particles sensed per ml of water) in 2 and 4 using 30 μm, 15 mg Si/L, and 0.25 mg Fe^{+3}/L demonstrates a rapid recovery of the flocs, which is characteristic of charge neutralization as shown in Figure (5.13). Although the resuspended flocs and reflocculated particles, do not exactly fit the initial and flocculated sample data, the data follow the same trend. The main difference relates to the difficulty in restoring initial conditions where there is no information about mixing energy and the length of time to be used. Failure to exhibit rapid recovery is an indication of polymer bridging. The results obtained using settled 5 μm, 75 mg Si/L and 1.5 mg polymer (percol 728)/L clearly indicate the extent of flocculation obtained under these conditions, Figure (5.14).

Resuspended flocs result in a trend that is different from the original one. Reflocculation of resuspended sample show the same trend as for small particles (< 1.0 μm). It is also observed that under these conditions resuspending and reflocculating the sample tends to increase the flocculation extent for particles greater than 12 μm in case of ferric chloride, and particles greater than 25 μm in case of polymer.

In summary, this chapter presented a number of techniques to quantitatively investigate and visually observe coagulation/flocculation mechanisms, floc geometry and modes of

deposition. Bridging and charge neutralization was identified as a significant mechanism with both polymer and ferric chloride, respectively. Amorphous and chain-like flocs represent the floc geometry observed. Smooth coating, dendritic and a combined mode of deposition were observed. Many previous observations are confirmed in this work by using the optical fibre endoscope.

Table (5.1) Jar test coagulant dosages as a predictor

Dosage reliability (Turbidity removal)	Reference
Understate	WPCF No.8, 1977
Good	Bratby, 1981
Overstate	Hudson, 1973

Table (5.2)*

Specific conductance of sample(umhos/cm)	Optimum voltage for electrophoresis	Volts/cm
0 - 300 max.	300	30
700	200	20
1500	133	13.3
3000	100	10
6000	67	6.7
10000	50	5
20000	40	4
30000	30	3
40000	25	2.5
60000	20	2

* Extracted from the Zeta-Meter manual, 1968, 2nd edition

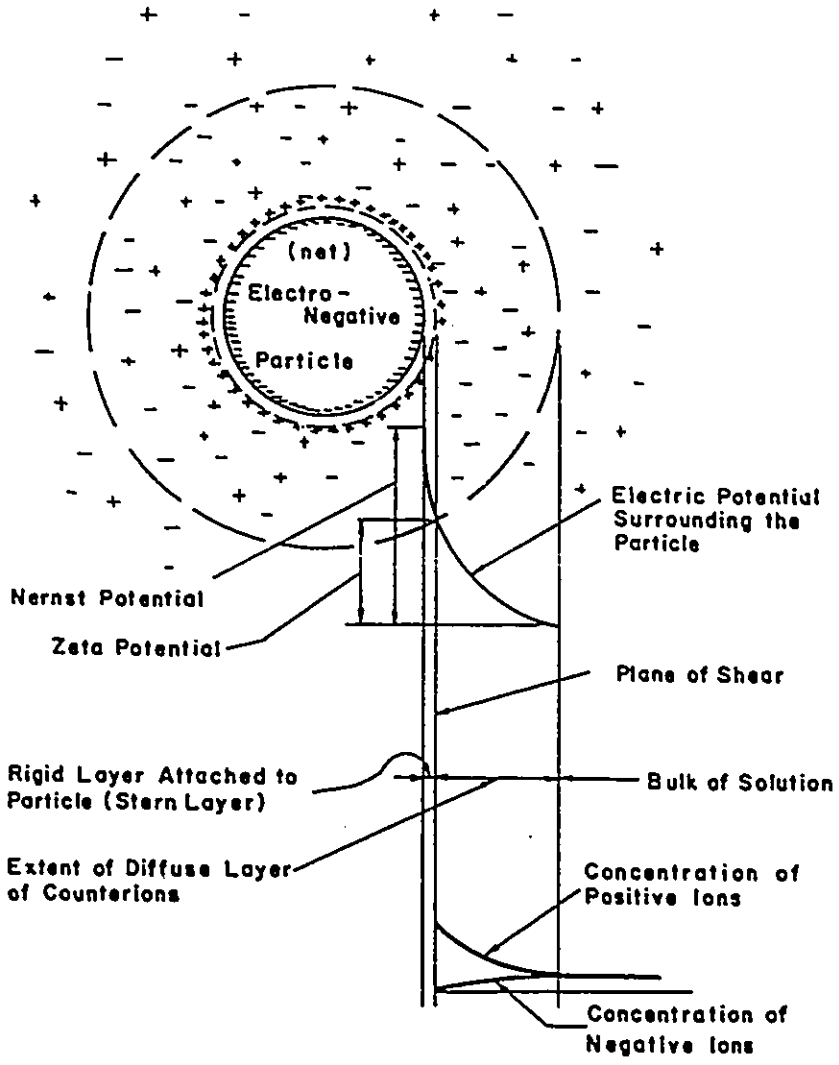

Figure 5.1 Concept of the zeta potential (after Riddick, 1966)

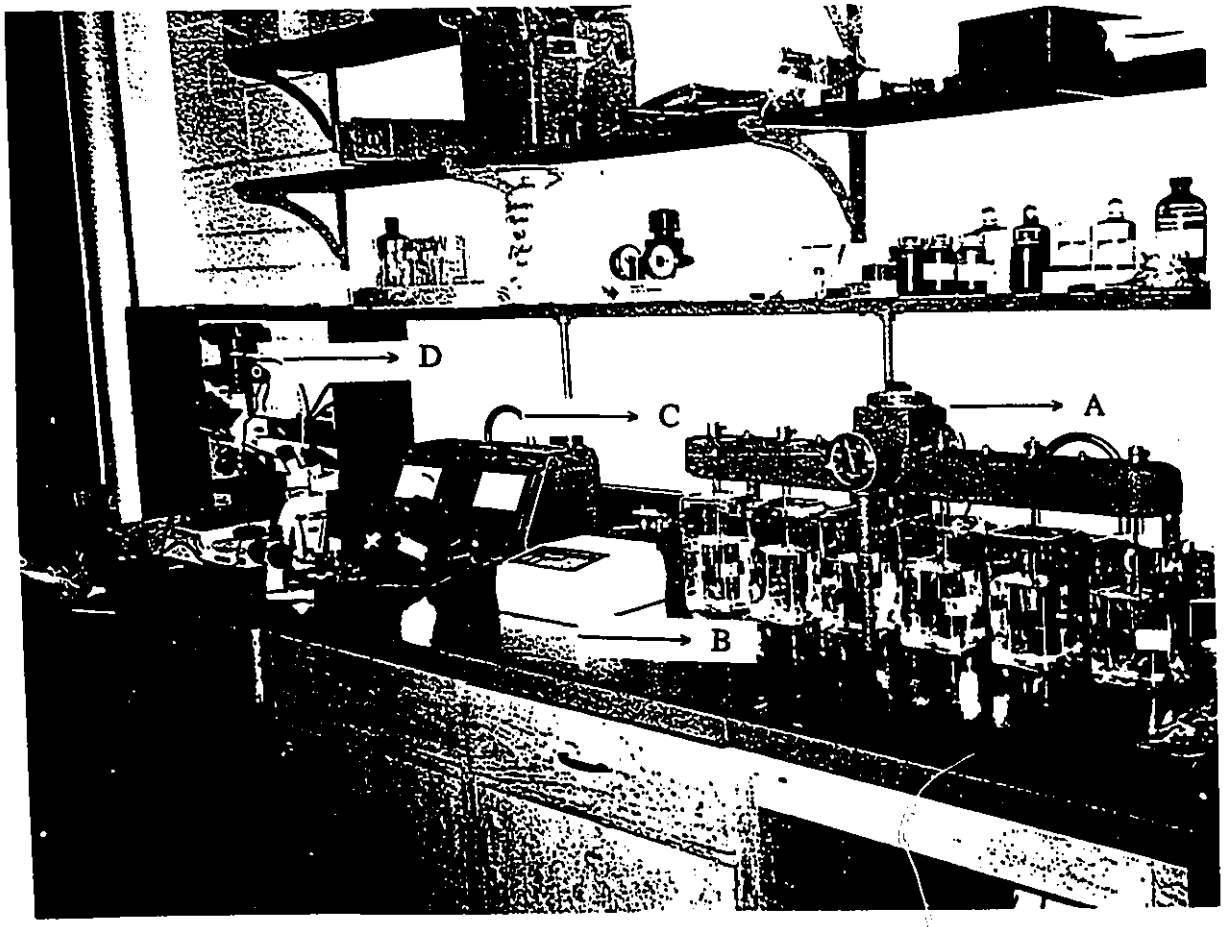

Figure 5.2 Coagulant dosage determination system and zeta meter with a camera mounted on light microscope for viewing flocs. A) Jar test; B) Turbidimeter (HACH 2100A); C) Zeta meter with stereoscopic microscope; D) Optical light microscope with a camera.

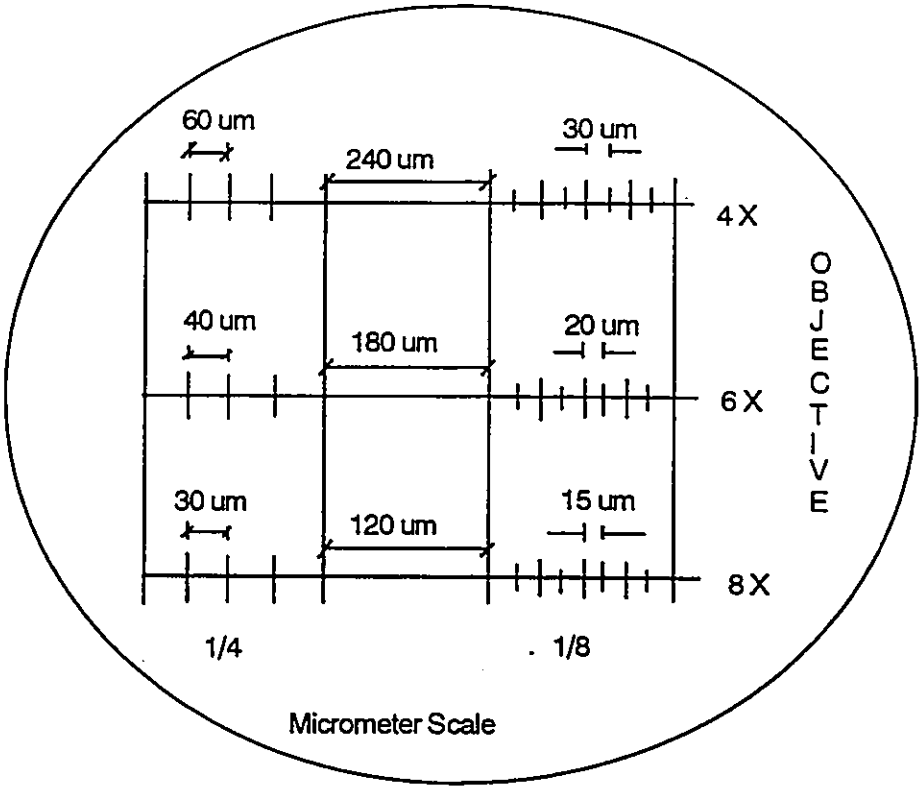

Figure 5.3 Full and multi-micrometer scale

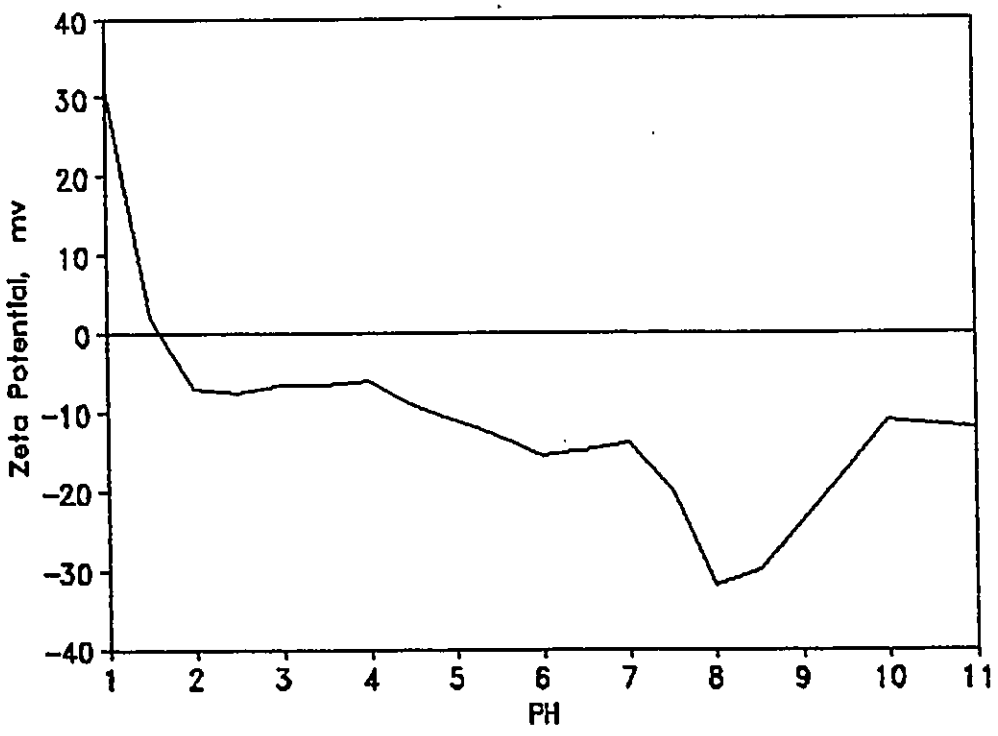

Figure 5.4 Zeta potential vs. pH for 5 μm, 15 mg silica particles/L suspended in tap water.

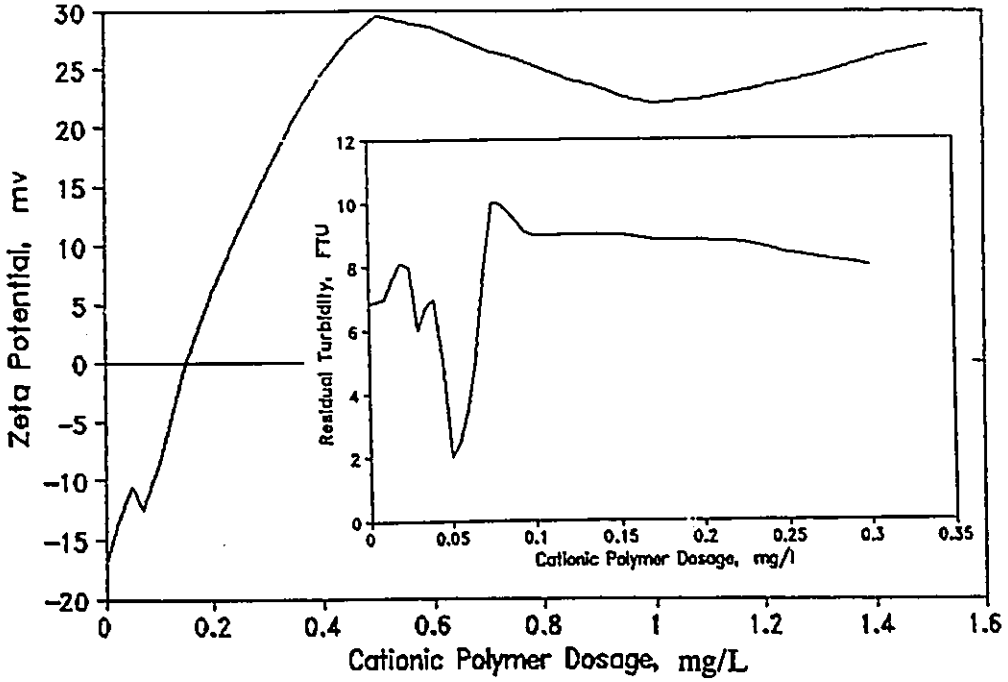

Figure 5.5 Zeta potential and residual turbidity for 5 μm silica particles in solution of varying cationic polymer (percol728) concentration.

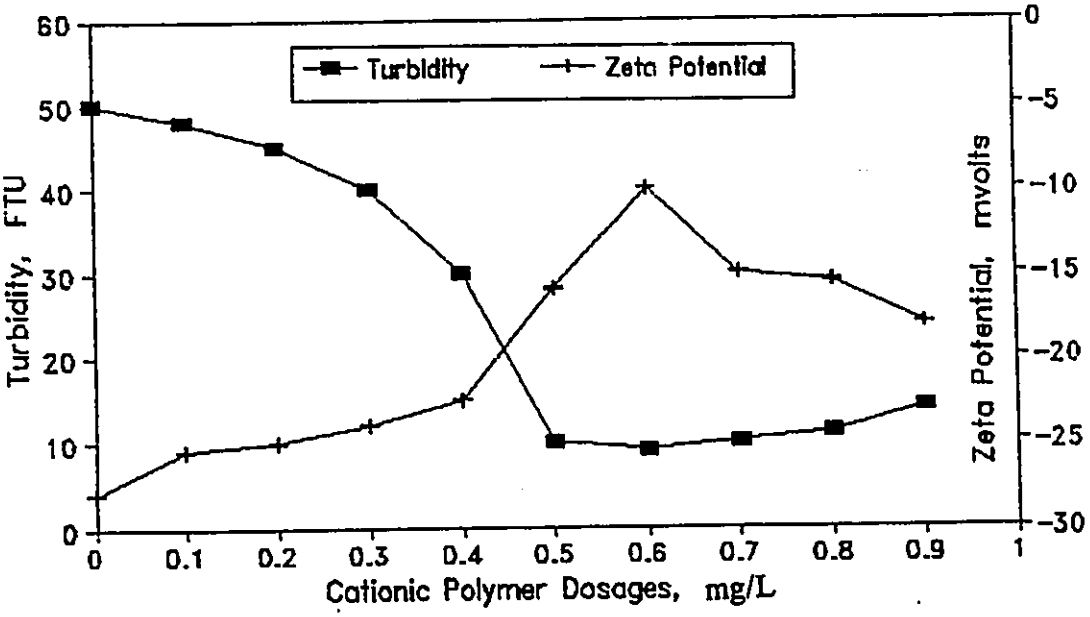

Figure 5.6 Zeta potential for settled 5 μm silica particles in solution of varying cationic polymer (percol 728) concentration.

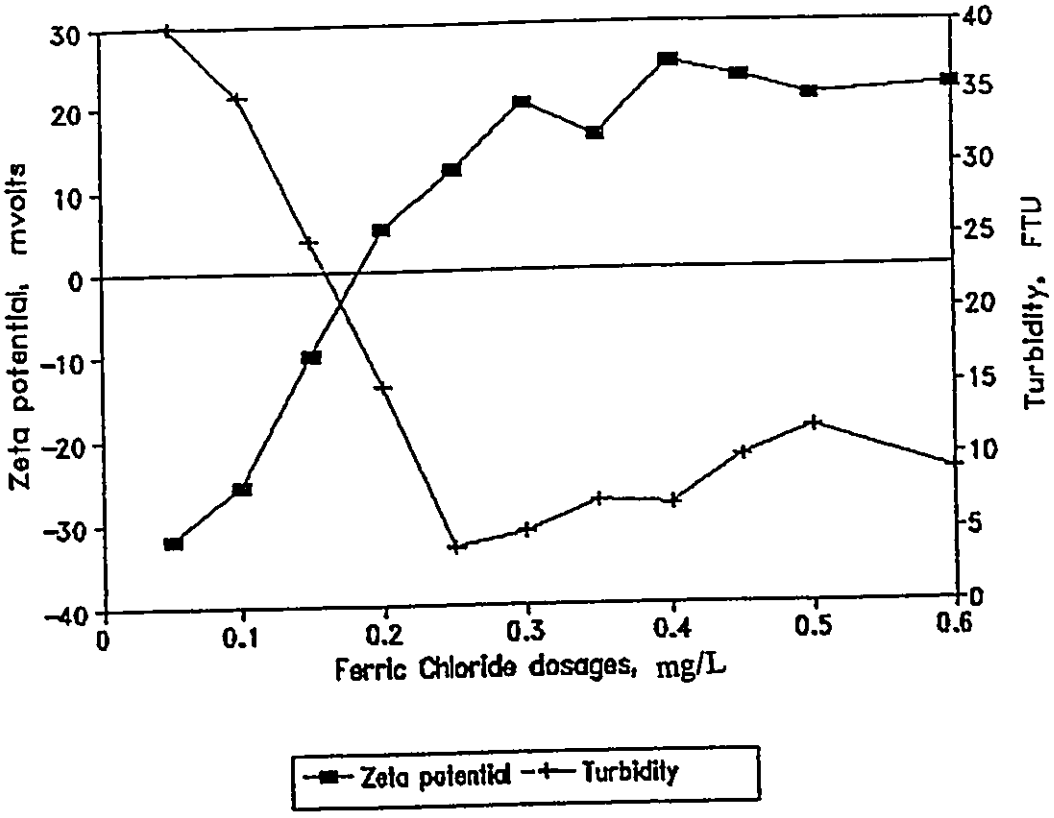

Figure 5.7 Zeta potential for 30 μm silica particles in solution of varying ferric chloride concentration.

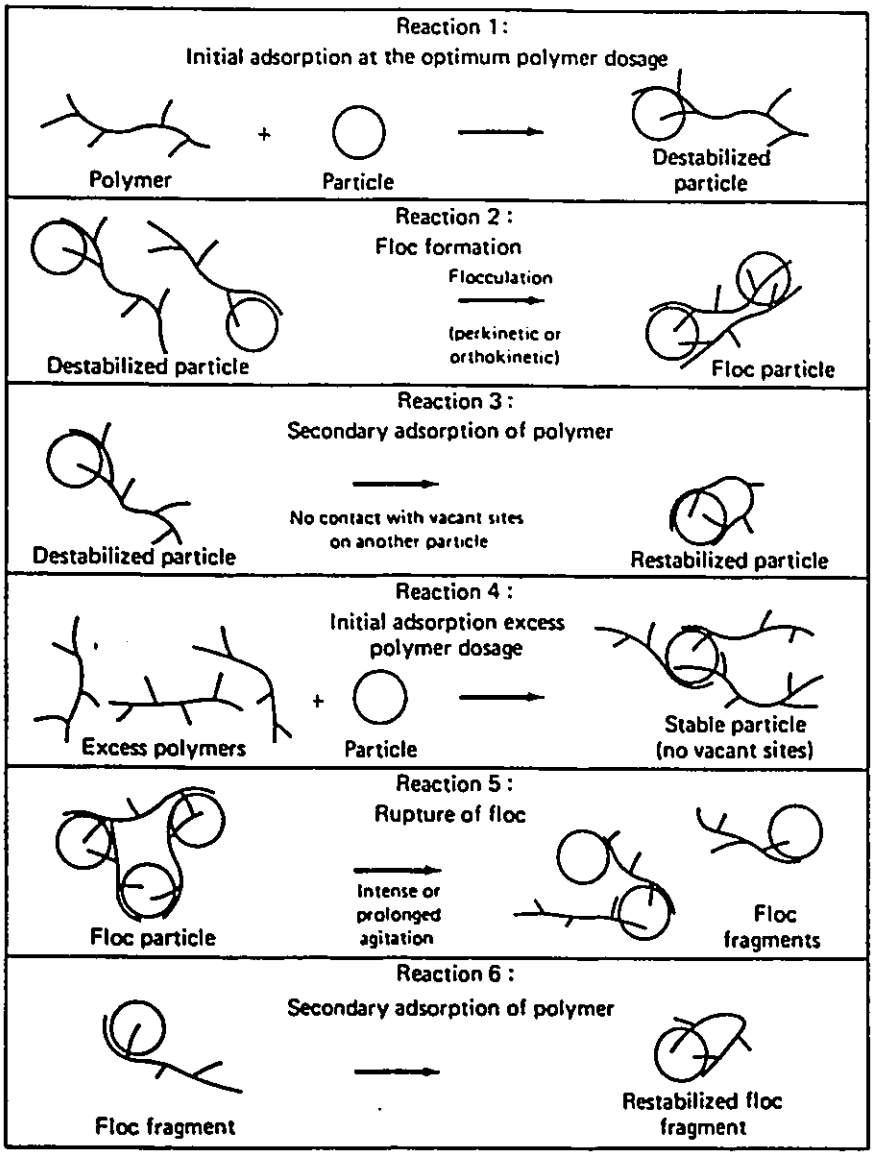

Figure 5.8 Schematic of reaction between colloid and polyelectrolyte (after O'Melia, 1969).

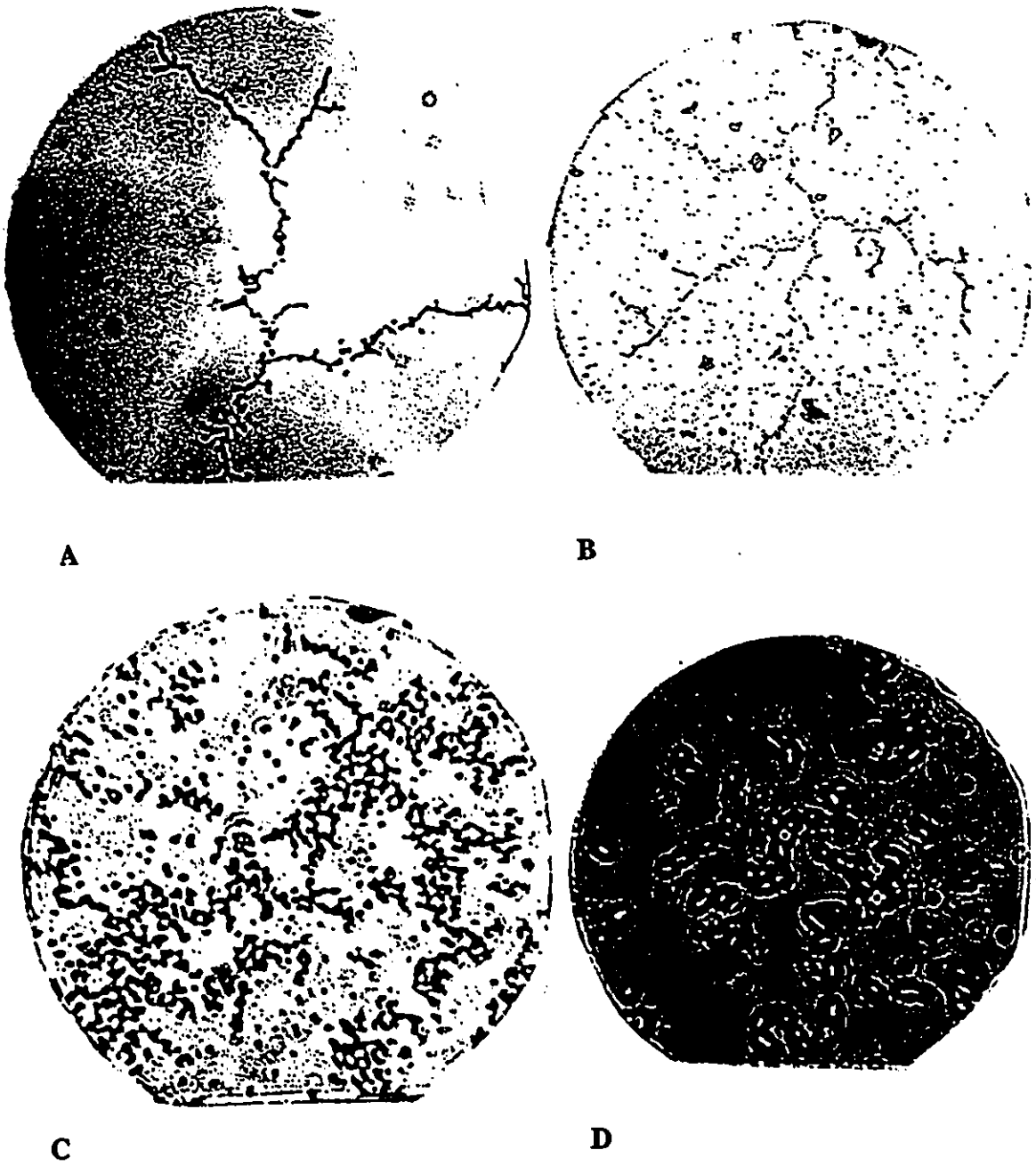

Figure 5.9 A Typical dendrite flocs acquired with the camera mounted on light microscope system. a) floc image after adjusting the focus for background noise removal, b) floc image with background noise, c) cluster of flocs, d) a group of 3, 4 and 5 particle flocs.

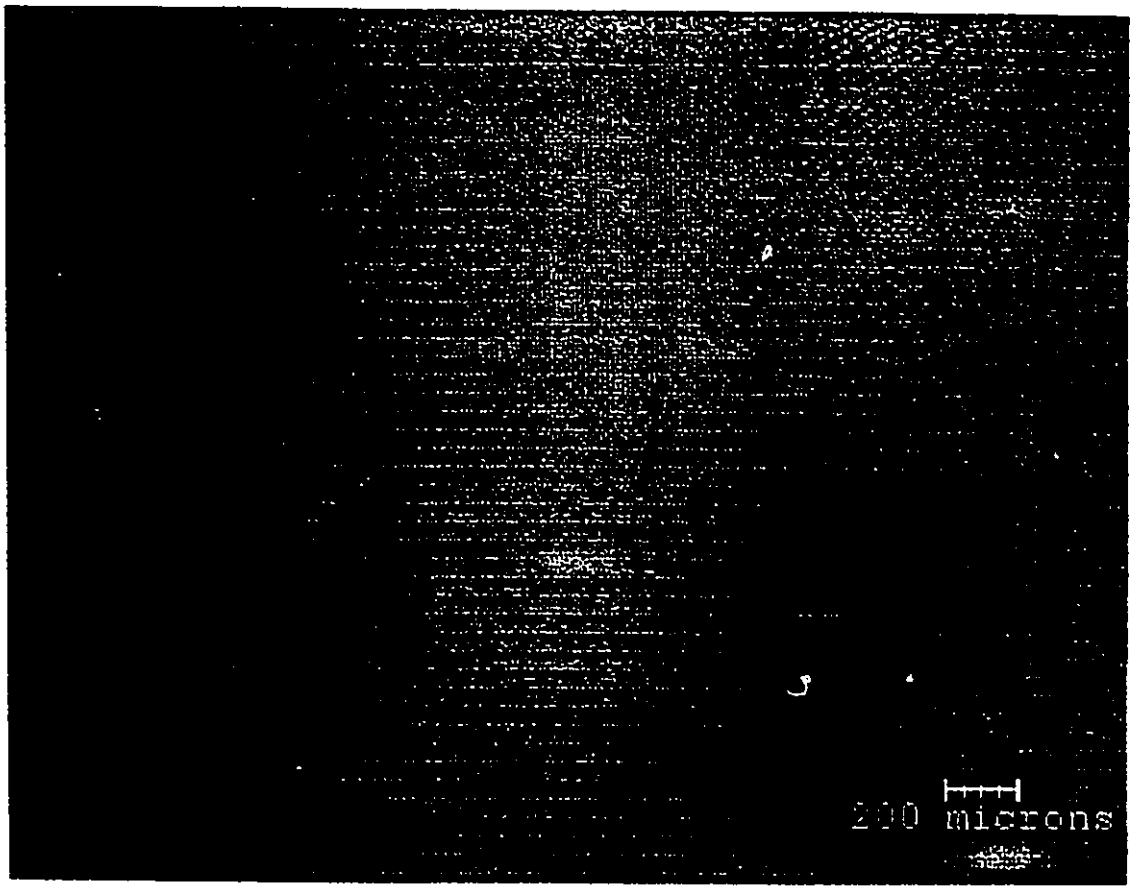

Sample: Floc Units in micrometers

Feature #	Area	Perimeter	Longest Diam.	Breadth	Area Equi. Diam.
1	7500.99	456.23	152.52	65.2	87.73

Volume of Sphere	Elongation Ratio
488697.47	0.44

Figure 5.10 **Floc size analysis using the "IMIX" system. Flocs are resuspended by gently backwashing (1.0 cm/sec) the filter bed (settled 5 μm, 5 mg Si/L, 0.45 mm sand, 50 cm bed depth)**

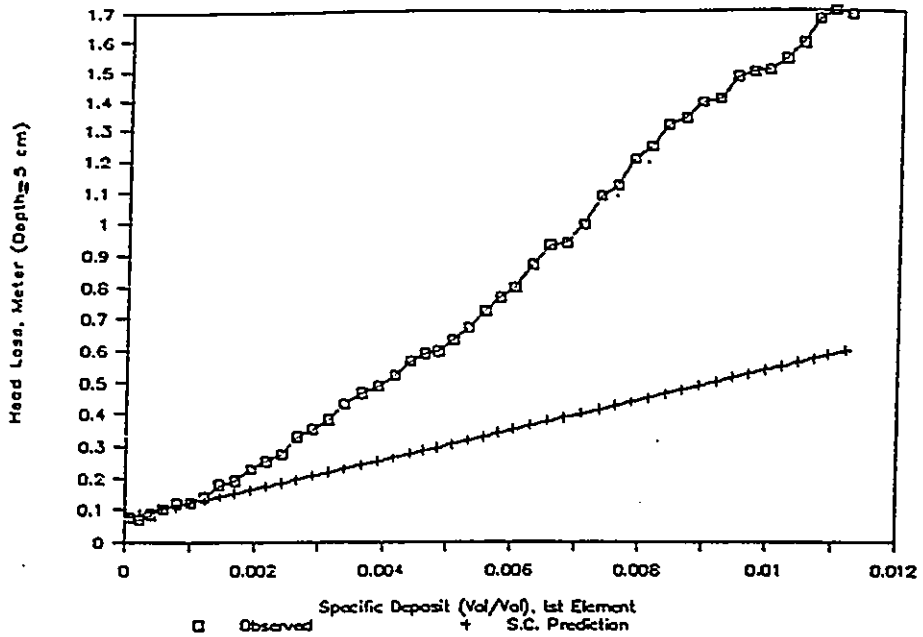

Figure 5.11 Head loss versus specific deposit comparison (settled 5 μm, 5 mg Si/L, 0.45 mm sand grains, 50 cm bed depth, V_0=0.1 cm/s).

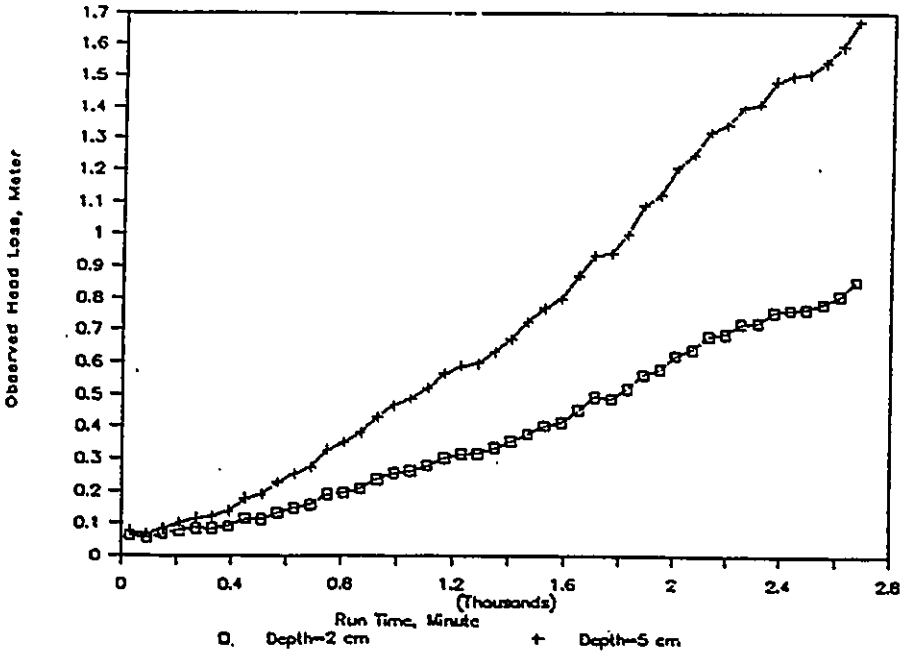

Figure 5.12 Observed head loss versus time (settled 5 μm, 5 mg Si/L, 0.45 mm sand grains, 50 cm bed depth, V_0=0.1 cm/s.)

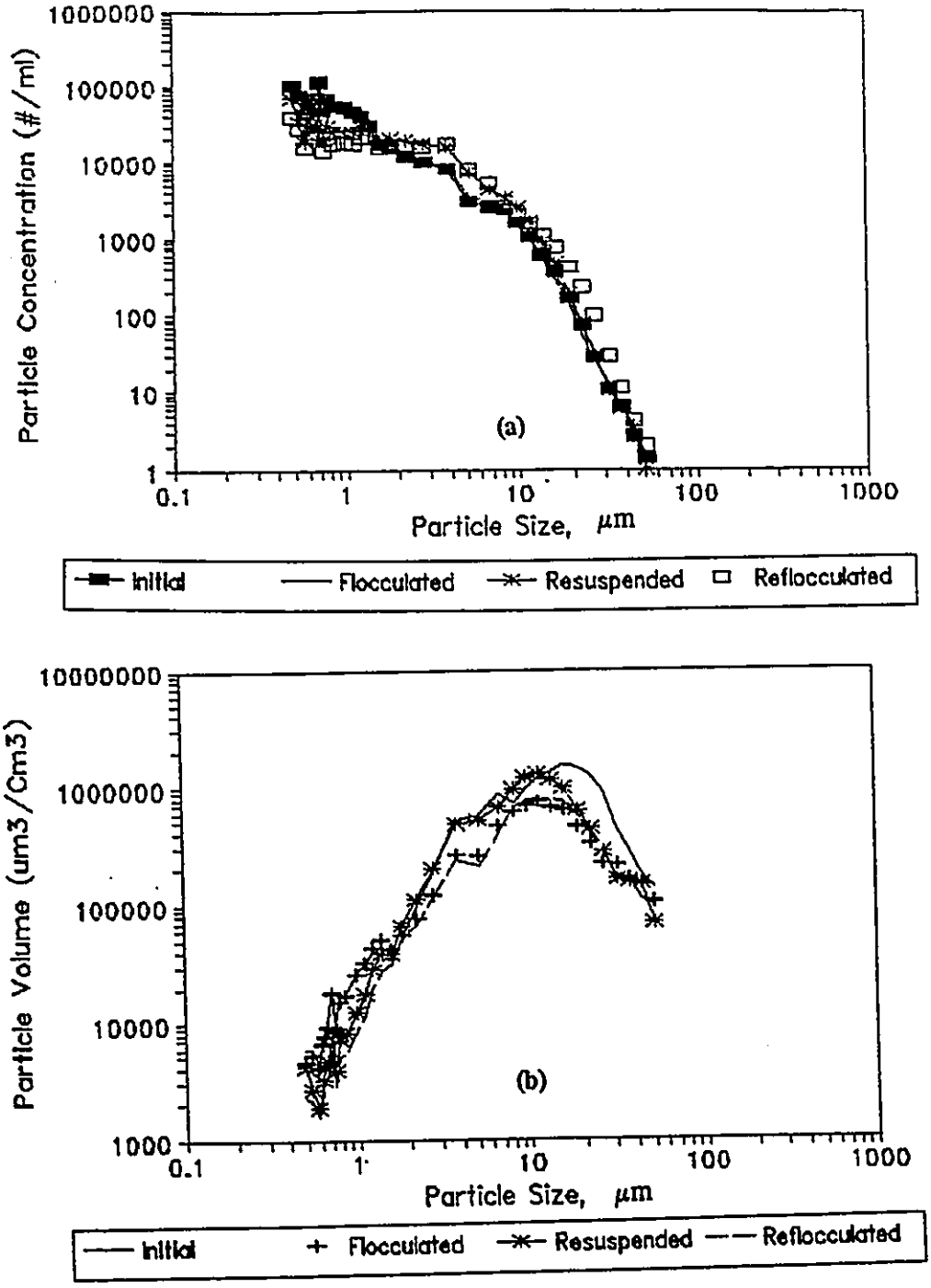

Figure 5.13 Quantitative verification of aggregation mechanism (30 μm, 15 mg Si/L, suspended in tap water, 0.25 mg Fe^{+3}/L). a) particle concentration versus particle size. b) volume of flocs per volume of sample ($\mu m^3/cm^3$) versus particle size.

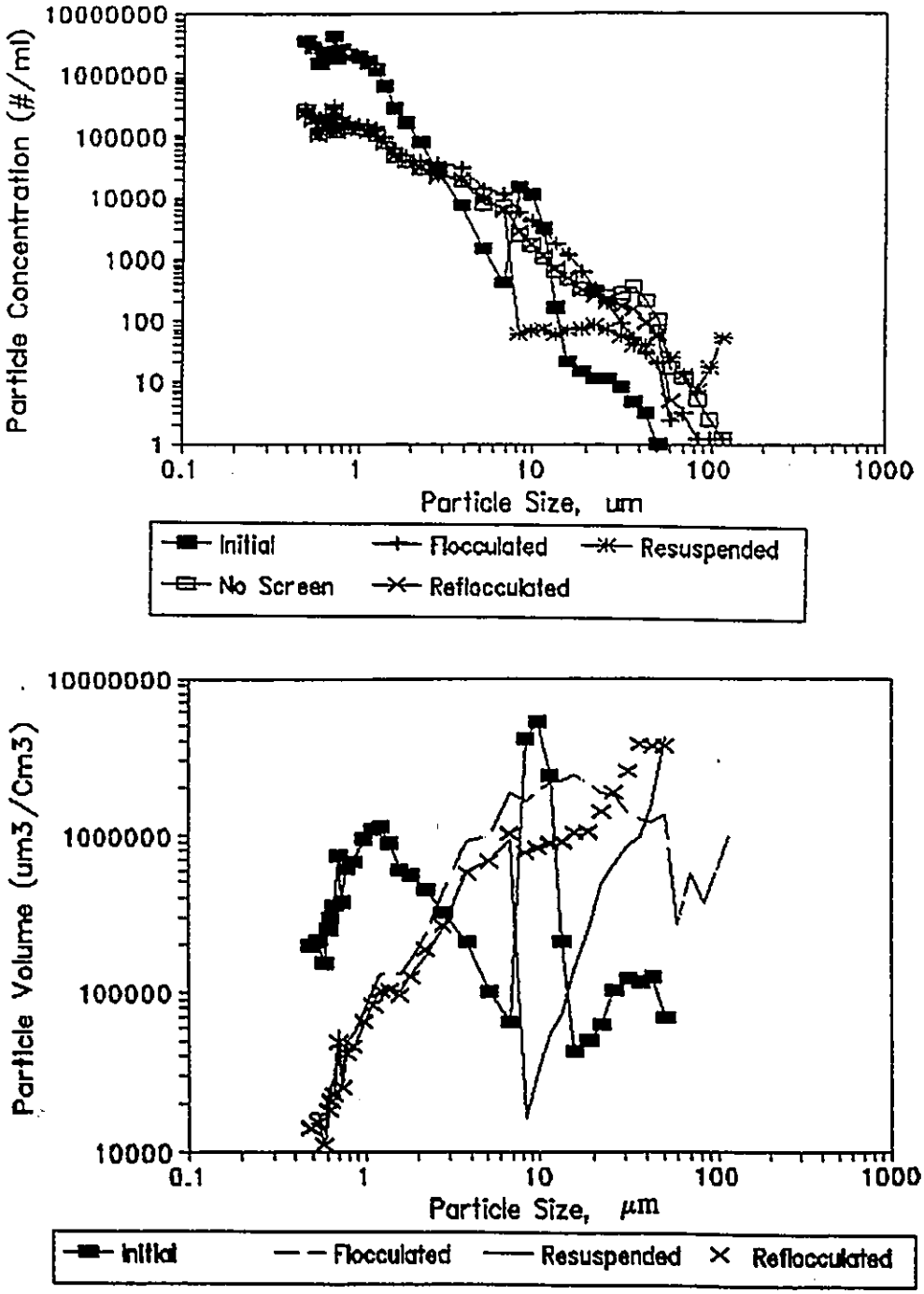

Figure 5.14 **Quantitative verification of aggregation mechanism (settled 5 μm, 75 mg Si/L, suspended in tap water, 1.5 mg polymer/L). a) particle concentration versus particle size. b) volume of flocs per volume of sample ($\mu m^3/cm^3$) versus particle size.**

CHAPTER SIX

PARTICLE CONCENTRATION MEASUREMENT

6.1 Introduction

The objective of a particle size distribution (PSD) monitoring system, as demonstrated by Monscvitz et al. (1976), Ensor et al. (1987), Beard and Tanaka (1976), Tate and Trussell (1979) and Hutchinson and Johnson Control Inc. (1984), is to avoid the confusion of turbidity monitoring problem; the problem with turbidity is that variation in number and sizes of particles in different samples can produce the same turbidity result. The other objective was to control a filtration water treatment plant. To meet this objective involves the determination of coagulant dosage (an optimal filtration particle size that gives deep filter media penetration can be achieved); the use of a filter backwash to produce a water with the lowest possible number of particles; and the gathering of information on particle removal efficiency and mechanism within the filter media.

Another significant aspect is that PSD plays an important role in head loss development as different deposition modes are related to different particle sizes. All head loss models developed in this work are related directly to the particle size and particle size distribution.

Most research work in water and waste water filtration ignores the PSD of the filtered suspension. In this study, change in PSD over time and depth in a pilot-scale filter, mass of solids and the amount of specific deposit are carefully correlated to the head loss under different operational conditions.

6.2 Measurement Of Particle Size And Particle Size Distribution

Characterization of particles (flocs) which are irregular in shape, is usually made by analyzing the particle size and particle size distribution. The most common methods used in particle counting are manual counting via microscopic examination, electrical resistance counter (based on change in current flow as particles pass through an orifice placed between electrodes), light scattering and light obscuration procedures. In the present experimental program, a combination of two Hiac-Royco product sensors, the light scattering 346B (small floc sensor) and light obscuration CMH-150 (large floc sensor) were used. Two sensors are used because there is no single instrument that provide counts over the wide range of 0.5 μm to 150 μm. The CMH-150 sensor sizes particles passing through the sensing zone (150 μm $\times$ 1000 μm) and obstruct the path of the collimated light causing the power produced by a photodiode to decrease Figure (6.1). The Hiac/Royco model 346B laser sensor (Figure 6.2) measures the amount of low angle forward scattered (collection angle 12° - 42°, Sommer and Harrison, 1990) light refracted by an individual particle as it passes through the beam of a helium neon laser. The laser sensor is capable of sizing particles in the 0.45 to 25 μm range. The automated particle counting system requires a continuous supply of particle-free water for diluting samples, because the sensors maximum allowable particle concentration is 2500 particles/ml. Several dilution factors are required to accommodate samples containing suspended solids concentrations which range from a maximum of 30 mg/L in the filter influent to near zero mg/L in the effluent. Particle size distribution data necessary to investigate filter performance and the impact on head loss development are difficult to obtain as data quality is subject to uncertainty due to instrument related measurement error and systematic errors which is presented and discussed in Section 6.3.

Observation of large flocs shows that there are many channels with essentially zero initial concentrations, which indicate that detection of large and fragile flocs using light obscuration procedure might prove inaccurate because large fragile flocs could break down into smaller fragments. It is also possible that the beam may transmit light through the boundary of semi-transparent flocs. Other system related errors are discussed in detail in section 6.3. The CMH-150 sensor was used to size flocs in the range 3 μm to 150 μm. The response of light scattering, or light obscuration from suspended particles (flocs), is related not only to the particle size but to the relative refractive index and optical geometry. An optical particle counter assigns a particle size to an electrical signal based on calibration correlation between the electrical signal and standard polystyrene latex (PSL) spheres in water (Monscvitz and Rexing, 1983). An optical particle counter provides an equivalent diameter of the calibration spheres. Since the optical properties of contaminating particles are generally unknown, the particle size remains unknown and the equivalent PSL diameter is used to characterize particle size. This process demonstrates a certain difficulty in accurately measuring particle size and count and therefore requires the use of an additional technique conducted (Sections 6.4 and 6.6) in conjunction with light scattering and obscuration (to derive data for the lower and upper bounds of both 346B and CMH sensors, respectively, and to account for particle count and size correction). The magnitude particle count, and sizing error introduced by system uncertainty and measurement errors are presented and discussed in Sections 6.4 and 6.6, respectively.

6.3 Measurement Error

Particles that are regular in shape and possess the same properties of the particles used in calibrating the sensors can be used to demonstrate the accuracy of the measurement technique.

However, in filtration processes, particles involved are flocs and usually irregular in shape. Therefore, particle diameter are difficult to measure, because of experimental and sampling errors (random), and systematic errors (bias). Measurement errors are usually due to optical material constants, such as particle refractive index, that differ between the calibration material PSL and the material of the unknown particle size during the monitoring process. Different classes of particles depending on size distribution, density and surface characteristic, may scatter light differently and thus influence the measured size (Yu et al., 1985). This supports Alvin (1988) who explained that different composition or shape of particles may produce different output, even of the same size group.

Measurement of particles in highly concentrated samples, and concentration variability of particles (flocs) suffer from noise due to over-concentration (exceeding the sensors maximum allowable particle concentration, 2500 particles/mL) which inhibits a proper particle size analysis dilution system. The technical problems associated with the analyzers were addressed by Sommer (1990), who explained that the major factors causing the presently available instruments to fall short of the theoretical possible performance related to a number of sources of noise" including:

a. Light scattered by windows and other components of the liquid flow cell,

b. Fluctuation in the illumination intensity (laser noise),

c. Optical inhomogeneity in the fluid due to nonuniform temperature, concentration, or flow turbulence, and

d. Electrical noise in the photo detector and amplifier.

Variability of sample flow rates, and the occurrence of false counts due to superposition of noise and signal also contribute to variability of particle count. Another important aspect of error is sampling, the sample may or may not be representative of the entire particles size

distribution (0.5 μm-150 μm), which must be present, especially in the upper bound of the CMH sensor since the sample mass could be controlled by a small number of large particles. Although an automatic method used for sampling from a moving stream, many channels in the upper bound of the CMH sensor with zero concentration was observed.

Additional factors which may affect the particle concentration measurement are:

a. Use of screen (60 mesh) about 300 μm in square openings just before the sensors (to protect the sensor from blockage) eventually results in retaining and/or breaking down the flocs. The effect of sampling before and after the screen on particle volume sensed is shown in Figure (6.3). The presence of the screen show the same trend as for no screen. It is also observed that with screen the flocs (for size greater than 20 μm) tends to be retained and/or breaking down causing the particle volume sensed to be less.

b. Use of static mixer to obtain a homogeneous-diluted sample may result in break down of the flocs into smaller fragments.

c. Plumbing required for sample to flow from sampling ports to the analyzer, could affect the distribution. Flocs break-up as they flow through narrow tubes, pumps and elbows.

d. Use of a low flow rate, 4.8 mL/min to meet the counting capability limitation may result in some flocs settling and others attaching to the wall.

e. Air bubbles which count as flocs in the upper bound of the CMH channels.

f. Coincidence counting error, i.e., more than one particle/floc reach the aperture of the sensors at the same time, count as one larger particles than originally anticipated.

The magnitude of sizing and particle count error resulted, because of system and measurement deficiencies are examined and calculated in the next sections.

6.4 Particle Count Correction

Particle count efficiency is defined as the ratio between on-line particle data and the actual data. Efficiency is a function of both concentration and particle size assuming a constant flow rate (Peacock et al., 1986). The literature review of previous research reveals that particle size analyzers experienced difficulty and uncertainty in obtaining true particle counts.

Flocs have been described as a solid matrix comprised of primary particles/coagulant/coagulant aid enveloping water. The relative proportion of solids and water may be characterized by floc density (or effective density), floc porosity or floc void ratio. The density function yields a relationship between floc density and size characterized by a rapid decrease with increasing floc size followed by an asymptotic approach to a constant. The resulting floc density curve is shown in Figure (6.4).

Comparison of mass calculated using on-line data and a floc density function, Bucens (1991) with observed mass are shown in Table (6.1). Total mass calculations underestimate those observed for some experiments, while exceeding others over the entire filter run. Such a variation may be attributed to one or more of the mentioned factors in Section 6.3, which may affect the measurements. Floc density function were suggested, primarily by Tambo and Watanabe (1979),

$$\rho_e = \rho_f - \rho_w = \frac{a}{(d_i/1)^{K_p}}, \qquad (6.1)$$

where, ρ_e is the floc effective density (g cm^{-3}), d_i is the floc diameter (cm), $d_1/1$ is dimensionless floc diameter (cm/cm), and a and k_p are constants (g cm^{-3}) and (-), respectively.

Tambo and Watanabe (1979) and Li and Ganczarczyk (1987) investigated the floc density function, evaluating floc effective density based on Stokes settling velocity and measured the floc

dimension perpendicular to the direction of settling. Tambo and Watanabe (1979) examined biological, aluminium/clay, iron/clay, and magnesium/clay flocs, all of which yield data, over the measured size range (200 μm to 2000 μm), and which fit equation (6.1). The density relationships are, however, only applicable to mature flocs consisting of a "large" number of primary particles.

The floc density function presented by Tambo and Watanabe (1979) was adopted by Bucens (1991) to account for the increase in suspended volume with time. The equation was modified to yield parameters which were more amenable to physical interpretation as,

$$\rho_e^i = (\rho_f^i - \rho_w)$$

$$= (\rho_s - \rho_w)\ \theta_1 \left[\frac{\theta_3}{d_i}\right]^{(3-\theta_2)}, \qquad (6.2)$$

in which $\rho_e{}^i$ is the effective floc density of size i, $\rho_f{}^i$ is apparent floc density of size i, ρ_w and ρ_s is the density of water and solid respectively, θ_1 and θ_2 are the dimensionless model parameters, equal to 0.48 and 1.52, respectively, and θ_3 represent the characteristic size of the initial distribution (9.7×10^4 cm).

Adjustment to on-line data based on differences between observed and calculated concentration should include the whole size range of both 346B and CMH-150 sensors, or adjustment should be for a limited range. Determining, whether considering the whole size range (0.50 μm-150 μm) or limited size range in the adjustment processes was done, in part, by monitoring the pumping system (sampling and dilution pumps) for both first, and second stage pumps. Monitoring analysis results reveal that major adjustment is required due to flow rate variability. Tables (6.2A and B) illustrate that the required particle count adjustment differs for flow path and for different dilution factors. On-line sampling, dilution, analysis particle sizing

and counting system are presented in Figure (6.5). The figure indicates the different flow paths required to achieve dilution needed by the system. A difference in particle count adjustment was also observed over the filter run when the dilution factor is essentially constant.

Analysis results indicate that the coefficient of variation changes with flow rate. Also observed are that different dilution factors give different values with both the CMH sensor (dilution factors 1:1-1:50), and with the laser (346B). The variation coefficient of both sample and dilution pumps as well as the bias values, vary with different dilution schemes. Despite the fact that many channels with initially zero concentration are observed, analysis strongly supports the overall range adjustment. An estimate of mass required for particle count adjustment may be used to avoid over-complication of on-line data adjustment by using results shown in Table (6.2A and B). New mass is calculated from observed overall mass and mass obtained using unadjusted on-line data with the density function (Equation 6.2). The procedure is summarized by the following steps:

a. Calculate the mass (gram) in each port using the unadjusted on-line data with the density function for each corresponding size.

b. Calculate cumulative mass.

c. Plot cumulative mass versus log particle size. The data should be plotted accumulatively as a percentage of undersize or oversize. As these points lie on an actual distribution, a smooth curve may be drawn through them to obtain a continuous cumulative curve.

d. Derive curve slope at the tails. Slope at the upper tail should be behind any point which shows no incremental increase in mass or with initially zero concentration.

e. Recalculate mass at upper bound as follows:

$$(Cum\ Mass)_i=(Cum\ Mass)_{i-1}+Slope\times(logd_{P_i}-logd_{P_{i-1}}), \tag{6.3}$$

whereby the raw mass is recovered from the undetected channels.

f. By including values obtained in e., calculate overall cumulative mass over filter run.

g. Determine the difference in mass between observed and calculated in f. above.

h. Distribute mass differences over entire particle size range, according to percentage of each total mass size contribution as follows,

$$(C.C.\ Mass)_i=(C.\ Mass)_i+\frac{(C.\ Mass)_i}{(T.C.\ Mass)}\ (Mass\ Difference), \tag{6.4}$$

where C.C. Mass = corrected cumulative mass in grams

C. Mass = cumulative mass in grams

T.C. Mass = total cumulative mass.

i. Derive mass frequency

j. Calculate volume for each corresponding channel

$$(Volume)_i=\frac{(Mass\ Frequency)_i}{(Density)_i}. \tag{6.5}$$

k. Calculate corrected number per mL

$$(number/ml)=(volume)_i\ /\left[\pi\times dp_i^3\ \times10^{-9}\times V_o\times\frac{t}{6}\right]. \tag{6.6}$$

The quantitative and statistical measures described in the Verification of Correction section below was used to verify the correction procedure.

6.5 Verification Of Correction

Quantitative measures and statistical verifications are used to verify the correction approach. Quantative measures are comparing output of correction method with data obtained from different proposed head loss equations, in terms of specific deposit. Another quantative measure is comparison of the amount of dry silica retained between sieves with amount of equivalent particle size from corrected data. The correction method would be considered verified when comparison of calculated and observed values shows a relative improvement in percentage standard error, and a fair correlation between corrected and predicted data using different proposed equations and data obtained from sieving analysis.

6.5.1 Methods Of Validation

The validity of the proposed correction approach for particle concentration was tested using two different methods for validation. First, the predicted histories of specific deposit were compared with the corrected values. Several head loss equations for depth filtration were used for the calculation. Equations proposed by Camp (1964), Mackrle (1965), Mohanka (1969), Shektman (1961) and Pendse (1978) are used. The parameter p in Mackrie (1965) and Mohanka (1969) head loss equation are not adjusted for the new experimental conditions. Specific deposit is predicted at the first layer (14 cm depth) according to these following equations:

Camp equation:

$$\left[\frac{H}{H_o}\right] = \left[1+\frac{\sigma}{(1-\varepsilon_o)}\right]^{4/3} \left[1-\frac{\sigma}{\varepsilon_o}\right]^{-3}. \qquad (6.7)$$

Mackrle equation:

$$\left[\frac{H}{H_o}\right] = \left[1+\frac{p\sigma}{\varepsilon_o}\right]^3 \left[1-\frac{\sigma}{\varepsilon_o}\right]^{3/2}. \tag{6.8}$$

Mohanka equation:

$$\left[\frac{H}{H_o}\right] = \left[1+\frac{p\sigma}{\varepsilon_o}\right]^2 \left[1-\frac{\sigma}{\varepsilon_o}\right], \tag{6.9}$$

in which

$$p = \frac{29}{S^{0.65}} = 9.05\left[\frac{\Psi d}{1-\varepsilon_o}\right]^{0.65}. \tag{6.10}$$

Shektman equation (Adin and Rajogopalan, 1989):

$$\left[\frac{H}{H_o}\right] = \left[1-\left[\frac{\sigma}{\varepsilon_o}\right]^{1/2}\right]^{-3}. \tag{6.11}$$

Pendse equation:

$$\left[\frac{H}{H_o}\right] = \left[1+\frac{\sigma}{(1-\varepsilon_o)(1-\varepsilon_d)}\right]^{4/3}\left[1-\frac{\sigma}{\varepsilon_o(1-\varepsilon_d)}\right]^{-3}. \tag{6.12}$$

The calculated values of deposit from head loss equations for different head loss ratio (H/H_o) with the corrected values are shown in Table (6.3). The comparison in Table (6.3) indicates that this approach is feasible. Different operating conditions are used for comparison. Stable and destabilized suspension using ferric chloride with different filtration velocities, are investigated. For the different velocities used, Camp's equation gives lower head loss ratio for

the same amount of deposit as shown in Figures (6.6) through (6.8). Mackrle and Pendse's equations give relationships that over predict head loss compared to experimental data. The results of Mohanka and Shektman tend to fall between the other equations.

The second qualitative measure used for validation is the comparison of a dry silica powder mass with that obtained from a stable suspension run (no aid). Amount of silica used in the sieve analysis is approximately 36 gram. The sieves (Endecotts Ltd., England) comprised the following apertures 150, 106, 75, 53, 45 and 38 μm, with geometric parameter equivalent to 126.1, 89.1, 63.0, 48.8 and 41.3 μm, respectively. The percentage amount of dry silica retained between two apertures is compared to the observed amount of equivalent particle size for stable suspension experiment. Silica particles are dried using an oven at 105 °C for several hours before use. A combination of judgment and graphical analysis is used to assess the adequacy of fit between sieved and corrected amount. From Figures (6.9 and 6.10) it is apparent that most data points fit close with corrected value.

Wire Mesh Series ASTM E11:81

Designation		Tyler Equivalent Designation
Standard, μm	Alternative	
150	No. 100	100 mesh
106	No. 140	150 mesh
75	No. 200	200 mesh
53	No. 270	270 mesh
45	No. 325	325 mesh
38	No. 400	400 mesh

Although the above-mentioned methods can be a graphical measure of the correction feasibility, statistical comparison may be necessary to provide further understanding of this approach as outlined in the next item.

6.5.2 Statistical Verification

A variety of simple statistic comparisons are appropriate to quantify correction verification status. Such measures are intended to supplement the qualitative comparisons discussed in the preceding section. Different tests were used to compare predicted with corrected amount of specific deposit and particle concentration. Correlation coefficients and the percentage standard error shown in Figures (6.11) through (6.13), are fair (range between 0.79-to-0.85). The percentage standard error shown in Figures (6.14) through (6.18), illustrates that the higher percentage standard error is associated with the large particles ($> 10\ \mu m$), this may be related to the existence of air bubbles and coincidence counting error, which may affect the measurement. Figures (6.14) through (6.18) give clear indication that the correction approach is appropriate as the percentage relative standard error values was reduced to less than 10 percent, compared to approximately 100 percent for the raw data. The quantitative, comparison of raw and corrected particle concentration and percentage standard error are included in Tables (6.4) through (6.9). These tables comprise data sets for three experiments, including both Laser and CMH sensors with different filtration velocities.

6.6 Particle Size Correction

Optical particle counters measure light scattered by individual particles passing through a small sensing volume. A photo detector collects and converts the scattered light into an

electrical pulse which is processed by counter electronics. The amplitude of the pulse generated depends on particle size, with larger pulses indicative of larger particles (Peacock et al., 1986). Study of published literature shows that signals generated by Laser and CMH sensors from suspended particles are related to the particle size and the relative refractive index and optical geometry. The true size remains unknown because the calibration correlation between electrical signal and standard polystyrene latex (PSL) spheres in water are assumed to be equivalent to the signal generated by flocs which have different surface characteristics (Sommer et al., 1990).

Giardia cysts added to the water are "seen" by FALS (Forward Angle Light Scattered) as equivalent in size to spheres of 1-5 μm in diameter which is considerably smaller than the 8-12 μm measured by optical microscopy techniques (Lewis et al., 1991). Lieberman (1988) wrote:

> "The actual size may have a different size (typically up to 30 percent) and may not be a sphere".

During the development of an automated particle counting system for filter monitoring, the results from an analysis of standard test spheres of 19.1 μm mean diameter taken with the CMH-150 sensor appear to underestimate true size by approximately 20 percent, Wood (1988). There is insufficient information available to correct the particle size measurement for the silica used in the experiments. Min-U-Sil (silica) has a different refractive index from PSL. In this work, each sensor type is challenged with two different PSL size ranges, 0.691 and 1.63 μm for Laser range, 8 and 19.1 μm for CMH to define sizing efficiencies of small and large particles. The results are shown in Table (6.10) as a cumulative percentage undersize versus different form of abscissae, i.e, d_p, d_p^2 and $\log d_p$. Various forms of mean diameters were evaluated graphically in different ways. The first and second methods are the ones quoted in Svarovsky (1990), where a mean diameter can be defined by using the general form,

$$g(\bar{x}) = \int_0^{\infty} g(x)\, f(x)\, d(x) = \int_0^{1} g(x)\, dF, \tag{6.13}$$

where f(x) is a particle size distribution frequency and g(x) is a certain function of particle size x.

$$\int f(x)\, dx = F(x). \tag{6.14}$$

Depending on the form of this function, several types of mean diameters x can be predicted as shown in Table (6.11). If the cumulative percentage distribution F(x), is plotted against g(x) for the corresponding size, $g(\bar{x})$ is then represented by the area under the curve with respect to the F(x) axis. The mean evaluated from this area using the corresponding equation for g(x) are presented in Table (6.11). Table (6.10) and Figure (6.19) are examples of such graphical evaluation of $\bar{x}_a$, $\bar{x}_q$, and $\bar{x}_g$. As example, the evaluation of the arithmetic mean $\bar{x}_a$ for 19.1 μm, F(x) is plotted against x and the area measured, giving $g(\bar{x}_a)=\bar{x}_a=16.28\ \mu$m. The quadratic mean $\bar{x}_q$ is determined from a plot of F(x) against x^2; the area is $g(\bar{x}_q)=\bar{x}_q{}^2=(16.53)^2\ \mu m^2$ thus $\bar{x}_q=16.53\ \mu$m. Similarly, the geometric mean $\bar{x}_q$ may be calculated from the corresponding area on the plot of F(x) against log(x) giving $\bar{x}_q=$ μm. The second method is based on the modified log normal distribution equation given by Svarovsky (1990).

$$dF(x) = A\ \exp\left[-b \ln^2 \frac{x}{x_m}\right] dx, \tag{6.15}$$

where

$$A = \left[\frac{b}{\pi}\right]^{1/2} \frac{\exp\left[\frac{-1}{4b}\right]}{x_m}, \tag{6.16}$$

and b is a new parameter called the steepness constant, and replaces σ_g:

$$b = \frac{1}{2\ln^2\sigma_g}, \tag{6.17}$$

The relationship between the mode and the median were assumed to take the form:

$$x_m = c\, x_g$$

where

$$c = \exp\left[\frac{-1}{2b}\right]. \tag{6.18}$$

Evaluation of the two parameters x_m and b in equation (6.15), may be determined from the plot of percentage log F(x) versus log d_p as the median size $x_{50}=x_g$ and σ_g is the ratio of the 84% size to the 50% size. The mode x_m and various mean diameter can then be determined.

$$x_m = cx_g; \quad x_a = c^{-1/2}x_g; \quad x_q = c^{-1}x_g \quad x_c = c^{-3/2}x_g; \quad x_h = c^{1/2}x_g. \tag{6.19}$$

The third method of particle diameter evaluation uses the arithmetic number average

$$D_p = \frac{\sum N_i \times D_{p_i}}{\sum N_i}. \tag{6.20}$$

The fourth method of evaluation uses the geometric mean (logarithmic) which is the same equation used by PSL particle manufacturer (Duke Scientific Corporation, 1986).

$$D_p = antilog \frac{\sum N_i \ln D_{p_i}}{\sum N_i}. \tag{6.21}$$

Finally, the fifth method of evaluation is the logarithmic number average

$$D_p = antilog \frac{\sum \log N_i \log D_{p_i}}{\sum \log N_i}. \tag{6.22}$$

Table (6.12) shows the results of various mean diameters obtained using the above mentioned methods labelled A, B, C, D and E, with the percentage instrument related measurement error for each standard PSL particle. Overall, percentage error may be considered as 10 percent (underestimate) for both 346B and CMH-150 sensors.

In summary, this chapter presented a number of methods to calculate the average diameter and explained sources of error associated with either the particle size analyzer and/or with the system. The chapter described how to evaluate and correct some of these errors. A method of quantifying the percentage error in laser and CMH channels is also presented. Setting the procedure to correct the number concentration supported with quantitative and qualitative validation is provided. This chapter also describes how to implement a statistical test to describe and evaluate the correction procedure for different sets of stable and destabilized suspension.

Experiment Number	Coagulant Type (Size), micrometer	Cumulative Mass, gram			
		Obser.	Calculated		
		Total	Total	346B	CMH
200,371 @	No Aid (5)	285.0	1130.8	83.77	1047
200,16 #	No Aid (5)	506.9	858.8	430.5	428.3
200,372 $	No Aid (5)	820.1	4775.8		
200,15 #	No Aid (30)	510.28	1252.4	357.68	894.7
200,263 @	Fe^{+3} (5)	263.33	155.22	10.79	144.4
200,01 #	Fe^{+3} (5)	410.0	428.75	216.1	212.6
200,315 $	Fe^{+3} (5)	793.5	517.85	20.61	497.2
200,261 @	Fe^{+3} (30)	270.9	368.5	26.70	341.8
200,02 #	Fe^{+3} (30)	400.0	603.2	81.66	521.5
200,346 $	Fe^{+3} (30)	737.4	771.12	93.2	677.9
200,325 @@	Fe^{+3} (30)	479.0	524.4	64.26	460.1

Table 6.1 **Comparison between observed mass and calculated mass using on-line data and density function.**
Key: (@) represent experiments with 15 mg Si/L, Vo=0.3 cm/s; (#) represent experiments with 15 mg Si/L, Vo=0.6 cm/s; ($) represent experiments with 15 mg Si/L, Vo=0.9 L/cm/s; (@@) represent experiments with 30 mg Si/L, Vo=0.3 cm/s

Table (6.2A) Sample dilution system data analysis.

Time Hour	Ist Stage Pump ml/min #2(2,25)	2nd Stage Pump ml/min #4(4,28)	Ist Satge Sample Pump Pump #1 (4,27)			2nd Stage Sample Pump Pump #3 (4,26)			Laser Pump (2,24)	CMH-150 Pump (2,24)	CMH Sampl Pump (2,26)
			6	7	8	6	7	8			
			16.7	9.7	4.8	15	4.8	4.8			
13:00	493	457	17	9.7	4.8	15	5.2	5.2	40	42	8.5
14:00	493	460	17	9.7	4.8	15.5	5.2	5.2	45	42.5	8.8
14:45	488	455	17	10	4.8	15.5	5.2	5.2	45	43	8.8
20:00	493	467	17.5	9.7	5	16	5.6	5.2	45	44.5	8.8
09:30	497	457	17.5	10	5	16	6	6	45	45	8.7
10:00	500	467	17	9.7	5	16	6	6	44.5	45.5	8.5
10:30	495	465	17	10	5	16	5.8	6	44.5	46	8.8
19:30	493	475	17	10	5	16	5.8	6	39.3	45.5	8.9
11:35	495	485	17	9.8	5	16	5.6	5.3	38.5	45	8.6
12:00	485	480	17	9.8	4.9	16	5.7	5.7	39	45	8.9
12:30	490	482	16.7	9.8	4.8	16	5.7	5.7	39	44.5	8.7
Actual Value	483	485	16.7	9.7	4.8	15	4.8	4.8	40	40	8
Average	492.9	469.1	17.06	9.83	4.92	15.82	5.62	5.6	42.25	44.41	8.727
Variance	17.09	103.09	0.054	0.019	0.009	0.113	0.089	0.14	8.932	1.741	0.02
Std Deviation	4.13	10.153	0.232	0.136	0.0948	0.336	0.298	0.37	2.988	1.319	0.141
C.V.	0.837	2.164	1.36	1.391	1.926	2.123	5.302	6.66	7.072	2.97	1.615
Sum R^2	170.91	1030.91	0.545	0.187	0.096	1.136	0.896	1.39	89.32	17.41	0.201
95% C.I L.L	484.8	499.2	16.605	9.562	4.734	15.161	5.035	4.87	36.393	41.824	8.45
95% C.I U.L	501	489	17.514	10.098	5.105	16.478	6.204	6.33	48.106	46.995	9

Table (6.2B) Combined sample system data analysis (different dilution factor).

CMH-150 Sensor

Dilution Factor	Pump No.	Std. Dev.	C.V.	Bias
1:1	2,24	1.32	2.97	4.41
1:5	2,24	1.32	2.97	4.41
	2,26	0.142	1.615	0.227
1:30	2,24	1.32	2.97	4.41
	2,25	4.13	0.837	9.9
	4,27	0.233	1.36	0.36
1:50	2,24	1.32	2.97	4.41
	2,25	4.13	0.837	9.9
	4,27	0.136	1.391	0.13

Laser Sensor (CMH-150 dilution actor=1:1)

Dilution Factor	Pump No.	Std. Dev.	C.V.	Bias
1:30	2,24	2.988	7.072	2.25
	2,25	4.13	0.837	9.9
	4,27	0.233	1.36	0.36
1:50	2,24	2.988	7.072	2.25
	2,25	4.13	0.837	9.9
	4,27	0.136	1.391	0.13

Laser Sensor (CMH-150 dilution ctor=1:5)

Pump No.	Std. Dev.	C.V.	Bias
2,24	2.988	7.072	2.25
2,25	4.13	0.837	9.9
2,26	0.141	1.615	0.727
4,27	0.233	1.36	0.36
2,24	2.988	7.072	2.25
2,25	4.13	0.837	9.9
2,26	0.141	1.615	0.727
4,27	1.36	1.391	1.3

Table (6.2B) (cont.)

Laser Sensor (CMH-150 dilution factor = 1:1)

Dilution Factor	Pump No.	Standard Deviation	C.V.	Bias
1:100	2,24	2.988	7.072	2.25
	2,25	4.13	0.837	9.9
	4,27	0.0948	1.926	0.12
1:1000	2,24	2.988	7.072	2.25
	2,25	4.13	0.837	9.9
	4,26	0.336	2.123	0.82
	4,27	0.233	1.36	0.36
	4,28	10.153	2.164	-15.9
1:5000	2,24	2.988	7.072	2.25
	2,25	4.13	0.837	9.9
	4,26	0.298	5.302	0.82
	4,27	0.136	1.391	0.13
	4,28	10.153	2.164	-15.9
1:10000	2,24	2.988	7.072	2.25
	2,25	4.13	0.837	9.9
	4,26	0.0948	6.658	0.8
	4,27	0.373	1.926	0.12
	4,28	10.153	2.164	-15.9

Laser Sensor (CMH-150 dilution factor=1:5)

Pump No.	Standard Deviation	C.V.	Bias
2,24	2.988	7.072	2.25
2,25	4.13	0.837	9.9
2,26	0.141	1.615	0.727
4,27	0.0948	1.926	1.2
2,24	2.988	7.072	2.25
2,25	4.13	0.837	9.9
2,26	0.141	1.615	0.727
4,26	0.336	2.123	0.82
4,27	0.233	1.36	0.36
4,28	10.153	2.164	-15.9
2,24	2.988	7.072	2.25
2,25	4.13	0.837	9.9
2,26	0.141	1.615	0.727
4,26	0.298	5.302	0.82
4,27	0.136	1.391	0.13
4,28	10.153	2.164	-15.9
2,24	2.988	7.072	2.25
2,25	4.13	0.837	9.9
2,26	0.141	1.615	0.727
4,26	0.0948	6.658	0.8
4,27	0.373	1.926	0.12
4,28	10.153	2.164	-15.9

Table (6.2B) (cont.)

Laser Sensor (CMH dilutor= 1:30)

Dilution Factor	Pump No .	Std. Dev.	C.V.	Bias
1:3000	2,24	2.988	7.072	2.25
	2,25	4.13	0.837	9.9
	4,26	0.298	5.302	0.82
	4,27	0.232	1.36	0.36
	4,28	10.153	2.164	-15.9

Laser Sensor (CMH dilution factor= 1:50)

Dilution Factor	Pump No.	Std. Dev.	C.V.	Bias
1:5000	2,24	2.988	7.072	2.25
	2,25	4.13	0.837	9.9
	4,26	0.298	5.302	0.82
	4,27	0.136	1.391	0.13
	4,28	10.153	2.164	-15.9

Table (6.3) Summary of experimental data for correction approach in determining specific deposit

(H/Ho)	Observed	Theoretical Amount of deposit					
		Mackrle	Camp	Mohanka	Shektman	Pendse	Average
A: Fe+3, 5 um 15 mg Si/l, V_0 = 0.3 cm/s)							
1	0	0	0	0	0	0	0
1.25	0.003833	0.001934	0.02357	0.003159	0.002205	0.004007	0.006975
1.5	0.007452	0.003617	0.042235	0.006036	0.006859	0.00718	0.0131854
1.75	0.011072	0.005117	0.057581	0.00867	0.01243	0.009789	0.0187174
2	0.014446	0.006475	0.070543	0.011196	0.018268	0.011997	0.0236958
2.5	0.021849	0.008872	0.0915	0.015799	0.029735	0.015555	0.0322922
3	0.027974	0.010957	0.107961	0.02	0.040364	0.018353	0.039527
B: Fe+3, 5 um 15 mg Si/l, V_0 = 0.6 cm/s)							
1	0	0	0	0	0	0	0
1.25	0.001814	0.001934	0.02357	0.003159	0.002205	0.004007	0.006975
1.5	0.005141	0.003617	0.042235	0.006036	0.006859	0.00718	0.0131854
1.75	0.008774	0.005117	0.057581	0.00867	0.01243	0.009789	0.0187174
2	0.010264	0.006475	0.070543	0.011196	0.018268	0.011997	0.0236958
2.5	0.014888	0.008872	0.0915	0.015799	0.029735	0.015555	0.0322922
3	0.018284	0.010957	0.107961	0.02	0.040364	0.018353	0.039527
3.5	0.021635	0.012724	0.1203345	0.0238	0.049575	0.019496	0.0451859
4	0.024485	0.014491	0.132708	0.0276	0.058786	0.020639	0.0508448
4.5	0.0272	0.015971	0.1599525	0.031012	0.0664	0.0215995	0.058987
C: Fe+3, 5 um 15 mg Si/l, V_0 = 0.9 cm/s)							
1	0	0	0	0	0	0	0
1.25	0.003985	0.001934	0.02357	0.003159	0.002205	0.004007	0.006975
1.5	0.008517	0.003617	0.042235	0.006036	0.006859	0.00718	0.0131854
1.75	0.013636	0.005117	0.057581	0.00867	0.01243	0.009789	0.0187174
2	0.019054	0.006475	0.070543	0.011196	0.018268	0.011997	0.0236958
2.5	0.026463	0.008872	0.0915	0.015799	0.029735	0.015555	0.0322922
3	0.041001	0.010957	0.107961	0.02	0.040364	0.018353	0.039527
3.5	0.052101	0.012724	0.1203345	0.0238	0.049575	0.019496	0.0451859
4	0.062919	0.014491	0.132708	0.0276	0.058786	0.020639	0.0508448
4.5	0.080092	0.015971	0.1599525	0.031012	0.0664	0.0215995	0.058987

Table (6.4) Comparison of particle concentration and standard error percentage of raw and corrected data.

Concentration corrected from a 5 μm suspension destabilized with 0.25 mg Fe^{+3}/L, using 15 mg Si/L, and Vo=0.3 cm/s

Particle Size, μm (346B)	Average Concentration Number/ml		% Standard Error	
	Raw	Corrected	Raw	Corrected
0.528	38892.35	1666812.01	12.35	4.68
0.5885	39732.27	104059.04	12.31	8.71
0.6325	51181.42	134008.47	12.68	9.42
0.6655	34961.26	91441.47	12.65	9.74
0.6985	13649.45	35685.48	13.22	10.08
0.7315	24325.58	63844.63	12.91	10.48
0.7645	18741.68	49105.94	13.21	10.98
0.7975	17337.28	45500.02	13.51	11.26
0.847	30693.37	80503.15	13.15	10.98
0.935	47990.26	125728.11	13.74	11.42
1.0725	40832.83	106551.63	14.30	11.82
1.21	4528.64	11810.99	14.45	11.73
1.3475	3397.72	8890.74	14.42	11.32
1.5125	4086.87	10641.07	12.71	10.41
1.7325	2892.79	7418.31	14.31	11.22
2.0075	6987.91	17999.83	12.73	9.83
2.4475	3209.17	8240.02	14.43	8.38
3.1075	2159.17	5512.06	16.98	5.51

Table (6.5) Comparison of particle concentration and standard error percentage of raw and corrected data.

Concentration corrected from a 5 μm suspension destabilized with 0.25 mg Fe^{+3}/L, using 15 mg Si/L, and Vo=0.3 cm/s

Particle Size, μm (CMH150)	Average Concentration Number/ml		% Standard Error	
	Raw	Corrected	Raw	Corrected
3.96	8109.93	20054.11	2.36	1.81
4.675	6794.53	16782.30	2.57	1.82
5.5	3993.44	9832.79	2.86	1.87
6.49	1566.52	3848.94	3.41	1.96
7.645	736.49	1800.19	5.01	2.11
9.02	249.61	602.98	9.08	2.91
10.67	140.05	335.12	12.41	3.75
12.65	90.26	216.83	13.82	4.27
14.85	62.92	150.16	16.61	5.22
17.49	40.67	96.95	16.41	4.74
20.68	26.11	62.09	16.58	4.53
24.42	20.14	47.81	18.68	4.89
28.82	10.61	25.38	17.14	5.13
34.1	4.91	12.34	22.43	5.04
40.15	2.31	7.63	30.48	6.09
47.3	0.58	4.28	47.94	4.17
56.1	0.59	2.83	35.97	5.47
66	0.06	1.68	83.58	5.06
77.77	0	1.05		5.06
91.85	0	0.65		5.06
108.35	0	0.41		5.06
127.6	1.06	0.24	18.86	5.06
150.7	1.44	0.15	15.46	5.06

Table (6.6) Comparison of particle concentration and standard error percentage of raw and corrected data.

Concentration corrected from a 5 μm suspension destabilized with 0.25 mg Fe^{+3}/L, using 15 mg Si/L, and 0.6 cm/s

Particle Size, μm (346B)	Average Concentration Number/ml		% Standard Error	
	Raw	Corrected	Raw	Corrected
0.528	1882571.	9989258.	21.58	9.31
0.5885	947437.9	389035.7	26.55	4.86
0.6325	725389.0	451036.5	26.74	12.03
0.6655	475314.7	437762.5	24.82	12.71
0.6985	398931.8	382414.4	14.98	8.93
0.7315	314706.9	311280.9	2.72	4.94
0.7645	300150.2	299069.4	2.07	4.71
0.7975	272484.8	271906.7	1.95	4.44
0.847	248138.1	247588.2	2.06	4.68
0.935	213547.2	213290.0	2.01	4.61
1.0725	175167.1	175851.5	2.04	4.52
1.21	143599.0	144687.0	2.01	4.38
1.3475	101685.5	102314.2	2.02	4.32
1.5125	70598.3	71019.6	2.04	4.16
1.7325	49974.2	50171.7	2.14	4.44
2.0075	34348.4	34607.7	2.18	4.42
2.4475	19469.5	19503.5	2.47	4.21
3.1075	10493.4	10644.2	3.08	4.79

Table (6.7) Comparison of particle concentration and standard error percentage of raw and corrected data.

Concentration corrected from a 5 μm suspension destabilized with 0.25 mg Fe^{+3}/L, using 15 mg Si/L, and Vo=0.6 cm/s

Particle Size, μm (CMH150)	Average Concentration Number/ml		% Standard Error	
	Raw	Corrected	Raw	Corrected
3.96	6743.84	6315.21	7.17	6.06
4.675	6002.55	5742.83	7.45	5.84
5.5	3526.61	3399.83	7.28	5.34
6.49	1547.51	1518.47	6.53	4.28
7.645	877.04	892.11	5.82	4.11
9.02	479.19	518.16	13.30	10.64
10.67	390.52	435.96	19.38	15.08
12.65	230.06	252.57	18.32	14.71
14.85	95.25	97.59	9.87	8.49
17.49	47.76	47.29	4.71	3.08
20.68	29.65	29.14	5.93	3.71
24.42	19.71	19.22	7.02	4.48
28.82	11.83	11.34	8.99	4.77
34.1	8.98	8.53	11.46	7.52
40.15	3.59	3.37	12.39	5.91
47.3	2.21	2.09	15.51	5.84
56.1	0.97	1.02	22.81	6.22
66	0.49	0.74	36.10	5.87
77.77	0.31	0.51	33.81	7.11
91.85	0.22	0.39	69.05	11.28
108.35	0.04	0.19	93.37	5.59
127.6	0.33	0.14	33.27	9.96
150.7	0.25	0.08	38.81	7.53

Table (6.8) Comparison of particle concentration and standard error percentage of raw and corrected data.

Concentration corrected from a 5 μm suspension destabilized with 0.25 mg Fe^{+3}/L, using 15 mg Si/L, and Vo=0.9 cm/s

Particle Size, μm (346B)	Average Concentration Number/ml		% Standard Error	
	Raw	Corrected	Raw	Corrected
0.528	57334.21	1771950.	18.89	7.91
0.5885	23737.34	35907.58	18.45	6.43
0.6325	10941.57	15915.66	14.83	5.97
0.6655	14363.36	20936.06	15.52	6.92
0.6985	16468.20	23798.56	15.02	6.91
0.7315	13745.74	20049.46	15.48	6.56
0.7645	18240.61	26896.67	17.06	6.42
0.7975	6226.05	9299.93	21.37	6.94
0.847	8196.52	12464.44	24.54	8.14
0.935	6025.67	9049.71	27.23	8.83
1.0725	5218.82	7847.81	27.33	9.06
1.21	4454.31	6632.57	26.94	8.81
1.3475	4000.93	6050.55	26.41	8.89
1.5125	3454.23	5159.71	28.47	9.61
1.7325	2102.21	3131.32	26.60	8.73
2.0075	1901.22	2842.52	26.95	9.19
2.4475	979.72	1456.51	28.04	9.29
3.1075	705.05	1045.61	26.11	8.56

Table (6.9) Comparison of particle concentration and standard error percentage of raw and corrected data.

Concentration corrected from a 5 μm suspension destabilized with 0.25 mg Fe^{+3}/L, using 15 mg Si/L, and Vo=0.9 cm/s

Particle Size, μm (CMH150)	Average Concentration Number/ml		% Standard Error	
	Raw	Corrected	Raw	Corrected
3.96	11529	16942	2.85	2.43
4.675	8741.97	12883	2.76	2.72
5.5	4905.62	7222.47	2.92	2.93
6.49	1851.63	2713.82	4.25	3.03
7.645	854.43	1235.89	8.81	3.32
9.02	313.21	439.41	18.31	5.41
10.67	204.31	281.31	25.17	6.83
12.65	134.68	182.22	30.52	8.19
14.85	100.95	135.95	32.28	8.91
17.49	81.87	110.44	31.07	8.38
20.68	55.55	74.21	29.46	7.61
24.42	41.39	60.09	23.19	5.28
28.82	37.51	51.06	17.21	3.55
34.1	31.78	45.03	10.38	3.81
40.15	22.23	31.63	9.15	3.47
47.3	14.22	20.35	9.23	3.48
56.1	4.91	7.33	11.71	4.68
66	0.98	1.95	21.98	10.17
77.77	0.42	1.87	38.56	5.42
91.85	0.14	1.09	61.63	6.08
108.35	0.28	0.71	37.77	5.92
127.6	0.71	0.42	19.93	5.71
150.7	0	0.26		5.71

Table (6.10) Experimental analysis of particle size

a. Standard Size=0.691 μm (laser, 346B)

Cumulative % Undersize	Particle Size	X^2	Log x
16.62338	0.535	0.286225	-0.27165
25.19481	0.575	0.330625	-0.24033
34.80519	0.605	0.33602	-0.21824
45.4545	0.635	0.40322	-0.19723
59.2207	0.665	0.44222	-0.17718
83.37662	0.695	0.483025	-0.15802
91.68831	0.725	0.525625	-0.13966
100	0.77	0.5929	-0.11351

b. Standard Size=1.63 μm (laser, 346B)

1.608969	1.1	1.21	0.041392
7.983876	1.22	1.4884	0.086359
70.09348	1.38	1.9044	0.139879
94.39401	1.58	2.4964	0.198657
97.72373	1.83	3.3489	0.262451
99.38012	2.22	4.9284	0.346352
100	2.82	7.9524	0.450249

Table (6.10) Continued

c. Standard Size=8 μm (CMH-150)

Cumulative % Undersize	Particle Size, micrometer	X^2	Log x
0.498613	3.6	12.96	0.5563
1.733497	4.25	18.0625	0.628389
6.92	5.0	25	0.69897
23.96	5.9	34.81	0.770852
69.314	6.95	48.30	0.841985
90.878	8.20	67.24	0.913814
97.32	9.7	94.09	0.986772
99.7	11.5	132.25	1.060698
100	13.5	182.25	1.130

Table (6.10) Continued

d. Standard Size=19.1 μm (CMH-150)

Cumulative % Undersize	Particle Size	X^2	Log x
0.281452	17.11	292.75	1.23325
0.576977	17.32	299.98	1.238548
0.956938	17.53	307.3	1.243782
2.040529	17.74	314.7	1.248954
4.03884	17.95	322.2	1.254064
8.865747	18.17	330.14	1.259355
18.73065	18.39	338.19	1.264582
35.80073	18.61	346.33	1.269746
63.94596	18.83	354.56	1.27485
90.06473	19.06	363.28	1.280123
97.14326	19.29	372.10	1.285332
99.04306	19.52	381.03	1.29048
99.7	19.76	390.45	1.2957
100	20	400	1.301

Table (6.11) Type of mean diameter*

Form of g(x)	Name of Mean Diameter x
$g(x) = x$	Arithmetic mean, $\overline{X}_a$ Arithmetic mean, $\overline{X}_a$
$g(x) = x^2$	Quadratic mean, $\overline{X}_q$
$g(x) = x^3$	Cubic mean, $\overline{X}_c$
$g(x) = \log x$	Geometric mean, $\overline{X}_g$
$g(x) = 1/x$	Harmonic mean, $\overline{X}_h$

*** Extracted from Svarovsky (1990).**

Table (6.12) Instrument-Related measurement error (%undersize actual flocs)

	Standard Particle Size, μm	0.691	1.63	8.0	19.1
A	$\overline{X}g$	0.630 (8.8)	1.467 (10)	7.2 (10)	17.34 (9.2)
	$\overline{X}a$	0.633 (8.4)	1.475 (9.5)	7.231 (9.6)	17.348 (9.1)
	$\overline{X}q$	0.637 (7.8)	1.484 (9.0)	7.262 (9.2)	17.357 (9.1)
	$\overline{X}h$	0.626 (9.4)	1.4577 (10.5)	7.168 (10.4)	17.33 (9.2)
B	Xa	0.60 (13.0)	1.385 (15.0)	6.70 (16.2)	16.28 (14.7)
	Xq	0.58 (16.0)	1.346 (17.0)	6.71 (16.1)	16.53 (13.4)
C	Dp	0.633 (8.4)	1.353 (17.0)	7.06 (11.7)	17.62 (7.7)
D	Arithma. Number Average	0.64 (7.4)	1.36 (16.5)	7.19 (10.1)	17.35 (9.1)
E	Logarith Number Average		1.385 (15.0)	6.97 (12.8)	17.228 (9.8)

Where

A Different types of mean diameter X are derived using log probability paper (Cumulative percentage undersize versus particle size).

B Arithmetic, geometric and quadratic means are evaluated graphically using the cumulative distribution plot.

C Weighting by number: The mean determined using the same equation used by PSL manufacturer (Duke Scientific Corporation):

$$\ln D_{P_g} = \frac{\sum N_i \ln D_{P_i}}{\sum N_i}.$$

D Arithmetic number average:

$$D_p = \frac{\sum N_i D_{P_i}}{\sum N_i}.$$

E Logarithmic number average:

$$Log D_p = \frac{\sum Log N_i Log D_{P_i}}{\sum Log N_i}.$$

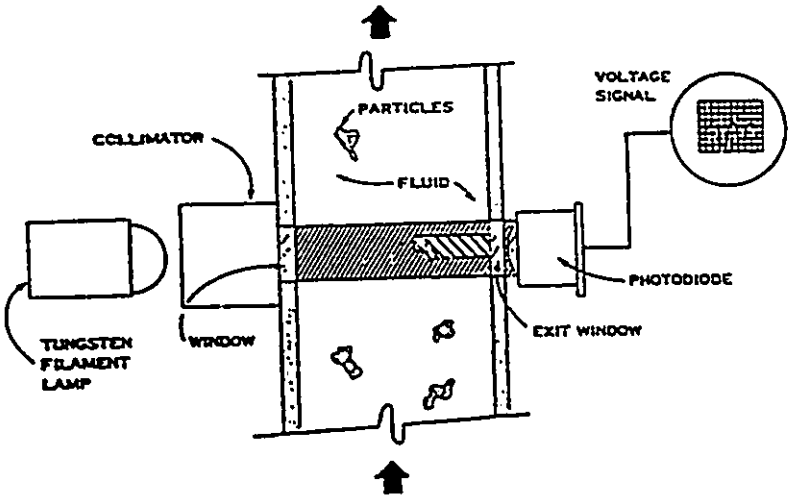

Figure 6.1 CMH-150 light occlusion sensor (extracted from Sommer, 1990)

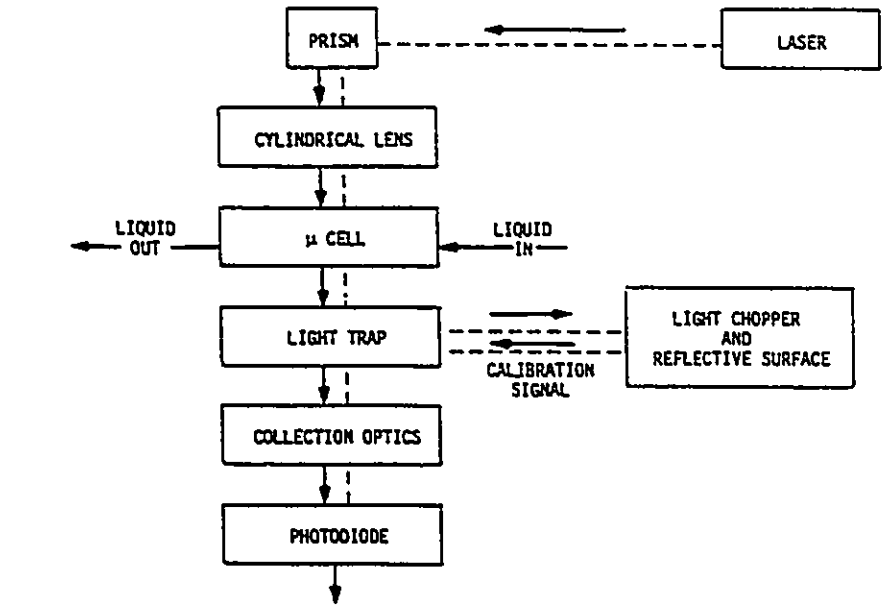

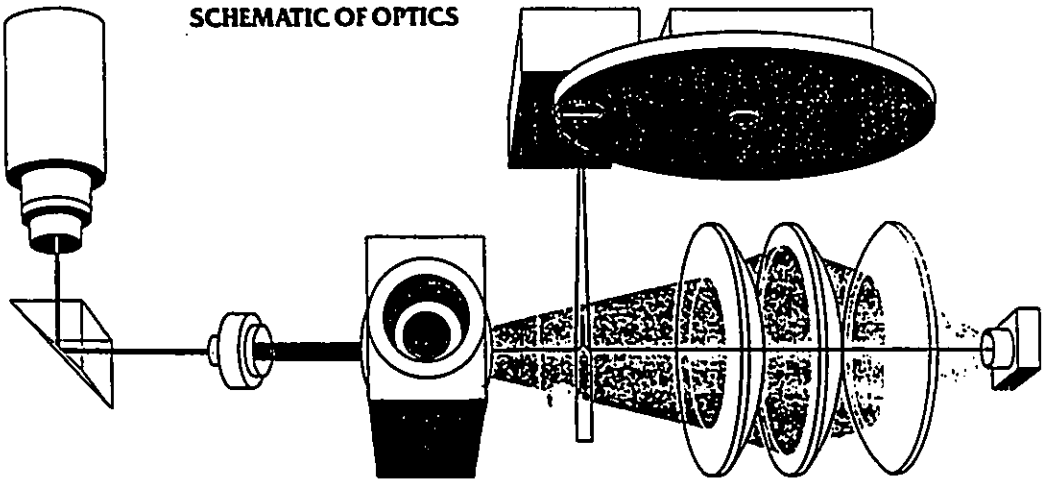

Figure 6.2 345B Near Forward Laser Scatter Sensor (Extracted from Hiac-Royco Brochures).

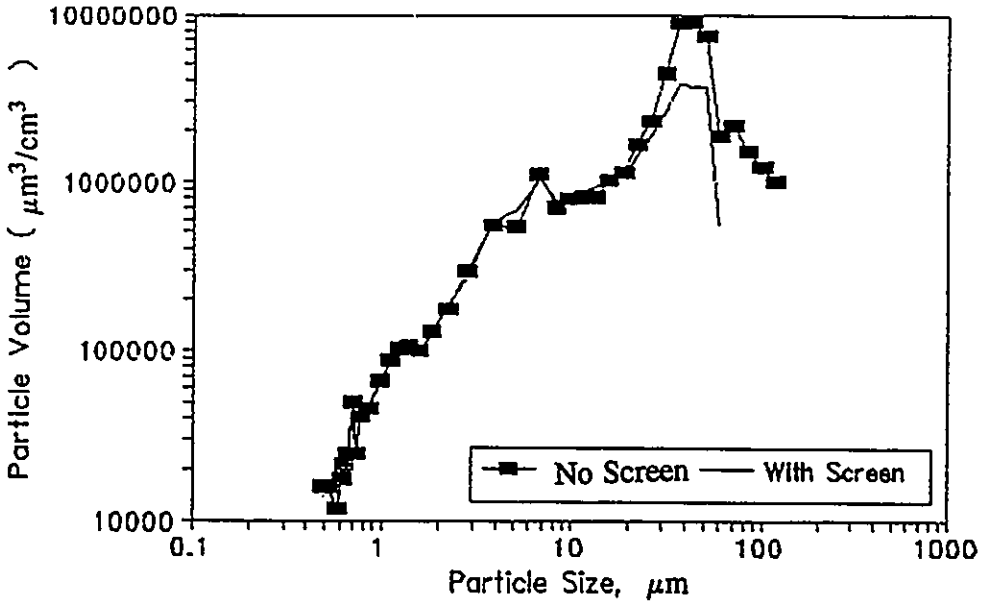

Figure 6.3 **Sampling effect before and after the screen on detected volume. Batch flocculation test (18 L), 5 μm 75 mg Si/L, percol 728.**

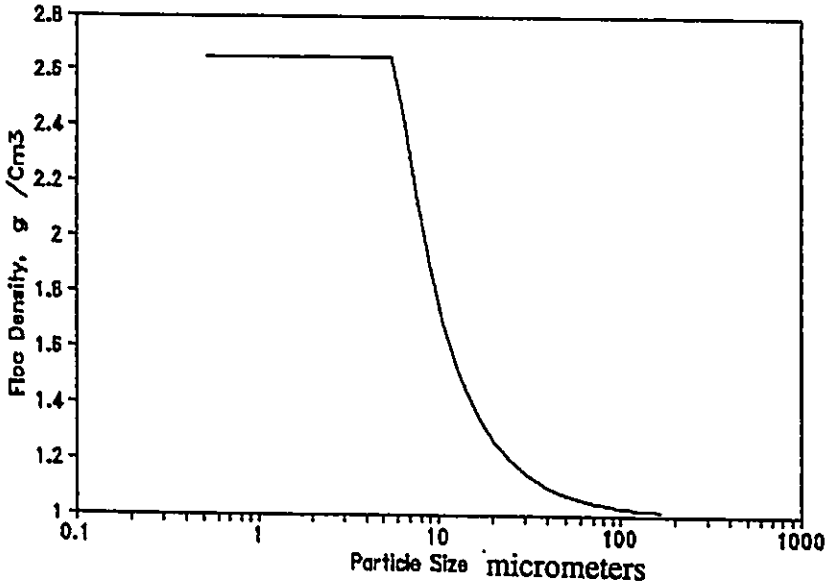

Figure 6.4 Floc densities versus particle size.

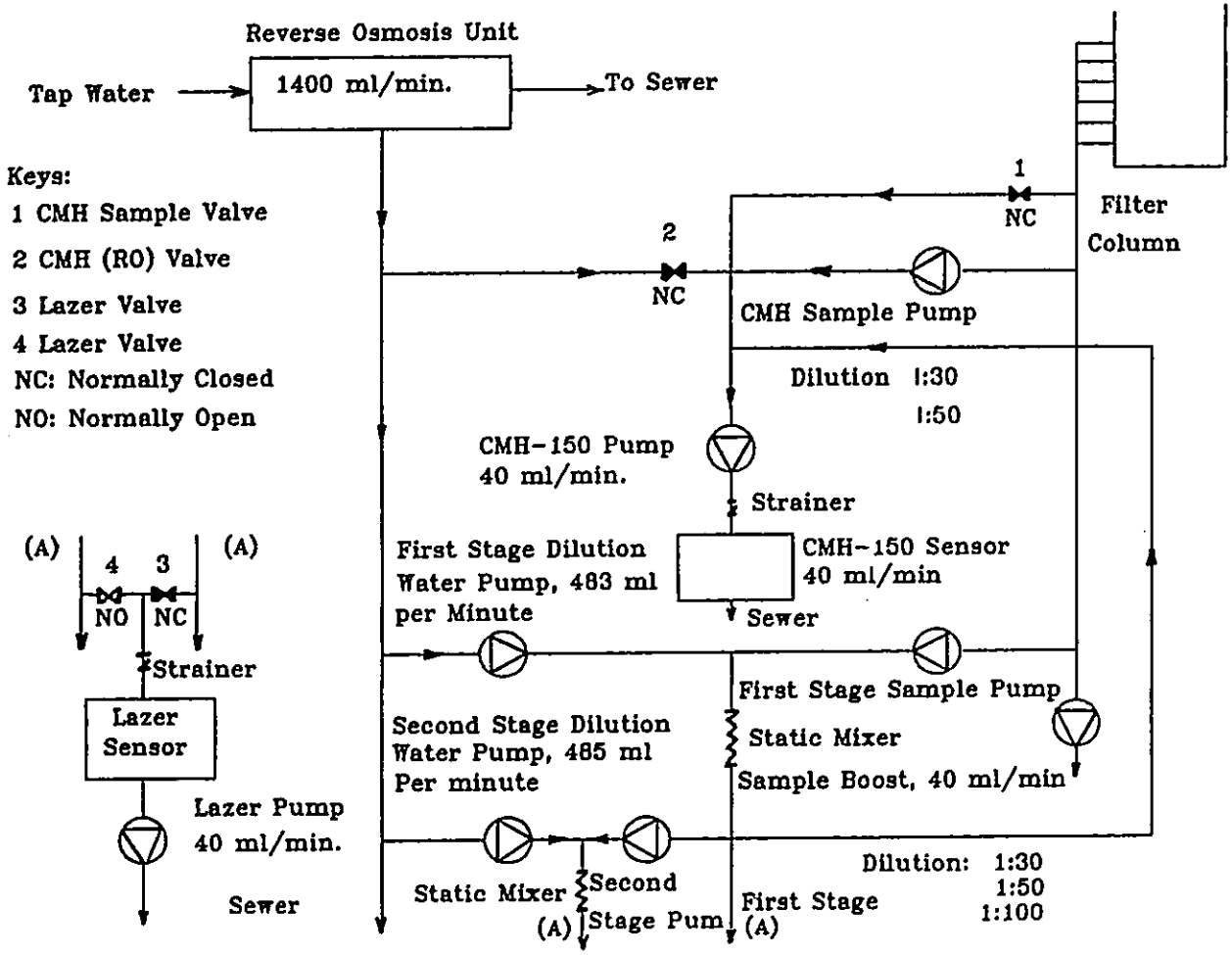

Figure 6.5 On-line sampling/dilution/analysis, particle sizing and counting system (adopted from J.Wood, 1988).

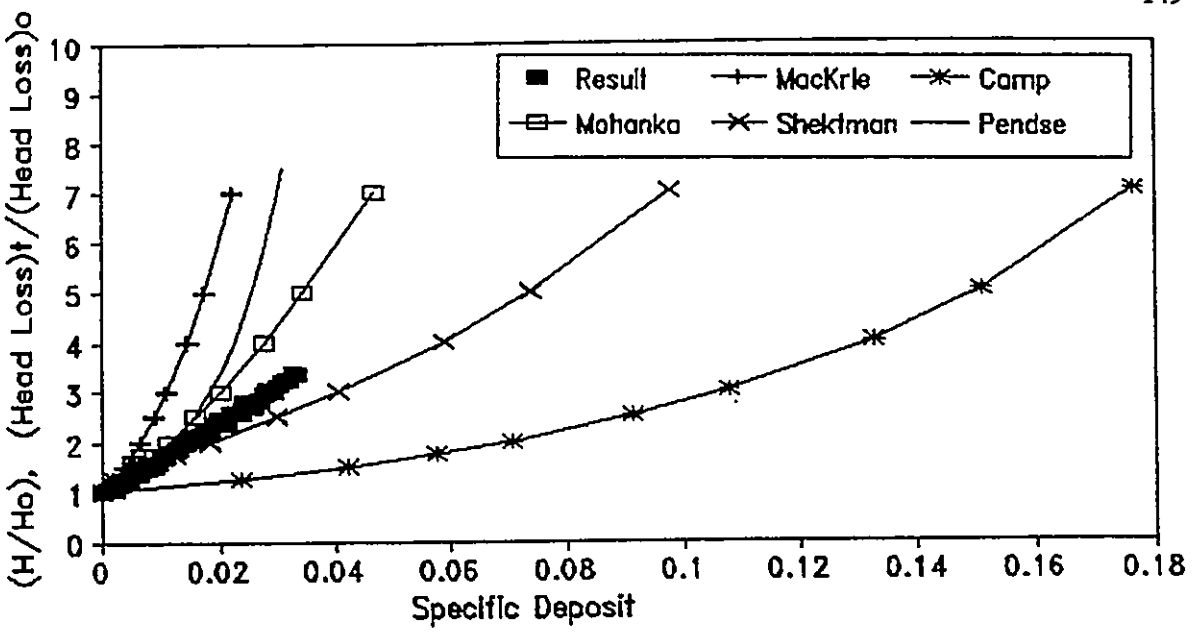

Figure 6.6 Validation of the correction approach. Comparison of observed and predicted head loss ratio (H/H_0) using Fe^{+3} experiment, 5 μm, 15 mg Si/L, Vo=0.3 cm/s.

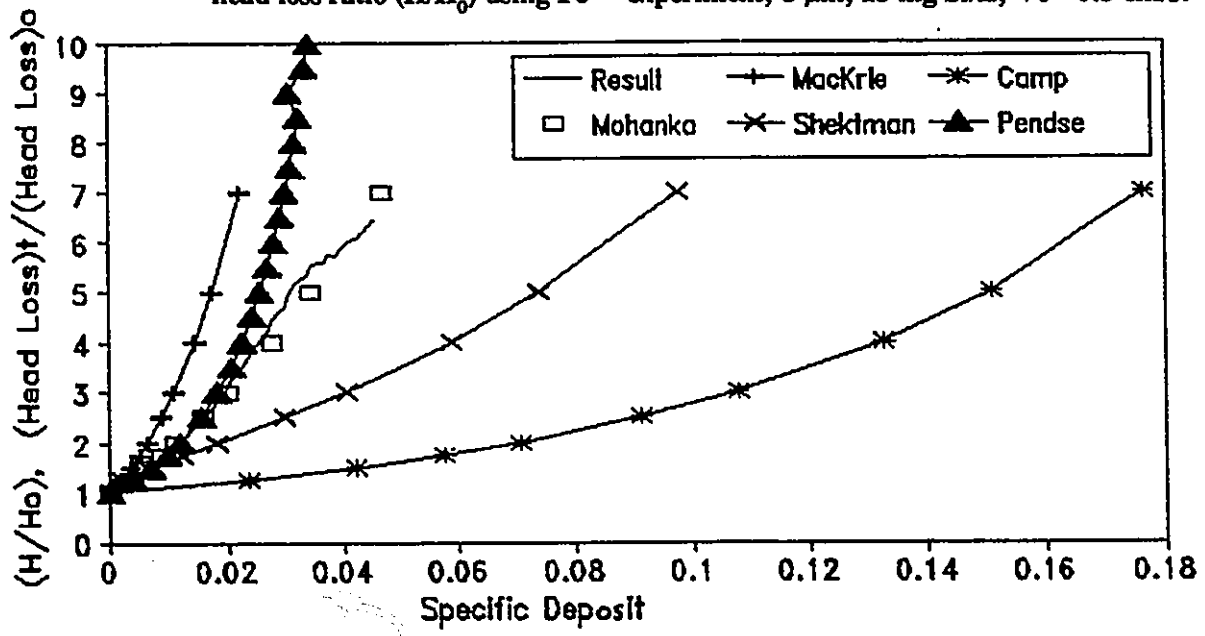

Figure 6.7 Validation of the correction approach using specific deposit data. Comparison of observed and predicted head loss ratio (H/H_0) using Fe^{+3} experiment, 5 μm, 15 mg Si/L, Vo=0.6 cm/s.

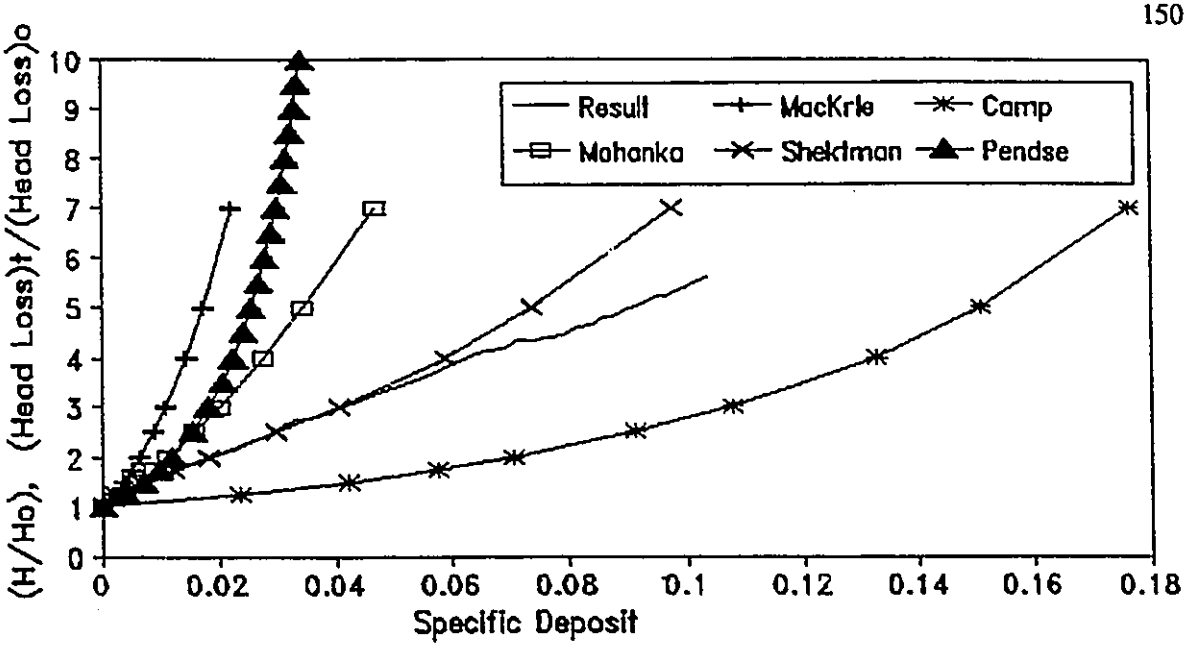

Figure 6.8 Validation of the correction approach using specific deposit data. Comparison of observed and predicted head loss ratio (H/H_0) using Fe^{+3} experiment, 5 μm, 15 mg Si/L, Vo=0.9 cm/s.

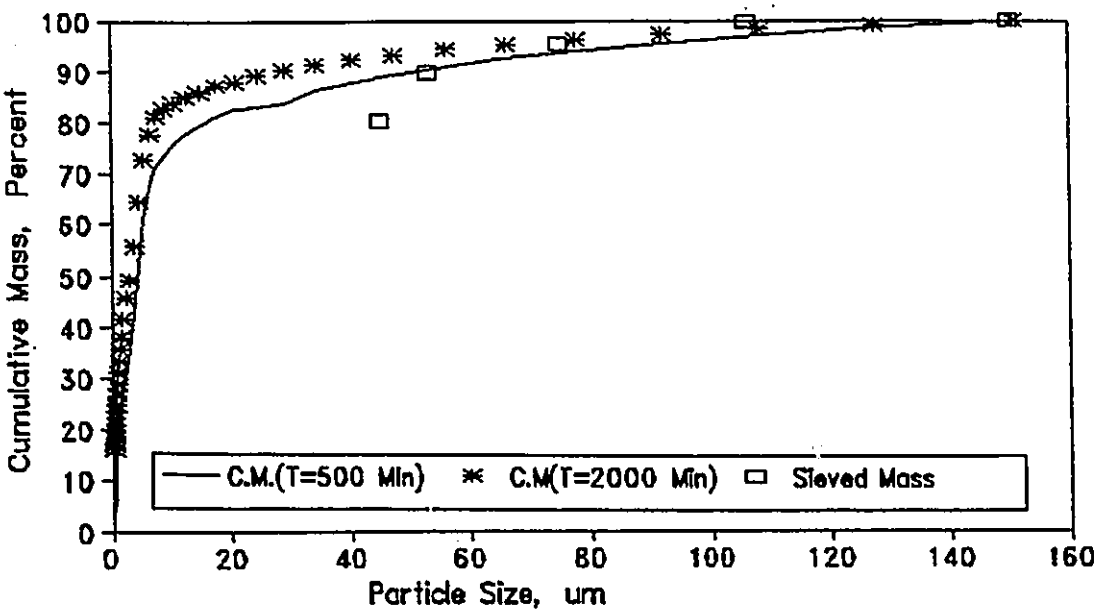

Figure 6.9 Validation of the correction approach using mass data. Cumulative mass comparison versus size of corrected mass and mass obtained by sieving a dry silica powder, using no-aid experiment, 5 μm, 15 mg Si/L, Vo=0.6 cm/s

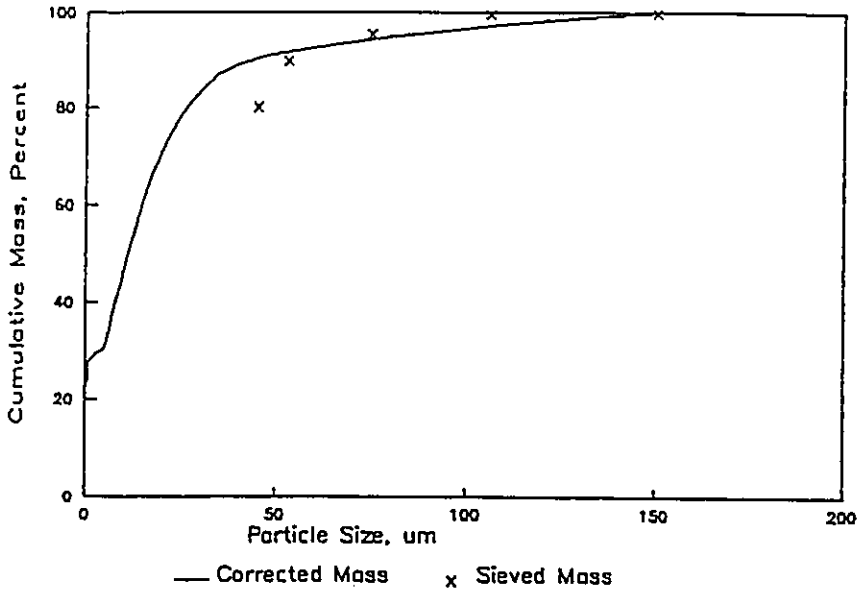

Figure 6.10 Validation of the correction approach using mass data. Cumulative mass comparison versus size of corrected data and data obtained by sieving a dry silica powder, using no-aid experiment, 30 μm, 15 mg Si/L, Vo=0.6 cm/s

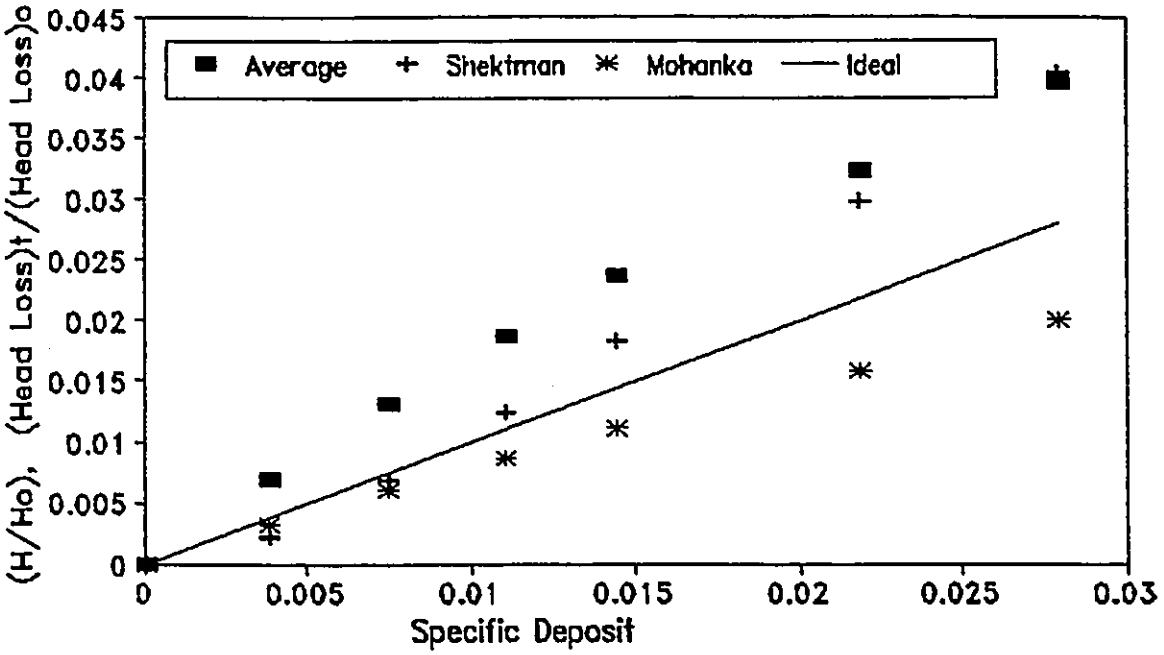

Figure 6.11 Validation of the correction approach using head loss ratio and specific deposit. Correlation between corrected and the prediction of different head loss equations, using Fe^{+3} experiment, 5 μm, 15 mg Si/L, Vo=0.3 cm/s

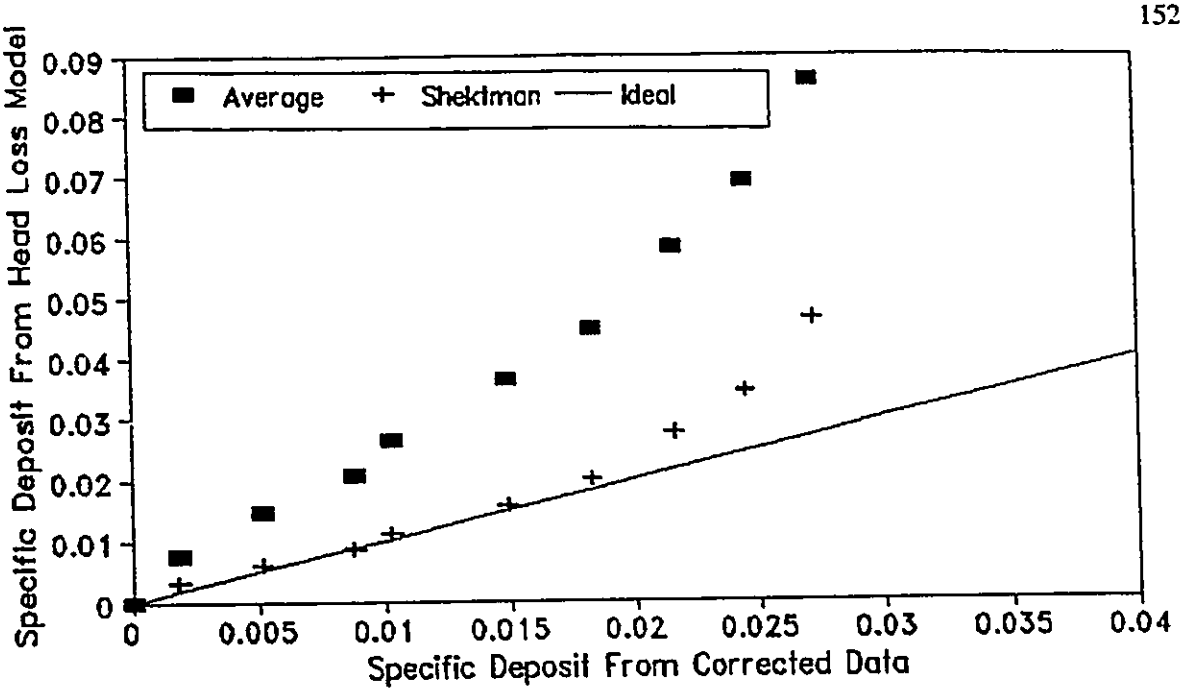

Figure 6.12 Validation of the correction approach using head loss ratio and specific deposit. Correlation between corrected and the prediction of different head loss equations, using Fe^{+3} experiment, 5 μm, 15 mg Si/L, Vo=0.6 cm/s

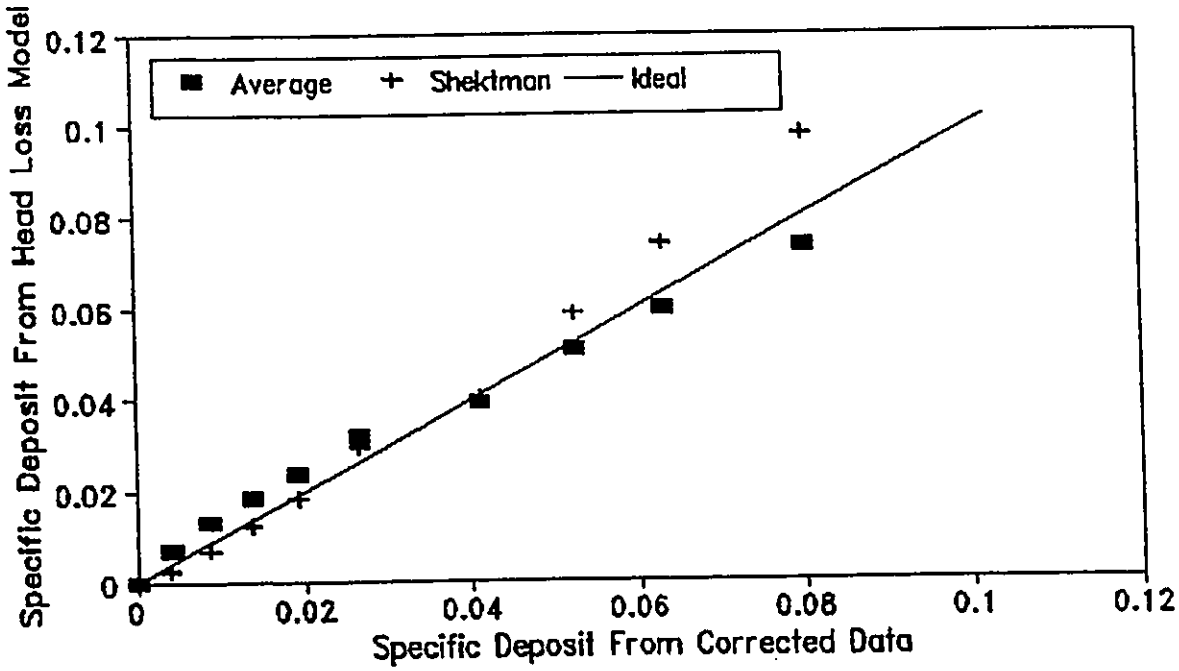

Figure 6.13 Validation of the correction approach using head loss ratio and specific deposit. Correlation between corrected and the prediction of different head loss equations, using Fe^{+3} experiment, 5 μm, 15 mg Si/L, Vo=0.9 cm/s

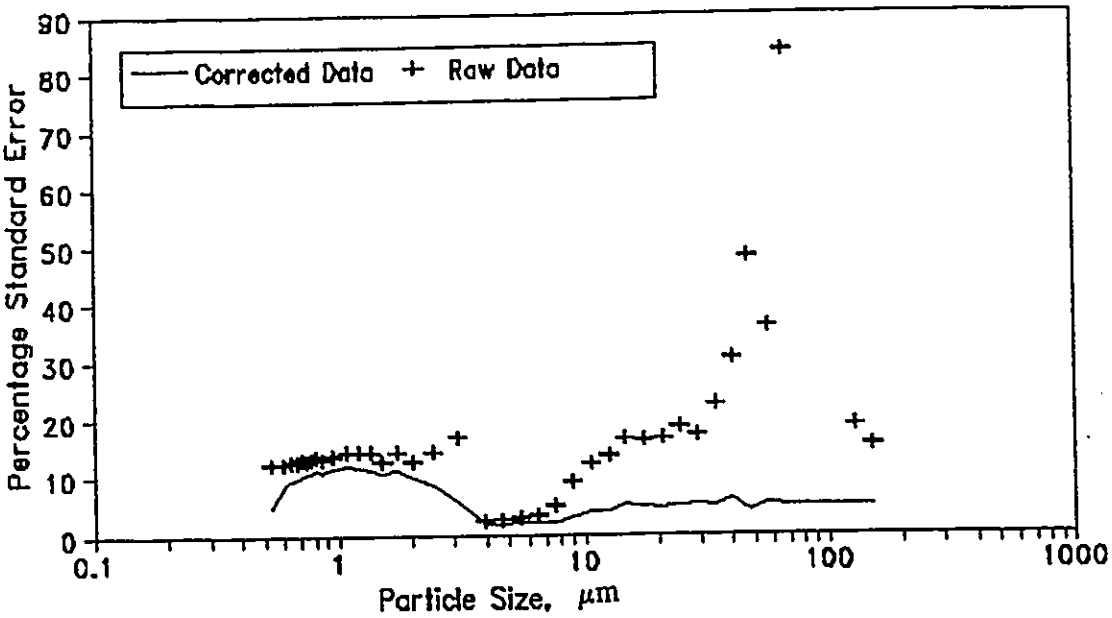

Figure 6.14 Relationship between percentage standard error and particles (flocs) size, using experiment with Fe^{+3}, 5 μm, 15 mg Si/L, Vo=0.3 cm/s

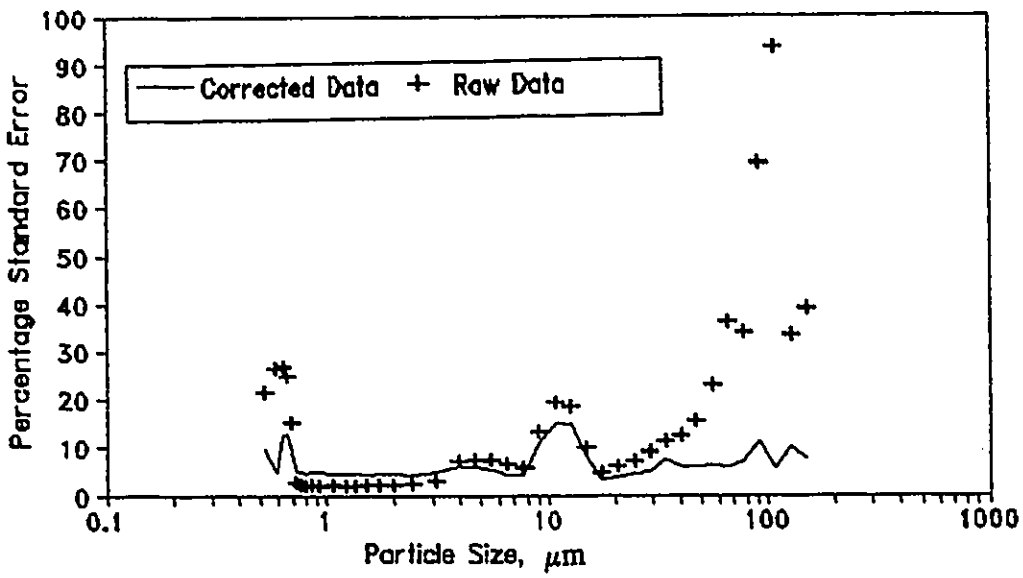

Figure 6.15 Relationship between percentage standard error and particles (flocs) size, using experiment with Fe^{+3}, 5 μm, 15 mg Si/L, Vo=0.6 cm/s

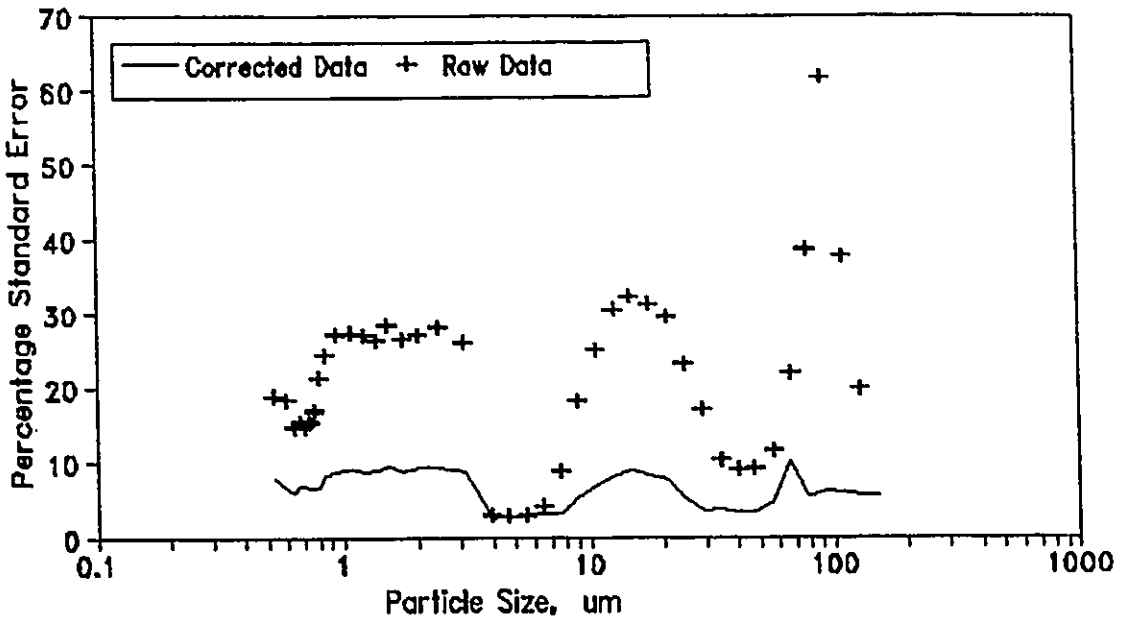

Figure 6.16 Relationship between percentage standard error and particles (flocs) size, using experiment with Fe^{+3}, 5 μm, 15 mg Si/L, Vo=0.9 cm/s

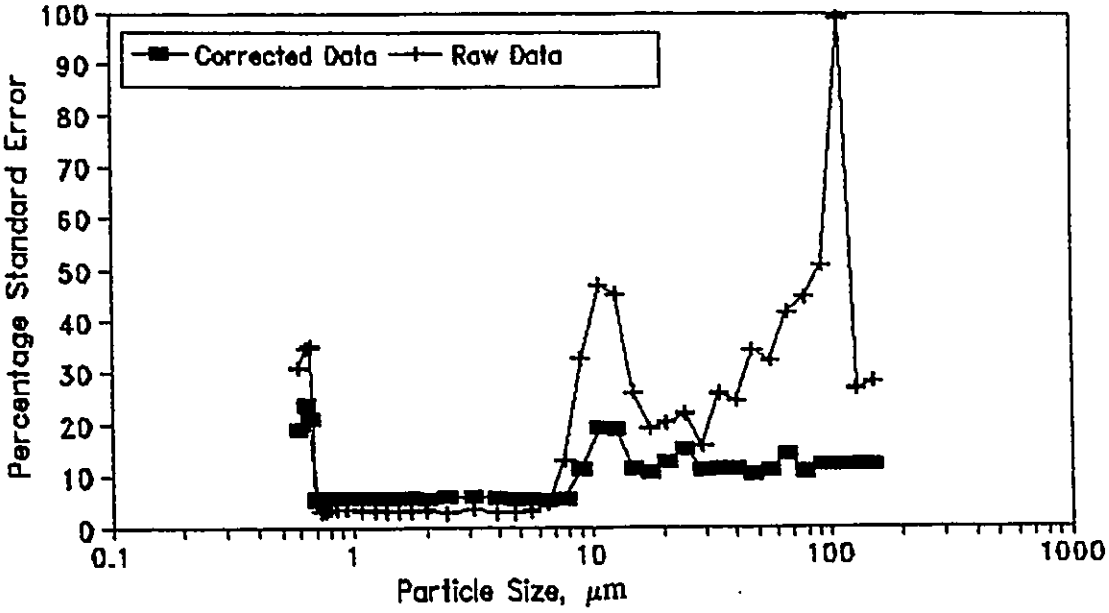

Figure 6.17 Relationship between percentage standard error and particles (flocs) size, using experiment with no aid, 5 μm, 15 mg Si/L, Vo=0.6 cm/s

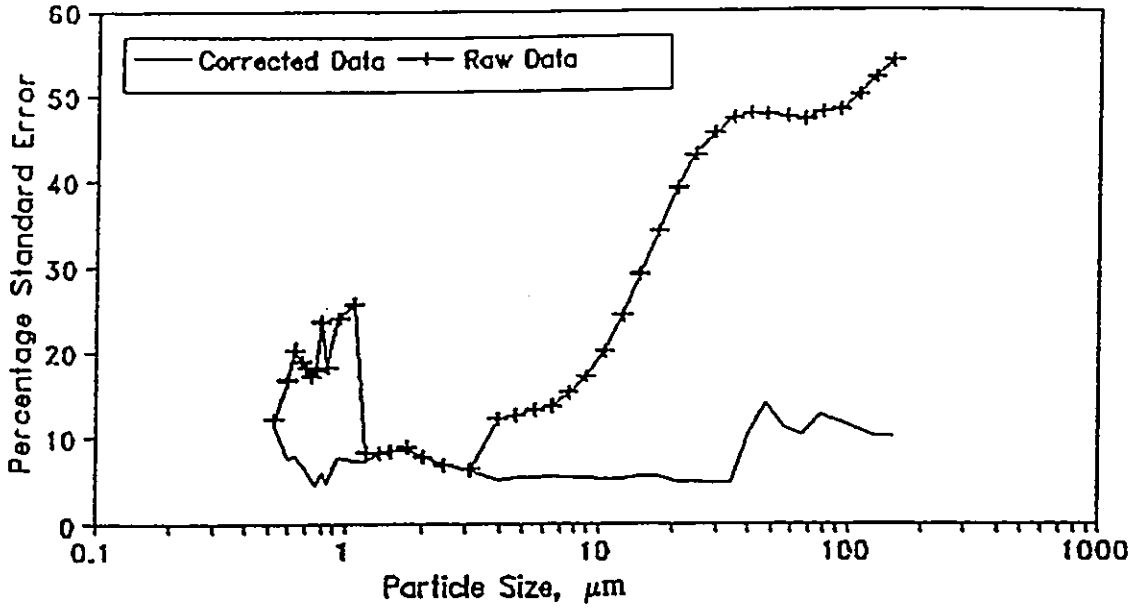

Figure 6.18 Relationship between percentage standard error and particles (flocs) size, using experiment with Fe^{+3}, 30 μm, 15 mg Si/L, Vo=0.9 cm/s

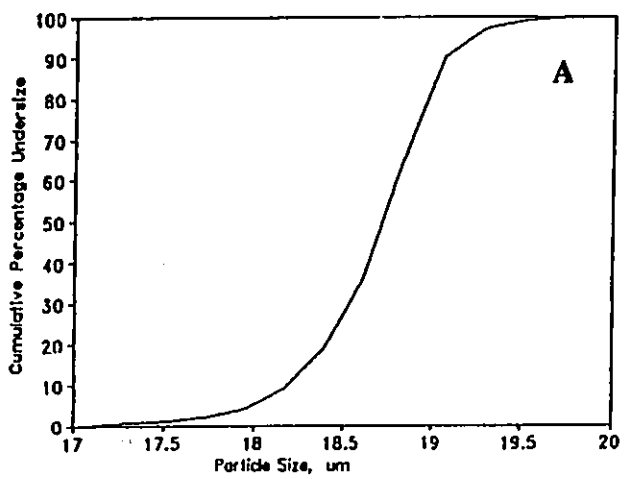

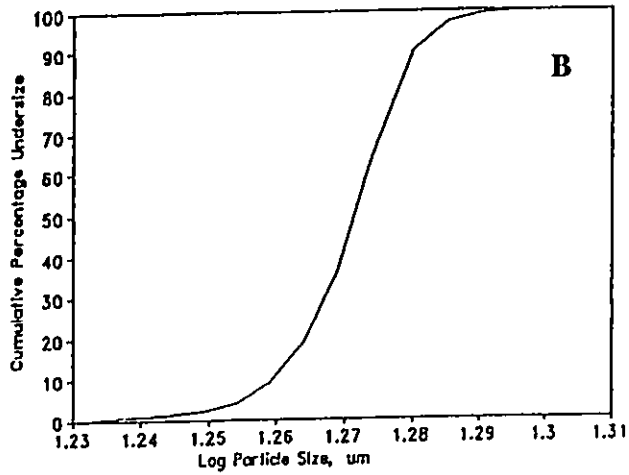

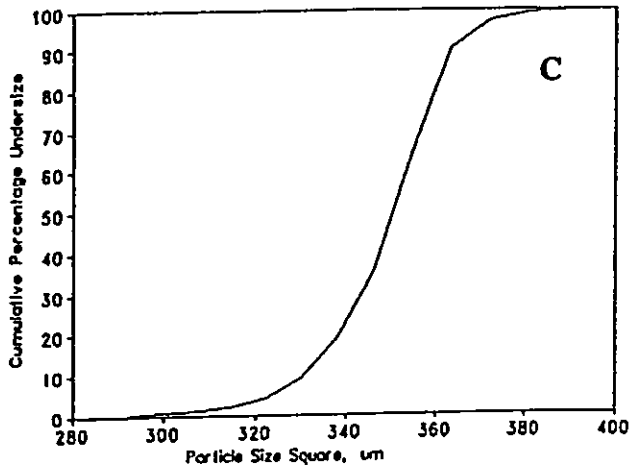

Figure 6.19 Graphical evaluation of different means. Cumulative percentage undersize versus different forms of particle size, using standard PSL (19.1 μm). (a) arithmetic mean, (b) geometric mean, (c) quadratic mean.

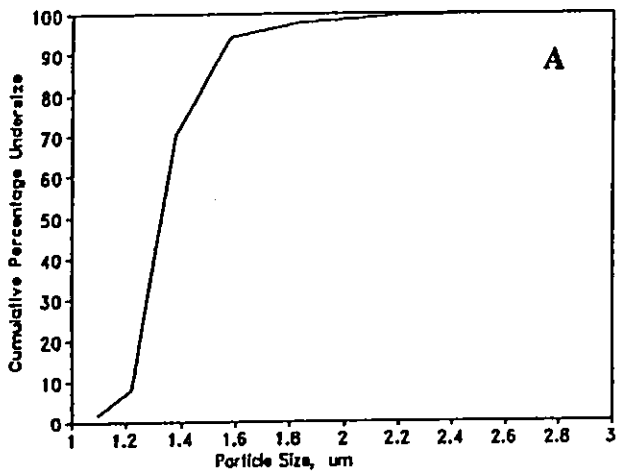

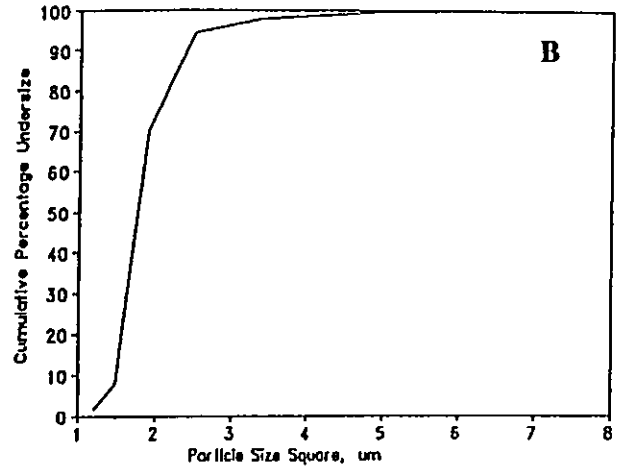

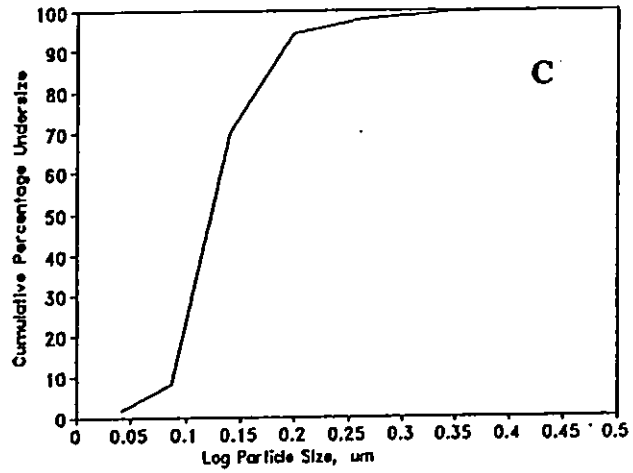

Figure 6.20 Graphical evaluation of different means. Cumulative percentage undersize versus different forms of particle size, using standard PSL (1.63 μm). (a) arithmetic mean, (b) quadratic mean, (c) geometric mean.

CHAPTER SEVEN

EXPERIMENTAL RESULTS AND ANALYSIS

7.1 Introduction

Filtration experiments using a granular bed composed of coarse filter grains (1.71 mm in diameter) and multi-sized particles in suspension were conducted. Results of pilot-scale filtration experiments are summarized, analyzed and discussed. The experimental data obtained, describes filtrate quality in terms of suspended solids concentration, head loss, amount of deposit and particle size distribution. These variables are the basis for comparison. A summary of experiments held under different conditions are shown in Table (4.4).

Insight into the kind of deposition, particle penetration and head loss build-up is achieved by using the amount of retained solids and head loss as a function of depth, different filtration velocity, different particle size, different particle concentration and different types of coagulant. Deposition morphology and degree of penetration are discerned from experimental observation and filter run results. Comparable figures of mass retained versus depth, head loss versus depth, specific deposit, as well as particle size distribution are shown to be important factors (particle size, coagulant type, filtration velocity and influent concentration) which influence the mode of deposition and head loss development. Procedure for data analysis, based on comparison between runs of dependent variables, except those in question, are held constant.

7.2 Presentation of the Head Loss Data

An investigation was carried out on how some factors, such as filtration velocity, particle

size concentration and coagulant type contribute to the development of certain deposition mode and how these parameters affect the head loss build up. The major parameter in filtration work, which can be measured as a function of depth of the filter media and time, is head loss. In all tests, head loss build-up occurred relatively slowly at the beginning. As the suspended solids accumulated in the bed, the geometry of the filter grains changed in different ways dependent on the type of coagulant used and influent particle sizes; (particles tended to accumulate on the filter grains in different configurations).

Filtration velocity played a role in determining which kinds of deposition dominated. The filtration velocity controlled the rate at which head loss increased. Increasing the filtration rate, increased the total amount of retained solids and the rate of head loss development, as one might expect. In a pilot plant with a particular head loss available, the head loss which remains for development during a run is reduced, which may shorten the run relative to results obtained with a lower filtration velocity. The head loss remains to develop is even expected to be less due to a higher amount of solids.

The head loss developed depends on particle size, coagulant type, retained amount of solids and how solids are distributed throughout the filter bed and within the single bed elements. Surface and in-depth removal of solids for both single bed element and overall bed depth are key factors in head loss build-up.

The variables of the testing programme were: coagulant type; filtration velocity; nominal particle size; and influent suspended solids concentration. The measured and derived quantities were: average effluent suspended solids concentration; of specific deposit (vol./vol.); mass of material deposited (gram); head loss developed; average suspended solids removal efficiency; volume of water filtered; depth of solids penetration (cm); and run time (minutes).

7.3 Reproducibility of Runs

Experimental results are meaningful if the data are reproducible. The reproducibility of the experiments was tested, for various coagulants, filtration velocities and influent concentrations by repeating each experiment once. Unfortunately, time and financial constraints prevented more repetition, from being carried out. Table (7.1) summarizes the experiments which were conducted to check the reproducibility of the pilot-scale filter.

The "replicated" filter runs were designed to determine if the head loss data were reproducible from run to run when the runs were conducted at different times. Statistical measure were used to account for the reproducibility of the experimental data. Calculated F-values with $F_{\nu_1,\nu_2,\alpha}$ value obtained from a statistical table (Box et al., 1978) were compared and the correlation between replicated runs were tested. In analyzing data, linear regression was applied to assess the degree of correlation between two runs. An example of assessing such a correlation, the results of replicated runs are plotted and a linear regression is depicted in Figure (7.1). All groups of replicated runs presented in Table (7.2) shows that the correlation between the replicated data are good. Comparison of the calculated F-values with that obtained from a statistical table (Box et al., 1978) indicated no significant difference between replicated experiments.

Average values for observed head loss in each of the replicate experiments are summarized in Table (7.3). The overall reproducing capability of the system were tested by plotting the average head loss of both ferric chloride and polymer runs versus the average of the replicate. Plot of the averages of replicated runs to assess the degree of correlation is given in Figure (7.2). Both the coefficient of determination (r^2) value of such a regression (0.966) and

the overlap of X=Y line with the line of best fit (LOBF), give an indication that both ferric chloride and polymer runs investigated , reproduced well from run to run.

7.4 Iron-Aided Runs

Table (7.4) summarizes the sets of filter runs used to compare the effect of filtration rate, particle size and influent concentration when using ferric chloride as a coagulant. Within each set of experiments, behaviourial variation resulting from a variation in particle size and particle concentration is represented by differences in filtration velocity. In many experiments, the behaviour of the top layer is different than that of layers at greater depths. The treatment of silica suspension with ferric chloride was characterized in the measurements by a linear increase in head loss.

A plot of the mass of suspended solids (gram) versus time at different ports, Figure (7.3) shows how the suspended solids concentration was distributed over the filter depth and how it varied with time. The general shape of the curves in Figure (7.3) indicate that a different trend of removal occured at different depths during the early stage of filtration. A smooth coating deposition mode was concluded from the results, since higher removal was observed in the top layer (depth = 14 cm) for the first 24 hours, while it was less in the lower layers. The effluent quality and removal efficiency improved however in the lower layer as the rate of mass deposition decreased in the upper layer. Comparing the mass of solids in different ports and at different times, say 500 and 2,000 minutes, in Figure (7.3), and comparing the differences in head loss in Figure (7.4), also support such an observation.

A comparison of head loss values versus retained amount of solids (flocs) for different filtration velocity, shown in Figure (7.5), reveals that the trend of behaviour is different, in

particular, for the first layer. Based on an equal amount of water treated (1000 L) and filtration rates of 0.3, 0.6 and 0.9 cm/s, the amount of mass accumulated within the filter bed element (144 g, 123 and 75 g, respectively) was found to be inversely proportional to the filtration rate. The distribution of cumulative mass deposit over filter depth was found to be more uniform at higher filtration velocities compared to low filtration velocities, as shown in Figure (7.6). Deeper penetration was observed at the higher filtration velocity (0.9 cm/s), whereas accumulation concentrated in the upper layer at the low filtration velocity (0.3 cm/s). This same observation was shown initially by Cleasby and Baumann (1962).

The rate of head loss development was influenced by the depth of deposit penetration and deposit geometry. In the upper two layers (32 cm depth) which have the maximum cumulative deposit, different dynamic responses were obtained.

For the same amount of mass deposit (80 gram), the head loss developed in the upper layer for a filtration rate of 0.9, 0.6 and 0.3 cm/s are observed to be lower, approximately equal and higher than the head loss developed in the second layer, respectively, Table (7.5). Mass distribution is more uniform over the depth of the first layer, uniform over the depth of the upper two layers and poorly-distributed over the depth of the upper layer and are characteristic of such response.

A transition from one type of morphology (smooth coating) to another (blocking mode) was observed at high filtration velocities (0.9 cm/s), as shown in Figure (7.7). This transition was attributed to increase in the total amount of retained solids, which resulted in an earlier clogging of the filter bed and subsequently exhausting a major part of the available head. Head loss per unit mass was observed to be steady with time in runs 200:261 and 200:002, but increased dramatically in run 200: 346. This may have been attributed to a significant change

in deposit geometry, Figure (7.5), or a change in removal efficiency.

As the filtration rate was reduced for a given particle size and concentration, the removal became more concentrated in the upper layer of the filter bed thereby causing a higher development rate of head loss in that layer with successively less head loss in each subsequent layer. Baumann and Haung (1974), found that increasing the filtration rate from 0.14 to 0.41 cm/sec has negligible effect on removal for a certain minimum bed depth, but did increase penetration of solids deeper in the bed. Baumann and Haung (1974), also stated that the head loss in excess of the value for the clean bed dependent on the amount of suspended solids accumulated and is not significantly affected by the flow rate. It should be noted that the head loss development rate were not only the amount of cumulated deposit dependent, but also related to the mode of deposition and deposit penetration.

Changing the silica particle size from 30 μm to 5 μm increased the particle number concentration and surface area of suspension. This decrease in size resulted in a significant increase in head loss when compared to that associated with the 30 μm silica, Figure (7.8), illustrates that for a given mass of retained particle, the suspension with the smaller particles contributed to a greater head loss when compared with that of the large particles (30 μm). This was attributed to a greater surface drag per unit mass.

Increasing the particle size, when mass concentration is fixed at 15 mg/L, resulted in a decrease of the particle number concentration, a decrease in the total particle surface area in the suspension, an increase in initial head loss, and a reduction in head loss development rate, since the surface area of the deposit is reduced. A change from 5 μm particle to the 30 μm particles resulted in approximately one order of magnitude decrease in head loss.

The head loss per unit mass of deposit changeed with an increase in mass deposit

differently for different filtration rates. This suggest is that the geometry of a deposit and deposit penetration changes when increasing the filtration rate. Based on equal amount of deposit accumulated (200 g) throughout the filter depth, more head loss per unit mass deposit observed, were 0.25 cm/g, with low filtration velocity (0.3 cm/s), compared to 0.44 cm/g, at higher filtration velocity (0.6 cm/s). The trend of the curves shown in Figure (7.9) are approximately the same.

In general, a decreasing, steady and finally an increasing rate of head loss per unit mass of deposited material are three stages depicted from the plots, for both small silica particles (5 μm) and large silica particles (30 μm) particularly, in the first layer. At the beginning, it appears that the solids were deposited in part on the surface of the filter grains as well as between the crevices. The effect of this deposition would have been to straighten the flow path and reduce the effect of deposited material on head loss. A further increase in deposit, appeared to cause the head loss rate to become steady for a certain period before it started to increase at a rate depending on filtration rate and depth of penetration.

Based on an equivalent mass of retained solids for comparison of head loss results, it is shown in Figure (7.10a) that a higher concentration (30 mg Si/L) of suspended solids produced more of a head loss than that of low concentration suspension. This effect probably suggest more interaction between particles, i.e, rapid increase in the number of particle-to-particle contact per unit volume of water treated, where, the shear force is weak. Figure (7.10b) shows that the reverse is true at a intermediate flow rate.

7.5 Polymer-Aided Runs

Different modes of deposition were recognized from the experimental observations of the

filter runs. Dendritic, combined and surface deposition were the three modes which were identified using the settled 5 μm, 5 μm and 30 μm silica, respectively. The observations indicated that the size of the suspended particles is an important factor influencing the mode of deposition.

Different experiments were performed using 5 μm silica at filtration velocity of 0.3, 0.6 and 0.9 cm/s. The experimental results of head loss using polymer with 5 μm silica and a filtration velocity of 0.6 cm/s, can be divided and as presented in Figure (7.11) into the following stages: a period of very little increase in head loss; a period of steady state attachment; a period of relaxation or a period of transformation from the smooth coating mode to the dendritic deposition mode; an exponential increase in loss after the dendritic deposition commences with possible dendritic structure interface; and finally a period of breaking a way of chains (limited chain length) or breaking a way the dendritic structure intermesh.

The dependence of head loss on filtration rates as expressed in Kozeny's equation for clean bed is well-established. It has been experimentally demonstrated in this work that the relationship between flow rate and head loss when a floc has accumulated is not of the same nature strictly given by Kozeny's equation, owing to the different deposition modes. The effect of increasing the filtration velocity is to increase the initial head loss and to increase the penetration of solids deeper into the filter bed thereby contributing to a lower head loss for the same amount of deposit when compared with what develops at a relatively low filtration velocity. Higher filtration velocity display removal with depth as shown by some spread of the cumulative mass deposit and head loss between filter bed elements, Figure (7.12).

Comparison of head loss versus cumulative mass retained for different filtration velocities illustrates that proportionality of degree of particles (flocs) penetration under different filtration rate is limited. Probably this happens because the dragging action of water is less than adhesive

force of flocs with 0.3 and 0.6 cm/s. At 0.9 cm/s, the dragging action is higher than the adhesive force which suggest more deposit penetration. Figures (7.13) a and b compare the amount of head loss developed versus cumulative mass retained for the first layer and overall depth respectively. Hydraulic shear effect is seen to occur when 15 gram, and approximately 200 gram of deposit accumulated in the first layer and overall depth, respectively.

Therefore, and as Figures (7.13) a and b shows the higher the mass retained, the lower head loss (first layer and overall depth), demonstrating that in-depth removal is achieved with high filtration velocity.

Figure (7.14) is fairly representative of conditions which lead to deeper penetration and lower head loss development. Mass deposit is even more uniformly distributed in the second layer. With the absence of surface removal, higher filtration velocity resulted in 1) an increase in initial head loss, 2) distribution of solids removed through a greater depth of the granular medium, 3) large storage capacity and, therefore, longer filter run, 4) equal water quality (effluent) associated with low head loss rate and 5) more volume treated for the same amount of solids, when compared to low filtration rate results.

Comparisons of the cumulative mass versus depth plots at different time intervals for different filtration velocities, Figure (7.15), provided another confirmation that the amount and distribution of mass deposit as a function of velocity and depth. As the velocity is increased wider distribution is obtained.

As stated earlier, the dependency of head loss on filtration rates, when flocs have accumulated has limitations, because of the formation of different deposit geometries. The dependency of head loss on the filtration rate and as presented in Figure (7.16) was valid for 0.3 and 0.9 cm/s, for the first layer and overall depth with both ferric chloride and polymer. For

0.6 cm/s, the rate of head loss per unit mass for the polymer run is 1.5 times that of the ferric chloride run in the first layer.

For an equal amount of mass deposit, the rate of head loss increase for 0.6 cm/s compared to 0.3 cm/s is proportional to filtration velocity ratio. The proportionality is not applicable when 0.9 cm/s was used, indicating a greater deposit penetration is achieved or different deposition pattern has been obtained. This will allow a higher final filter load with lower amount of head loss as can be seen in Figure (7.13). This result supports the fact, that it is difficult to obtain a dendritic structure at high filtration velocities, in which a high hydraulic shear is exerted and the chain length is limited.

The effect of particle size is illustrated in Figure (7.17), in which head loss as a function of filter depth at different time intervals is presented. The family of the curves shows that for large particles (30 μm silica), the lower 72 cm of the bed is essentially clean for the entire run and exhibits linear increase of head loss with depth. More than 85 percent of the head loss is developed within the first layer while the rest of the bed shares the burden of 15 percent only. Surface accumulation of approximately 1 cm depth above the surface was observed. The set of curves for small particles (5 μm silica) show that the solids are captured deeper in the filter bed as the data exhibited a curvilinear trend when compared to that of large particles (30 μm).

In summary, the analysis of the results of experiments 200: 161 and 200: 014, presented in Table (7.6) indicates that increasing the nominal size from 5 μm to 30 μm contributed, to 1) a change in deposit morphology, 2) an increase in head loss by 27 percent for the same amount of deposit, 3) a decrease in the length of the run by 20 percent, 4) decrease in the volume of water treated by 22 percent, and 5) a suspended solids removal efficiency increase when the silica size was increased. This can be attributed to the increase in large particle population, which is

more easily removed.

Large silica particles (30 μm) with polymer as coagulant aid and different filtration velocity results in different modes of deposition. Two runs are compared 200:014 and 200:304 with 0.6 and 0.3 cm/s, respectively. For an equal mass (150 gram) of particle (floc) removed the build-up of head loss is extremely small with 0.3 cm/s when compared with that corresponding to the run at 0.6 cm/s, as shown in Figure (7.18), this suggests that the storage capacity of the top filter layer was being utilized. It is interesting to note, that it had been observed experimentally that all suspensions resulted in little head loss for considerable initial removals. The head loss developed with cumulative retained mass in the first layer and overall depth were relatively identical at the early stage of the filtration run. Higher increase in head loss for 0.6 cm/s than that of 0.3 cm/s, suggested the possibility that the deposition morphology may have been different, as shown in Figure (7.18). A comparison of cumulative mass retained, and head loss versus depth plots, Figure (7.19) indicates that the first layer was able to cope with the higher suspended solids loading and increasing the filtration velocity using 30 μm affect the mode of deposition when compared to low filtration velocity. For a specific amount of retained mass the build-up of head loss indicates that a different mode of deposition occurred for different filtration velocities, as shown in Figure (7.20).

Visual observation and the use of optical fibre endoscope techniques, confirmed that surface removal with nearly 1 cm depth of deposit on the filter surface is obtained with run 200:014; while in-depth removal is obtained with run 200:304. Comparison of head loss versus retained amount of solids (overall depth) when the run was terminated, for both runs, as presented in Figure (7.18), showed that with 0.6 cm/s the amount of head loss was four times that with 0.3 cm/s.

In summary, comparing "surface removal" tendency with "depth removal" tendency, surface removal tended to produce short filter runs with an exponential increase in head loss. Depth removal tended to produce longer filter runs with a relatively linear increase in head loss. which confirms the observation made by Oulman, et al. (1979).

For settled 5 μm silica, the deposition geometry was in dendritic form, where the particles in the influent suspension were mostly fine particles. The analysis of head loss development is meaningful only in the upper most layer, where the head loss increased exponentially. The uppermost layer of the filter was used for the purpose of comparison between runs, because it retained the greatest portion of the solids and offered the greatest hydraulic gradient values. In deeper layers, there was little deposition since the concentration leaving the top layer and reaching the lower layers was close to zero. The effect of removal in the top layer is illustrated in Figure (7.21), in which the head loss as a function of bed depth at different time interval is presented. The family of the curves suggests that the upper layer attained a maximum storage, while the subsequent layers were essentially clean for the entire run as reflected by the linear increase of head loss for those layers and the fact that the curves are parallel. However, the polymer dosage applied to the influent suspension was not excessive as to cause an excessive loss of head at the surface of the filter media, and there was no considerable increase in head loss at the initial stage of filtration indicating the absence of filter performance improvement due to surface deposition effect.

The suspended solids which were filtered out usually consisted of polymer chains containing fine silica particles. The flocs adhered to surface of the filter media or to previously deposited flocs. A strong exponential head loss versus mass deposit curves, as presented in Figure (7.22), indicates that the removal occurred by bridging mechanism. The result follows

neither "surface removal" tendency (short filter run), nor "depth removal" tendency (long filter run with low head loss development rate), but rather it tended to produce long filter run with higher head loss value.

7.6 Min-U-Sil 30 μm With Polymer and Ferric Chloride

Using the same particle size and filtration velocity of 0.6 cm/s, and a concentration of 15 mg Si/l, with a different coagulant provided a basis to compare the effect of coagulant aid on head loss build-up. As presented in Figure (7.23), two types of head loss curves were observed. In the polymer run, the upward bend in the curve indicated a different trend of deposition than usually observed in polymer runs. For ferric chloride runs, the head loss curves are nearly linear. Figure (7.23) which clearly indicates that the first layer contribution was about 80 percent with respect to the total amount of mass retained for polymer. For the ferric chloride run, the percentage was about 30, which mean the polymer contribution to the deposit in the first layer was 2.7 times that of the ferric chloride run. Figures (7.23) indicates the same kind of deposition in the early stage of filtration using 30 μm silica with both ferric chloride and polymer. As the filter run proceeded, head loss values for the polymer run were almost 2.5 times that of ferric chloride for equal amount of removed mass.

The analysis of the mass deposit and head loss versus depth, summarized in Figure (7.24), revealed that for polymer, there is a sharp decrease in the amount of deposit between the first layer and subsequent layers, whereas a wide spread of mass deposit between filter bed elements was observed for ferric chloride. The ferric chloride trend is a sign that all filter bed elements were used for storage, i.e., the entire filter played an active role in filtration, which in turn gave an indication of smooth coating. This conclusion is reached based on two

factors: firstly, by the fact that the capacity of the filter for accumulating solids was used (i.e., all unit bed elements shared the burden of accumulating solids) which resulted in a lower rate of head loss development. Higher removal is observed in the top layer (depth = 14 cm) for the first 24 hours, while it is less in the lower layer. However, effluent quality and removal efficiency improved in the later run for the lower layers as the rate of mass deposition decreased in the upper layer. And second, by visual observations of deposit within the granular filter media, using an optical fibre endoscope. The sharp decrease of head loss with depth, signals surface removal. The head loss versus depth plot, Figure (7.24), duplicates that of mass deposit.

At a low filtration rate (0.3 cm/s) the mass data indicated different dynamic responses. For example, with the lesser penetration in polymer run (200:264), the upper element attained a maximum of more than 80 percent of the total mass. The rest of the bed shared the burden of the 20 percent. The upper element in iron-aided run (200:262), on the other hand contained only 50 percent of the solids at the end of the run. In iron-aided experiments the head loss development per unit mass increased as the filtration rate increased, except for 0.9 cm/s, where the head loss rate was smaller, since the deposited material was more uniformly distributed throughout the filter bed.

A different trend of head loss behaviour was observed for run 200:261, at different depths. This may have been attributed to small strong flocs, which represented a substantial part of flocs population. The high density associated with small flocs (Tambo and Watanabe, 1986) which means stronger flocs due to less water content when compared to larger flocs. Therefore, due to the large pore space within the filter grains when compared with floc size, there was a good chance for the flocs to achieve greater depth before attaching to a collector surface, or attaching to previously retained floc. Hence there is a possibility of generating less head loss.

7.7 No-Aid Runs (control)

The two grades (5 and 30 μm) exhibited similarity in head loss for the same amount of mass deposited in most of the runs. The general shape of the head loss curves reflects the type of deposition. A linear plot for the 5 and 30 μm silica at different filtration velocity, suggests in-depth removal in which the pore-space was only partially filled and the flow path remain mostly open.

The average removal efficiency of mass of suspended solids was 56 and 47 percent for 30 μm and 5 μm, respectively. The PSD plot for large particles (30 μm), indicated removal of large-sized particles with no significant change seen in the small size range. As presented in Figure (7.25) no indication show any significant improvement in removal efficiency of fine particles, with time during the filtration process.

The rate of head loss development was almost zero at 0.6 cm/s, while at 0.9 cm/s, it changed slightly over filter depth as shown in Figure (7.26). For a deposit of equal mass, the same trend of head loss behaviour was observed in the first layer and overall depth at 0.6 cm/s. At the higher filtration rate, of 0.9 cm/s the head loss per unit mass was higher in the first layer than throughout the overall depth, although the amount of deposited mass was even less than that observed in the second layer.

These observations suggest that either, the deposit geometry may have undergone a change from one mode to another or the head loss per unit mass may have been affected by the residual coagulant present in the tap water (residual alum = 0.1−0.3 mg/L), Frazer (1992). Some differences in the surface properties of the media from run to run (depending on how thorough the backwashing was) may have also contributed to such an effect. The second possibility, together with the differences in surface properties, seems most likely, as the plot of

head loss is not curved up, even when the run was terminated, Figure (7.27).

An increase in the influent mass increased the total amount of retained solids and the rate of head loss development, as shown in Figure (7.27). No sign of decreasing run length related to the effect of increasing filtration rate, particle size and influent concentration was observed. This is not a general conclusion, because the run time was arbitrarily terminated at 48 hours, before the complete storage capacity was used and the designed head exhausted.

For 5 μm silica, Figure (7.28) indicates that there was a consistent particle concentration for each channel size and over an entire run. Analysis of the cumulative mass percentage versus particle size for both laser and CMH range at different times reveals an improvement in mass removal exceeding 200 percent of both small and large particles was achieved, Figure (7.29).

There was no observed effect on the mode of deposition when increasing the filtration rate, although there was a slight effect on the head loss rate at 0.9 cm/s, as shown in Figure (7.30). An increase in the rate of filtration contributed to a degradation of effluent quality, and a reduction in the amount of retained solids over filter depth.

A comparison of total solids retained, based on different filtration rates using 5 μm silica, indicates that 50, 62 and 65 grams of solids were retained at filtration velocities of 0.3, 0.6 and 0.9 cm/s, respectively. These values reflect that 60 and 137 percent reduction in total solids deposit based on the assumption of similar removal efficiencies obtained when 0.6 and 0.9 cm/s are used compared to 0.3 cm/s. A comparison of solids retained for each layer is listed in Table (7.7). The same phenomena was duplicated when 30 μm silica as used instead of 5 μm silica.

The effect of increasing particle size with 0.9 cm/s, for instance, was to increase the amount of retained solids, thereby improving effluent quality, and reducing the head loss

development rate because of the fact that less surface area associated with 30 μm than 5 μm silica, as shown in Figure (7.31).

7.8 Effect of Particle Size

The effect of different particle size in suspension together with different coagulant aid was partially examined in the previous sections. A 15 mg Silica per litre was filtered through 1.71 mm sand grains at a flow rate of 0.6 cm/s. Solids were retained on the surface of the filter bed which caused the bed to ripen quickly thereby leading to faster head loss build-up. Data shown in Figure (7.32) for run 200:161 (5 μm) were for the same conditions as used for run 200:014 (30 μm), except for particle size. This set of curves shows that solids were retained at a somewhere lower depth since the amount of deposit was distributed in the top and other subsequent layers. However, the results shown in Figure (7.33) suggest that the particle size exhibited some influence on head loss increase as seen in the overall depth result. For a given mass of removed particles, the suspension with 30 μm size particles resulted in a greater head loss than that associated with the 5 μm suspension because of the large flocs which blocked the filter pores at the surface of the filter bed.

Habibian and O'Melia (1975) and Tobiason (1987) on the other hand concluded that large particles in suspension produce less head loss. This conclusion is limited for a single specific case and is not valid for a wide range of particles size in suspension. It is determined in this case that head loss build-up depends not only on the amount of deposit, but also on the mode of deposition and depth of penetration of flocs down the filter column. The conclusion of such a dependency is based on tests running 0--24/48 hours instead of 0-5 hours.

Head loss versus cumulative mass deposit for runs 200:161 and 200:014 are presented

in Figure (7.33). This figure illustrates that at the early stage of the filter run, the 5 μm silica resulted in a greater head loss when compared to that using 30 μm because initially all the removed particles were subjected to the stream line, closest to the filter grains, where the small particles contributed to more surface area than large particles. The reverse was true as the filter run proceeded. In iron-aided runs, as previously observed in Figure (7.8) the two grades (5 and 30 μm) exhibited different amounts of head loss for equal amount of retained mass.

A comparison of silica size effect was examined in runs 200:261 (30 μm) and 200:263 (5 μm), in which both were operated at 0.3 cm/s, with 15 mg Si/L influent concentration and an iron dosage of 0.25 mg/L. Both runs were terminated at the same time. Less penetration was observed with the 30 μm silica relative to the 5 μm silica. Logically, increasing the particle size contributed to a reduction in the specific surface area of the deposit, an increase in the density of the deposit, an increase in the suspension stability based on an increasing amount of coagulant per unit surface area of suspension, and a reduction in head loss rate.

As the filtration rate was increased, the silica size effect was also increased. A summary of the results from runs 200:001 and 200:002 with 5 μm and 30 μm silica sizes, respectively, are presented in Figure (7.34). Both runs were operated at 0.6 cm/s, 15 mg silica/L influent concentration and an iron dosage of 0.25 mg Fe^{+3}/L. Although the effluent quality in run 200:001 was poorer than that in run 200:002 and a greater particles penetration was observed, the 5 μm run was associated with head loss of higher magnitude when compared with that of the 30 μm silica run. These observations indicated that the greater surface drag per unit mass associated with the 5 μm silica contributed to a higher head loss development rate. A change to the smaller size increased the suspension stability since the effective dosage associated with the increased surface area was reduced. A dosage reduction would have resulted in increasing both

the depth of solids penetration and effluent concentration.

7.9 Effect of Coagulant Aid

The primary objective of analyzing the effect of different parameters was to provide an insight into the geometry of the deposit and depth of particle penetration. The depth of penetration was affected by coagulant mass per unit mass of suspension, filtration rate, and deposit geometry. The effect of different coagulants was particle size dependent. For the large particle (30 μm) and low influent concentration (15 mg/L), the amount of mass deposited is presented in Figures (7.24). For the polymer, the last three layers of the filter bed remained fairly clean for the entire run, and a linear head loss increase with depth was exhibited. The major head loss build-up occured in the top layer of the filter bed. Iron run characteristic is the in-depth removal with all filter bed elements sharing burden of head loss. As previously stated and presented in Figure (7.23) for an equal mass of deposit, ferric chloride run resulted in lower head loss than polymer run. During the early stages of the filter run, the ratio of head loss using ferric chloride and polymer was close to unity, suggesting the same kind of deposition for both coagulants. The ratio started to decrease and approached 0.5 as the deposition geometry changed to a blocking mode; where the ability of the flocs to reach the subsequent layers diminished. The coagulant type appeared to have no effect on the removal of small particles, and consequently had no effect on the observed head loss development. The experimental data showed that the head loss curve, for the 5 μm silica and 0.6 cm/s filtration rate was similar for both ferric chloride and polymer runs, as can be seen in Figure (7.35). For both grades (5 μm and 30 μm) and with low and high influent concentrations (15 and 30 mg/L), differences in head loss rate were observed when the filter-aided runs were compared with no-aid runs; see, e.g. Figures (7.36) and (7.37).

Filtration rate seems to have had some effect on head loss rate. As presented in Figure (7.38), the higher filtration rate (0.9 cm/s) causes a higher head loss when using ferric chloride than when using polymer, based on equal mass of deposit. The influent concentration effect is shown in Figure (7.39). The figures indicate that the mass deposit ratio between 15 mg/L and 30 mg/L influent concentration, for the first and overall depth of 1.35 and 0.45 corresponds to head loss ratio of 3.3 and 1.06, respectively. From Figure (7.39) there appeared to be more in-depth removal associated with a high influent concentration. This was not the case for the second elements, where less than a half of the deposit accumulated with 15 mg/L when compared to that corresponding to 30 mg/L. This phenomena may indicate more voluminous deposit resulted in increased particle removal.

When large particles and high influent concentration were used, three different trends were obtained. This effect was significant as different deposition geometry seemed to have dominated each kind of coagulant. The results presented in Figure (7.37) for the first layer and overall depth indicated an order of magnitude increase in head loss. The coagulant ranking in order of increasing head loss rate per unit mass and time was no aid, ferric chloride and polymer, respectively.

It is fairly evident that no difference in head loss development was observed, using percol 351 (anionic) when compared to percol 728 (cationic), as presented in Figure (7.40). The adsorption of the anionic polymer on negative surfaces was indicated, observed and has been explained by different researchers (Ives and Gregory, 1967; Ives, 1980; Stumm and Morgan, 1981; Tobiason and O'Melia, 1987). There is a general agreement among researchers that anionic flocculant perform well because of the relatively high level of indifferent electrolytes and (particularly, calcium ions) hydrogen bonding which provides salt linkages for the anchorage of

polymer anionic group to the silica surface. The effect of the anionic compared to cationic polymer appears to be confined to the amount of deposit accumulated within the filter depth. Deeper penetration was observed and more solids retained in subsequent layers than the top layer with percol 351, as demonstrated in Figure (7.40).

7.10 Effect of Influent Concentration

Table (7.8) summarize sets of filter runs, which were used to compare the effect of influent concentration. The effect of suspended solids concentration is demonstrated in Figures (7.10), (7.27), and Figure (7.41). The results were unexpected as can be seen in Figures (7.41). Logically, increased influent solids concentration should produce more head loss per unit time. This can be justified when the number of particle-to-particle contact per unit volume of water treated is rapidly increased under favoured chemical conditions. An interesting observation is obtained from the comparison of head loss results. Based on equal mass deposit, the suspension with 30 mg Silica per litre resulted in less head loss than was caused by the 15 mg per litre suspension for both 5 and 30 μm silica. This could have been due to the distribution of the deposit within the filter bed depth, for different initial solids concentration.

This head loss observations due to the increase in number concentration and surface area of suspension, resulted from increasing the mass concentration, and an increase in suspension stability resulted from a reduction in the effective dosage causing the particles to penetrate deeper, thereby increasing the effluent concentration. This was observed both in polymer and ferric chloride runs, but was not observed in no-aid runs.

The mass deposit versus depth at different time interval are compared. In case of the polymer, an in-depth filtration with 30 mg/L was observed, considering the removal efficiency

is approximately the same (> 90 percent) for both run 200:313, and run 200:273, Figure (7.42). In case of ferric chloride, run 200:002, and run 200:345, Figure (7.43) reveals that the trend of removal and head loss build-up were the same with deeper solids penetration associated with higher solids concentration. Comparison of 300 and 600 gram of mass deposited with 15 and 30 mg/L influent concentration, respectively, does not result in doubling the head loss value. Retained mass ratio of 2 is equivalent to head loss ratio of 1.2. This observation illustrates that head loss build-up was not only a function of deposit amount, but also of the deposition mechanism and degree of penetration.

Increasing influent concentration from 15 to 30 mg/L, resulted in increasing the solids flow and rate of deposit accumulation, thus shortening the run time and decreasing the effluent quality. The mean average percentage removal was 90 and 84 for 15 and 30 mg/L suspension, respectively. A better distribution of the solids within the bed was achieved because of the increased particle stability at higher solids concentration. This caused an increase in the ultimate quantity of the deposited material at the end of a run and a slower head loss development rate. Figure (7.43) which represents the head loss profile for the initial and final head loss values versus depth gives a quick comparison for the trend of head loss development. The ratio of accumulated deposit is not equivalent to the concentration ratio. Table (7.9) shows the deposit ratio in each layer at a given time for 15 and 30 mg/L influent concentration.

A summary of filtration performance for selected experiments is presented in Table (7.9). The time to achieve equal mass removal of 200 gram and the corresponding head loss developed, provide a basis for comparison of the various individual runs. The effect of different important parameters within any given run, kind of deposition and even the depth of penetration an information which may be derived from these results.

The effect of different deposit geometry, various filtration velocities and coagulant mass on depth of deposit penetration is presented in Table (7.10). A summary of literature investigation and condition compared with results in this study are given in Table (7.11).

7.11 Summary of Model Prediction Comparisons

The head loss models can be used to predict the changes with time, mass or specific deposit as affected by bed depth, media size, bed porosity, filtration velocity and geometry parameter for different coagulant type with different influent concentration. Most of the head loss models reported in the literature allow a description of the change of pressure drop with retention, for the experiment from which they are formulated, but they do not allow an accurate prediction in a new operating conditions. The models formulated in this work is predictive since parameter value obtained from only one experiment could be used to predict the experimental results for different sets of conditions. For the same amount of specific deposit, the predicted head loss values was different in some cases. This is because it is initial head loss, initial geometry parameter and particle surface area dependent. It was found that the present results (filtration of 5 μm and 30 μm silica particles through coarse sand, 1.71 mm in diameter) could satisfactorily predicted with values as a function of specific deposit. This is due to the significant variation of head loss profile when a certain single value of γ used. Therefore an empirical equation is suggested between γ and specific deposit. A study and analysis was made for the models prediction in order to distinguish the role of different operating conditions in developing any of the deposit morphology. The predicted results were then compared with experimental results as well as other head loss equations reported in the literature. It can be seen that they fit reasonably well compared to other proposed equations. This results is an indicative that the

empirical relationships established between model coefficient and other parameters could successfully be used to predict head loss profile for other operating conditions.

Criteria such as PSD or surface area average diameter in filtration are rarely measured in practice or previous research work so the dendrite or combined mode model can not be compared with independent data. The ability of the smooth coating model to predict quantitatively the head loss through filter bed elements for large silica particles (30 μm) with ferric chloride is appreciable. The ability of the combined model to predict quantitatively the head loss through filter bed elements for small silica particles (5 μm) with polymer is good.

Comparing the experimental results with the model prediction, shows how the change in head loss are related to the amount, extent and modes of deposition. Comparison with the experimental results obtained in this work, in particular, ferric chloride experiments, with V_o = 0.3 and 0.6 cm/s, influent concentration = 15 mg/L and particle size of 30 μm showed the smooth coating head loss model quite satisfactory. Results are shown in Figures (7.44) and (7.45).

The effects of particle size on model applicability for a new condition (particle size of 5 μm) are shown in Figures (7.46) and (7.47). Results shown in Figures (7.46) and (7.47) are for experiments with V_o = 0.3 and 0.6 cm/s, respectively. The figures show that head loss increased with decreasing particle size. However, there appear to be some differences in observed head loss trend and thereby the model prediction with variation in filtration velocities. Results shown in Figure (7.47) suggest that the filtration velocity exhibits an influence on the geometry of deposit, extent of particle penetration and consequently, the head loss increase. The effect of higher filtration velocity (0.6 cm/s) became more pronounced at higher degrees of deposition. Again, Figure (7.48) illustrated such an influence at high influent concentration along

with 30 μm silica particles.

Two different modes of deposition formed, by using polymer along with small silica particles (5 μm and < 5 μm) suspension, combined mode and dendritic deposition. Results shown in Figures (7.49) and (7.50) for experiments with $V_o = 0.6$ and 0.1 cm/s; filter media diameter = 0.171 and 0.046 cm; and influent concentration of 15 and 5 mg silica/L, respectively. The agreement between observed and predicted head loss is good. This good agreement is consistent with the fact that introducing the factors α_s and α_d and the factor γ as a function of specific deposit fits the experimental data rather well. However, the trend of head loss behaviour is different when influent concentration were increased to 5.8 mg/L, while all other conditions are kept constant. Results are presented in Figure (7.51).

Table 7.1 Replicated Experiment

Experiment Number	Coagulant Type	Influent Concentration, mg/L	Filtration Velocity, cm/s	Particle Size, m
264 304	percol 728	15	0.3	30
160 161	percol 728	15	0.6	5
343 376	Fe^{3+}	30	0.6	30
262 346	Fe^{3+}	15	0.9	30

Table 7.2 Comparison of Calculated F-Value with $F_{\nu_1\nu_2\alpha}$

Experiment Number	Calculated F-Value					$F_{\nu_1\nu_2\alpha}$*	r^{2+} for observed vs. replicated	
	Unit Bed Element Number						Depth of filter bed, cm	
	1	2	3	4	5		14	86 (overall depth)
304 264	0.67	1.10	0.62	1.20	1.35	1.73		
160 161	0.66	0.54	0.64	0.73	1.04	1.65	0.981	0.985
343 376	0.95	0.88	1.05	0.93	0.95	1.86	0.994	0.997
262 346	0.63	0.48	0.76	1.19	1.48	1.68	0.997	0.997

*ν_1 degree of freedom of numerator
ν_2 degree of freedom of denominator
r^{2+} coefficient of determination
α probability

Note: Correlation coefficient (r) = $\sqrt{r^2}$

Table 7.3 Comparison of Average Head Loss in Replicated Experiments

Experiment Number	Filter Bed Depth, cm	Head Loss, m		Experiment Number	Filter Bed Depth, cm	Head Loss, m	
		Average	Std*			Average	Std
304	14	0.108	0.0516	343	14	0.403	0.206
	32	0.048	0.0138		32	0.342	0.177
	50	0.039	0.0004		50	0.242	0.116
	68	0.030	0.0004		68	0.159	0.062
	86	0.032	0.0005		86	0.115	0.035
264	14	0.132	0.062	.376	14	0.387	0.211
	32	0.056	0.013		32	0.350	0.189
	50	0.041	0.006		50	0.233	0.113
	68	0.037	0.004		68	0.155	0.065
	86	0.038	0.004		86	0.113	0.036
160	14	0.931	0.404	262	14	0.263	0.108
	32	0.280	0.034		32	0.272	0.106
	50	0.099	1.4E-3		50	0.242	0.085
	68	0.067	1.0E-4		68	0.199	0.063
	86	0.049	4.7E-5		86	0.179	0.048
161	14	0.889	0.269	346	14	0.360	0.166
	32	0.234	0.018		32	0.390	0.180
	50	0.093	9.0E-4		50	0.308	0.125
	68	0.068	7.4E-5		68	0.231	0.083
	86	0.051	4.9E-5		86	0.190	0.057

* Standard deviation

Table 7.4 Summary of Iron-Aided Runs

Set No.*	Particle Size, μm	Concentration, mg/L	Experiment: Run number under different conditions		
			Filtration velocity, cm/s		
			0.3	0.6	0.9
1	5	15	200 : 263	200 : 001	200 : 315
2	30	15	200 : 261	200 : 002	200 : 346
3	30	30	200 : 325	200 : 345	200 : 344

*1 Runs with 5 μm particle size and 15 mg Si/L,
2 Runs with 30 μm particle size and 15 mg Si/L,
3 Runs with 30 μm particle size and 30 mg Si/L.

Table 7.5 Summary Table of Different Dynamic Responses

Parameter	Filtration Velocity, cm/s					
	0.3		0.6		0.9	
	1st layer	2nd layer	1st layer	2nd layer	1st layer	2nd layer
Head loss, m	0.086	0.065	0.133	0.130	0.153	0.160
Mass deposit, g	50	20	33	26	19	22
Time to achieve 80 g of removal	800		700		300	
Depth at which 80% of removal achieved	25.5		42.0		46.0	
Dynamic response	Poorly distributed		Uniformly distributed		More uniformly distributed	

Table 7.6 Summary of Filtration Performance for Selected Experiments

Run No.	Particle Size, μm	Influent Conc., mg/L	Coagulant	V_0 cm/s	Time* minute	Head Loss, Meter
200 : 203	5	15	Fe^{3+}	0.3	2250	0.39
200 : 001	5	15	Fe^{3+}	0.6	1470	1.18
200 : 315	5	15	Fe^{3+}	0.9	780	1.20
200 : 261	30	15	Fe^{3+}	0.3	2000	0.49
200 : 002	30	15	Fe^{3+}	0.6	1500	0.77
200 : 346	30	15	Fe^{3+}	0.9	720	1.03
200 : 260	5	15	percol 728	0.3	2220	0.60
200 : 161	5	15	percol 728	0.6	1320	1.21
200 : 347	5	15	percol 728	0.9	700	1.16
200 : 204	30	15	percol 728	0.3	2500	0.40
200 : 014	30	15	percol 351	0.6	1110	1.50
200 : 313	30	30	percol 728	0.6	1440	1.56
200 : 316	5	30	Fe^{3+}	0.6	1170	0.61
200 : 325	30	30	Fe^{3+}	0.3		
200 : 015	30	15	No Aid	0.6	*	–
200 : 016	5	15	No Aid	0.6	*	–
200 : 332	30	30	No Aid	0.6	810	0.34
200 : 345	30	30	Fe^{3+}	0.6	1220	1.15
200 : 013	5	15	percol 351	0.6	2280	0.37
200 : 304	30	15	percol 728	0.3	*	–
200 : 371	5	15	No Aid	0.3	2650	0.646
200 : 372	5	15	No Aid	0.9		

*Time required to achieve 200 gram of mass removal

Table 7.7 Comparison of Solids Retained (gram) In Each Layer at Time 1000 Minute

Filtration Velocity, cm/s	Depth From Surface, cm				
	14	32	50	68	86
0.3	14.0	14.0	7.5	10.0	5.0
0.6	14.0 (100)	15.0 (87)	12.0 (25)	11.0 (82)	10.5 (0)
0.9	18.0 (133)	16.0 (162)	10.0 (125)	9.5 (215)	10.5 (43)

( ) Percentage of solids reduction due to increasing filtration velocity

Table 7.8 Summary of Filter Runs used to Compare the Effect of Influent Concentration

Coagulant Type	Influent Concentration		Notes
	15	30	
Iron-Aided	200 : 261 200 : 002	200 : 325 200 : 345	30 μm, V_0 = 0.3 30 μm, V_0 = 0.6
Polymer-Aided	200 : 161 200 : 014	200 : 273 200 : 313	5 μm, V_0 = 0.6 30 μm, V_0 = 0.6
No-Aided	200 : 015	200 : 332	30 μm, V_0 =0.6

Table 7.9 Deposit Ratio ($Mass_{30}/Mass_{15}$) At Different Layers

Run. No.	Influent Concentration	Deposit Ratio at Different Depth, cm					Total Influent Solids, gram	Time, Minute
		14	32	50	60	86		
200 : 002 200 : 345	15 30	1.86	2.5 3	3.1 2	2.8 6	5.0 8	374.0 947.0	2500 2500
200 : 161 200 : 273	15 30	0.8	1.7 5	2.6	2.0	1.3 3	252.0 557.0	1500 1500

Table 7.10 Depth of Penetration of Removed Material at Which 80 percent of Solids Removed, cm

Run No.	Time, Minutes					
	500	750	1000	1500	1750	2000
200 : 015	59.0	59.6	60.0	60.4	60.8	61.5
200 : 016	65.4	63.8	65.6	62.7	64.2	63.5
200 : 371	55.0	54.6	53.0	55.7	57.3	52.3
200 : 332	65.4	63.9	64.2	63.5	63.5	68.8
200 : 372	64.2	64.6	58.5	61.1	62.3	60.0
200 : 374	51.5	53.0	53.0	48.5	51.9	46.5
200 : 375	50.5	60.4	58.5	59.0	59.0	59.0
200 : 263	32.7	33.5	37.7	47.7	52.3	56.5
200 : 001	48.0	48.8	51.2	54.6	58.8	62.3
200 : 315	51.2	52.7	54.2	62.7	65.0	56.2
200 : 261	25.3	25.3	27.3	30.0	31.5	35.0
200 : 002	38.0	43.0	45.4	48.5	48.5	47.7
200 : 346	50.0	53.0	57.7	63.0	64.6	66.2
200 : 013	27.7	28.5	31.5	30.7	31.0	35.0
200 : 014	↑	↑	↑	17.3	19.2	20.7
200 : 160	20.0	22.7	25.4	24.6	26.9	30.0
200 : 161	17.7	21.5	24.6	28.5	30.8	31.5
200 : 264	↑	↑	↑	13.8	14.3	16.2
200 : 304	↑	↑	↑	19.2	16.5	15.8
200 : 259	31.2	36.2	47.7	48.0	51.2	52.7
200 : 347	36.9	37.7	38.5	41.2	42.7	43.9
200 : 273	32.0	42.7	48.5	57.7	←	←
200 : 086	27.7	28.9	46.2	31.2	45.4	40.0
200 : 313	20.3	21.2	24.6	29.2	30.7	32.3

Table (7.10) cont'd.

Run No.	Time, Minutes					
	500	750	1000	1500	1750	2000
200 : 015	59.0	59.6	60.0	60.4	60.8	61.5
200 : 325	21.5	24.6	27.3	32.3	35.4	39.6
200 : 326	29.2	36.5	42.3	57.3	60.4	←
200 : 316	47.3	51.5	53.9	55.8	56.9	58.8
200 : 344	54.6	60.4	64.6	←	←	←
200 : 345	41.5	45.4	49.2	58.5	62.3	64.6
200 : 343	41.2	43.0	49.2	58.0	58.5	←
200 : 377	45.8	50.0	51.2	51.5	←	←
200 : 361*	22.0	18.6	11.0	12.1	17.9	8.3
200 : 362*	13.8	6.0	7.1	22.3	←	←
200 : 369*	22.7	20.0	16.5	↑	↑	↑
200 : 370*	21.3	22.5	23.0	24.2	←	←
200 : 262	51.0	53.5	58.0	62.0	65.0	66.4
200 : 085	49.0	50.7	52.0	53.6	54.5	56.0
200 : 274	45.6	51.2	55.7	58.0	61.3	64.0
200 : 331	50.1	50.6	56.4	57.6	59.2	60.3

Legend:
↑ More than 80 percent of material removed at this time
← The run terminated before this time
* Settled 5 μm (<5 μm) silica run with polymer (percol 728)
+ Settled 5 μm (<5 μm) silica run with Ferric chloride.

Notes:

Compare run 200 : 002 and run 200 : 014 to illustrate different deposit geometry effect.

Compare run 200 : 264 and run 200 : 161 to illustrate the effect of different filtration velocity.

Compare run 200 : 001 and run 200 : 002 to illustrate insufficient coagulant mass per unit mass of suspended solids effect.

Table 7.11 Summary of Literature Investigation and Condition

Particle Characteristic			Filter Media Characteristic			Coagulant		Mode of deposition	Reference
Particle size, μm	Particle conc., mg/L	Particle type	Media size, mm	Porosity	Filtration velocity, cm/sec	Type of coagulant	Coagulant conc., mg/L		
0.1	9.7	PSL	0.397 (L.B.)	0.36	0.136	polymer (CAT-Floc)	0.07		Yao and Habibian (1971)
1.305		PSL	9.6 μm		13.8			dendrites	Tien et al. (1977)
0.1 1.0 7.6	9.7 37.2 14.7	PSL	0.38	0.36		Polymer (CAT-floc) PEI-18		dendrites	O'Melia and Ali (1978)
3-35 3-35		GMS GMS	1.75	0.40	0.132-0.833	Non-ionic polymer (Praestol, A968)			Tien and Gimbel (1982)
0.109 1.099 7.60	48					Polymer CAT-Floc PEI-6 PEI-18 PEI-600 PEI-1000	 0.029 0.050 0.024 0.025		Haibian and O'Melia (1975)

Table (7.11) cont'd.

Particle Characteristic			Filter Media Characteristic			Coagulant		Mode of deposition	Reference
Particle size, μm	Particle conc., mg/L	Particle type	Media size, mm	Porosity	Filtration velocity, cm/sec	Type of coagulant	Coagulant conc., mg/L		
15	50		200 μm 300 μm 50 μm0 (G.B.)	0.395	2.18			blocking mode	Pendse, Tien and Turian (1978)
4-25	5.0 7.0	(hydrous ferric oxide flocs)	0.59-0.84 (sand)		0.204 0.408				Fox and Cleasby (1966)
0.091-15.2	5-100	PSL	0.49-0.52 (sand)	0.41	(0.0264-0.158)				Russel and Ghosh
0.091-15.2 0.481	10-100 50	PSL PSL	0.5 (sand) 0.5 (sand)	0.40 0.40	(0.0264-0.158) 0.133	Polymer PEI-18 PEI-600	0.01-22.0 0.18 0.12		Ghosh et al. (1975)
0.5-150 (5 μm)	15	PSL	1.71	0.43	0.6	Polymer (percol 728)	0.05	combined mode (smooth coating + dendrite)	This study
Settled 5 μm	5	Silica	0.45	0.36	0.1	percol 728	0.05	dendrite	This study

Table (7.11) cont'd.

Particle Characteristic			Filter Media Characteristic			Coagulant		Mode of deposition	Reference
Particle size, μm	Particle conc., mg/L	Particle type	Media size, mm	Porosity	Filtration velocity, cm/sec	Type of coagulant	Coagulant conc., mg/L		
0.5-150 (30 μm)	15	Silica	1.71	0.43	0.6	Ferric chloride	0.25	smooth coating	This study
0.5-150 (30 μm)	15	Silica	1.71	0.43	0.6	percol 351	0.05	surface removal	This study
0.5-150 (30 μm)	30	Silica	1.71	0.43	0.6	Ferric chloride	0.25	blocking mode	This study
0.5-150 (30 μm)	15	Silica	1.71	0.43	0.3	percol 728	0.05	smooth coating	This study

Legend:

L.B. = Latex beads
PSL = polystyrene latex particles
GMS = Glass micro spheres
G.B. = Glass beads

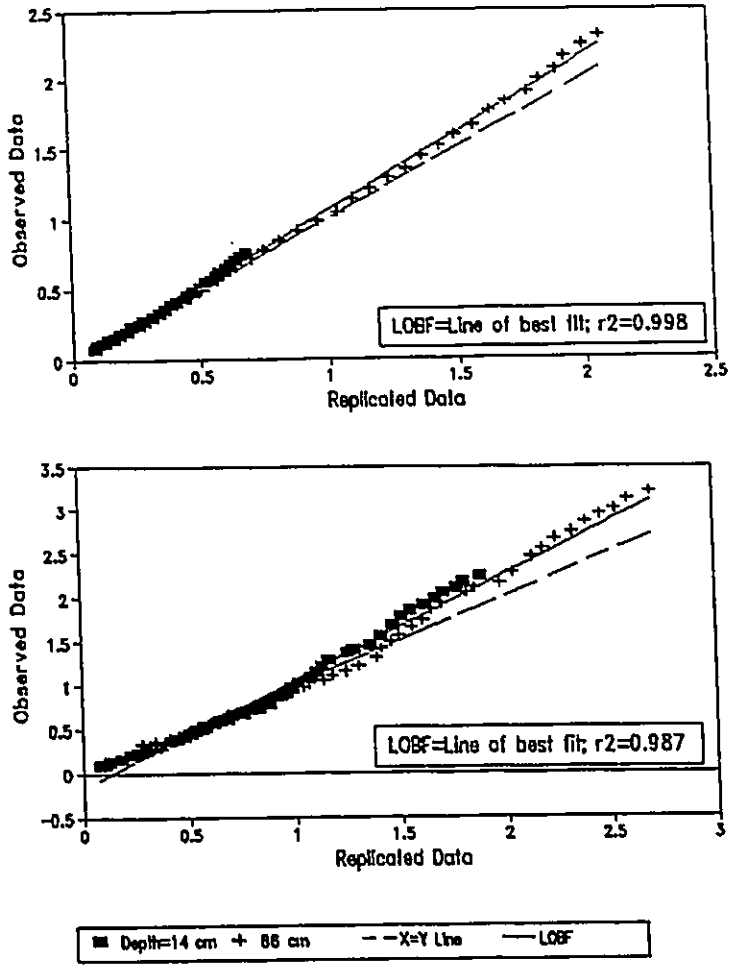

Figure 7.1 **Observed versus replicated head loss data (verification the reproducing capability between runs)**

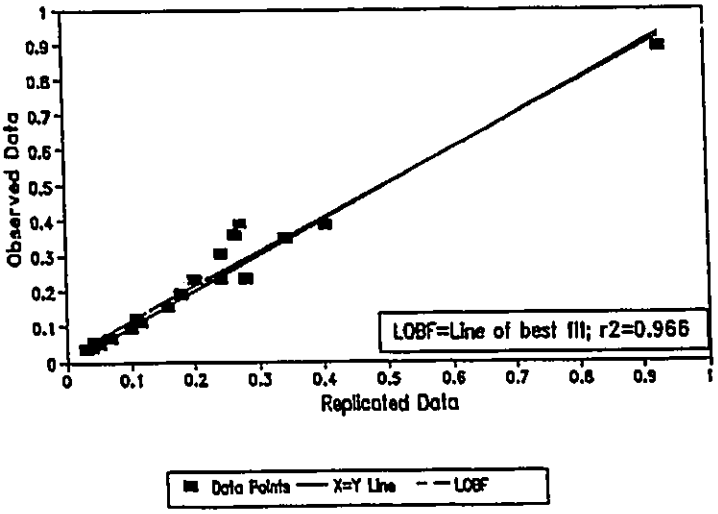

Figure 7.2 **Observed average versus replicated average head loss data (verification the overall reproducing capability of the system**

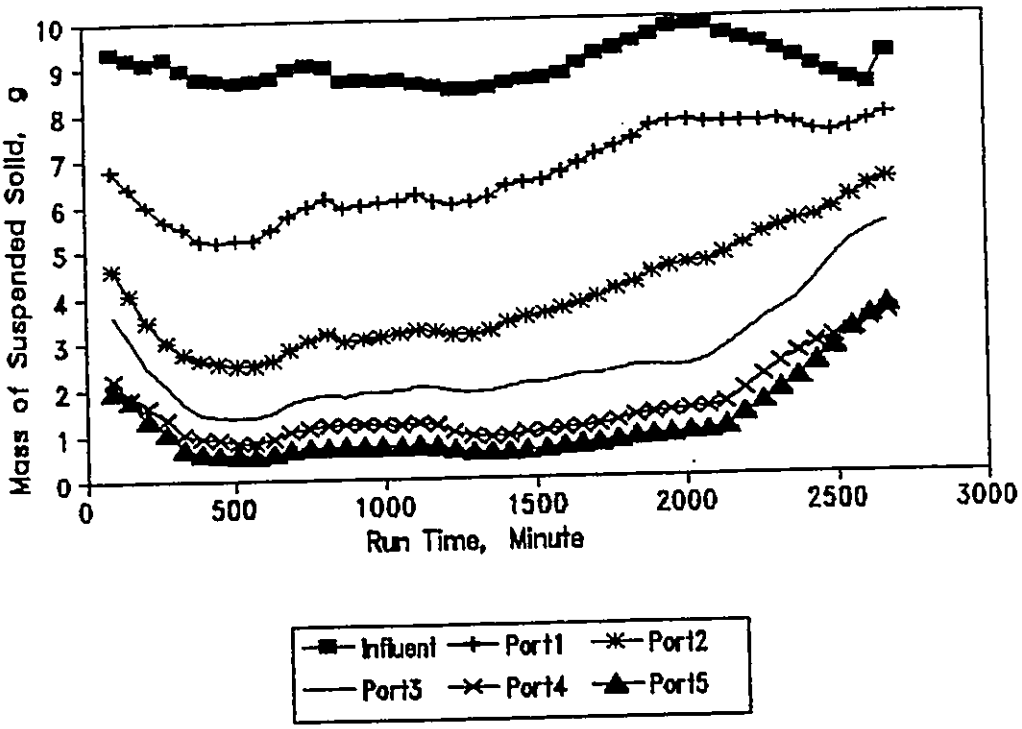

Figure 7.3 Mass of suspended solids versus time (Fe^{3+}, 30 μm, 15 mg Si/L, V_o = 0.6 cm/s)

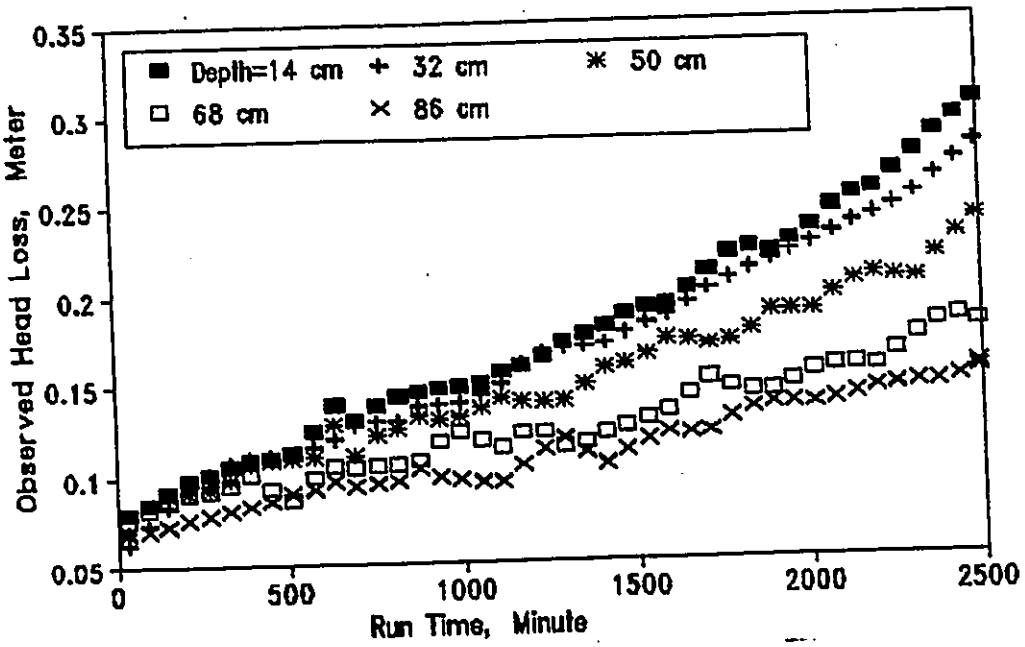

Figure 7.4 Observed head loss versus time (Fe^{3+}, 30 μm, 15 mg Si/L, V_o = 0.6 cm/s)

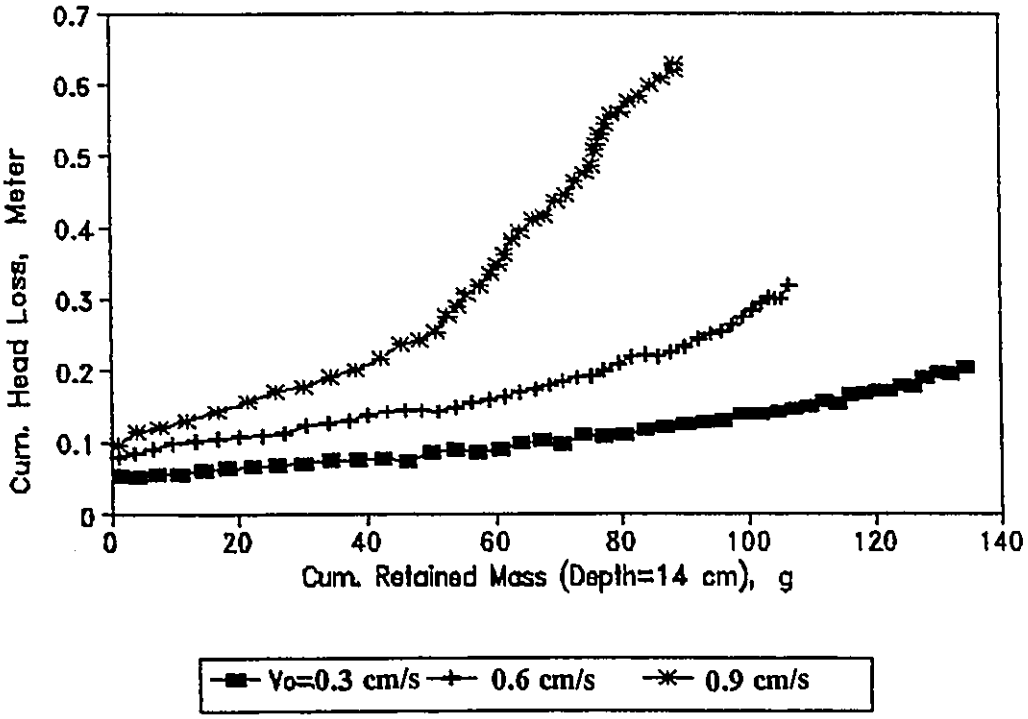

Figure 7.5 Head loss versus cumulative mass deposit comparison (Fe^{3+}, 30 μm, 15 mg Si/L, V_0 = 0.3, 0.6 and 0.9 cm/s)

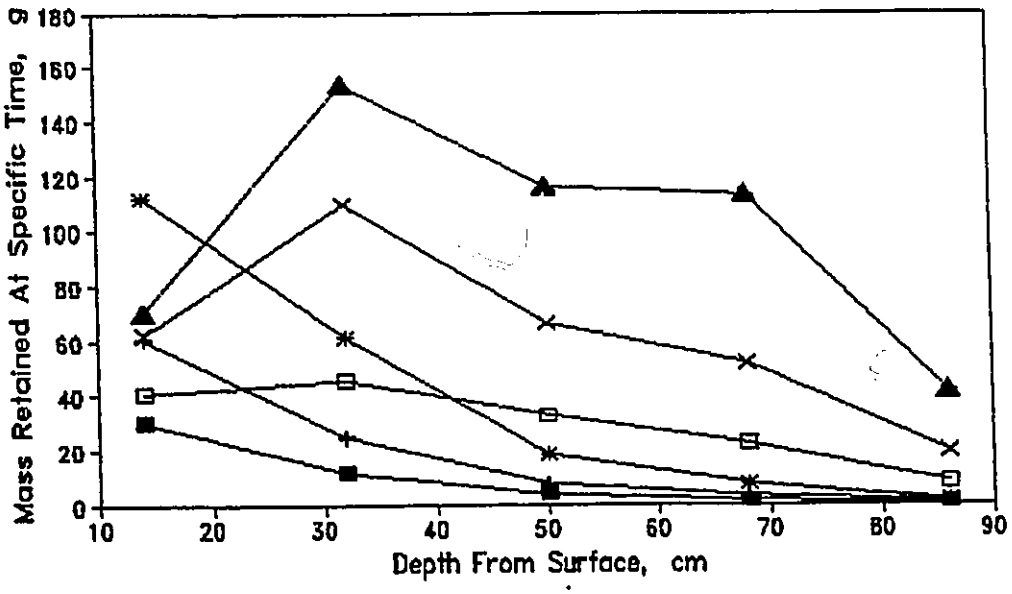

Figure 7.6 Mass retained at specific time versus depth (Fe^{3+}, 30 μm, 15 mg Si/L, V_0 = 0.3 and 0.9 cm/s)

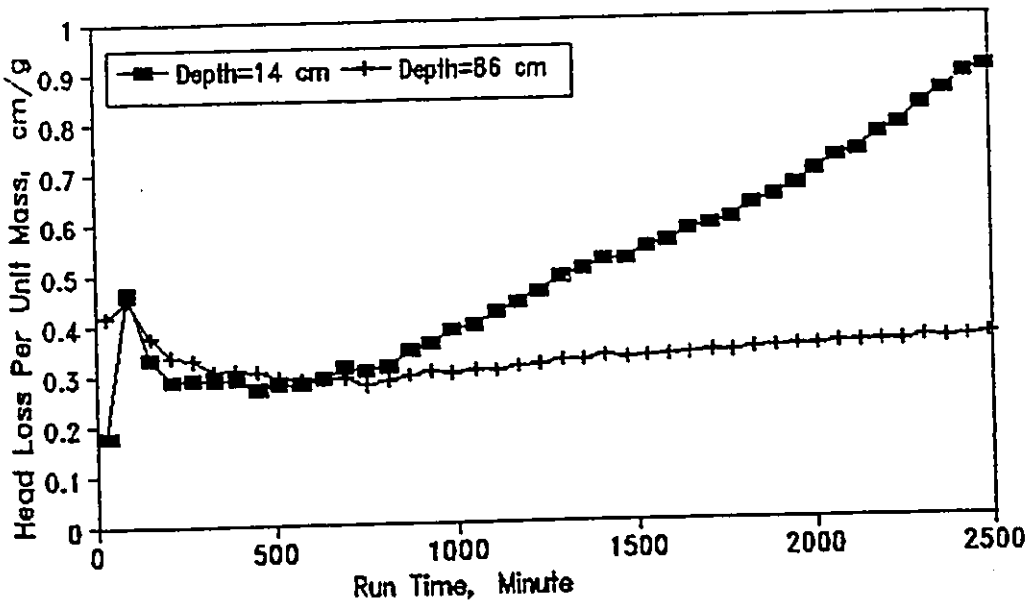

Figure 7.7 Head loss development rate versus time (Fe^{3+}, 30 μm, 15 mg Si/L, V_o = 0.9 cm/s)

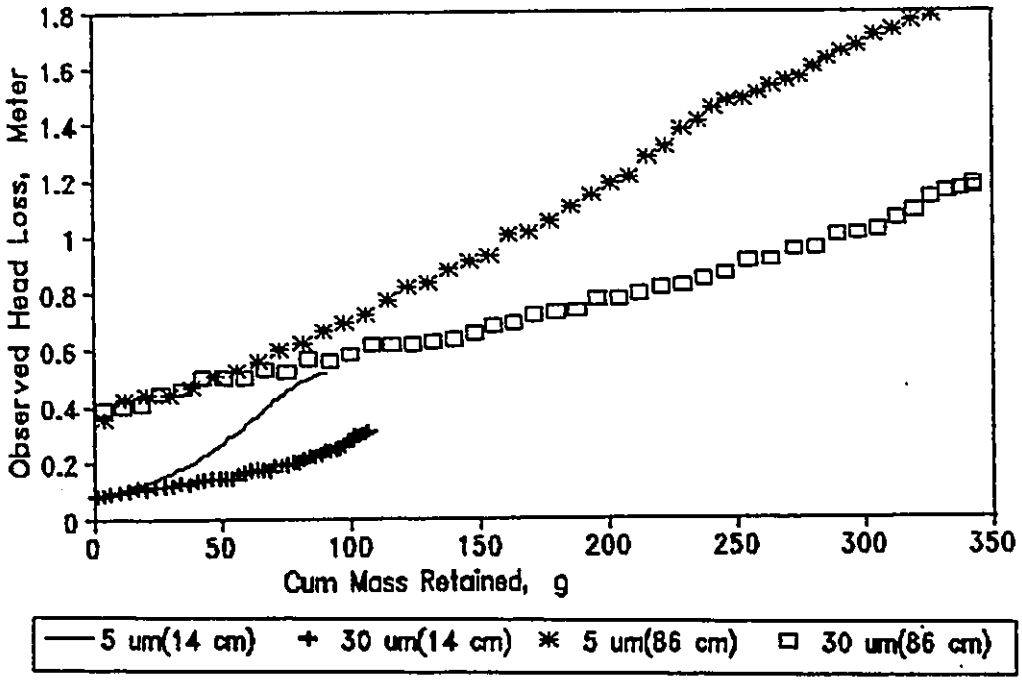

Figure 7.8 Comparison of head loss versus retained mass (Fe^{3+}, 5 and 30 μm, 15 mg Si/L, V_o = 0.6 cm/s)

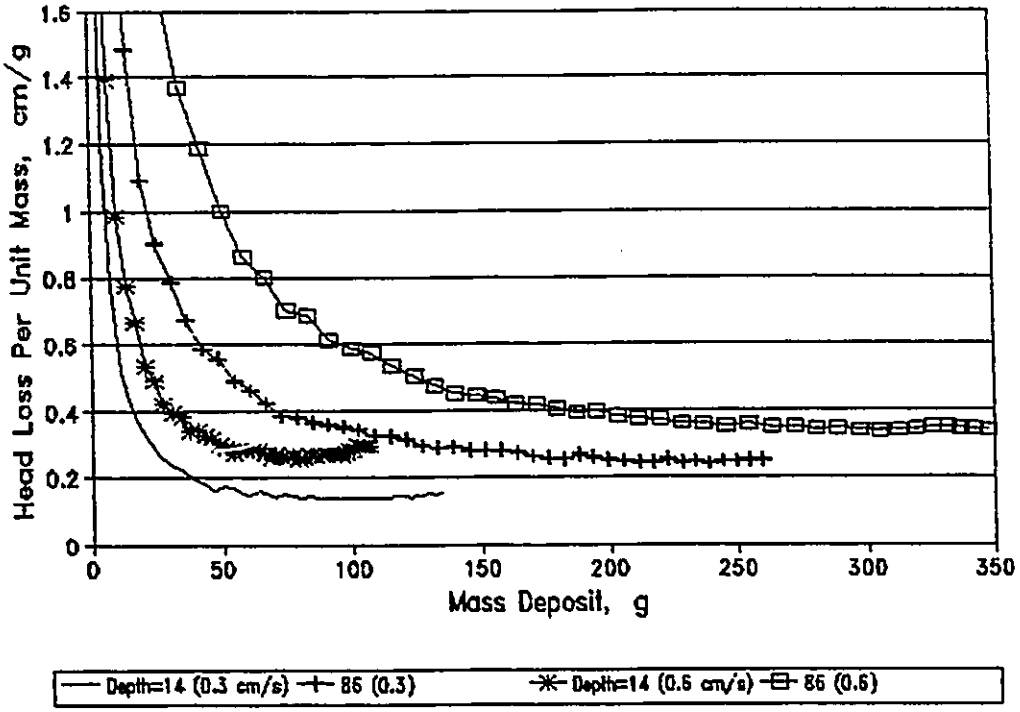

Figure 7.9 Head loss per unit mass deposit versus mass deposit at different filtration velocities (Fe^{3+}, 5 μm, 15 mg Si/L, V_o = 0.3 and 0.6 cm/s)

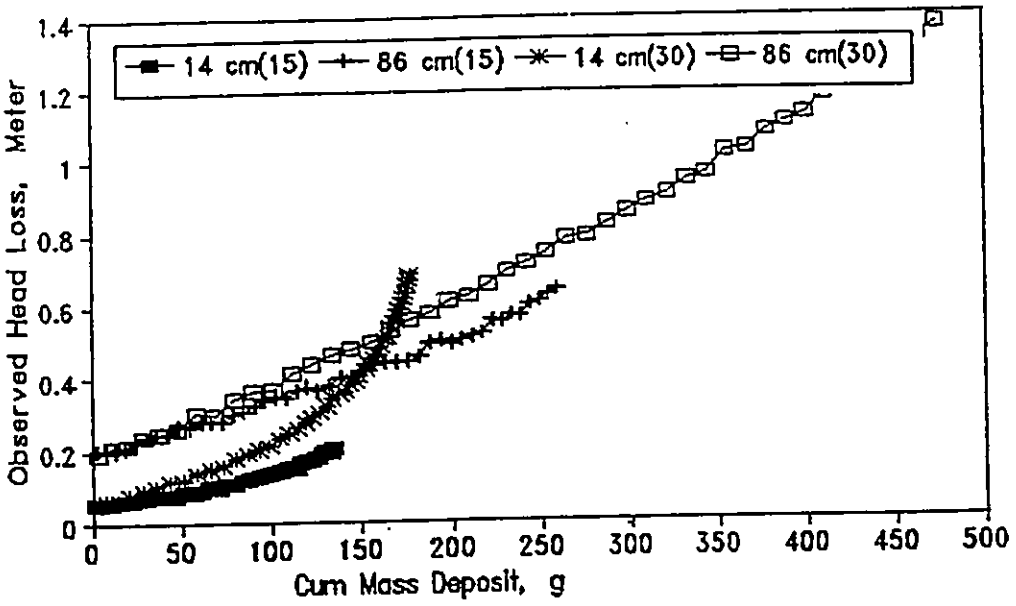

A

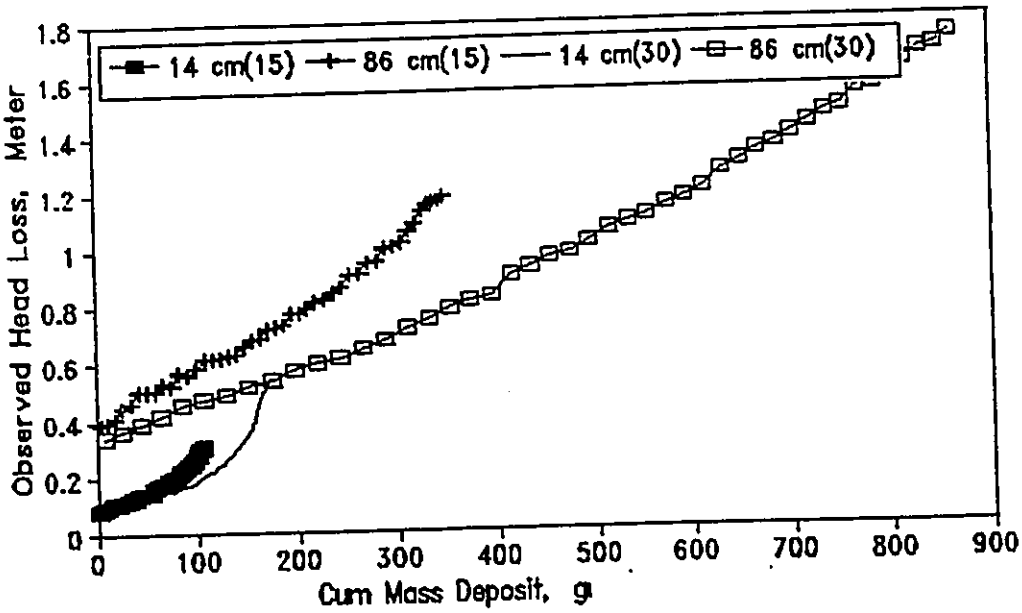

B

Figure 7.10 **Comparison of head loss versus cumulative mass deposit for different suspended solid concentration (Fe^{3+}, 30 μm, 15 and 30 mg Si/L). a) 0.3 cm/s, and b) 0.6 cm/s**

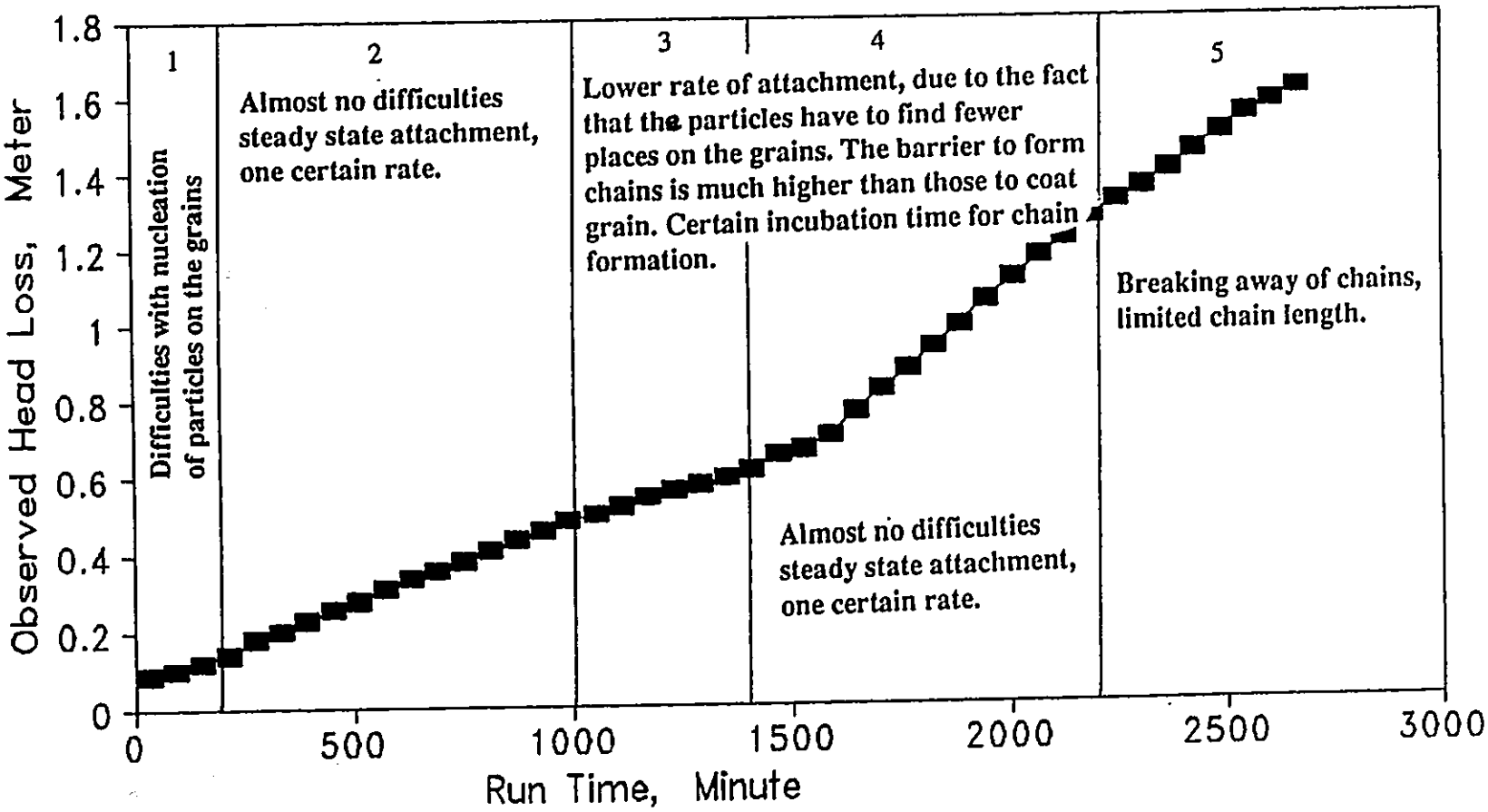

Figure 7.11 Head loss versus time, smooth coating and chain argument (polymer, 5 μm, 15 mg Si/L, V_0 = 0.6 cm/s)

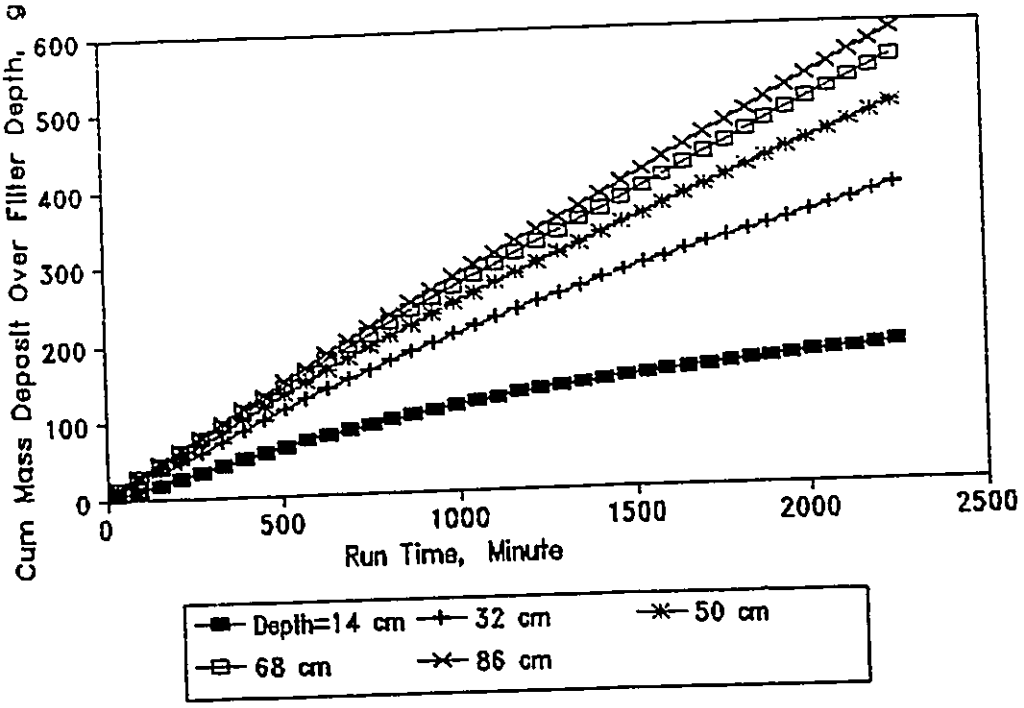

A

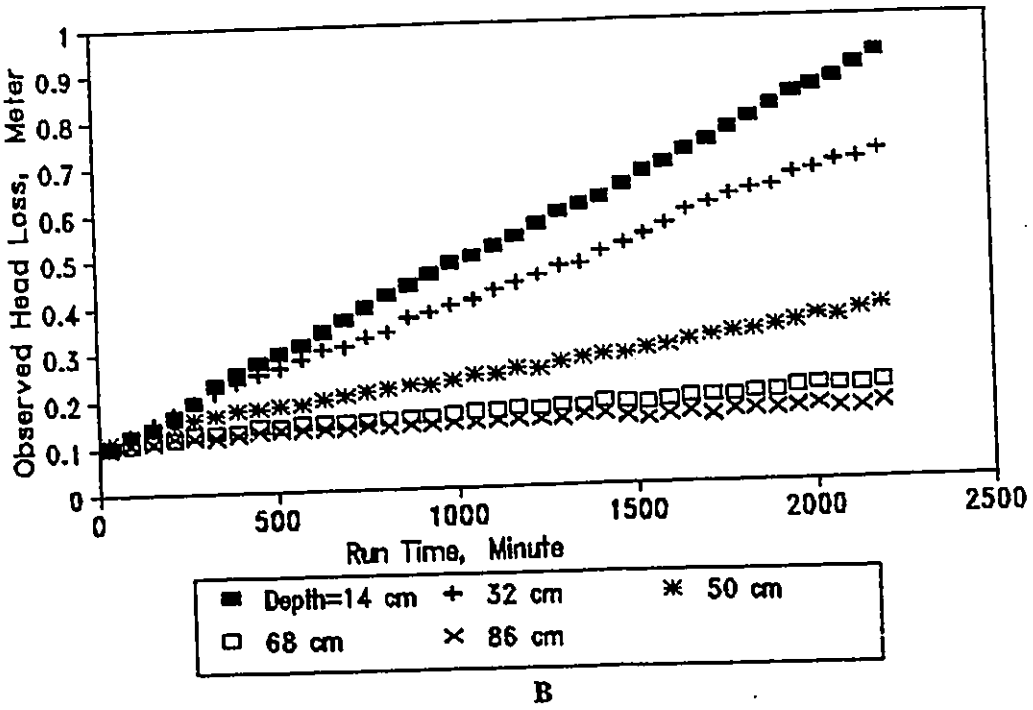

B

Figure 7.12 a) observed mass of suspended solids at different ports versus time, b) observed head loss versus time (polymer, 5 μm, 15 mg Si/L, V_o = 0.9 cm/s)

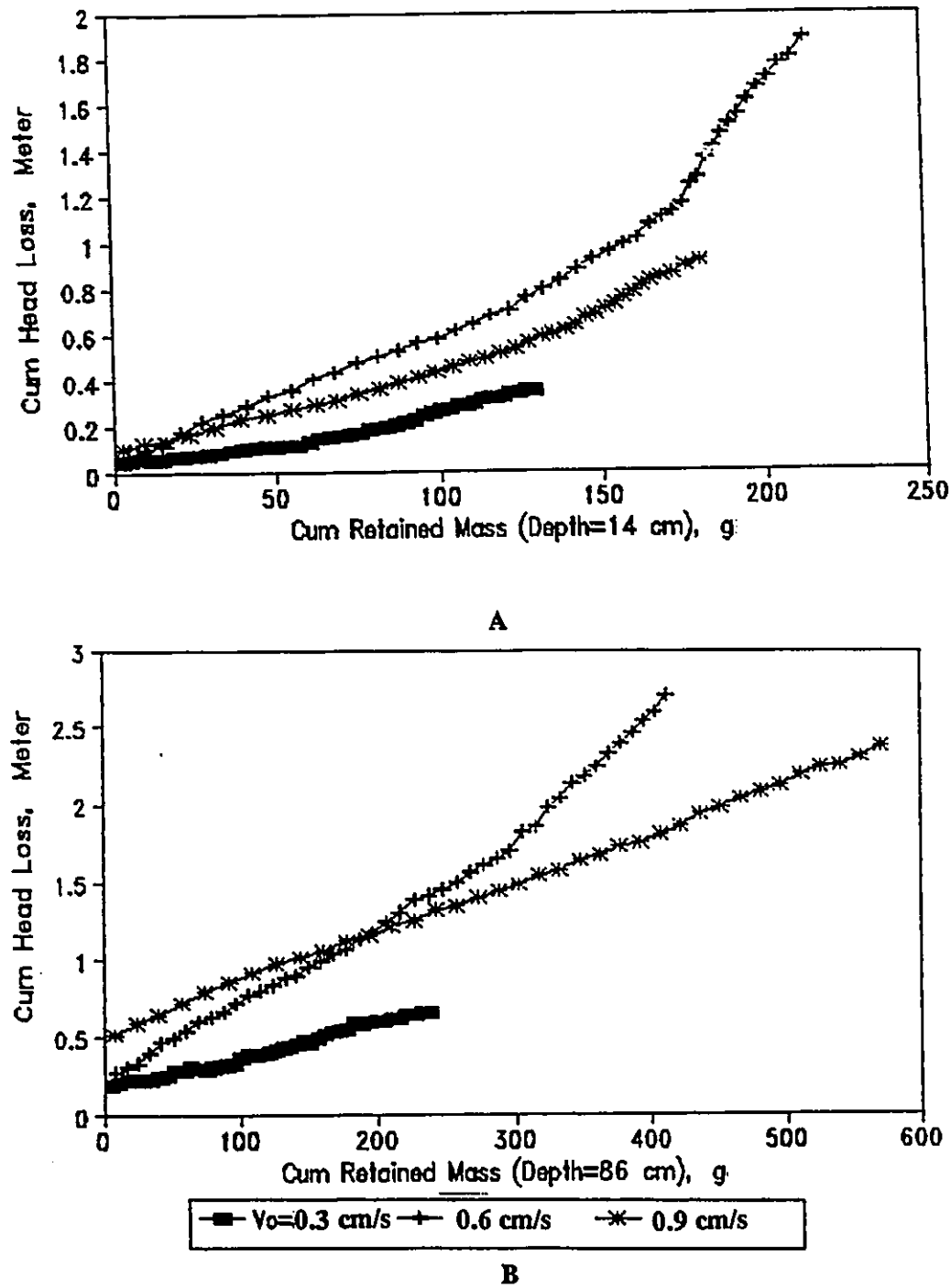

Figure 7.13 Comparison of head loss versus cumulative mass deposit at different filtration velocities; a) First layer, b) overall depth (polymer, 5 μm, 15 mg Si/L, V_0 = 0.3, 0.6 and 0.9 cm/s)

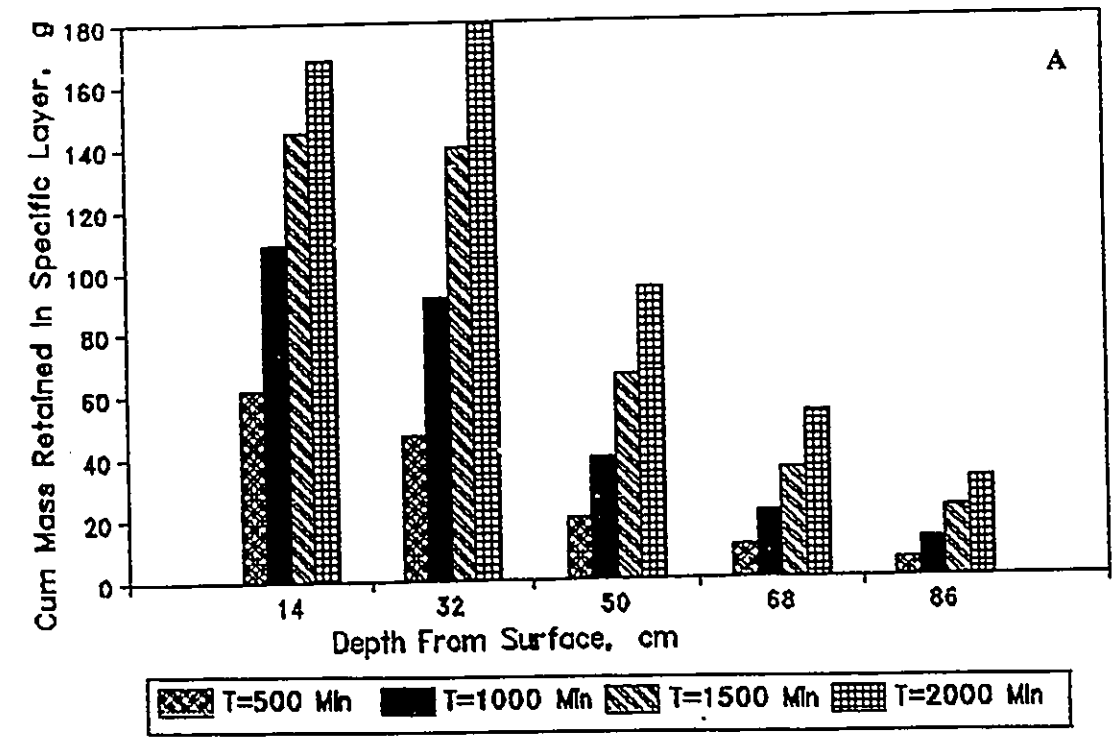

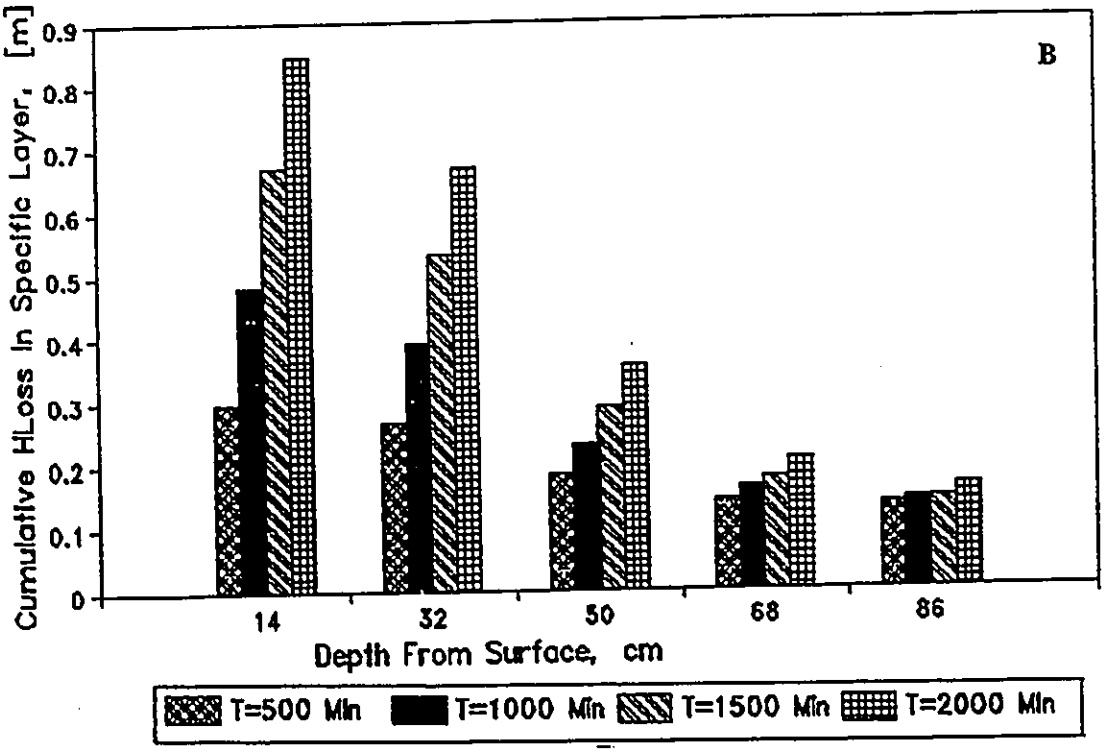

Figure 7.14 Bar-diagram of a) cumulative mass deposit in specific layers, b) head loss in specific layers (polymer, 5 μm, 15 mg Si/L, V_0 = 0.9 cm/s)

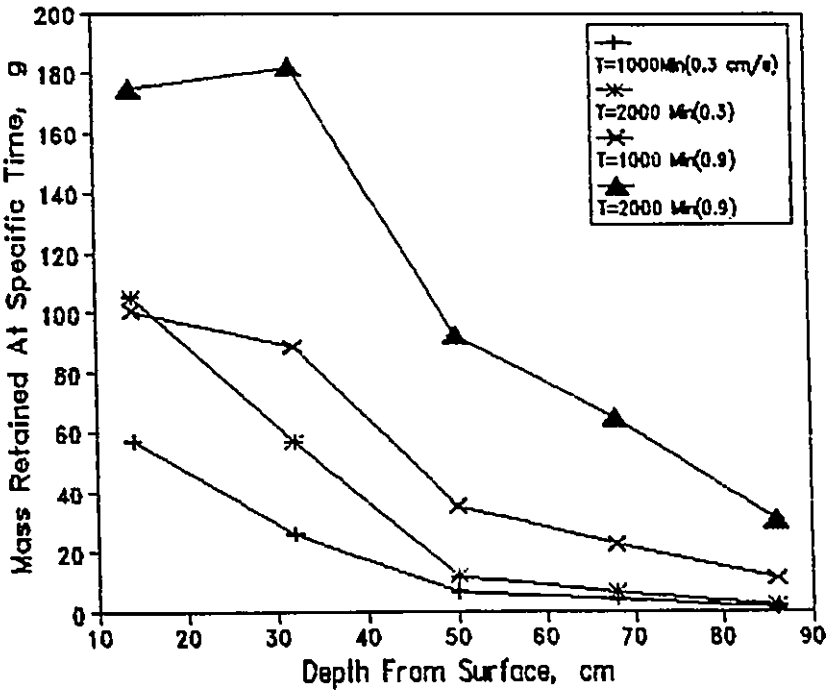

Figure 7.15 Mass deposit versus depth at different time intervals (polymer, 5 μm, 15 mg Si/L, V_0 = 0.3 and 0.9 cm/s)

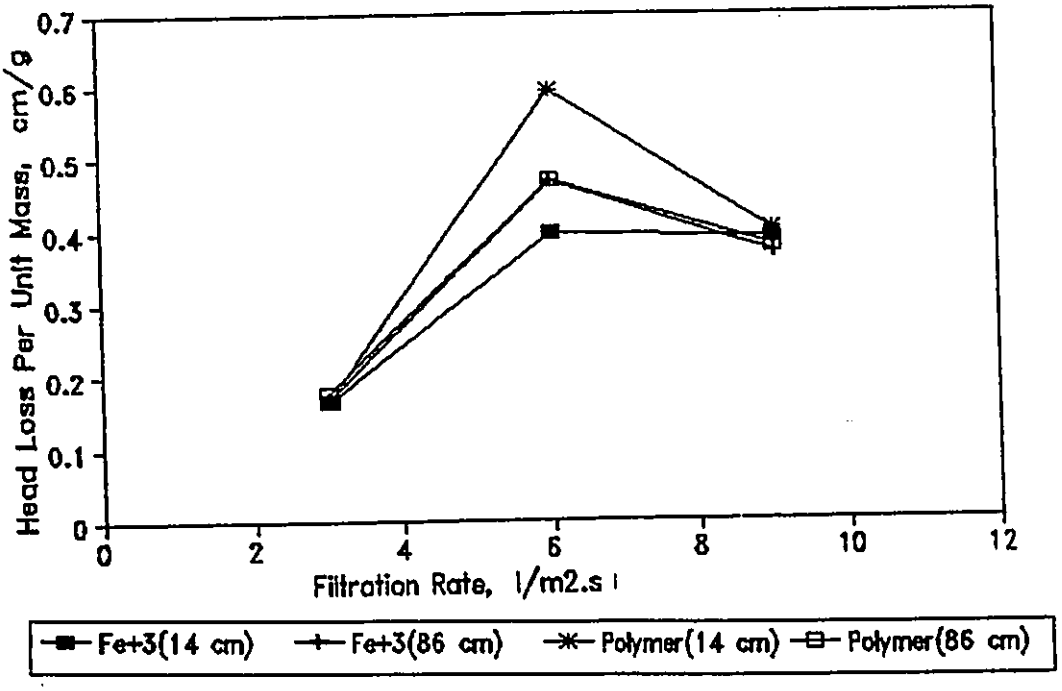

Figure 7.16 Comparison of head loss rate versus filtration rate (Fe^{3+} and polymer, 5 μm, 15 mg Si/L, V_0 = 0.3, 0.6 and 0.9 cm/s)

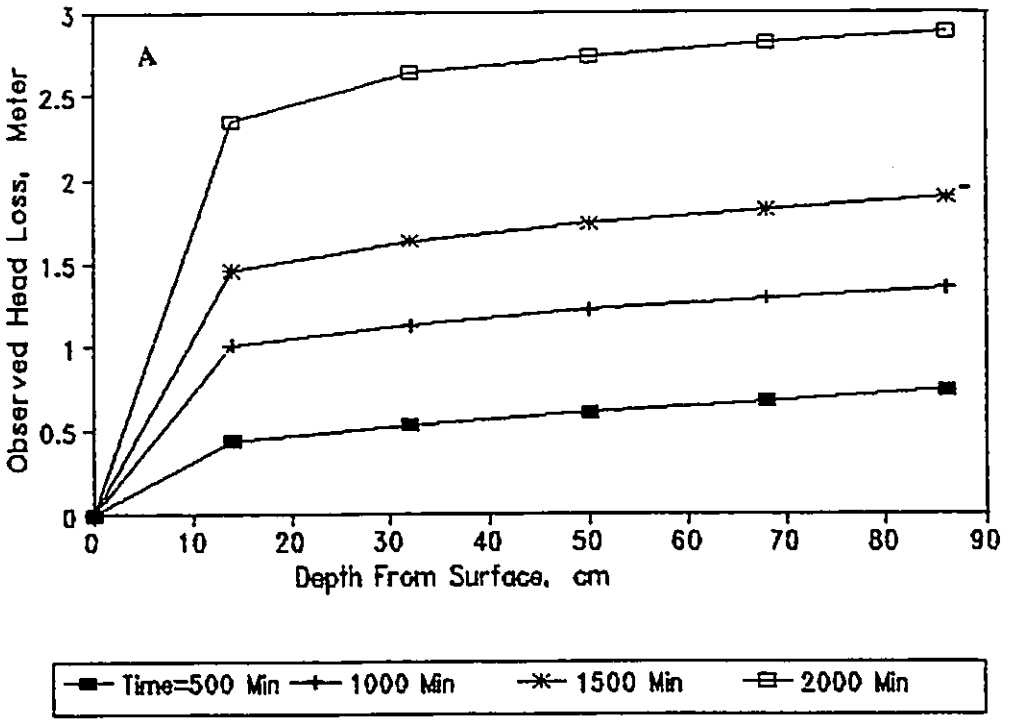

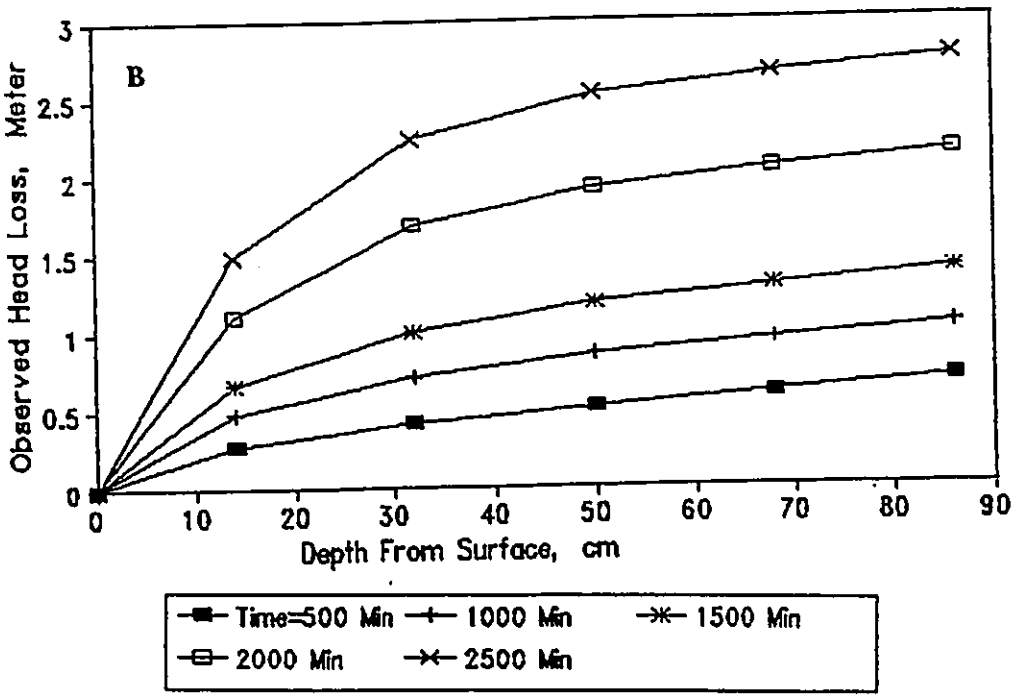

Figure 7.17 **Observed head loss rate versus depth at different time intervals (polymer, 5 and 30 μm, 15 mg Si/L, V_o = 0.6 cm/s)**
a) 30 μm, b) 5 μm

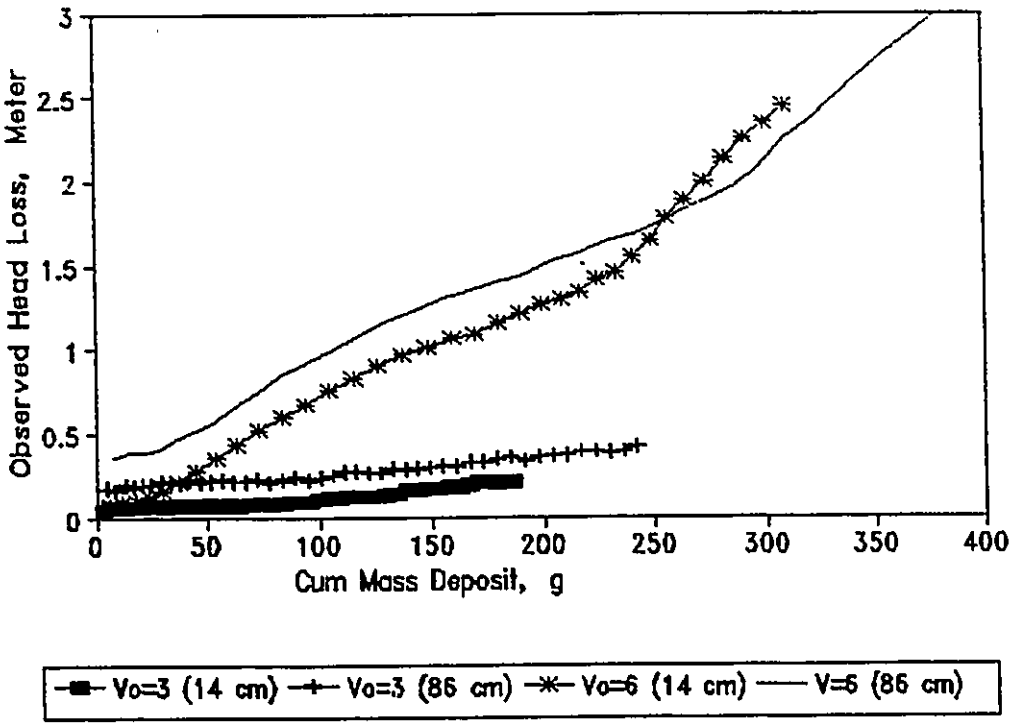

Figure 7.18 Comparison of head loss versus cumulative mass deposit at different filtration velocity (polymer, 30 μm, 15 mg Si/L, V_o = 0.3 and 0.6 cm/s)

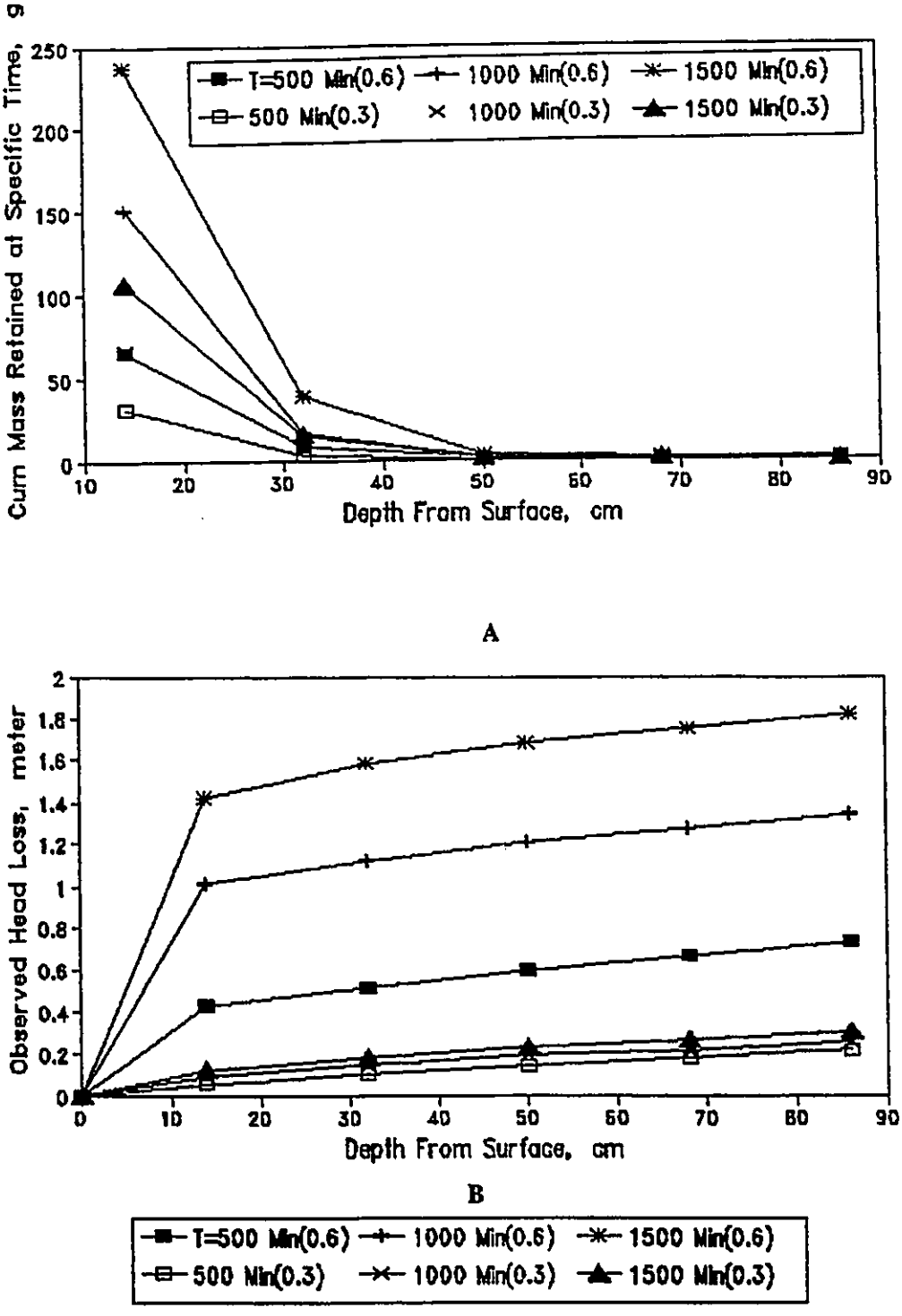

Figure 7.19 Mass deposit and head loss versus depth at different time intervals (polymer, 30 μm, 15 mg Si/L, V_0 = 0.3 and 0.6 cm/s)
a) Mass deposit, b) Head loss

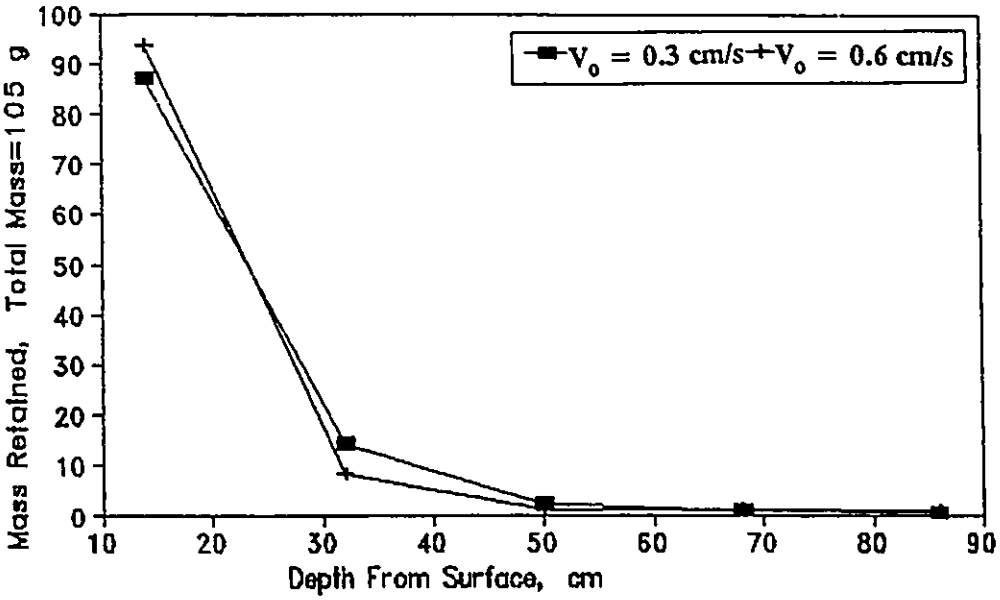

A

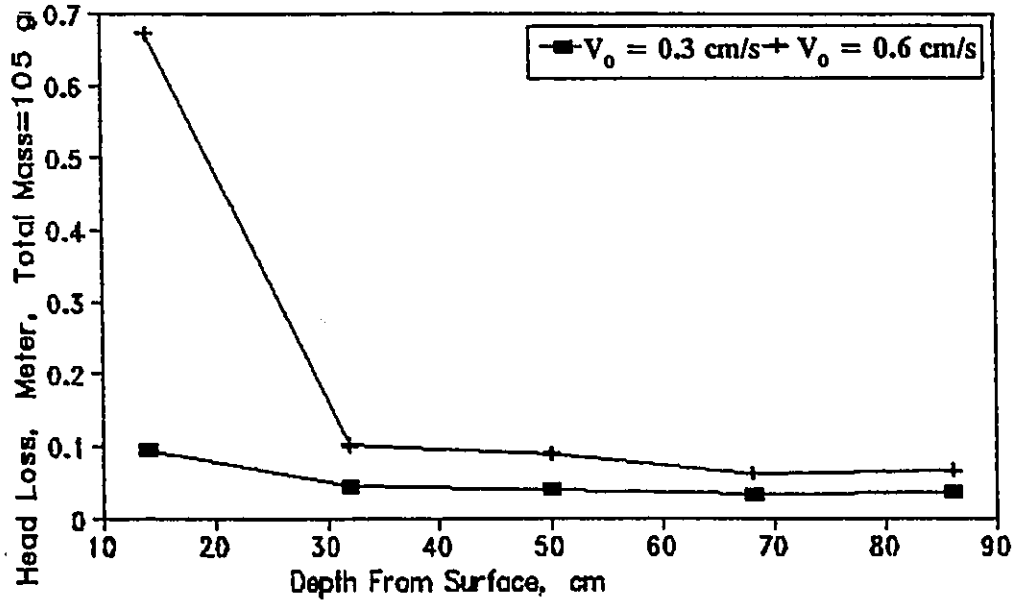

B

Figure 7.20 Comparison of mass deposit and head loss versus depth for different filtration velocity (polymer, 30 μm, 15 mg Si/L, V_0 = 0.3 and 0.6 cm/s) a) Mass deposit vs. depth, b) Head loss versus depth

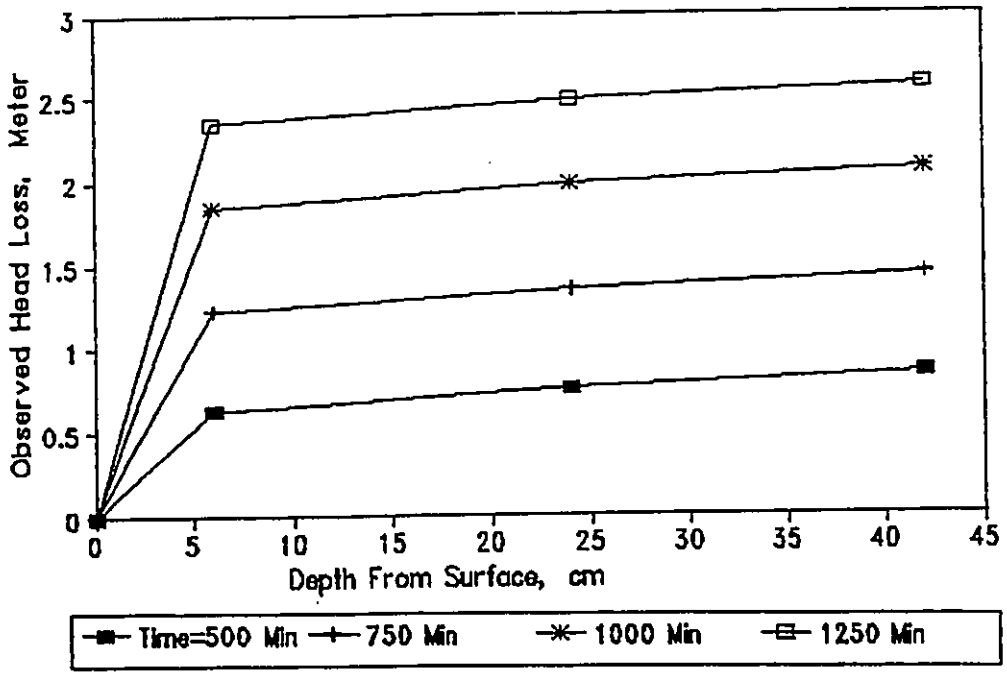

Figure 7.21 Observed head loss versus depth (polymer, settled 5 μm, 5.8 mg Si/L, V_0 = 0.1 cm/s)

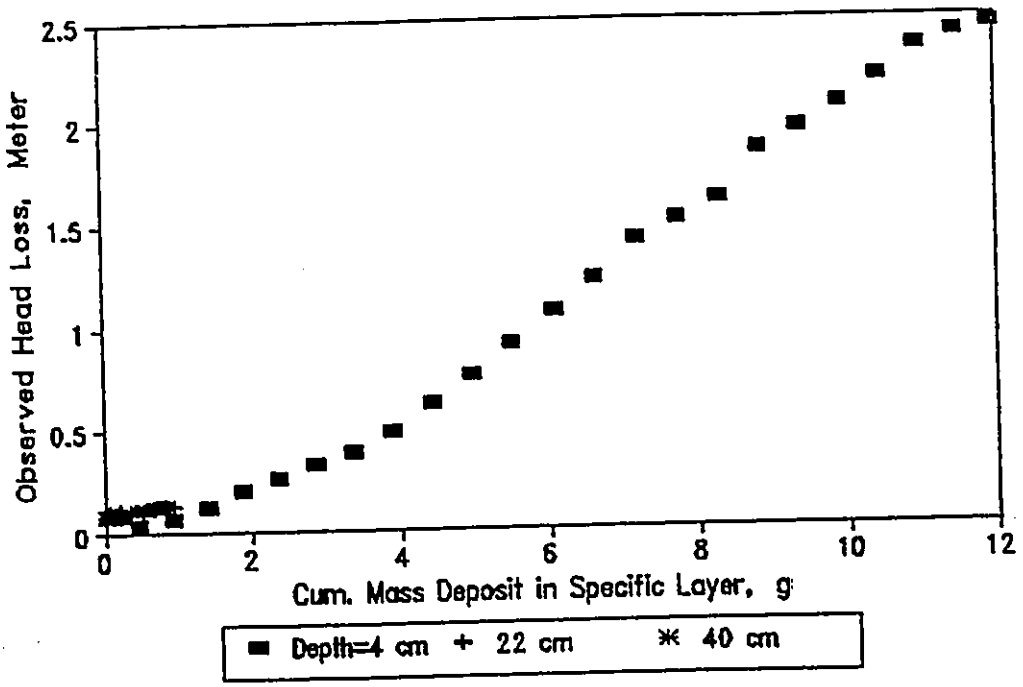

Figure 7.22 Head loss versus cumulative mass deposit (polymer, settled 5 μm, 5.8 mg Si/L, V_0 = 0.1 cm/s)

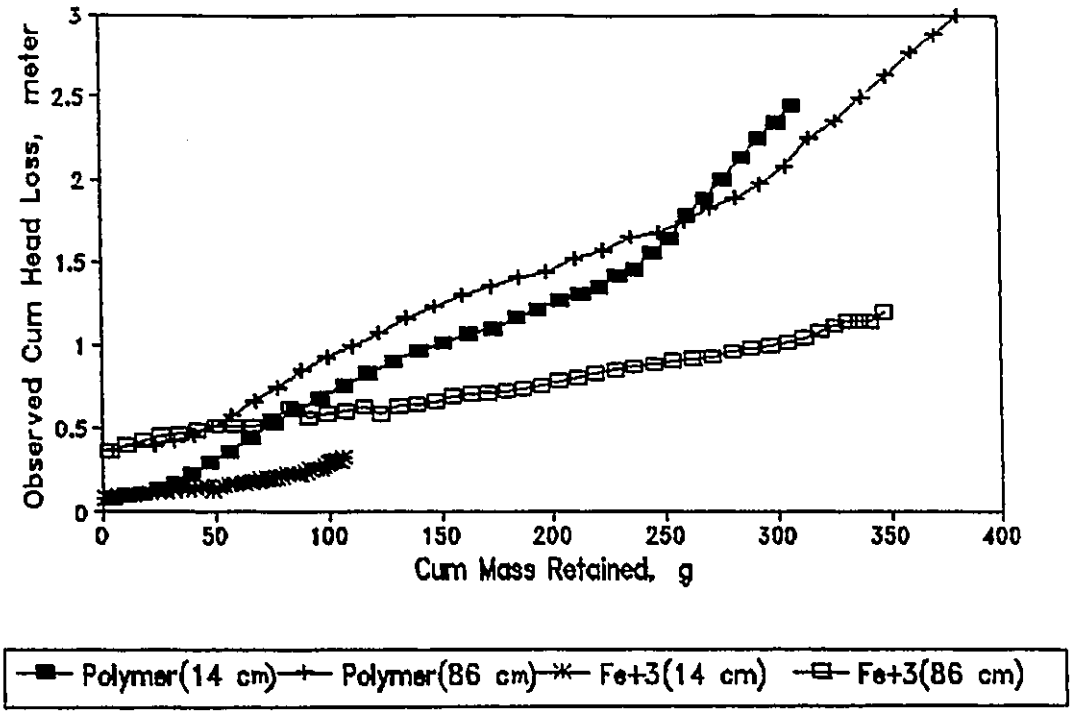

Figure 7.23 Head loss versus cumulative mass comparison, depth = 14 and 86 cm (Fe^{3+} and polymer, 30 μm, 15 mg Si/L, V_0 = 0.6 cm/s)

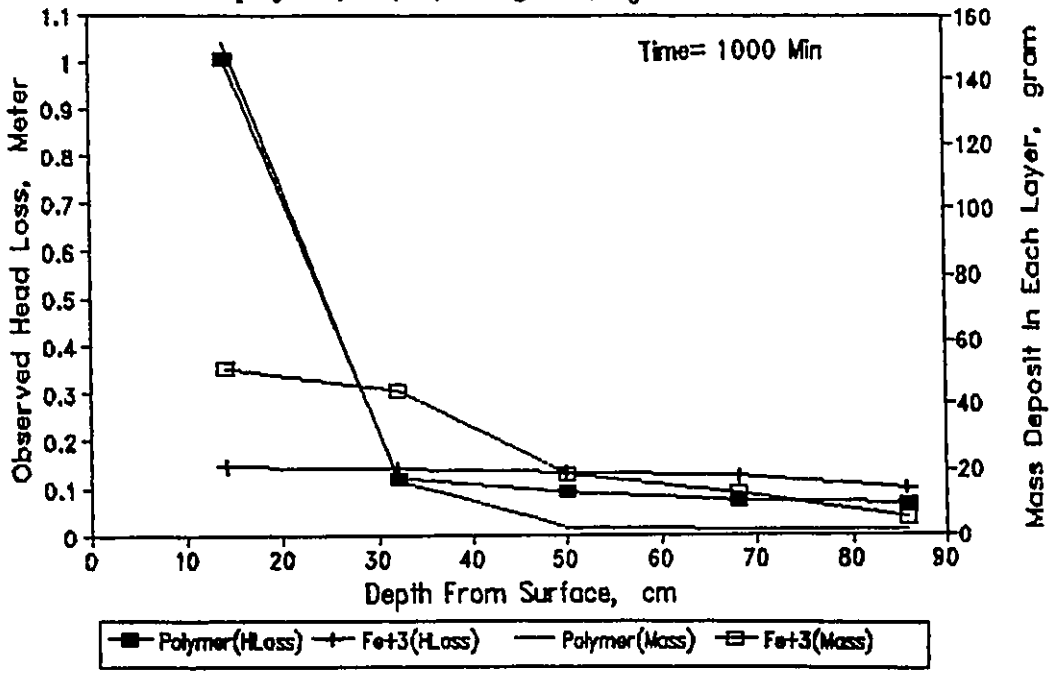

Figure 7.24 Comparison of mass retained and head loss at specific time versus depth (Fe^{3+} and polymer, 30 μm, 15 mg Si/L, V_0 = 0.6 cm/s)

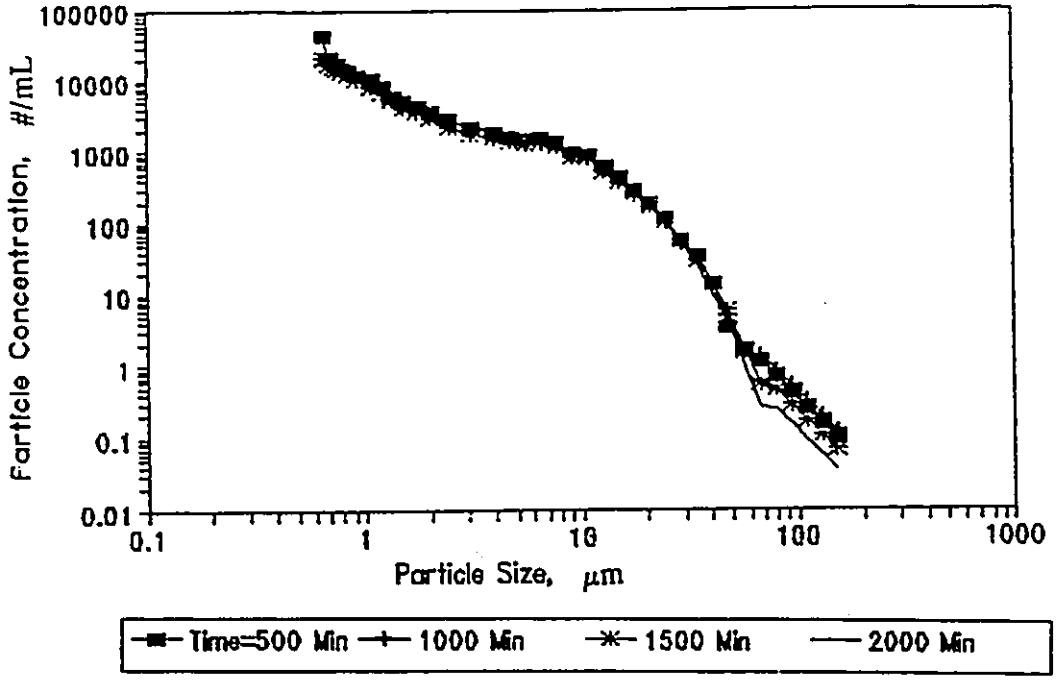

Figure 7.25 Particle concentration (#/ml) for the effluent versus particle size (No-aid, 30 μm, 15 mg Si/L, V_0 = 0.6 cm/s)

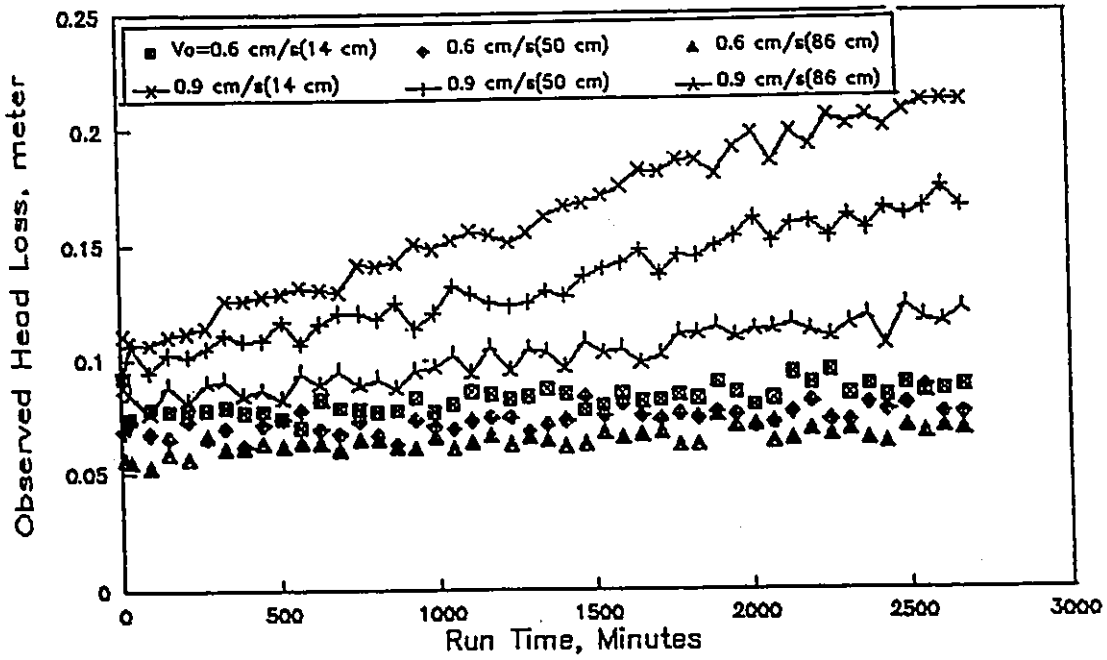

Figure 7.26 Head loss versus time for different depths (No-aid, 30 μm, 30 mg Si/L, V_0 = 0.6 and 0.9 cm/s)

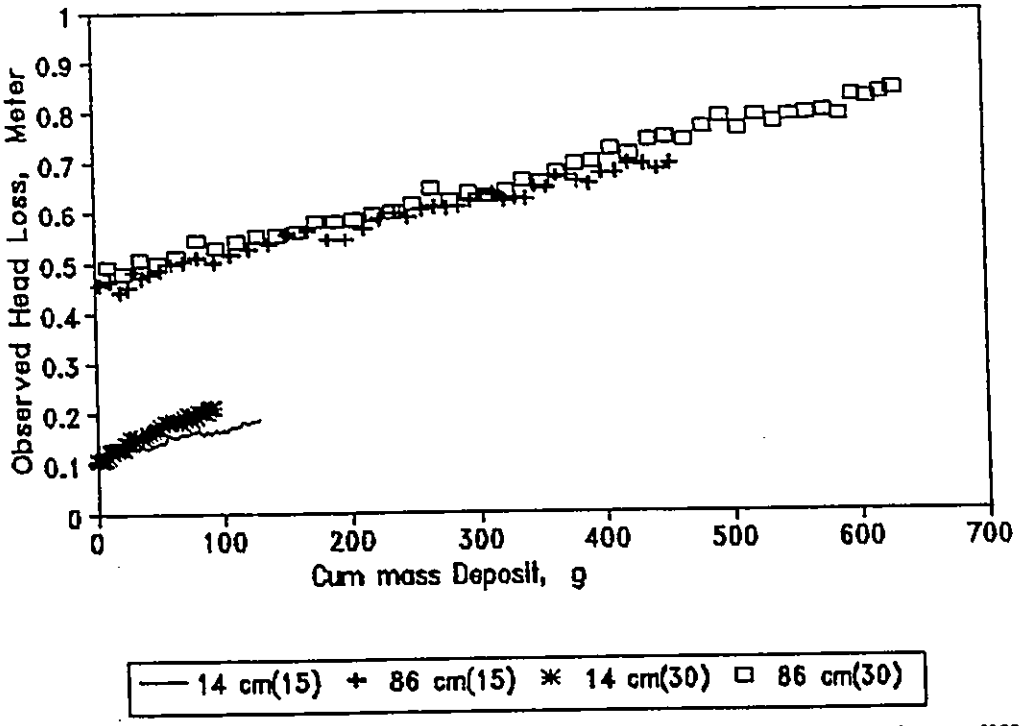

Figure 7.27 Comparison of head loss versus cumulative mass deposit at different concentration (No-aid, 30 μm, 15 and 30 mg Si/L, V_0 = 0.9 cm/s)

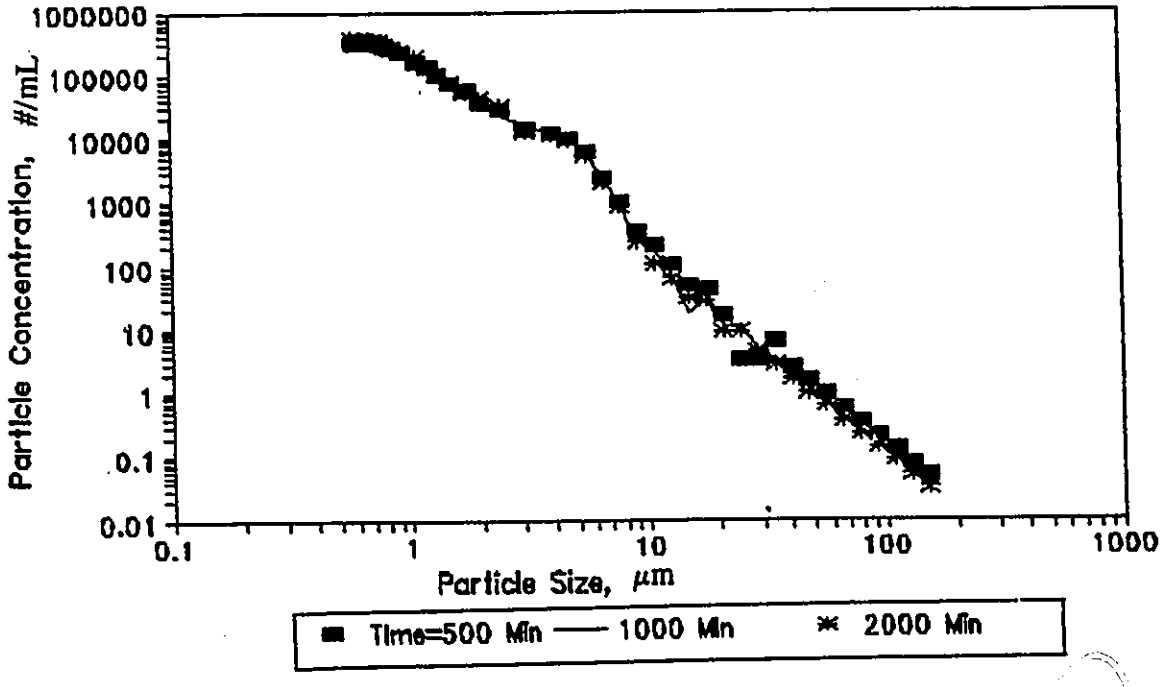

Figure 7.28 Particle concentration (#/ml) versus particle size (No-aid, 5 μm, 15 mg Si/L, V_0 = 0.6 cm/s)

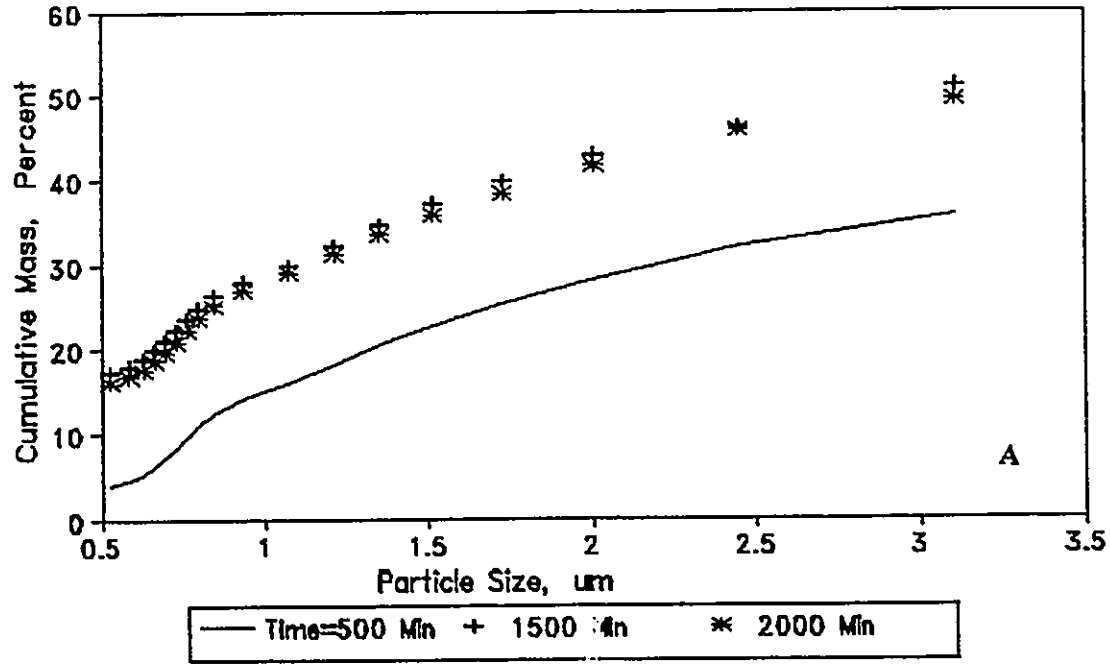

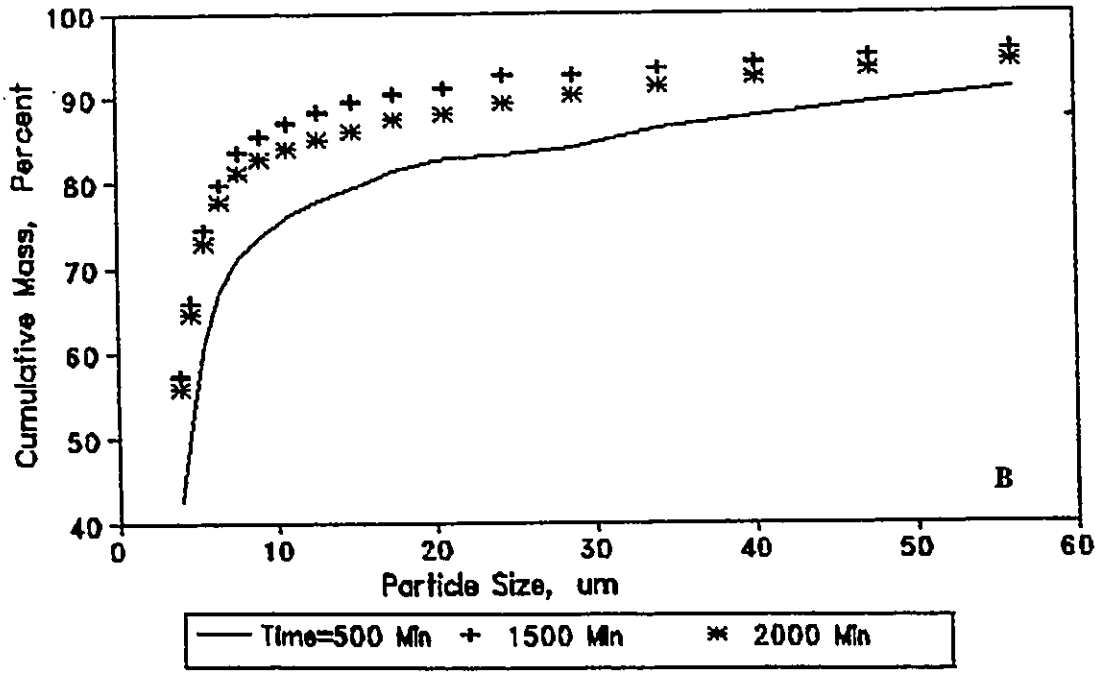

Figure 7.29 Comparison of mass percentage (cumulative) versus particle size at different time intervals (No-aid, 5 μm 15 mg Si/L, V_0 = 0.6 cm/s)
a) Laser size channels, b) CMH-150 channels

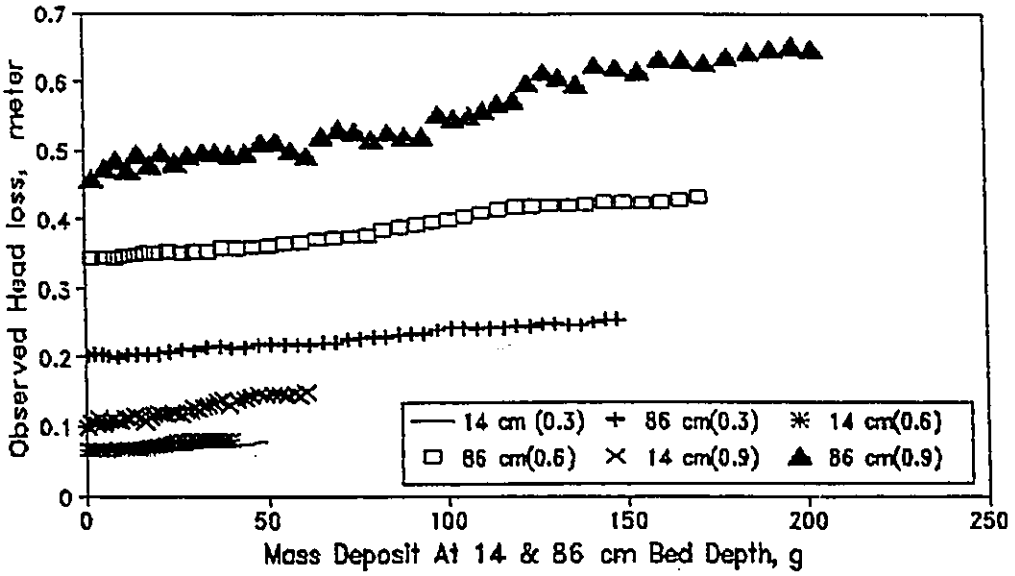

Figure 7.30 Comparison of head loss versus cumulative mass deposit for different filtration velocities at 14 cm and 86 cm depth (No-aid, 5 μm, 15 mg Si/L, V_o = 0.3, 0.6 and 0.9 cm/s)

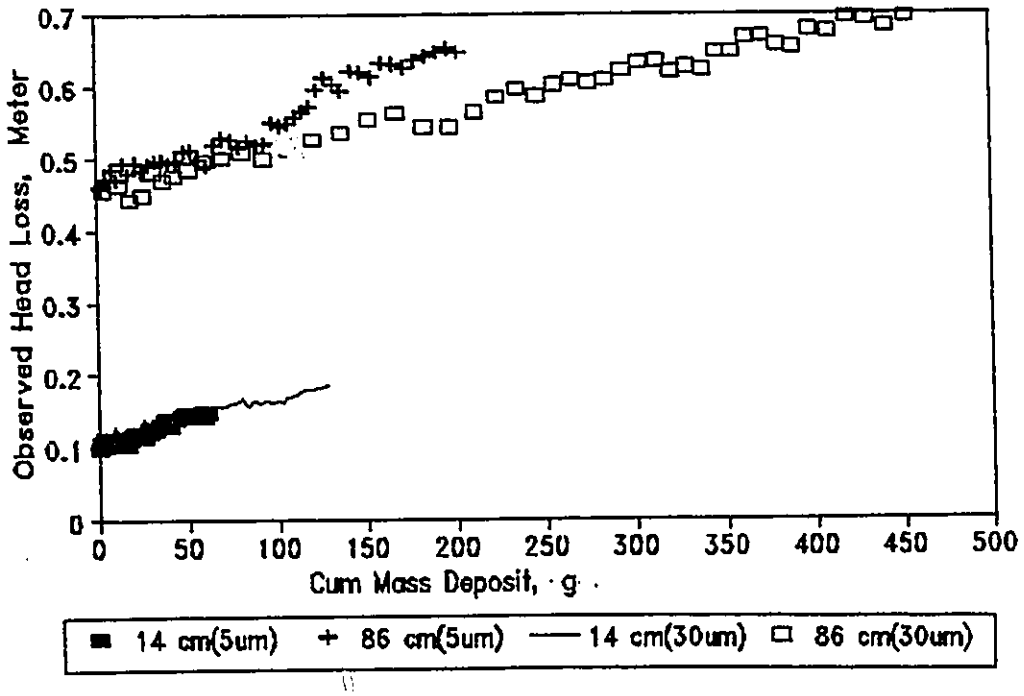

Figure 7.31 Comparison of head loss versus cumulative mass deposit for different particle size (No-aid, 5 μm and 30 μm, 15 mg Si/L, V_o = 0.9 cm/s)

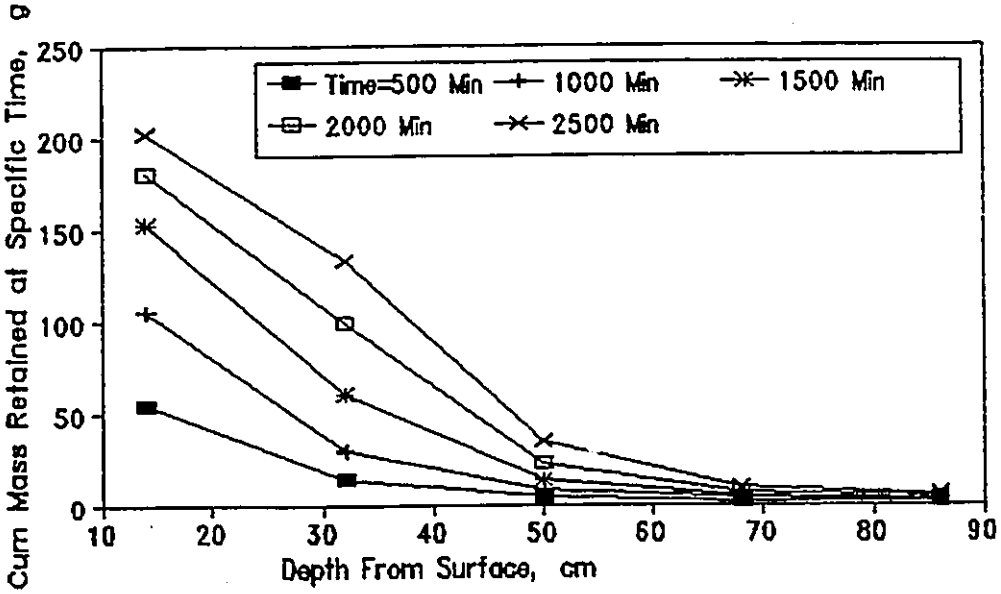

Figure 7.32 Mass deposit versus depth at different time intervals (polymer, 5 μm, 15 mg Si/L, V_o = 0.6 cm/s)

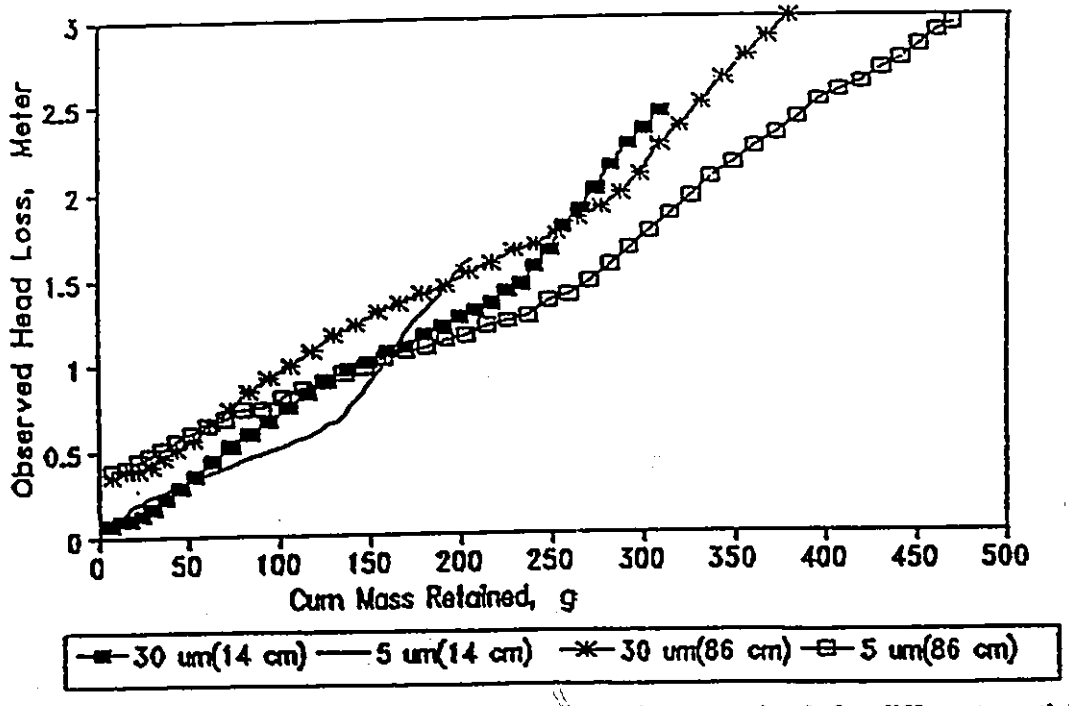

Figure 7.33 Comparison of cumulative mass deposit versus depth for different particle size (Fe^{3+}, 5 μm and 30 μm, 15 mg Si/L, V_o = 0.3 cm/s)

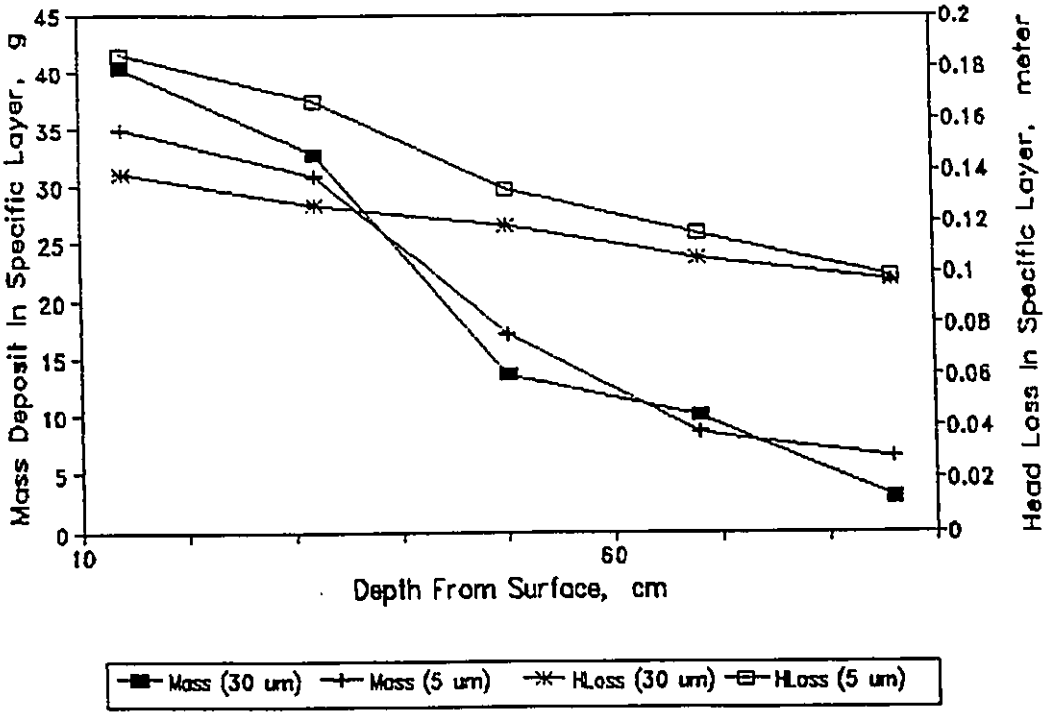

Figure 7.34 Comparison of mass deposit and head loss versus depth for different particle size (Fe^{3+}, 5 μm and 30 μm, 15 mg Si/L, V_o = 0.6 cm/s)

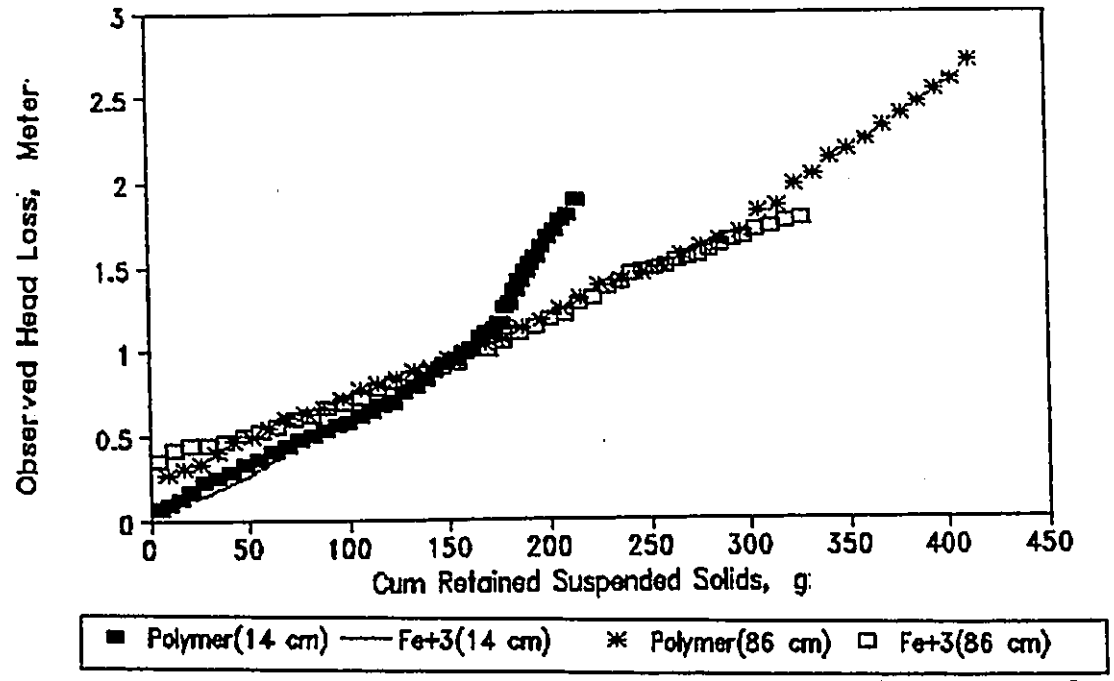

Figure 7.35 Comparison of head loss versus cumulative mass deposit for different coagulants (Fe^{3+} and polymer, 5 μm, 15 mg Si/L, V_o = 0.6 cm/s)

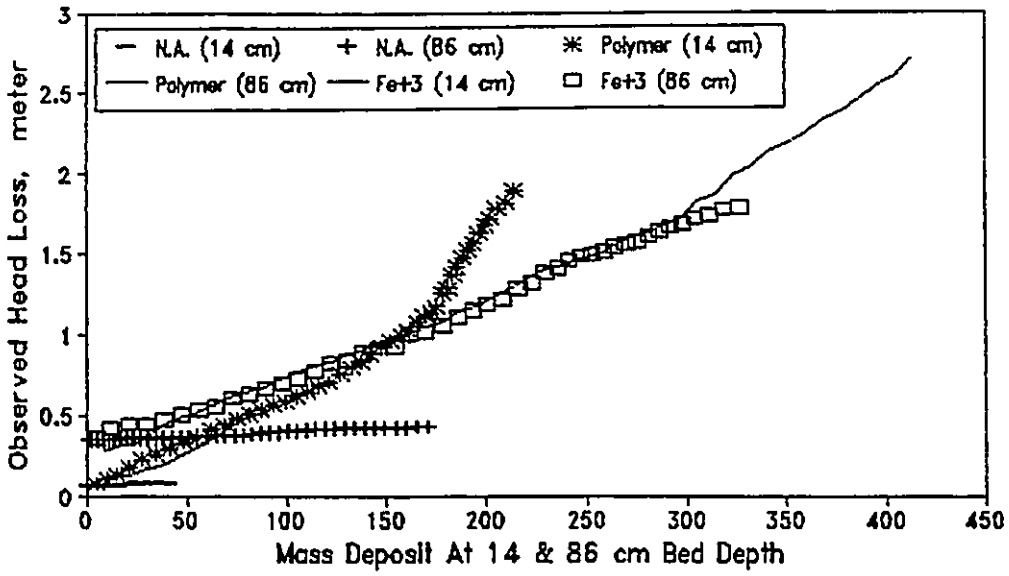

Figure 7.36 Comparison of head loss versus cumulative mass deposit for different coagulants at 14 cm and 86 cm depth (No-aid, Fe^{3+} and polymer, 5 μm, 15 mg Si/L, V_0 = 0.6 cm/s)

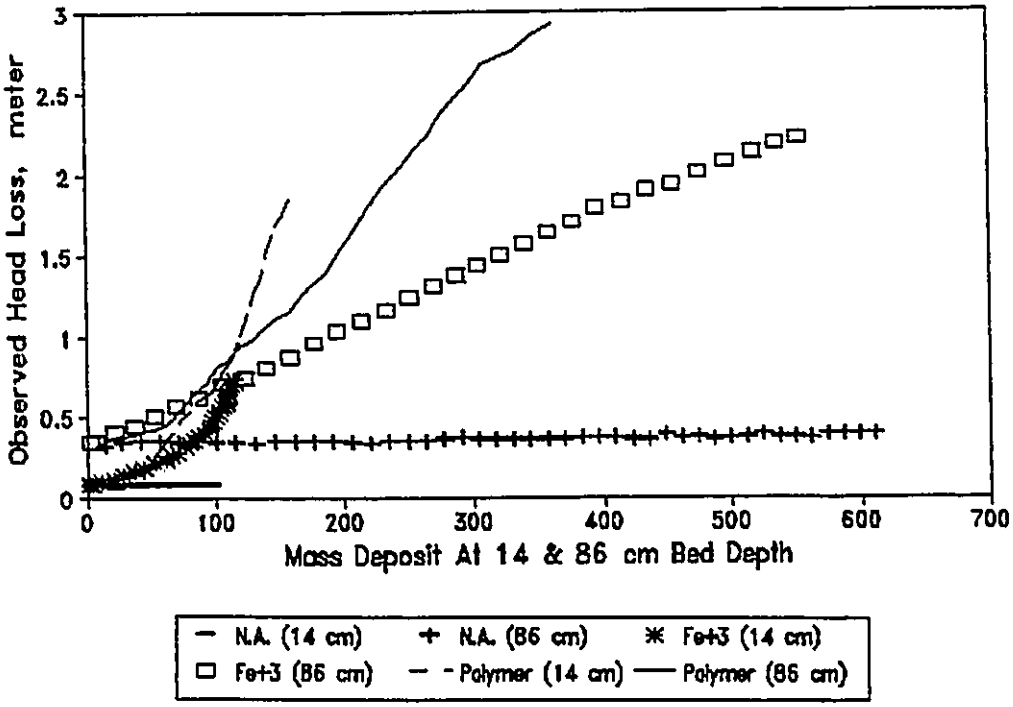

Figure 7.37 Comparison of head loss versus cumulative mass deposit for different coagulants at 14 cm and 86 cm depth (No-aid, Fe_{3+} and polymer, 30 μm, 30 mg Si/L, V_0 = 0.6 cm/s)

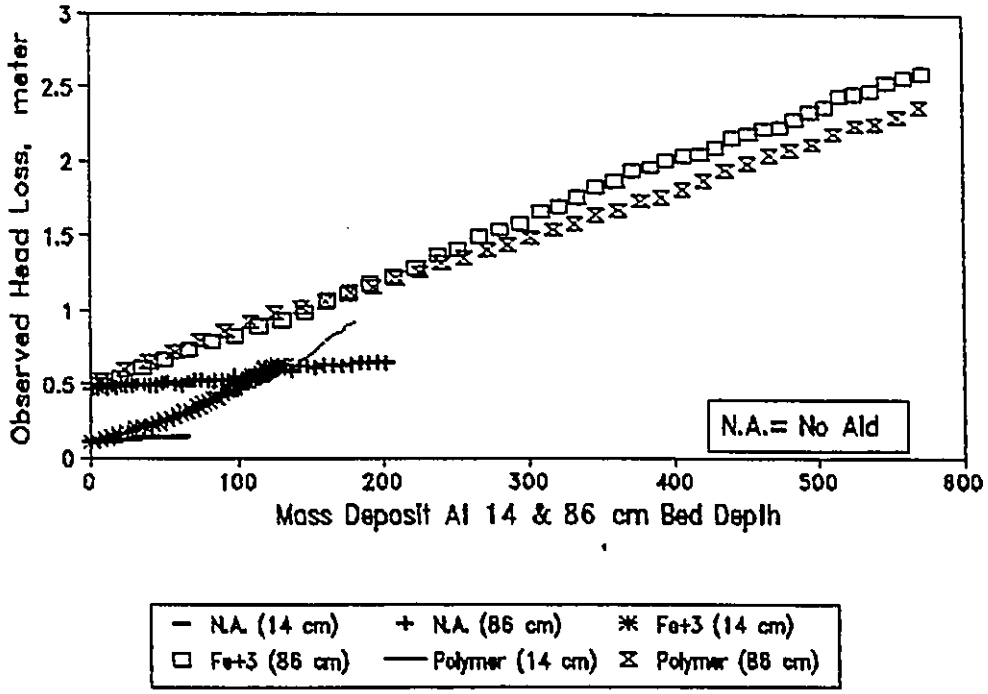

Figure 7.38 **Comparison of head loss versus cumulative mass deposit for different coagulants at 14 cm and 86 cm depth (No-aid, Fe^{3+} and polymer, 5 μm, 15 mg Si/L, V_0 = 0.9 cm/s)**

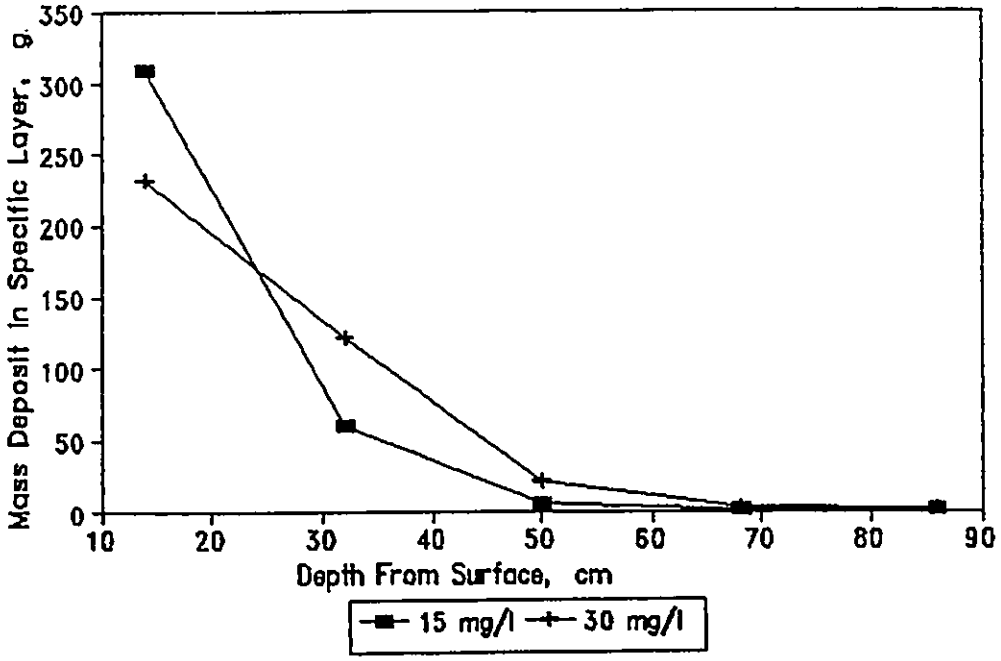

A

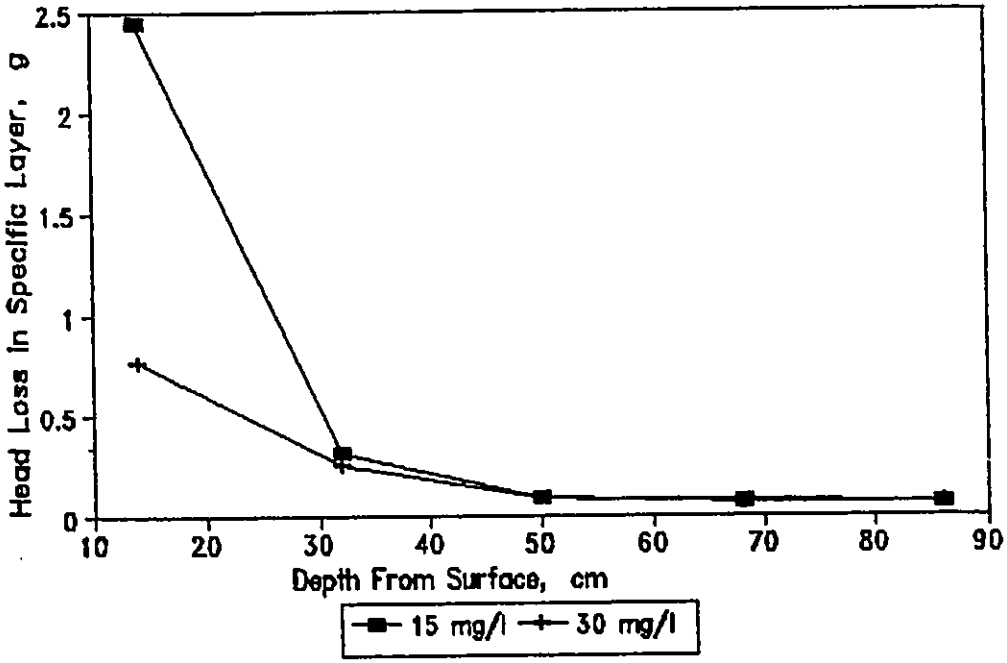

B

Figure 7.39 Comparison of head loss and mass deposit versus depth for different concentration (polymer, 30 μm, 15 and 30 mg/L, V_o = 0.6 cm/s) a) mass deposit, b) head loss

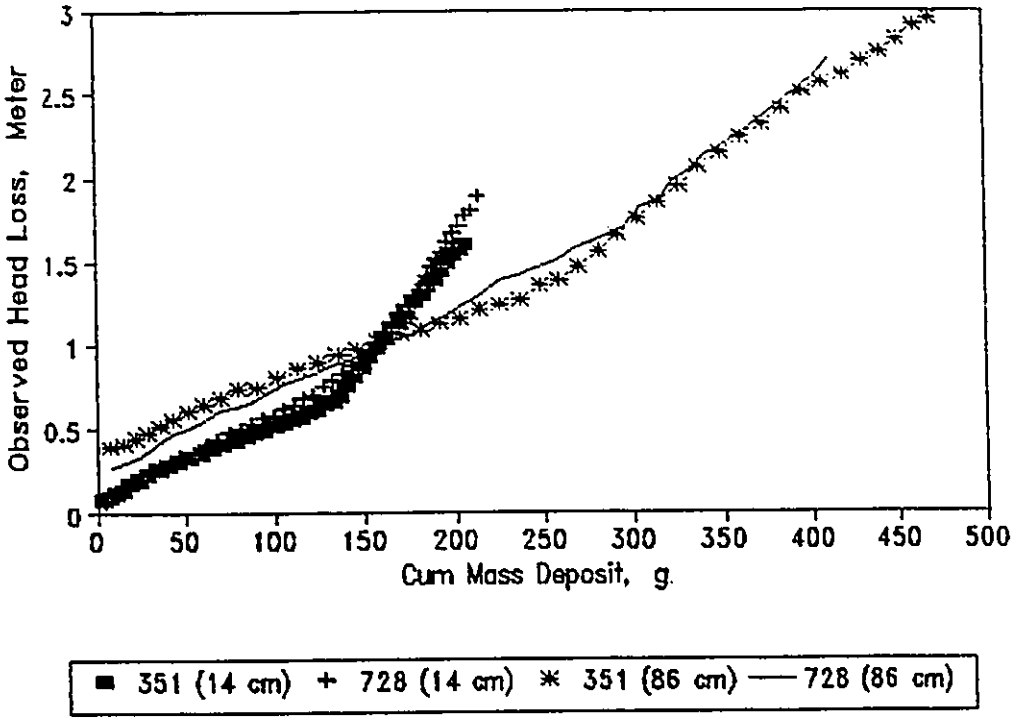

Figure 7.40 Head loss versus cumulative mass deposit (polymer, 5 μm, 15 mg Si/L, V_0 = 0.6 cm/s)

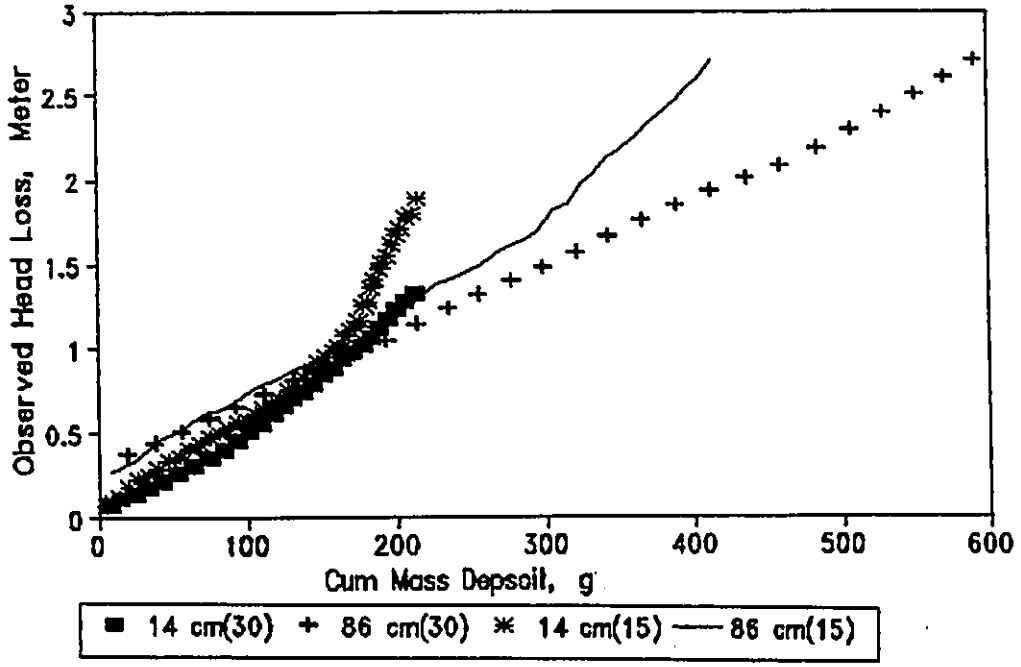

Figure 7.41 Head loss versus cumulative mass deposit for different influent concentration (polymer, 5 μm, 15 and 30 mg/l, V_0 = 0.6 cm/s)

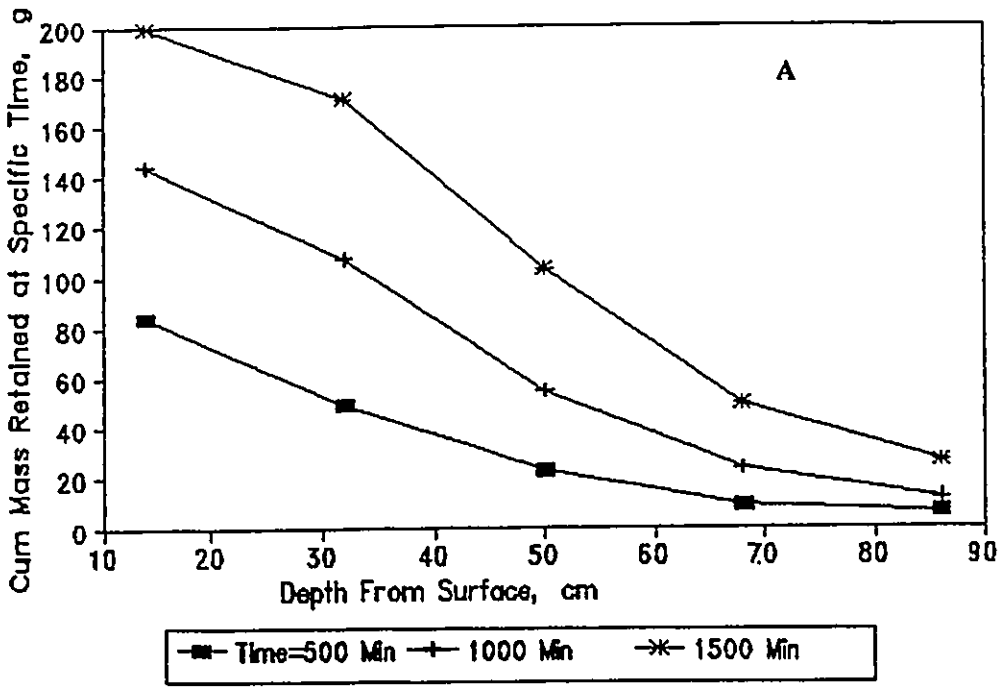

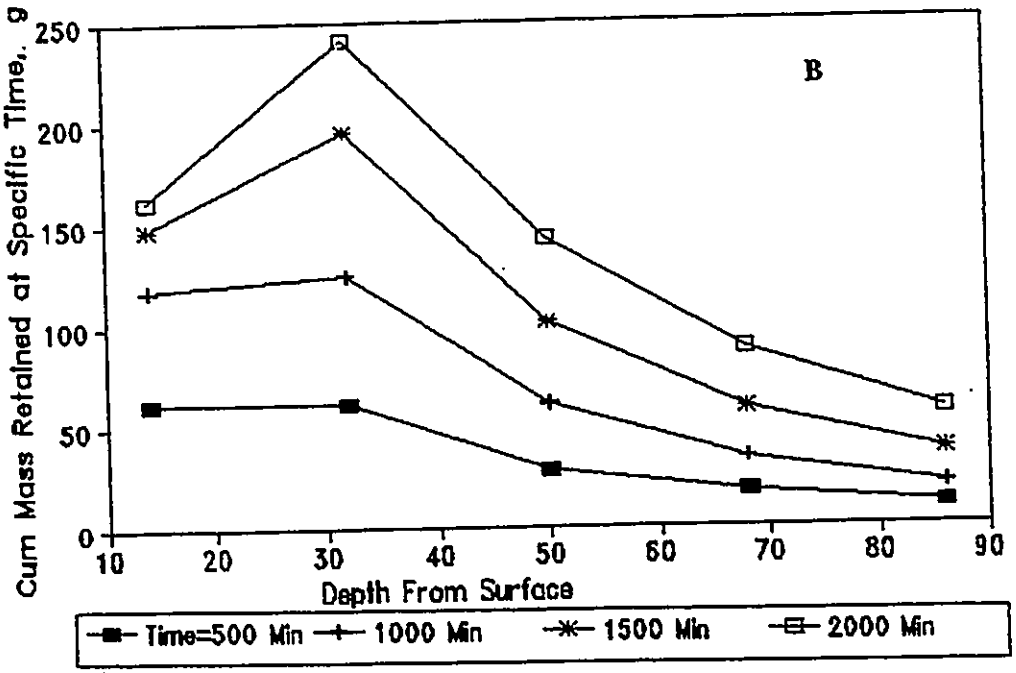

Figure 7.42 Mass deposit versus depth at different time intervals, (polymer, 5 μm and 30 μm, 30 mg Si/L, V_0 = 0.6 cm/s). a) 5 um and b) 30 um

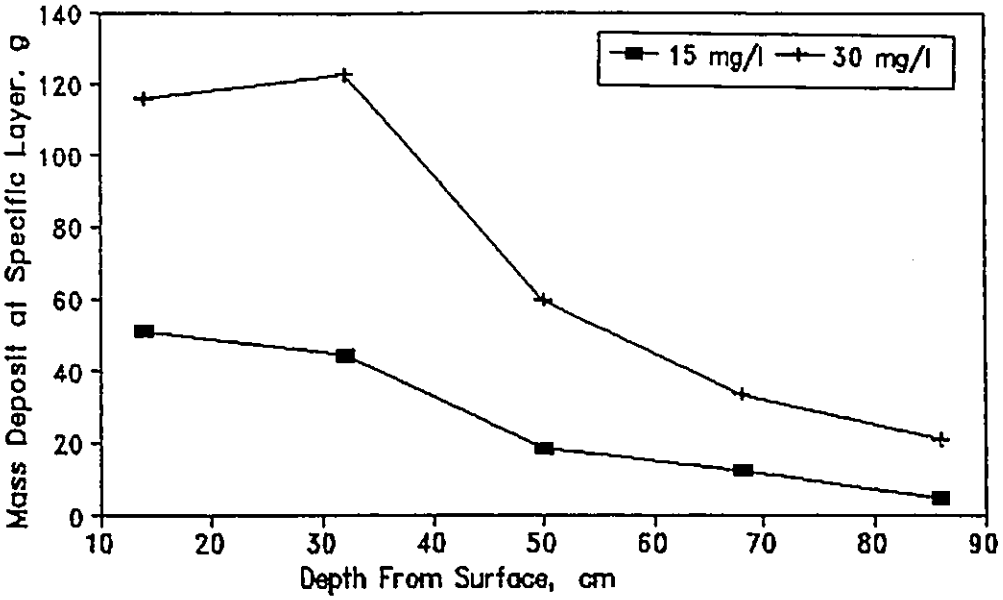

A

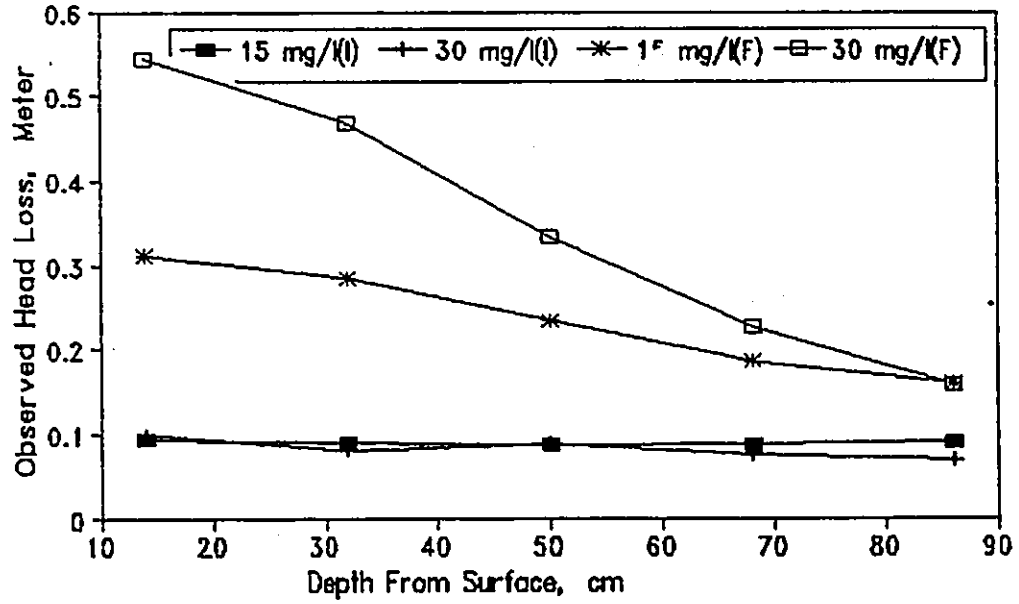

B

Figure 7.43 **Comparison of head loss versus depth for different influent concentration (Fe^{3+}, 30 μm, 15 and 30 mg Si/L, V_0 = 0.6 cm/s), A = mass deposit, B = head loss (I=Initial, and F=Final)**

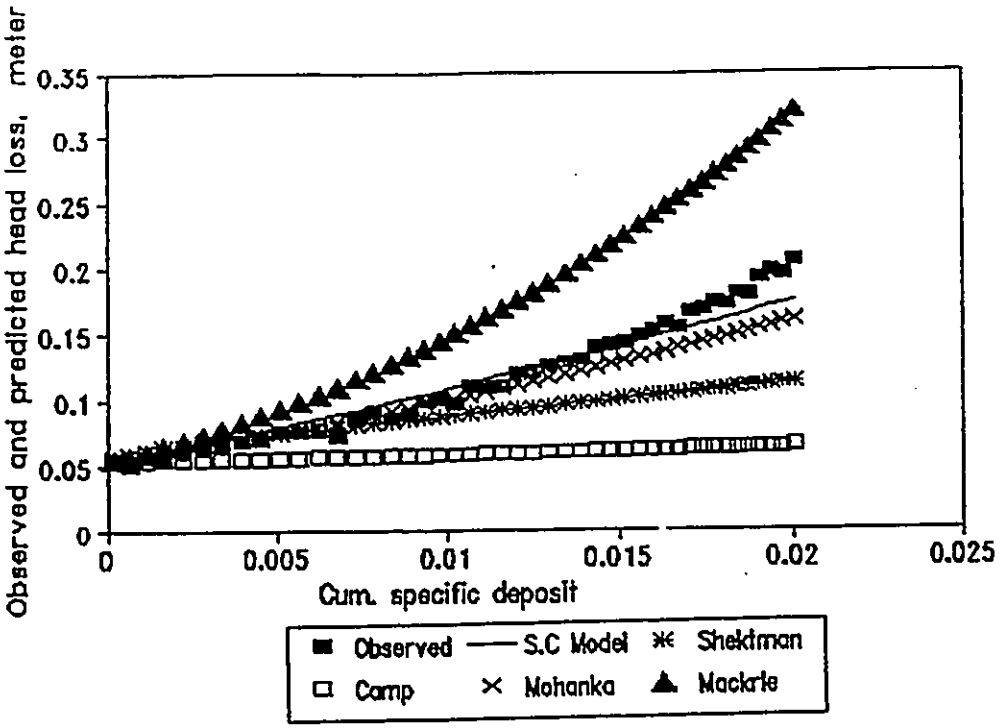

Figure 7.44 Comparison of observed and predicted head loss versus cumulative specific deposit for the first layer (Fe^{+3}, 30 μm, 15 mg Si/L, V_0 = 0.3 cm/s)

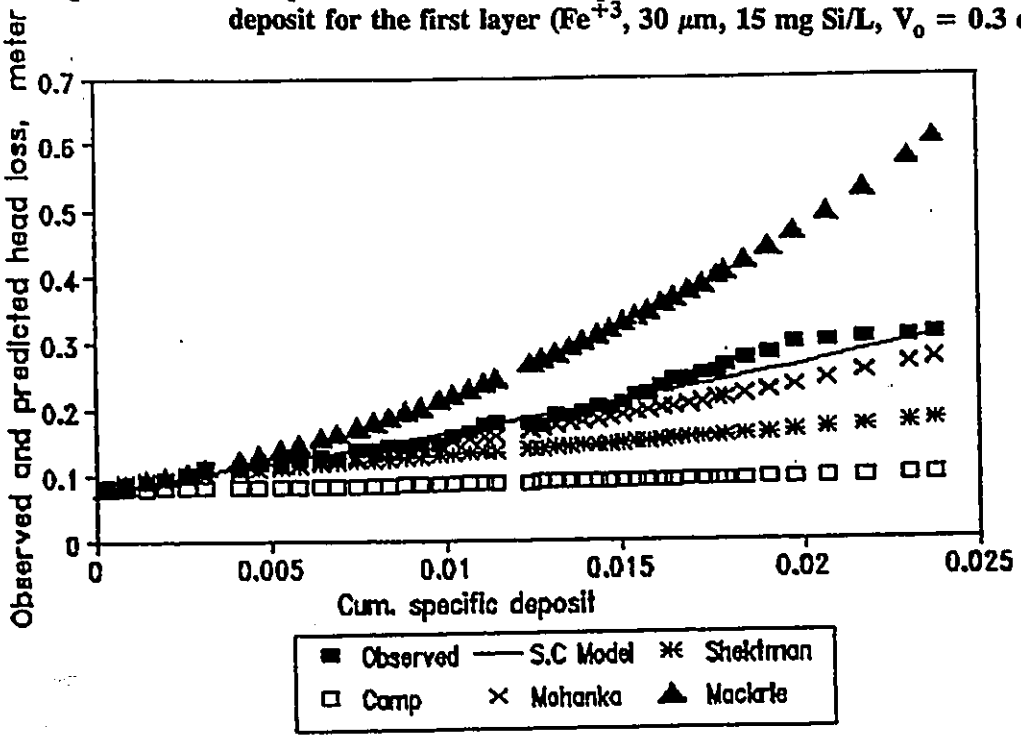

Figure 7.45 Comparison of observed and predicted head loss versus cumulative specific deposit for the first layer (Fe^{+3}, 30 μm, 15 mg Si/L, V_0 = 0.6 cm/s)

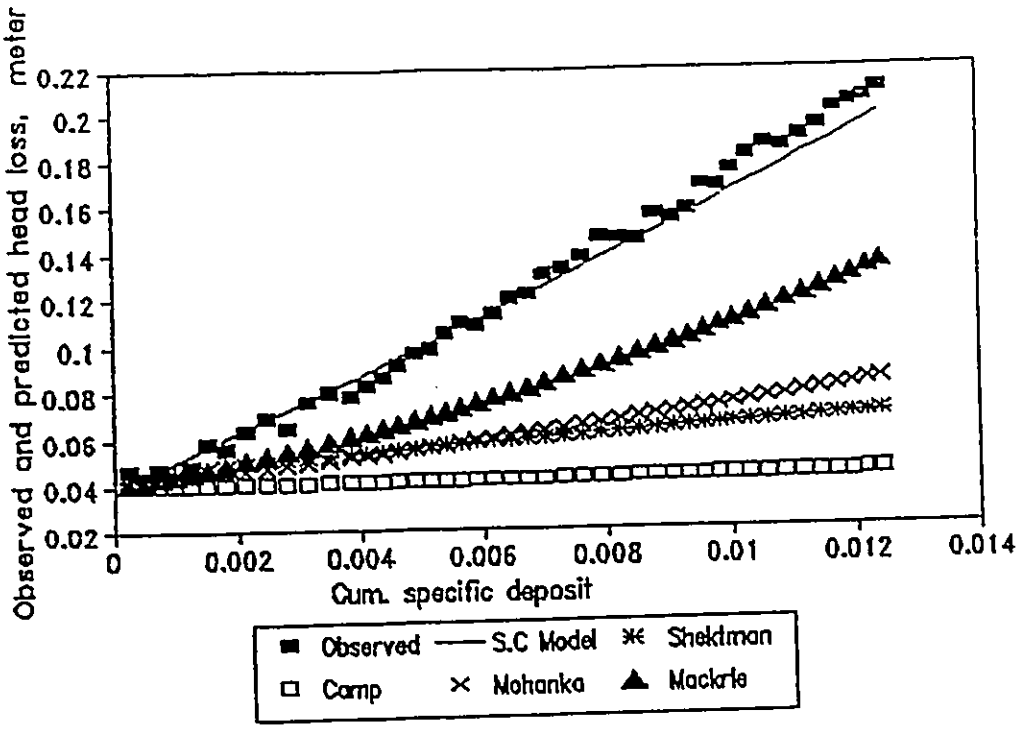

Figure 7.46 Comparison of observed and predicted head loss versus cumulative specific deposit for the first layer (Fe^{+3}, 5 μm, 15 mg Si/L, V_0 = 0.3 cm/s)

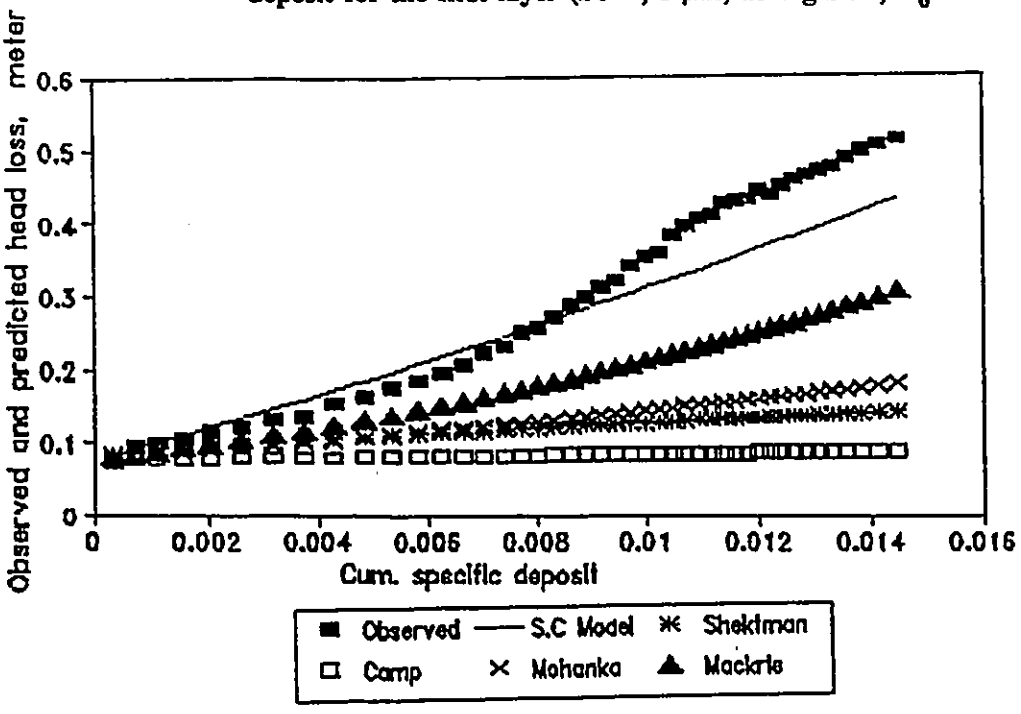

Figure 7.47 Comparison of observed and predicted head loss versus cumulative specific deposit for the first layer (Fe^{+3}, 5 μm, 15 mg Si/L, V_0 = 0.6 cm/s)

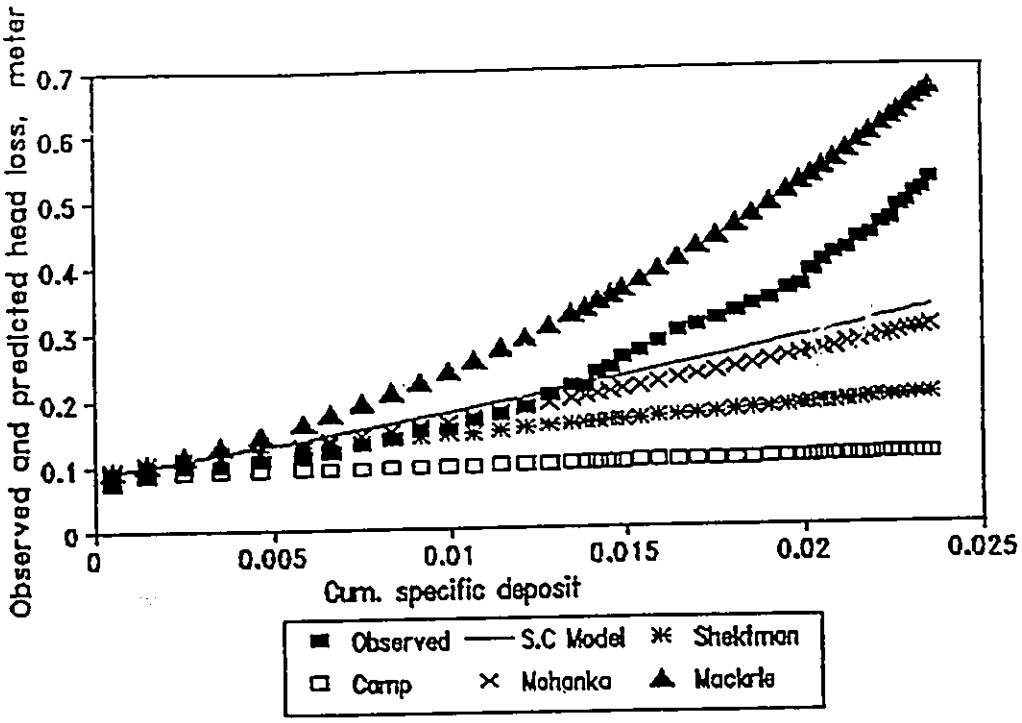

Figure 7.48 Comparison of observed and predicted head loss versus cumulative specific deposit for the first layer (Fe^{+3}, 30 μm, 30 mg Si/L, V_0 = 0.6 cm/s)

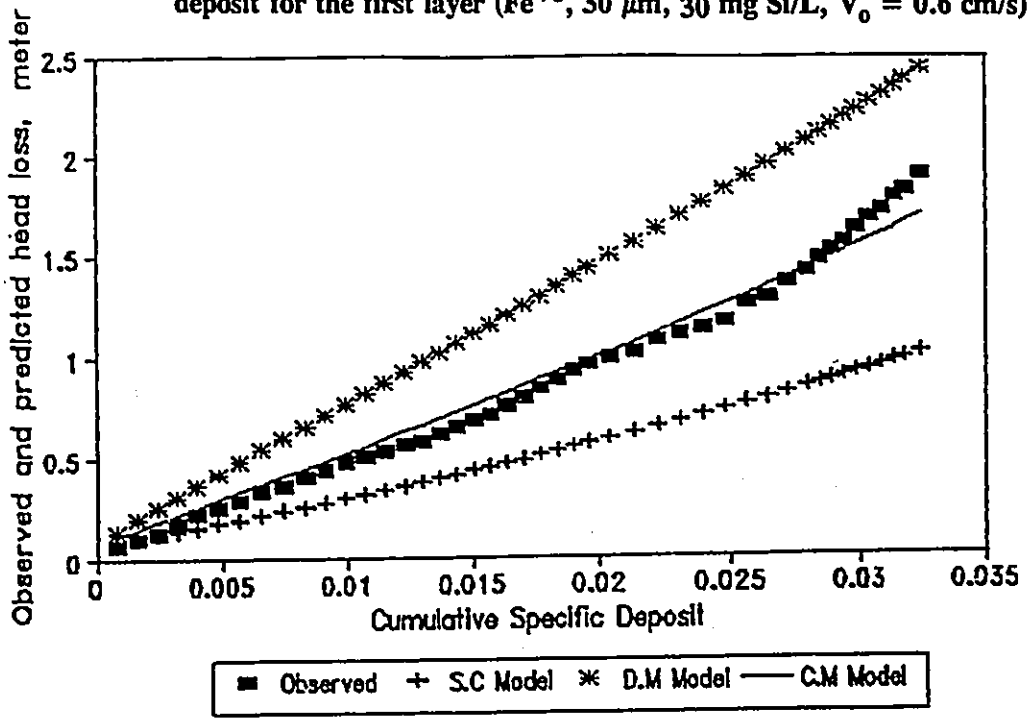

Figure 7.49 Comparison of observed and predicted head loss versus cumulative specific deposit for the first layer (polymer, 5 μm, 15 mg Si/L, V_0 = 0.6 cm/s)

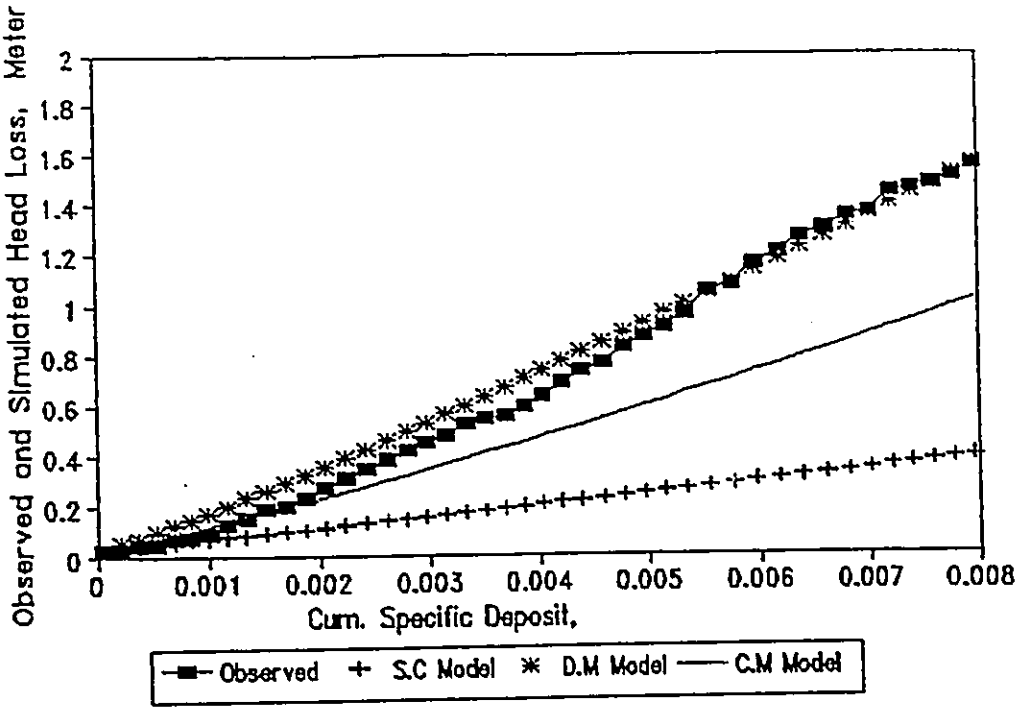

Figure 7.50 Comparison of observed and predicted head loss versus cumulative specific deposit for the first layer (polymer, settled 5 μm, 5 mg Si/L, V_0 = 0.1 cm/s)

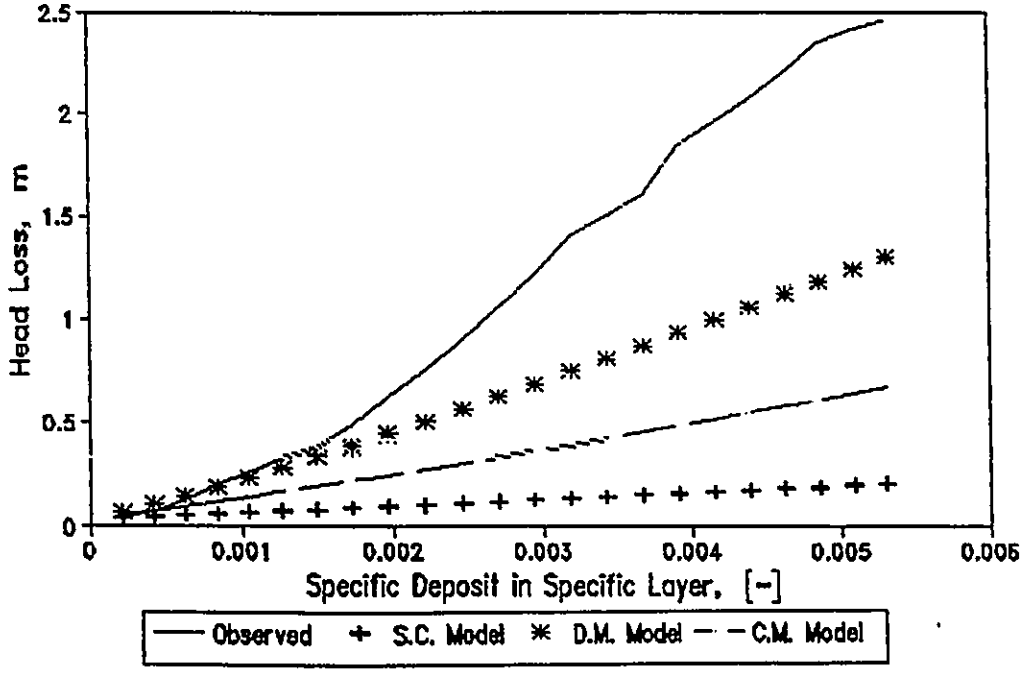

Figure 7.51 Comparison of observed and predicted head loss versus cumulative specific deposit for the first layer (polymer, settled 5 μm, 5.8 mg Si/L, V_0 = 0.1 cm/s)

CHAPTER EIGHT

CONCLUSIONS, CONTRIBUTIONS AND RECOMMENDATIONS

8.1 Conclusions

1. The amount of deposit within a filter bed was found to affect the increase of head loss. The amount of head loss was found to be a function of the geometry of deposit, and depth of deposit penetration. This conclusion is in agreement with that of previous studies in which suspension size distribution has been found to affect the overall distribution and morphology of deposit.

2. The depth of deposition was found to be affected by the amount of coagulant mass per unit mass of suspension, filtration velocity and deposit geometry. In general, deeper penetration was associated with less amount of coagulant mass, higher filtration velocity, thereby confirming the previous observations.

3. Particle size distribution data which is necessary to investigate filter performance and its impact on head loss development, are difficult to obtain as data quality is subject to uncertainty due to, measurement error and systematic error. Appropriate correction approach was evidenced by the fact that: a) the relative standard error was reduced to less than 10 percent in most cases, and b) the corrected data correlated well with theoretical predictions obtained using different head loss equations.

4. Suspensions having the same influent concentration but different in particle sizes, exhibit a wide range in head loss development. For ferric chloride runs, there is a clear particle size effect. The curves for small size particles show higher head loss when compared with those for larger particles. The opposite is true with polymer where large particles contribute to different modes of deposition (surface removal), resulting in higher head loss, shorter filter run and less volume of water treated. When no-aid is used, the overall depth results indicate that small particles produced higher head loss.

5. For the same particle size, coagulant mass and filtration velocity; it was observed in some cases that low influent concentration may contribute to higher head loss than is observed at high concentrations of suspension. This conclusion is in agreement with a recent publication in which similar comparison have been made, based on equal volume of particles (flocs) retained. Although this result may be contrary to expectations, the behaviour could be attributed to: a) increase in number population of the suspension, b) increase in surface area of the suspension which would result in a significant reduction in mass of dosage per unit mass of suspension, and, c) therefore the effect of a and b above is an increase in suspension stability causing the particles to penetrate deeper down the filter bed and contribute to lower head loss. This is not similar to the case when a destabilized suspension (ferric chloride) was used with low filtration velocity (0.3 cm/s). A greater concentration is associated with more local deposit, leading to constriction/blocking. Hence, the increased concentration would result in a greater rate of deposition. The effect of concentration is demonstrated when an exponential increase in head loss (30 mg/L) is compared to a corresponding linear (15 mg/L) increase. It is

concluded that initially, removal of suspended matter occurs at greater depth . Later on, removal takes-place near the top of the bed.

6. Dendritic deposition mode is evidenced when settled 5 μm silica suspension with polymer (Percol 728) was used. Neither "surface removal" nor "depth removal" trends were observed. This deposition mode tends to produce a longer filter run with exponential increase in head loss.

7. Different coagulant and different filtration velocities were found to have little or no effect on the head loss in case of small particle size.

8. Difference in filtration velocities caused different modes of deposition for suspension destabilized using polymer with large particle size (30 μm) and having the same influent concentration. Smooth coating and surface deposition for the case of 0.3 and 0.6 cm/s respectively, were observed. The experimental results indicate that the capacity of the filter bed for accumulating solids would be more successfully utilized, resulting in a significant reduction in head loss in case of 0.3 cm/s than 0.6 cm/s. This may mean that the deposition of suspended solids promotes deeper penetration and inhibits surface removal without deteriorating effluent quality. For the same amount of deposit in the first layer the head loss for the case of 0.6 cm/s is seven times that of the 0.3 cm/s case. This conclusion was confirmed as the data was successfully reproduced in more than one filter run.

9. The control of deposit geometry is possible through the selection of desirable process variables such as flow rate, particle size, coagulant type and influent concentration.

10. For an equal mass of deposit, use of ferric chloride resulted in lower head loss than use of polymer for suspension having the same particle size (30 μm), influent concentration (15 mg/L) and filtration velocity (0.6 cm/s). The difference in head loss is slight and negligible with 5 μm silica.

11. Qualitative (optical fibre endoscope with video recording and microscopic observations) and quantitative (filtration and batch flocculation test) measurement were found to be useful tools for direct viewing, validating and recording of deep bed filtration phenomena.

8.2 Contributions

The principal contributions of the present research program are:

1. Further extension to the theory of filtration.

2. Combination of a two mode model of deposition rather than a one mode model.

3. Confirmation of the proposed deposition morphology; visually and quantitative evidence. The existence of long particle dendrites in filtration was demonstrated using different techniques. Flocs obtained from a jar test sample were photographed using a camera mounted on an optical light microscope. The flocs were recorded on video cassette

during a gentle backwashing of the filter bed using an optical fibre endoscope and were retained for further image analysis.

4. Identification of the different modes of deposition within a set of polymer or ferric chloride experiments for the coagulant used; variation in behavioral is attributed to differences in particle size. Behavioral variation in different test sets is due to different coagulants. Dendritic, a combination of smooth coating with dendrite and a combination of smooth coating with blocking mode deposition are associated with polymer and settled 5 μm, 5 μm and 30 μm silica suspension, respectively. Polymer like behaviour and smooth coating are associated with ferric chloride and 5 μm and 30 μm silica suspension. This also suggests that no single mode of deposition governs the deposition process over the entire filter run.

5. The development of a method whereby particle size distribution (PSD) data can be easily corrected. A computer program was developed which incorporates all of the correction steps.

6. Inclusion of a geometry parameter in a combined mode model; i.e., the model considers the relative values of the fraction of particles which contribute to smooth coating and dendrite deposition.

7. Implementation of a 0-24/48 hour and use of a pilot scale filter column with 100 cm filter media depth and 20 cm diameter, uses the same rate of flow through the same porous medium as in the full-scale facility.

8. The significant effect of deposit morphology on head loss build-up is demonstrated in this work.

9. Development of predictive models i.e., parameters obtained from one experiment can be readily used to predict the experimental results for a different set of conditions, using the same parameter values.

8.3 Recommendations

1. The effect of ionic strength on the floc size should be studied in greater details as it may be found to have a strong influence on the particle flocculation, filtration mechanism and deposit morphology.

2. A correction procedure for particle size needs to be developed on the basis of sufficient experimental data in order to take into account the scattered cross section of different spherical particle size. This correction procedure is important in the particle size range of 0.1-150 μm.

3. The effectiveness of different deposit geometries in removing colour bodies, and other water quality parameters such as coliforms, viruses, parasites and algae, from waste water has yet to be tested.

4. Criteria such as in-line monitor of particle size and its distribution, in the large scale filtration processes should be attempted, so that the results of the model parameters can be compared with field data.

5. More detailed consideration of current setting of particle size analysis system and larger orifice sizes is required to reduce the concentration uncertainty and extend the flocs detection in the upper bound.

REFERENCES

Abdul-Alim A.H. and Hamelec A.E. (1973) Shear Degradation Of Water Soluble Polymer I. Degradation Of Polyacrylamide In A High Shear Couette Viscometer. J. Appl. Polym. Sci., 17, 3769.

Adin A., Baumann E.R. and Cleasby J.L. (1979) The Application of Filtration Theory To Pilot Plant Design. J. Am. Wat. Wks.Ass. 71, 1, 17-27.

Adin A. (1978) Solution of Granular Bed Filtration Equations. J. Envir. Engng. Div., Am.Soc. Civ. Engrs. 104, EE3, 471-484.

Adin A. and Rebhun M. (1974) High-Rate Contact Flocculation-Filtration With Cationic Polyelectrolytes. J. Am. Wat. Wks. Ass. February 258-262.

Adin Avner and Rajagopalan Raj (1989) Breakthrough Curves in Granular Media Filtration. J. Envir. Engng. Div. 115, 4, August, 785-798.

Adin A. and Rebhun M. (1977) A Model to Predict Concentration and Head-Loss Profiles in Filtration. J. Am. Wat. Wks. Ass., August, 444-452.

Alvin F. Bieberman (1988) Calibration Requirements And Methods For Liquid-Born Particle Counters. J.Envir. Sci. 31, May/June.

Albeldawi M.F. (1990) Evaluation of Two-Stage Filtration System In Treating The Iron And Steel Mill Effluent. Report (Internal) Presented To The Waste Water Technology Centre(Burlington), Ontario, Canada.

Averil D.W. and Wood J.A. (1987) Examining Granular Media Filter Performance With The Aid Of Particle Size Analysis. Paper Presented At The 60th Annual Conference Of The WPCF, October.

AWWA Coagulation Committee (1989) Committee Report: Coagulation As An Integrated Water Treatment Process. J. Am. Wat. Wks. Ass. 81, 10, 72-78.

Baumann E.R. and Ives K.J. (1987) The Evidence of Wormholes In Deep Bed Filters. Proc. Filtech Conf. Utrecht, September, 1, 151-164.

Beard J.D. and Tanaka T.S. (1976) A Comparison of Particle Counting and Nephelometry in Evaluation Filtration Plant Performance. AWWA Water Quality and Technology Conference Proceeding.

Bieberman A.F. (1988) Calibration Requirements and Methods for Liquid-Born Particle Counter. J. Envir. Sci., May/June, 31, 34-36.

Black A.P., Singley J.E., Whittle G.P. and Moulding J.S. (1963) Stoichiometry of the coagulation of Colour-Causing Organic Compound With Ferric Sulphate. J. Am. Wat. Wks. Ass., 55, October, 1347-1366.

Black A.P. and Manuel R.V. (1969) Effect of Particle Size On Turbidity Removal. J. Am. Wat. Wks. Ass., 209-214.

Black A.P. and Hannah S.A. (1961) Electrophoretic Studies Of Turbidity Removal By Coagulation With Aluminium Sulphate. 53.

Black A.P., Birkner F.B. and Morgan J.J. (1965) Destabilization of Dilute Clay Suspensions With labelled Polymers. J. Amm. Wat. Wks. Ass., 57, 12, 1547-1560.

Boyd R.H. and Ghosh M.M. (1973) An Investigation of The Influences of Some Physicochemical Variables on Porous-Media Filtration. Paper presented at The Annual Conference, J. Am. Wat. Wks. Ass., May, 94-98.

Box G.P., Hunter W.J., Hunter J.S. (1978) Statistics for Experimenters: An Introduction to Design, Data Analysis, and Model Building. John Wiley and Sons, New York.

Bratby, J.R. (1981) Optimizing Coagulants And Flocculant Aids For Settling. J. Am. Wat. Wks. Ass., 312-319.

Bratby J.R. (1981) Interpreting Laboratory Results For The Design Of Rapid Mixing And Flocculation System. J. Am. Wat. Wks. Ass., April, P. 73.

Brink D.R., Suing Iu Choi, Mohammad AL-Ani and Hendricks D. (1988) Bench Scale Evaluation of Coagulants For Low Turbidity Waters. J. Am. Wat. Wks. Ass., April, 199-204.

Bucens P.G. (1991) Measurement and Interpretation of Floc Size Distribution. Unpublished Master Thesis, McMaster University/Civil Engng. Dept.

Camp T.R. (1964) Theory Of Water Filtration. J. Sanit. Engng. Div., Am. Soc. Civ. Engrs. 90, 3, SA4, 1-30.

Cleasby J.L. (1966) Experimental Evaluation of Sand Filtration Theory. J. Sanit. Engng. Div., Am. Soc. Civ. Engrs., October, 92, SA5, 61.

Cleasby J.L. (1969) Approaches To A Filterability Index For Granular Filters. Paper presented At The Annual Conference, San Diego, May, 372-381.

Cleasby J.L. (1969) Approaches to a Filterability Index for Granular Filters. J. Am. Wat. Wks. Ass., 372-381.

Cleasby J.L. (1982) Unconventional Filtration Rates. Proceedings-24th Annual Public Water Supply Engineer's Conference-Unconventional Water Treatment, Champaign 111, USA, April, 49-57.

Cleasby J.L. and Baumann E.R. (1962) Selection of optimum filtration rates for sand filters. Bulletin 198 of The Iowa Engineering Experimental Station, The Iowa State University Bulletin, LX, No.34.

Clough G. and Ives K.J. (1986) Deep Bed Filtration Mechanisms Observed With Fibre Optic Endoscopes And CCTV. Proceeding of The Fourth International Filtration Congress, Ostend, 8, Part II, 13.21-13.26.

Coad M.A. and Ives K.J. (1981a) Investigation of Deep Bed Filters using Tracers. Filtech Conference, 98, 131-136.

Coad M.A. and Ives K.J. (1981b) Deposition and Flow Pattern in the Pores of Deep-Bed Filters. Proceedings of the 2nd World Congress of Chemical Engineering, Montreal, Quebec, 111-114.

Cooper D.W. and Grotzinger S.J. (1989) Comparing Particle Counter: Cost Vs. Reproducibility. J. Envir. Sci., September/October, 32-34.

Craft T.F. and Eicholtz G.G. (1970) Mechanism of Rapid Filtration in a Uniform Filter Bed. Wat. Resou. Res., 6, 257.

Craig K. (1985) Direct Filtration: An Australian Study. J. Am. Wat. Wks. Ass., December, pp. 56-61.

Darby J.L., Attanasio R.E. and Lawler D.F. (1992) Filtration of Heterodisperse Suspensions: Modelling of Particle Removal and Head Loss. Wat. Res., 26, 6, 711-726.

Darby J.L., Lawler D.F. and Wilshusen T.P. (1991) Depth Filtration of Wastewater: Particle Size and Ripening. J. Wat. Pollut. Control Fed., 63, 3, May/June, 228-238.

Darby J.L. and Lawler D.F. (1990) Ripening In Depth Filtration: Effect of Particle Size on Removal and Head Loss. Envir. Sci. Techno., 24, 7, 1069-1079.

Deb A.K. (1969) Theory Of Sand Filtration. J. Sanit. Engng. Div., Am. Soc. Civ. Engrs., 95, 399-422.

Dentel S.K. and Gossett J.M. (1988) Mechanism of Coagulation With Aluminium Salts. J. Am. Wat. Wks. Ass., 80, 4, April, 187-198.

Diaper E.W.J. and Ives K.J. (1965) Filtration Through Size Graded Media. J. Sanit. Engng. Div., Am. Soc. Civ. Engrs., 91, SA3, 89-114.

Ditter W., Eisenlauer J. and Horn D. (1982) Laser Optical Method For Dynamic Flocculation Testing In Flowing Dispersions. In The Effect of Polymers on Dispersion Properties (Edited By Th. F. Tadros), 323-342, Academic Press. New York.

Dixon J.K., et al., (1967) Effect of Structure of Cationic Polymers on The Flocculation and The Electrophoretic Mobility of Crystalline Silica. J. Collo. Interf. Sci., 23, 4, 465-473.

Edzwald J.K. (1984) Removal of Trihalomethane Precurssor by Direct Filtration and Conventional Treatment. Report No. EPA-600/2-84-068, U.S. Environmental Protection Agency, Cincinnati, Ohio.

Eikebrokk B. and Fettig J. Treatment of Coloured Surface Water By Coagulation/Direct Filtration: Effect of Water Quality, Type of Coagulant and Filter Aid.

Eliassen R. (1941) Clogging of Rapid Sand Filters. J. Am. Wat. Wks. Ass., New York, N.Y., 33, 926-942.

Ensor D.S., Donovan R.P. and Locke B.R. (1987) Particle Size Distribution In Clean Rooms. J. Envir. Sci., 30, November/December, 44-49.

Fitzpatrick J.A., Zitnay L.W., and Spielman L.A. (1974) Advances In The Design Of Granular Bed Filters. Proceeding 1st World Filtration Congress, Paris, May, A7.1-A7.5.

Fox M. and Cleasby J.L. (1966) Experimental Evaluation of Sand Filtration Theory. J. Sanit. Engng. Div., Am. Soc. Civ. Engrs., 92, SA5, October, 61-70.

Francois R.J. and Van Haute A.A. (1985) Backwashing and Conditioning Of Deep Bed Filters. Wat. Res. 19:11:1357, 1357-1362.

Frazer J. (1992) Internal Report, Waste Water Technology Centre, Burlington, Ontario, Personnel Communication.

Ghosh M.M., Jordan T.A. and Porter R.L. (1975) Physicochemical Approach to Water and Wastewater Filtration. J. Envir. Engng. Div., Am. Soc. Civ. Engrs. 101, EE1, 71-85.

Gillberg L., Eger L. and Jepsen Svend-Erik (1990) The Effect of Five Coagulant on The Concentration and Distribution of Small Particles in Sewage Water. In "Chemical Water and Waste Water Treatment", Edited By Hermann H. Hahn, and Rudolf Klute.

Glaser H.T. and Edzwald J.K. (1979) Coagulation and Direct Filtration of Hymic Substances with Polyethylenimine. Envir. Sci. Techno., 13, 299-305.

Grace H.P. (1956) Structure and Performance of Filter Media. AIChE. Journal, 2, 3, 307-336.

Graham N.J. (1988) Filter Pore Flocculation As A Mechanism In Rapid Filtration. Wat. Res. 22, No. 10, 1229-1238.

Graham N.J. (1986) Orthokinetic Flocculation In Rapid Filtration. Wat. Res., 20, 6., 715-724.

Grant D.C., Benjamin Y.H. and Fisher W.G. (1989) Particle Capture Mechanism In Gases and Liquid: An Analysis Of Operative Mechanisms in Membrane/Fibrous Filters. J. Envir. Sci., 32, July/August, 43-51.

Gregory J. (1986) Flocculation., In Progress In Filtration and Separation, (Edited by Wakeman R.J.), 55-99.

Gregory J. (1987) Flocculation By Polymer And Polyelectrolytes. In Solid/Liquid Dispersion, (Edited By Th. F. Tadros), 163-181, Academic Press, New York.

Gros H. (Sulzer Bros. Ltd.) (1979) Optimization of Deep-Bed Filtration In Water and Waste water Treatment. Proceeding of The Second World Filtration Congress, London, U.K.

Habibian M.T. (1971) The Role of Polyelectrolyte in Water Filtration. unpublished Ph.D. dissertation, University of North Carolina, Chapel Hill, North Carolina.

Habibian M.T. and O'Melia C.R. (1975) Particles, Polymers, and Performance In Filtration. J. Envir. Engng. Div., Am. Soc. Civ. Engrs. 101, 4, 567-583.

Hall W.A. (1957) An analysis of sand filtration. J. Sanit. Engng. Div., Am. Soc. Civ. Engrs., 83, SA3, Paper 1276, 1-9.

Hannah S.A., Cohen J.M. and Robeck G.G. (1967) Control Techniques For Coagulation-Flocculation. J. Am. Wat. Wks. Ass., September, 59:149, 1149-1163.

Hauarhoff J. and Cleasby J.L. (1988) Comparing Aluminium And Iron Coagulants For In-Line Filtration Of Cold Water. J. Am. Wat. Wks. Ass., April, 80, 4, 168-175.

Heertjes P.M. and Lerk C.F. (1967) Functioning Of Deep Bed Filters. Trans. Inst. Chem. Eng., 45, 129.

Hsiung K.Y. (1986) Filterability Study on Secondary Effluent Filtration. J. Envir. Engng. Div., Am. Soc. Civ. Engrs., 98, SA3, June, 505-513.

Hsiung K.Y., and Cleasby J.L. (1968) Prediction of Filter Performance. J. Sanit. Engng. Div., Am. Soc. Civ. Engrs., 94, SA6, 1043-1069.

Hsiung K.Y. (1974) Determining Specific Deposit by Backwashing Techniques. J. Envir. Engng. Div., Am. Soc. Civ. Engrs., 100, EE2, 353-361.

Chiang Hsu-Wen and Chi Tien (1984) Transient Behaviour of Deep Bed Filters. In "Solid-Liquid Separation", Chapter Twenty, (Edited By Gregory, J.).

Chiang Hsu-Wen and Tien Chi (1985) Analysis of Deep-Bed Filtration, Part1: Analysis of Two Limiting Situations. AIChE Journal, August, 31, 8, 1349-1359.

Chiang Hsu-Wen and Tien Chi (1985) Analysis of Deep-Bed Filtration, PartII: Experiment. AIChE Journal, August, 31, 8, 1360-1371.

Hudson H.E. (1973) Evaluation Of Plant Operating And Jar Test Data.J. Am. Wat. Wks. Ass., 65, May, 368-375.

Hudson H.E. Jr. (1968) Physical Aspects of Filtration. Paper Presented At The AWWA Annual Conference, Cleveland, June.

Hutchinson C., William and Johnson Controls Inc. (1984) On-Line Particle Counting For Filtration Control. Instrumentation Society Of American International Conference And Exhibition. Houston, Texas, 183-195.

Ison C.R., and Ives K.J. (1969) Removal Mechanisms In Deep Bed Filtration. Chem. Engng. Sci. 24, 717-729.

Ives K.J. (1960) Rational Design of Filters. Proceedings Institution of Civil Engineers, 16, 189-193.

Ives K.J. (1961) Filtration Using Radioactive Algae. J. Sanit. Engng. Div., Am. Soc. Civ. Engrs. 87, SA3, 23-37.

Ives K.J. and Sholji I. (1965) Research On Variables Affecting Filtration. J. Sanit. Engng. Div., Am. Soc. Civ. Engrs., 191, 1, SA4, 1-18.

Ives K.J. and Gregory J. (1966) Surface Forces in Filtration. Proceedings of the Society for Water Treatment and Examination", 15, 93-116.

Ives K.J. and Gregory J. (1967) Basic Concepts of Filtration. Proceeding of The Society For Water Treatment And Examination, 16, 147, Part 3.

Ives K.J. (1969) Theory of Filtration. Special Subject No. 7, 8th International Water Supply Congress, Vienna 1969, International Water Supply Association, London.

Ives K.J. (1970) Rapid Filtration. Wat. Res., 4, 3, 201-223.

Ives K.J. and Cleasby J.L. (1971) Filtration of Water and Wastewater. CRC, Critical Review in Envir. Engng., 2, 293, August, 293-335.

Ives K.J. (1975) Specifications for Granular Filter Media. Effluent and Water Treatment Journal, June, Reader Service, No. 11, 296-305.

Ives K.J. (1975) Capture Mechanisms In Filtration. In The Scientific Basis of Filtration, (Edited By Ives, K.J.), Noordhoff, International, Leyden.

Ives K.J. (1978) A New Concept of Filterability. Progress Water Technology, 10, 5/6, 123-137.

Ives K.J. (1980) Deep Bed Filtration: Theory and Practice, Filtration and Separation. March/April, 157-166.

Ives K.J. (1982) Fundamental of Filtration. Water Filtration Proceeding Symposium, Antwerp, (ediged by Weiler R. and Janseens, J.G.), May (U.K.), 1-11.

Ives K.J. (1985) Deep Bed Filters. From Mathematical Models and Design Method in Solid-Liquid Separation, edited by Rushton, A., NATO, ASI Series.

Ives K.J. (1989) Filtration Studied With Endoscopes. Wat. Res., 23, 7, 861-1164.

Iwasaki T. (1937) Some Notes On Sand Filtration. J. Am. Wat. Wks. Ass., 29, 10, 1591-1602.

Janssens J.G. (1982) Statistical Analysis of Variable Affecting Direct-Filtration. Water Filtration, Proceeding Symposium, (Antwerp), 4.65-4.80.

Kane Lamer and Linford (1964) Filtration and Electrophoretic Mobility Studies of Flocculated Silica Suspension. J.A.C.S., 86, 3450.

Kreissl J.F., Robeck G.G. and Sommerville G.A. (1968) Use of Pilot Filters to Predict Optimum Chemical Feeds. J. Am. Wat. Wks. Ass., March, 299-314.

LaMer V.K and Healy T. (1963) Adsorption-Flocculation Reaction of Macromolecules at The Solid-Liquid Interface. Rev. Pure Appl. Chem., 13, 3.

Lash L. (1975) Granular Media Filtration For Trace Particle Removal. AlchE, Symposium Series, 71, 151, 136-114.

Letterman R.D. (1976) Optimizing Deep Bed Water Filters using a Deposit Distribution Concept. Filtration and Separation, July/August, 343-350.

Letterman R.D., Rami R.S. and Edward J.D. (1979) Direct Filtration Using Polyelectrolyte Coagulants. J. Am. Wat. Wks. Ass., June, 332-338.

Lewis C.M. and Manz D.H. (1991) Light-Scatter Particle Counting: Improving Filtered-Water Quality. J. Envir. Engng. Div., 117, 2, Mar/Apr., 209-223.

Li D.H. and Ganczarczyk J.J. (1987) Stroboscopic Determination of Settling Velocity, Size, Porosity of Activated Sludge Flocs. Wat. Res., 21, 3, 257-262.

Lieberman A.F. (1988) Calibration Requirement and Methods For Liquid-Borne particle Counter. J. Envir. Sci., May/June, 34-36.

Ling J.T. (1955) A Study Of Filtration Through Uniform Sand Filters. J. Sanit. Engng. Div., Am. Soc. Civ. Engrs., 81, paper 751, 1-35.

Lynggaard-Jensen A. and Thorsen E. (1982) Filtration and Contact Filtration in Full-Scale as Well As Pilot-Scale, of The Effluent From A Waste Water Treatment Plant Including Simultaneous Precipitation. Water Filtration Proceeding Symposium Antwerp.

Mackie R.I., Horner R.M.W., and Jarvis R.J. (1987) Dynamic Modelling of Deep-Bed Filtration. AIChE Journal, November, 33, 11, 1761-1775.

Mackie R.I. (1989) Rapid Gravity Filtration - Towards a Deeper Understanding. Filtration and Separation, January/February, 32-35.

Mackrle V. and Mackrle S. (1961) Adhesion In Filters., J. Sanit. Engng. Div., Am. Soc. Civ. Engrs., 87, 17, 17-32.

Mark R. Wiesner and Pierre Mazounie (1989) Raw Water Characteristics and The Selection Of Treatment Configurations For Particle Removal. J. Am. Wat. Wks. Ass., May, 80-89.

Maroudas A. and Eisenklam P. (1965) Clarification of Suspension:A Study of Particle Deposition In Deep Bed Granular Media. Part 1 – Some Observation On Particle Deposition. Chem. Engng. Sci., 20, 867.

Maroudas A. and Eisenklam P. (1965) Clarification of Suspension:A Study of Particle Deposition In Deep Bed Granular Media. PartII- A theory of Clarification. Chem. Engng. Sci., 20, 975-888.

McDowell L.M., Hunt J.R. and Sitar N. (1986) Particle Transport Through Porous Media. Wat. Resou. Res., December, 22, 13, 1901-1921.

Metcalf and Eddy (1980) Wastewater Engineering Treatment, Disposal, Reuse. 2nd Edition, Ed Cerra, F. J. and Maisel, J. W., McGraw-Hill Inc., United States of America.

Mints D.M. (1966) Modern theory of Filtration. Special Report No. 10, International Water Supply Congress Proceedings, Barcelona, Spain.

Moffett J.W. (1968) The Chemistry of High-Rate Water Treatment. J. Am. Wat. Wks. Ass., Novenber, 60, 1255-1270.

Mohanka Shyam S. (1969) Multilayer Filtration. J. Am. Wat. Wks. Ass., October, 504-511.

Monscvitz J.T., Rexing D.J., William R.G. and Heckler J. (1978) Some Practical Experience In Direct Filtration. J. Am. Wat. Wks. Ass., October, 70:10, 584-588.

Monscvitz J.T. and Rexing D.J. (1983) Direct Filtration Control By Particle Counting. American Annual Conference Proceedings.

O'Melia C.R. and Crapps D.K. (1964) Some Chemical Aspects Of Rapid Sand Filtration. J. Am. Wat. Wks. Ass., 56, 1326-1344.

O'Melia C.R. (1969) A Review Of The Coagulation Process. Public Works, May.

O'Melia C.R. (1972) Coagulation and Flocculation. In "Physico-Chemical Process For Water Quality Control", Chapter Two, (Edited by W.J. Weber, Jr.), 61-109, John Wiley and Sons, Inc., New York, 1972.

O'Melia C.R. (1985) Particles Pretreatment And Performance In Water Filtration. J. Envir. Engng. Div., Am. Soc. Civ. Engrs., 111, 6, 874-890.

O'Melia C.R. and Ali W. (1978) The Role Of Retained Particles In Deep Bed Filtration. Prog. Wat. Techno., 10, (5/6), 167-182.

Oulman C.S., Saatci A.M., and Baumann E.R. (1979) Direct Filtration:Particle Removal With Polymer. AIChE, Symposium Series, 75, 190, 87-96.

Payatakes A.C. and Tien Chi (1976) Particle Deposition in Fibrous Media with Dendrites Like Pattern: A Preliminary Model. J. Aerosol Science, 7, 85-100.

Payatakes A.C., Brown D.H., and Tien Chi (1977) On The Transient Behaviour of Deep Bed Filtration. Paper Presented At AIchE National Meeting, Texas.

Payatakes A.C., Parks H.Y. and Petrie J.A. (1981) A Visual Study of Particle Deposition and Re-entrainment During Depth Filtration of Hydrosorb with a Polyelectrolytes. Chem. Engng. Sci., 36, 1319-1335.

Payatakes A.C., Tien Chi and Turan R.M. (1974) Trajectory Calculation of Particle Deposition in Deep Bed Filtration; Part I, Model Formulation. AIChE Journal, 20, 5, September, 889-899.

Peacock S.L., Accomazzo M.A. and Grant D.C. (1986) Quantitative Count Calibration Of Light Scattering Particle Counters. J. Envir. Sci., July/August, 23-27.

Pelton R.H. (1981) A Model For Flocculation In Turbulent Flow. Colloids and Surfaces 2, 277-291.

Pendse H., Tien Chi, Rajagopalan R. and Turian R.M. (1978) Dispersion Measurement In Clogged Filter Beds: A diagnostic Study On The Morphology Of Particle Deposit. AIChE, 24, 3, May, 473-485.

Rajagopalan R. and Tien Chi (1977) Single Collector Analysis of Collection Mechanism in Water Filtration. The Canadian J. Chem. Engng., June, 55, 246-264.

Rajagopalan R. and Karis T.E. (1979) Effect of Electrokinetics On The removal of Colloidal Particles From Liquid. AIChE Symposium Series, 73-81.

Rajagopalan R. and Tien Chi (1979) The Theory of Deep Bed Filtration. 179-269.

Ramaley B.L., Lawler D.F., Wright W.C. and O'Melia C.R. (1981) Integral Analysis Of Water Plant Performance. J. Envir. Engng. Div., 107, EE3., 547-562.

Rebhun M.Z. Fuhrer and Adin Avner (1984) Contact Flocculation-Filtration of Humic Substances. Wat. Res., 18, 8, 963-970.

Rice A.H. (1974) High-Rate Filtration. J. Am. Wat. Wks. Ass., April, 258-262.

Riddick T.M. (1964) Role Of Zeta Potential In Coagulation Involving Hydrous Oxides. Tappi, 47, 1, 171A-179A.

Riddick T.M. (1966) The Role of Zeta Potential and Polymers in the Coagulation of Raw Waters. Trans. 16th Conference of Sanitary Engineering, University of Kansas, Lawrence, pp. 37-45.

Rong-Jin Leu and Ghosh M.M. (1988) Polyelectrolyte Characteristic and Flocculation. J. Am. Wat. Wks. Ass., April, 80, 4, 159-167.

Sakthivadivel R., Thanikachalam V. and Seetharaman S. (1972) Head-Loss Theories In Filtration. J. Am. Wat. Wks. Ass., April, 233-238.

Sembi S. and Ives K.J. (1983) Optimization of Size Graded Water Filters. Filtration and Separation, September/October, 397-402.

Sholji I. (1977) Filtration and Separation. A graduate course notes, University of Baghdad/Civil Engng. Dept., Baghdad, Iraq

Shull K.E. (1967) Filterability Techniques For Improving Water Clarification. J. Am. Wat. Wks. Ass. 59:1164, 1164-1171.

Smith C.V. (1967) Electrokinetic Phenomena In Particulate Removal By Rapid Sand Filtration. J. Am. Wat. Wks. Ass., June, 81, 170.

Sommer Holger T. and Harrison C.F. (1990) Performance Of Optical Particle Counter For Semiconductor Process Liquid. Presented at Microcontamination 90, Conference And Exhibition, Santa Clara, California. Private Communication From Dr. H.T. Sommer: Vice President of Research and Development for Hiac/Royco.

Sommer Holger T. (1990) Reliability and Count Accuracy of Optical Particle Counters. Paper Presented At 36th Annual Meeting Of The Institute Of Environmental Science, April. Private Communication From Dr H.T. Sommer: Vice President of Research and Development for Hiac/Royco.

Sommer Holger T. (1990) Performance of Monochromatic and White Light Extinction Particle Counter. Presented At IES International Conference on Particle Detection, Metrology, and Control, Arlington, Virginia. Private Communication From Dr. H.T. Sommer: Vice President of Research and Development for Hiac/Royco, 1-14.

Spielman L.A. and Fitzpatrick J.A. (1973) Theory for Particle Collection Under London and Gravity Forces. Journal of Colloid and Interface Science, 42, 3, March, 607-623.

Stanley D.R. (1955) Sand Filtration Studied with Radiotracers. Proc. Am. Soc. Civ. Engrs., 81, Separate No. 592.

Stewart R.F. (1986) Control of Structure In Particulate Solids Suspension. In "Solid-Liquid Separation", Chapter Nine, (Edited by Gregory J.).

Stumm W. and Morgan J.J. (1981) Aquatic Chemistry: An Introduction Emphasizing Chemical Equilibria in Natural Waters. A Wiley Interscience Publication, New York, N.Y.

Stumm W. and O'melia C.R. (1968) Stoichiometry Of Coagulation. J. Am. Wat. Wks. Ass., May, 60, 514-539.

Stump V.L. and Novak J.T. (1979) Polyelectrolyte Selection For Direct Filtration. J. Am. Wat. Wks. Ass., June, 338-342.

Svarovsky L. (1990) Characterization of Particles Suspended in Liquid. In "Solid-Liquid Separation". Third Edition, (Edited By Ladislav Svarovsky).

Tambo N. and Watanabe Y. (1979) Physical Characteristic Of Flocs-I. The Floc Density Function And Aluminium Floc. Wat. Res., 13, 409-419.

Tate C.H. and Trussell R.R (1979) The Use of Particle Counting In Developing Plant Design Criteria. J. Am. Wat. Wks. Ass., December, p. 691.

Tchobanoglous G. (1970) Filtration Techniques In Tertiary Treatment. J. Wat. Pollut. Control Fed., April, 42, 4.

Tien Chi, Turian R.M. and Pendse Hemant (1979) Simulation of The Dynamic Behaviour of Deep Bed Filters. AIchE, 75, 190, 82-86.

Tien Chi and Payatakes A.C. (1979) Advances In Deep Bed Filtration. AIchE Journal, September, 25, 5, 737-759.

Tien Chi, Chiu-Sen Wang and Barot D.T. (1977) Chainlike Formation Of Particle Deposits In Fluid Particle Separation. Science, May, 196, 983-985.

Tien Chi and Gimbel R. (1985) On The Development Of A Comprehensive Model Of Deep Bed Filtration. Progress In Water Filtration, Part I, (1.1-1.13).

Tobiason J.E. (1987) Physicochemical Aspects of Particle Deposition in Porous Media. unpublished Ph.D. dissertation, John Hopkin University, Baltimore, Maryland.

Tobiason J.E. and O'Melia C.R. (1988) Physicochemical Aspects of Particle Removal in Depth Filtration. J. Am. Wat. Wks. Ass., December, 80, 54, 54-64.

Trewek G.P. and Morgan J.J. (1977) Size Distribution of Flocculated Particles: Application of Electronic Particle Counters. Envir. Sci. Techno., July, 11, 7, 707-714.

Vande Hulst H.C. (1957) Light Scattering By Small Particles. John Wiley and Sons, New York, N.Y.

Verdegan B.M., Thibodeau L. and Stinson J.A. (1990) Using Monodispersed Latex Spheres In Nonpolar Liquids To calibrate Particle Counter. Microcontamination, February.

Vigneswaren S. and Tulachan R.K. (1988) Mathematical Modelling of Transient Behaviour of Deep Bed Filtration. Wat. Res., 22, 9, 1093-1100.

Vigneswaren S. and Jing Song Chang (1989) Experimental Testing of Mathematical Models Describing The Entire Cycle of Filtration. Wat. Res., 23, 11, 1413-1421.

Vingaswaran S. and Ben Aim R. (1985) The Influence of Suspended Particle Size Distribution in Deep-Bed Filtration. AIChE Journal, 31, 2, February, 321-324.

Wang C.S., Beizaie M. and Tien Chi (1977) Deposition of Solid Particles on a Collector: Formulation of a New Theory. AIChE Journal, 23, 6, 879-889.

Weber W.J. (1972) Phsiochemical Processes For Water Quality Control. John Wiley & Sons, New York.

Wood J.A. (1988) Development of Automated Particle Counter System For Filter Monitoring. Filtration And Separation, July/August, 243-247.

WPCF Manual Of Practice No. 8, 1988, Wat Pollut. Control Fed., New York.

Yao K., Habibian M.T. and O'Melia C.R. (1971) Water And Wastewater Filtration:Concept and Application. Envir. Sci. Techno., 5, 11, November, 1105-1112.

Yapijakis C. (1982) Direct Filtration: Polymer In Backwash Serves Dual Purpose. J. Am. Wat. Wks. Ass., 74:8:426, 426-428.

Yu C.H., O'Connor J.T. and Brazos B.J. (1985) Particles, Pretreatment, and Performance in Water Filtration. Discussion, J. Envir. Engng. Div.

Zeta-Meter Manual (1968), Zeta-Meter Inc.2nd Edition, New York, N.Y.

APPENDIX A

ENDOSCOPE AND MICROSCOPIC IMAGES OF FLOCS AND SYSTEM

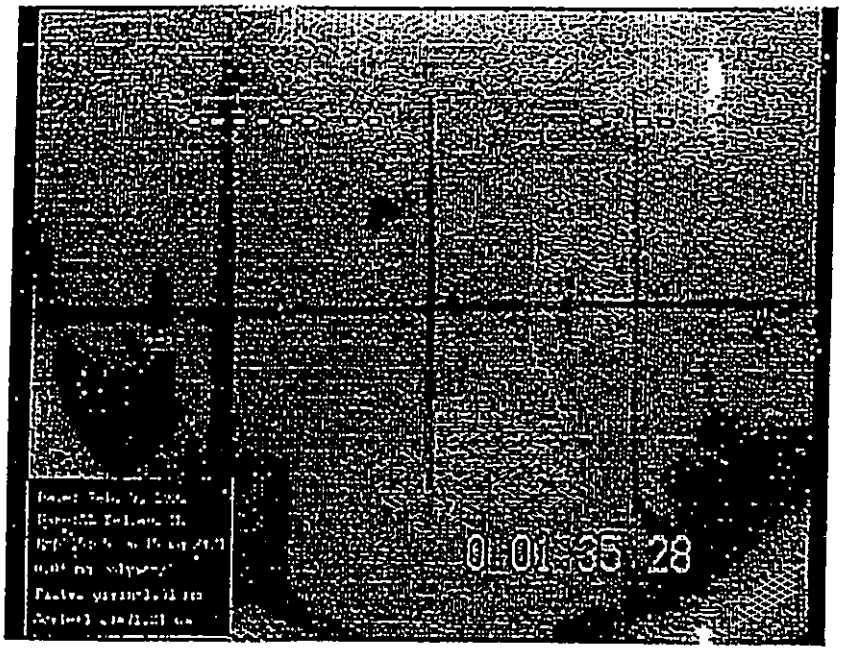

A

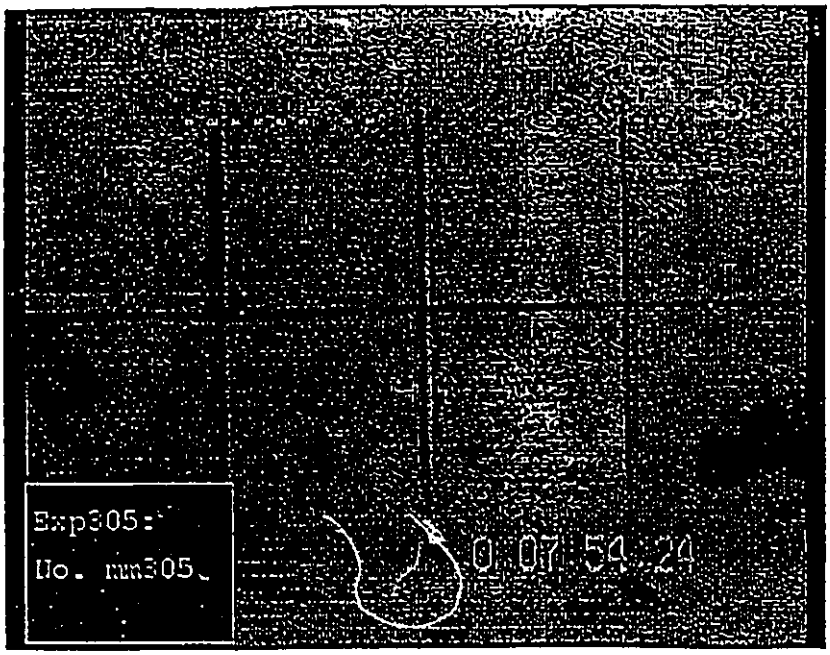

B

Figure A.1 **Endoscope view of deposit on sand grains within the filter bed (top layer). a) With deposit, b) With much of deposit on sand grains.**

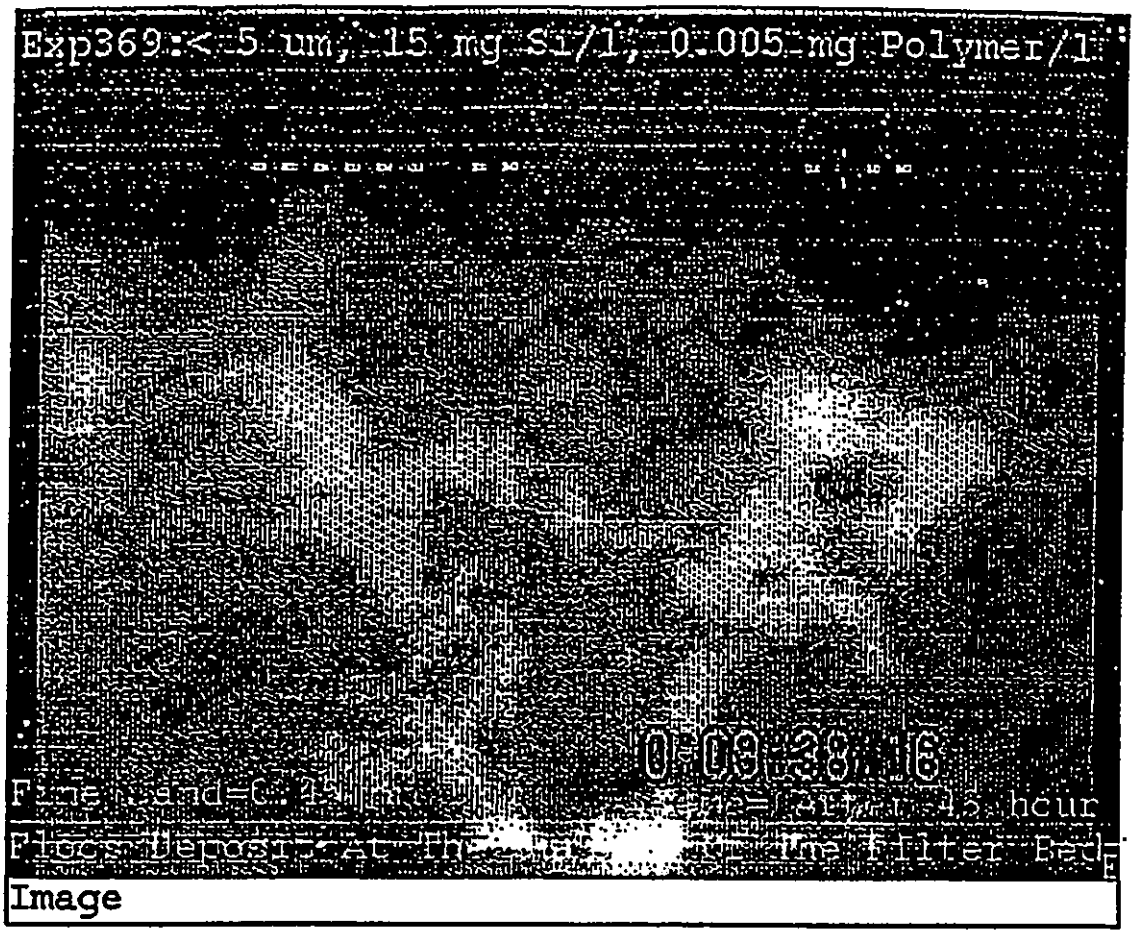

Figure A.2 **Endoscope view at the surface of the filter bed showing deposit as a cloud.**

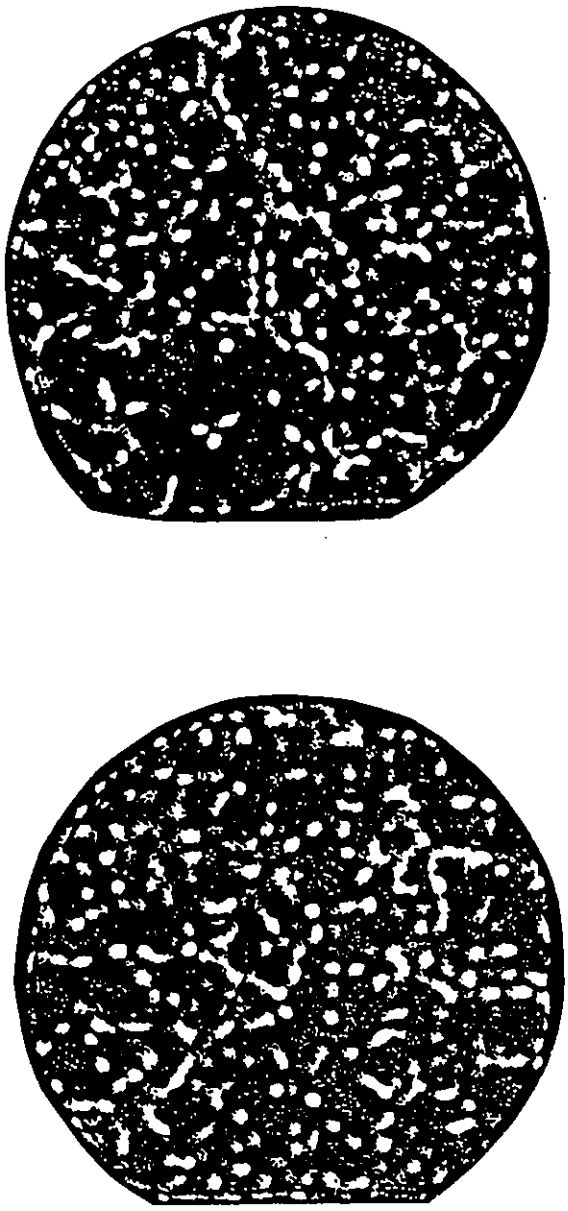

Figure A.3 Negative image of dendrite flocs acquired with the camera mounted on microscope at different points of settled 5 μm silica sample, destabilized by using polymer (percol 728).

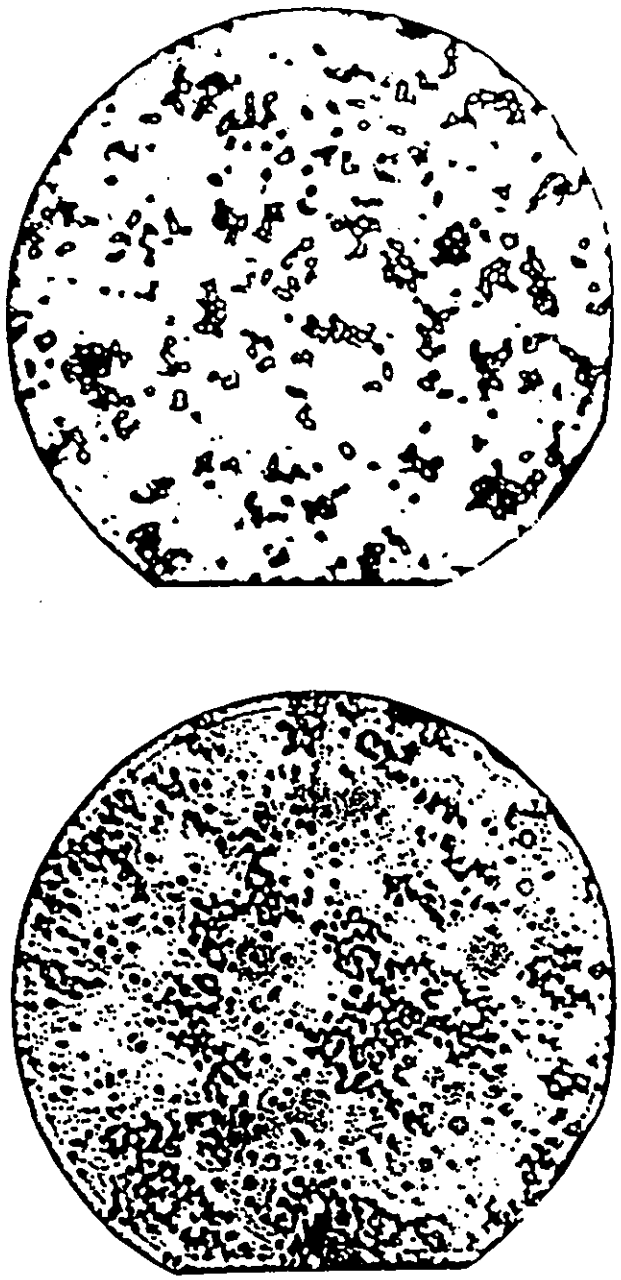

Figure A.4 **Dendrite flocs acquired with the camera mounted on microscope. a) destabilized 5 μm (Fe^{3+}) clusters b) destabilized settled 5 μm (percol 728) clusters.**

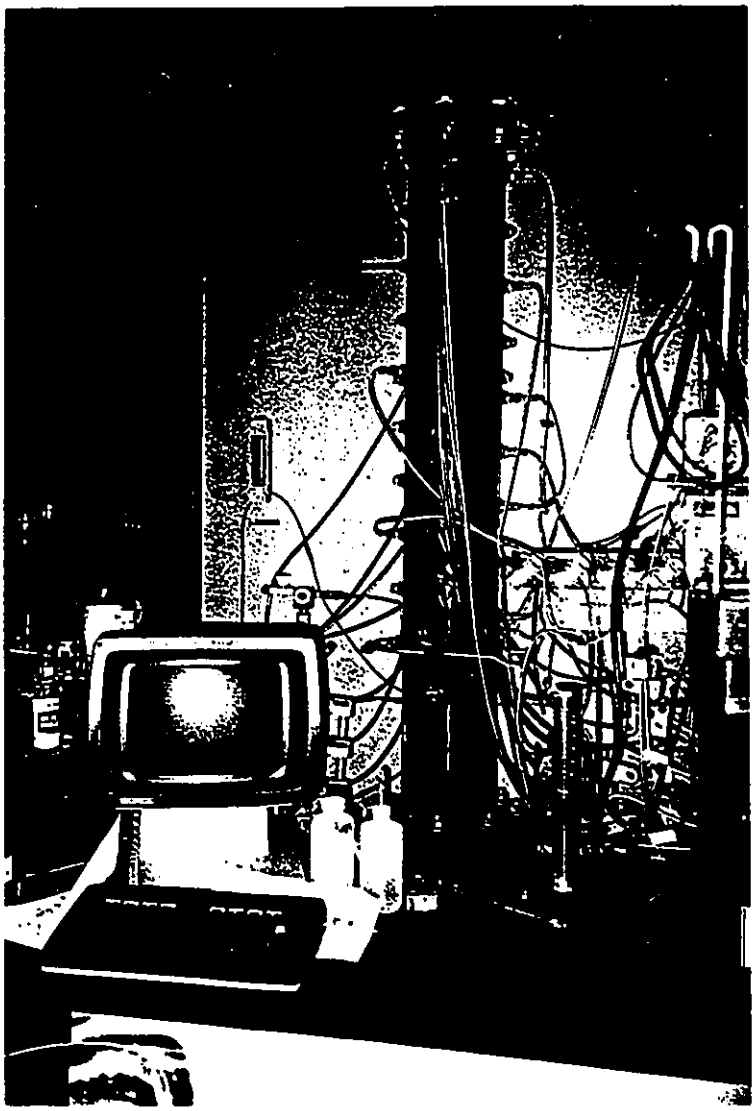

Figure A.5 Pilot-scale filter column.

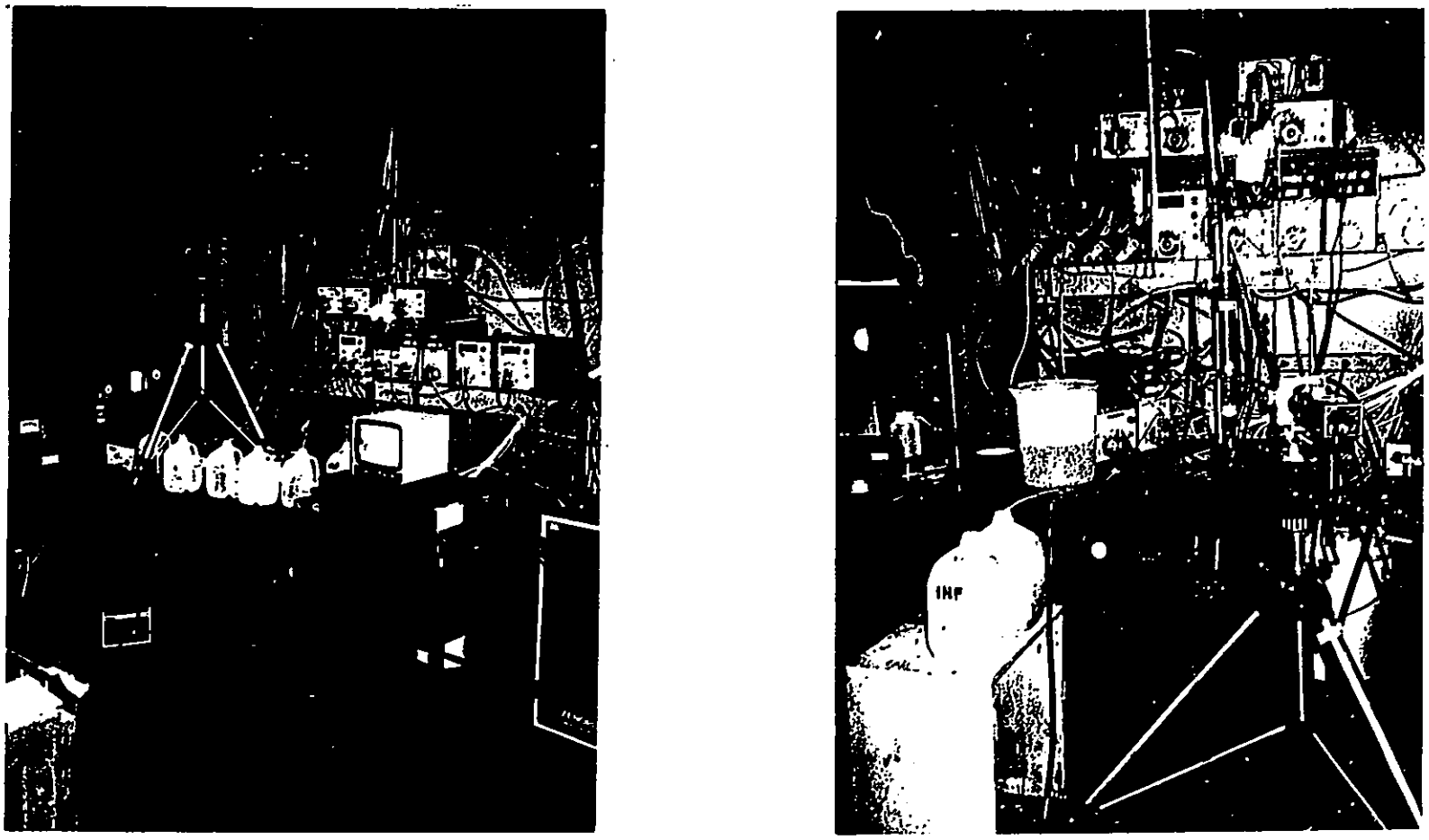

Figure A.6 The experimental system with the endoscope mounted on the filter wall, viewing the deposition on the sand. a) Pilot-scale filter column, b) bench-scale filter.

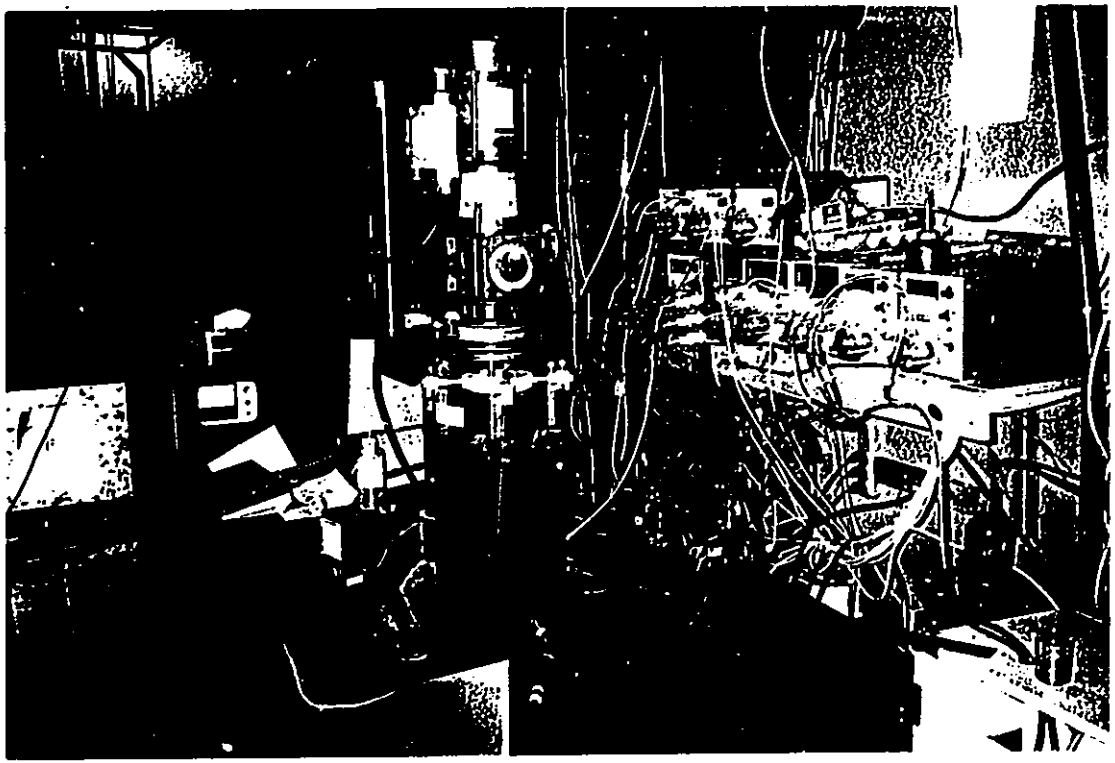

Figure A.7 **Batch flocculation system used as a mean for quantitative validation of charge neutralization and bridging mechanism.**

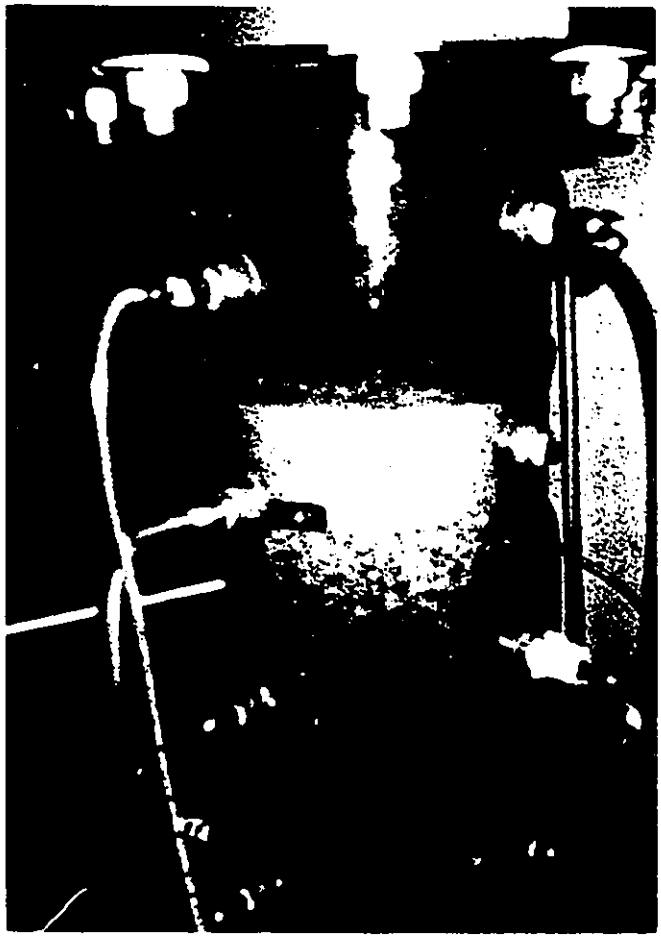

Figure A.8 **Filter column with white silica deposit showing depth of deposition.**